UNIVERSITY OF SOUTHAMPTON

FACULTY OF PHYSICAL SCIENCES AND ENGINEERING

Department of Electronics and Computer Science

Research in Field Distortion by Cavity Presence in HVDC Cable and the Associated Partial Discharge Characteristics

by

Miao HE

Thesis for the degree of MPhil

December 2016

UNIVERSITY OF SOUTHAMPTON

<u>ABSTRACT</u>

FACULTY OF PHYSICAL SCIENCES AND ENGINEERING

<u>Department of Electronics and Computer Science</u>

Thesis for the degree of MPhil

RESEARCH IN FIELD DISTORTION BY CAVITY PRESENCE IN HVDC CABLE AND THE ASSOCIATED PARTIAL DISCHARGE CHARACTERISTICS

by Miao HE

This thesis explores the electric field enhancement by a single cavity presence inside a high voltage direct current cable and the associated partial discharge characteristics at the steady state. Electrical conductivity is indicated to be important in determining the field enhancement inside the cavity and the field distortion in the region surrounding the cavity. The volume of the region possibly influenced by the cavity is given, and it is never higher than five times the cavity radius for a single spherical cavity. The conclusions are applicable across the range of cavity locations, cavity sizes, temperature differences, and material properties studied in the project.

At the present stage, no numerical model on partial discharge at direct-current voltage is published. In this project, preliminary modelling and simulation work is researched based on Niemeyer's model, which is an accepted model at alternating-current voltage, with modification according to its physical mechanism. Electrical conductivity of the insulation bulk is important in determining the characteristics of partial discharge, including the discharge repetition rate and discharge magnitude. The conclusion is applicable across the current through the conductor, cavity location and fresh and aged material studied in the project.

Table of Contents

List of Figures

I

List of Tables

DECLARATION OF AUTHORSHIP

I, Miao HE,

declare that this thesis entiled "Research in Field Distortion by Cavity Presence in HVDC Cable and the Associated Partial Discharge Characteristics" and the work presented in it are my own and has been generated by me as the results of my own original research.

I confirmed that:

- this work was done wholly or mainly while in candidature for a research degree at this University;

- where any part of this thesis has previously been submitted for a degree or any other qualification at this University or any other institution, this has been clearly stated;

- where I have consulted the published work of others, this is always clearly attributed;

- where I have quoted from the work of others, the source is always given. With the exception of such quotations, this thesis is entirely my own work;

- I have acknowledged all main sources of help;

- where the thesis is based on work don by myself jointly with others, I have made clear exactly what was done by others and what I havd conrtributed myself;

Signed: …………………………………………………………………………………...

Date: …………………………………………………………………………………

Acknowledgements

x

Definitions and Abbreviations

Name	Explanation	First Appearance
A	Experimental constants from Townsend equations	Equ(2.16)
	Constant 1 determining the electrical conductivity at DC voltage	Equ(3.5)
B	Experimental constants from Townsend equations	Equ(2.16)
	Constant 2 determining the electrical conductivity at DC voltage	Equ(3.5)
	Parameters in streamer criterium	Equ(5.3)
a	Constant depending on gas composition	Equ(2.15)
	Distance coefficient from the cable center	Equ(3.35)
b	Constant depending on gas composition	Equ(2.15)
	Radius coefficient the from cavity center	Equ(3.37)
C_{rad}	volume ionization law parameter	Equ(5.16)
C	Rate constant in determining discharge occurrence probability	Equ(2.21)
D	Distance from the cable center	Equ(4.4)
D_c	Distance from the cavity center	Equ(5.21)
d	Distance between two electrodes	Equ(2.9)
dy	Length of the selected part of cable for analysis	Equ(3.4)
E	Electric field	Equ(2.12)
E_0	Electric field when no cavity appears	Equ(3.36)
$\overrightarrow{E_{app}}$	Field vector produced by externally applied field	Equ(2.20)
E_c	Electric field in the middle of insulation	Equ(3.13)
$\overrightarrow{E_c}$	Cavity field vector	Equ(2.20)
E_i	Electric field at the innermost later	Equ(3.7)
E_o	Electric field at the outermost later	Equ(3.7)
E_{occ}	Discharge occurrence field	Equ(5.8)
E_{over}	Over field	Equ(5.6)
$(E/p)_{cr}$	The critical value of pressure reduced electric field	Equ(5.3)
$\overrightarrow{E_q}$	Field vector produced by charge on cavity surface	Equ(2.20)
E_r	Residual field	Equ(5.6)
E_{ref}	Electrical conductivity measuring field	Equ(3.26)
E_{rmin}	Minimum residual field	Equ(5.6)
$E_{s\infty}$	Inception field	Equ(5.6)
E_x	Electric field at any location in the insulation layer	Equ(3.25)
e	Charge value of a single electron	Equ(5.12)
f	Geometry factor determined by cavity shape	Equ(2.20)
	Modification factor in deriving temperature distribution across the insulation	Equ(3.17)
$f(X_i)$	Discharge magnitude	Equ(2.25)
h	Plank's constant	Equ(2.2)

I	Leakage current through insulation at DC steady state	Equ(3.1)
i_r, i_θ	Unit vectors of the insulation coordinate system	Equ(4.1)
J	Current density	Equ(3.2)
K	Coefficient determined by the cavity shape	Equ(3.33)
K_u	Kurtosis	Equ(2.26)
k	Product of local electric field, electrical conductivity and distance from cable center	Equ(3.6)
k_b	Boltzmann constant	Equ(3.5)
L	Cable length	Table(3.1)
l	Cavity height	Equ(5.17)
M	Factor in simplifying the expression of critical temperature difference for field reversal occurrence	Equ(3.11)
N	Air number density	Equ(2.12)
	Amount of discharge	Equ(2.25)
N_{dt}	the amount of detrapped electrons	Equ(5.13)
N_{dt0}	Number of detrappable electrons produced in discharge	Equ(5.12)
$N_{\_e}$	Amount of electron arriving at the anode	Equ(2.6)
N_e	Generation rate of the first electron	Equ(5.19)
N_{e1}	Generation rate of the first electron from surface emission	Equ(5.14)
N_{e2}	Generation rate of the first electron from volume generation	Equ(5.18)
n	Parameters in streamer criterium	Equ(5.3)
n_e	Electron amount	Equ(2.8)
o	Distance coefficient from the cavity center	Equ(5.21)
P	Factor in simplifying the expression of electric field distribution across the insulation	Equ(3.24)
p	Gas pressure	Equ(2.15)
Q_t	Amount of charge on the t-th layer	Equ(5.10)
q	Elementary charge	Equ(3.5)
	Amount of surface charge	Equ(5.2)
Ramp	Voltage ramp value	Table(5.1)
R_b	Resistance value of the dielectric in series to the cavity	Equ(2.23)
R_c	Resistance value of the cavity	Equ(2.23)
	Cavity radius	Table(3.1)
r	Distance from cavity center	Equ(4.2)
r_i	Inner radius of the insulation layer	Equ(3.6)
r_m	Distance of the middle of insulation to the cable center	Equ(3.15)
r_o	Outer radius of the insulation layer	Equ(3.6)
r_x	Distance of point on the insulation to the cable center	Equ(3.17)
S	Area through which leakage current flows through	Equ(3.2)
S_k	Skewness	Equ(2.25)
T	Temperature	Equ(3.5)
T_c	Temperature in the middle of insulation	Equ(3.15)
T_i	Temperature at the innermost later	Equ(3.7)
T_o	Temperature at the outermost later	Equ(3.7)

T_{ref}	Electrical conductivity measuring temperature	Equ(3.26)
T_x	Temperature at any location in the insulation layer	Equ(3.21)
t	Time	Equ(2.17)
U_0	applied voltage	Equ(5.15)
U_0^{inc}	the inception voltage	Equ(5.15)
V	Externally applied voltage level	Equ(2.23)
$V_{c,\infty}$	Voltage across the cavity without discharge consideration	Equ(2.23)
V_{eff}	effective ionization volume	Equ(5.17)
V_{min}	Inception voltage	Equ(2.24)
V_r	Residual voltage	Equ(2.24)
V_s	Gas breakdown voltage	Equ(2.14)
	Photon frequency	Equ(2.2)
v	Cavity voltage	Equ(5.4)
	ratio of the applied voltage to the inception voltage	Equ(5.15)
v_0	Fundamental photon frequency	Equ(5.14)
v_a	Attachment coefficient	Equ(2.17)
v_i	Ionization coefficient	Equ(2.17)
v_r	Residual residual voltage	Equ(5.5)
v_{rmin}	The minimum residual voltage	Equ(5.5)
$v_{s\infty}$	Inception voltage	Equ(5.4)
W	Factor in simplifying the expression of electric field distribution across the insulation when the other electrical conductivity expression is used	Equ(3.31)
X_{xy}, Y_{xy}, Z_{xy}	Coordinate value of points on xy plane	Equ(3.37)
X_{xz}, Y_{xz}, Z_{xz}	Coordinate value of points on xz plane	Equ(3.38)
X_{yz}, Y_{yz}, Z_{yz}	Coordinate value of points on yz plane	Equ(3.39)
x	Distance from cable center	Equ(3.4)
	Townsend 1st coefficient	Equ(2.8)
α	Temperature coefficient in determining electrical conductivity	Equ(3.26)
	gas ionization coefficient	Equ(5.18)
β	Field coefficient in determining electrical conductivity	Equ(3.26)
	exponent in approximation for effective ionization coefficient	Equ(5.17)
γ	Townsend 2nd coefficient	Equ(2.5)
ΔE	Field difference across the insulation layer at steady state	Equ(3.9)
	Electric field collapsed in discharge	Equ(5.7)
ΔT	Temperature difference across the insulation layer at steady state	Equ(3.8)
$ΔT_{cri}$	Critical temperature difference for field reversal occurrence	Equ(3.12)
Δt	Length of time period since last discharge	Equ(5.20)
Δv	Over voltage	Equ(5.4)
ε	Electron energy	Equ(2.17)
$ε_0$	Vacuum permittivity value	Equ(3.33)
$ε_r$	Relative permittivity of XLPE	Equ(3.33)

	Field distortion by the cavity presence	Equ(3.36)
η	gas attachment coefficient	Equ(5.18)
η_{AC}	Field enhancement by the air-filled cavity at AC voltage	Equ(3.33)
η_{DC}	Field enhancement by the air-filled cavity at DC voltage	Equ(3.34)
η_i	volume controlling volume ionization coefficient	Equ(5.16)
	Central angle of the selected part of cable for analysis	Equ(3.4)
θ	Angle value determining the location in the region surrounding the cavity	Equ(3.37)
	Angle value determines the location	Equ(4.1)
μ	Average discharge magnitude	Equ(2.25)
$(\rho/p)_0$	pressure reduced gas density	Equ(5.16)
	Discharge variance	Equ(2.25)
σ	Electrical conductivity of dielectric at DC voltage	Equ(3.3)
σ_0	Empirical value of material electrical conductivity at the measuring temperature and field	Equ(3.26)
σ_{air}	Electrical conductivity of air	Equ(3.34)
σ_i	Ionization cross section by electron	Equ(2.17)
σ_s	Electrical conductivity of cavity surface	Equ(5.9)
σ_{XLPE}	Electrical conductivity of XLPE	Equ(3.34)
	Discharge repetition rate at DC voltage	Equ(2.24)
τ	Decay time constant	Equ(5.13)
φ	Thermal activation energy	Equ(3.5)
Φ	Work function	Equ(5.14)
ϕ_{rad}	radiation quantum density	Equ(5.16)
2D	Two-dimension	
3D	Three-dimension	
DC	Direct current	
FEA	Finite Element Analysis	
HVAC	High voltage alternating current	
HVDC	High voltage direct current	
PD	Partial discharge	
XLPE	Cross-linked polyethylene	

Chapter 1. Background

This section introduces the research project, including the advantages of the High Voltage Direct Current (HVDC) transmission system, recent achievements on the field distribution in the presence of cavities in high voltage cables, definition of partial discharge, discharge research essence and development, aim of the project and the structure of this thesis.

1.1 HVDC Cable

Development of the HVDC cable has been historic, and the development in the last few years has been fast in terms of capacity and voltage. The first commercial direct current (DC) generator appeared in the year 1879 [1], and the first HVDC underground cable was delivered to transmit energy from the Pearl Street Station to New York's financial district three years later [1, 2]. The system was capable of lighting up 7,200 incandescent lamp bulbs [1]. In 1979, a 900 MW, $\pm$463 kV system was established in the United Kingdom with the initial converters being supplied by English Electric/GEC, and the capacity and voltage level were further expanded to be 2,000 MW and $\pm$500 kV in no more than 10 years [1]. Both the capacity and voltage level kept further increasing, and a long-distance power transmission system rated up to 10 GW at the voltage level $\pm$800 kV was under construction ten years ago [1].

The HVDC system has several advantages over the High Voltage Alternating Current (HVAC) system, especially in case of the ease of grid connection and the power flow control. It also has certain environment influences as demonstrated in the published studies [3–6] as noted below:

- Power flow can be fully controlled accurately and quickly;

- System connection is much easier, and network unsynchronisation or fault transmission between two grids waiting to be connected hardly happens in network connections via the HVDC system;

- Lower energy losses are involved in long distance HVDC power transmissions, and the capital cost can be lower due to the bipolar lines. The HVDC transmission distance can be theoretically infinite, and accordingly, it is more proper in long distance transmissions;

- The HVDC system is more suitable for integrating renewable energy, for example, transmitting offshore energy to the mainland, due to the low voltage ride-through capacity of variable structure speed control (VSSC) HVDC.

However, converters and inverters are associated with the HVDC system construction, and the expense increases in the capital cost and the maintenance cost at the application [2, 7]. Long distance helps compensate the weakness.

HVDC cable is an important equipment in the electric power transmission and distribution system [2, 8, 9]. The overhead line costs less in power transmission, but a cable is more attractive in electric power transmission and distribution, especially in the open sea or in urban areas due to its much less visual and environmental impact [2, 10]. The HVDC cable is the first choice and a flexibly technical solution in long-distance sea crossing power transmissions in transmitting offshore power to the mainland. In 2007, the European Commission proposed a European climate and energy 20/20/20 target in battling the global climate change: by the year 2020, the greenhouse gas emission will be reduced by 20%, the energy efficiency will be improved by 20%, and the share of renewable energy will increase by 20% [6, 11]. Therefore, the application of the HVDC cable helps achieve the goal: offshore energy helps reduce traditional fuel consumption, limits the greenhouse gas emission and enhances the use of renewable energy.

The polymer insulating cables have advantages over the mass impregnated cables. First, at the same capacity level, the polymeric cables are more flexible, smaller in size, lighter in weight and cost less [8]. Second, the operational temperature of the Cross-linked polyethylene (XLPE) cable can be as high as 90℃, while the value for the mass impregnated cable is 55℃. Polymeric cables can be more compact for the same power rating. Third, operation of the polymer cable is safe. Oil concentration in the upper insulation layer can possibly decrease due to the oil migration in the mass-impregnated cable with high temperature. This risk is not possible in polymeric cables [2]. However, the phenomena of space charge accumulation can be more significant in the polymeric cables, which results in field distortion, electrical tree generation and electrical breakdown [8].

1.2 Field Distortion by Cavities

The presence of an air-filled cavity or void in the insulation will alter the local electric field distribution. In the region surrounding the cavity, the electric field is distorted due to the variation in electric field lines distribution, and therefore, electric field line density [12]. The electric field inside the air-filled cavity can possibly be raised to a destructive level so that partial discharge tends to happen inside the cavity as the air breakdown strength is lower than that of the surrounding dielectric.

The research concerning field distortion by a single spherical or ellipsoidal cavity in high voltage cables via Finite Element Analysis (FEA) has been published in [12–15]. The cavity location, cavity size, cavity shape and relative permittivity value of the material surrounding the cavity and inside the cavity are the factors that determine the cavity field. The cavity field is stronger when the cavity is closer to

the conductor. The presence of the cavity enhances the local field when the relative permittivity of the material inside is higher than the value of the material outside, while the cavity has a reduction effect on the local field when the relative permittivity value inside the cavity is higher [13]. Field stress inside and outside the spherical cavity is stated in [12]; the presence of a prolate cavity results in a more serious field enhancement in the cavity than that by a spherical or an oblate one. The equation describing the field enhancement by a spherical cavity is proposed in [14–16].

Though the type of voltage applied is not specified in the publications [12-15], it can be believed that the research is for the field distortion at AC voltage. Relative permittivity is concluded to be the key factor in determining field distortion as the insulation tends to be capacitively graded. Temperature distribution is not considered in the research, as it may not have significant impact on the permittivity of the insulation. However, the temperature distribution is important for DC voltage applications as the electric field distribution depends on the conductivity, and the electrical conductivity value depends on the local temperature.

A 2D model is used in cavity field enhancement research due to the reduction in calculation time [13]. However, the results cannot be accurate enough, especially when the spherical or ellipsoidal cavity is under analysis [12]. A 2D model is inherently weak in geometry description as both the cable length and cavity height cannot be accurately described through the model. A single spherical cavity described in the model is a cylindrical one instead in practice. Although the simulation time may be significantly longer, a 3D model can be a possible solution to the issue as the geometry built in the model agrees with the real condition.

Accordingly, in indicating the local effect of a spherical or ellipsoidal cavity on the temperature or electric field, the reference for the model selection should be given in solving the problem accurately in a time-efficient way. To understand the partial discharge characteristics at DC voltage, the field strength inside the cavity at DC voltage, which has been little studied, is essential, as it is believed that the cavity field is important in determining discharge occurrence [12, 13]. Similar to the published work, the location and the shape of the cavity, and material properties are to be considered in drawing a widely applicable conclusion.

1.3 Partial Discharge

In this part, definition, research essence and the development of partial discharge are to be introduced.

1.3.1 Partial Discharge Definition

Partial discharge (PD) is the discharge that occurs in the dielectric or insulation system [17]. Different from breakdown that leads to insulation failure directly, partial discharge is defined as

"localized electrical discharges that only partially bridges the insulation between conductors and which can or cannot occur adjacent to a conductor. Partial discharges are in general a consequence of local electric stress concentrations in the insulation or on the surface of the insulation. Generally, such discharges appear as pulses having a duration of much less than 1µs."

in standard IEC 60270 [17–19]. PD degrades insulators gradually and finally results in insulation failure.

1.3.2 Partial Discharge Research Essence

Three indicators represent the insulation weakness: sparks, arcs and electric discharge [20]. Generally, when the term PD is discussed, it mainly refers to the partial discharge at AC voltage [21]. Partial discharge has drawn a great interest in research for a long time due to its negative effects on high voltage systems. First, partial discharge causes great energy loss and gradual dielectric degradation [17]. It consequently reduces the system reliability, quality and electricity productivity, and raises the repair and compensation cost [17, 22, 23]. The problems become more and more serious with the increase in population concentration in modern cities [24]. PD research helps improve quality and production of electricity, and reduces maintenance expense. Second, PD is normally the first indicator of insulation failure, and the research in partial discharge can help determine the location of defects inside [22]. The equipment has a potential in maintenance, and can therefore be repaired instantly when electric failure is about to occur, and the expense is limited. Furthermore, the detected PD characteristics can help predict the potential equipment lifetime [17].

It has been introduced that the HVDC transmission system has advantages over the HVAC system, and therefore, the PD research at DC voltage becomes increasingly important in helping to understand the aging process, enhance system reliability, reduce system failure, and limit the energy loss in operation in HVDC systems. There is a lack of research on DC PD: the theories or tools in identifying defect types inside systems and separating noise from PD impulses are not enough; the HVDC PD test is incomplete, and DC PD is low in both repetition rate and magnitude, and the destruction caused on the dielectric is not as serious as that at AC [21, 25].

1.3.3 Partial Discharge Research Development

Before the definition of 'partial discharge' ever appeared, the term 'local breakdown' was used in describing the local failure in solid insulation, and 'spark-over' was popular in gaseous dielectric [26–28]. Dakin et al. [26, 29] first defined corona discharge as 'a partial breakdown of insulation due to the increased stress in one component of different insulating material in series'. However, definitions proposed in earlier times were not accurate enough. Confusions were not completely addressed until

Kreuger proposed the definition of corona, surface discharge and internal discharge in 1964 [30]. Nevertheless, the definition and explanation referred more to the discharge location than the physical mechanism behind the discharge activities [26]. The nature and mechanism of partial discharge were discussed and studied in the last fifty years [31–35]. A journal paper, by R. J. Van Brunt, published in 1991 indicated that PD characteristics, including PD initiation, and discharge development for various PD types at AC or DC voltage, could be described in a stochastic way [36]. The effect of various external and internal elements, such as voltage magnitude and frequency, temperature, gas pressure, void shape and size, on discharge characteristics is researched and published in [37–42]. An electric tree can possibly appear after long-term degradation. The growth and propagation of electric trees was introduced and discussed in [43].

In the last few decades, PD research developed quickly due to the evolution in computer-based PD measurement and analysis techniques [37, 44–46]. The negative effects of PD at the interface between insulation and electrode and at the defect is concentrated on in these publications, as well as the mechanism behind the insulation degradation. The simulation based approach was developed recently, and various associated models were proposed in analysing the discharge characteristics at AC voltage. A capacitance model, despite a weakness in assumption and description, was proposed and had been accepted for a long time [22, 23, 26]. It describes PD activities in a simple manner. G. C. Crichton et al. proposed a model called Pedersen's model' in 1993 [47]. Induced charges in PD activities are considered in this model, and the results are better in describing PD activities. Similarly, L. Niemeyer produced a new model, namely Niemeyer's model, in 1995 [48]. The result is better than Pedersen's as it matches both initial and long-time aged insulators [47–49], and the simulation results agree with experiments in both PD patterns, discharge magnitude and discharge repetition rate with proper settings of the parameter values.

The term 'PD at DC voltage' was proposed for the first time [21] in the 1960s, and the mechanism behind the DC PD was discussed in [50]. In the last two decades, the DC PD research was mainly taken up by Delft University of Technology, Netherlands on the classification and the analysis of PD activity [21]. Recently, a PD test at DC voltage or at combined AC and DC voltage research is mainly applied on oil-paper insulation. Oil-paper insulation is widely applied in transformers [51]. Compared with PD at AC voltage, cavity discharge or internal discharge in solid dielectrics at DC voltage is less investigated [24].

Modelling or simulation work can help understand the effect of external factors on discharge characteristics (repetition rate and discharge magnitude) in an easier way. So far, there is no model available for describing PD characteristics at DC voltage. The solution can possibly be that the model accepted at AC voltage is referred to with the change in applied voltage form and modification according to the physical mechanism behind the DC PD.

1.4 Aim of the Project

Cavity field is an important factor in understanding discharge characteristics, and it is therefore important to understand the field stress at the cavity before the DC PD characteristics are studied. The brief review in this chapter has indicated that there is a lack of research on electric field distortion by the spherical or ellipsoidal cavity at DC steady state and partial discharge modelling work in HVDC cable applied with the voltage of constant magnitude and polarity.

In this project, these two points are to be researched via FEA. Electrical conductivity is a key factor in field distribution at DC voltage, and it depends on the local temperature and field strength. Therefore, to understand the field distortion, the effect of cavity location, cavity size, temperature distribution across the insulation and material properties have been studied. This project focusses on DC steady state.

The study on DC PD modelling work is preliminary, as there are a limited number of experiment and modelling results currently. A published model available for the AC PD research has been used with the modification according to the mechanism of DC PD. The effect of cavity location and the current level through the conductor on discharge characteristics has been considered due to their influence on the material conductivity.

The research on the field distortion and temperature distribution is mainly at the DC steady state, and the transition stage is not considered in the research. The reason is that in the PD research, the voltage with constant magnitude and polarity after the ramping stage is applied on the cable for a long time (10 hours in the project). The cable is therefore mainly at the steady state, and results from the steady state research can help understand the PD characteristics at DC voltage.

1.5 Thesis Structure

There are seven chapters in this thesis. In the first chapter, advantages of the HVDC cable and the present research on field enhancement by cavity in the insulation and partial discharge are introduced. The aim of the project is also presented in this chapter.

The second chapter is 'Introduction'. The basic theories of partial discharge, including gas breakdown theory, PD categories, PD processes and the associated physical phenomena, and PD analysis and detection methods are introduced.

The third chapter is 'HVDC XLPE Cable Analysis at Steady State'. Equations describing electric field and temperature distribution across the insulation without the cavity are derived and proposed, and a speculation on field enhancement by the single air-filled cavity at the DC steady state is stated. The

difference in cavity geometry description between 2D and 3D models is introduced in the chapter. The method through which data is extracted from the model in understanding the electric field and temperature distribution across the insulation and field distortion at or surrounding the cavity is introduced.

The fourth chapter is 'HVDC XLPE Cable Simulation Results at Steady State'. According to the data provided in Chapter 3, the validity of the equations proposed in the third chapter via the comparison between simulation results and calculation results from the corresponding equations is proved. 2D and 3D models are compared to provide the reference for model selection. Field strength and field distortion at or surrounding the cavity are illustrated, and the volume of region possibly distorted by the cavity is given. The effect of cavity size, cavity location, temperature difference across the insulation and material properties is considered while drawing a widely applicable conclusion.

Preliminary research on partial discharge characteristics is stated in the following two chapters. The fifth chapter is 'Partial Discharge Modelling Work in HVDC XLPE Cable'. Important equations in discharge modelling work and the charge decay process, which is the main reason for the difference between AC and DC discharge characteristics, are discussed in the chapter. The sixth chapter is 'HVDC XLPE Cable Partial Discharge Modelling Results'. According to the data listed in the previous chapter, DC PD simulation results are illustrated. The effect of cavity location, loading level, or current through the conductor, and material properties are discussed in this chapter.

The final chapter is 'Conclusions and Future Work'. The results obtained through the work are summarised, and the new contributions to the field are outlined in this chapter. In further improving the project, work to be undertaken or finished in the future is briefly introduced in the final part of this chapter.

Chapter 2. Introduction

In this chapter, basic theories of partial discharge are introduced, including the gas breakdown theory, PD categories, PD processes and the associated physical phenomena, PD analysis and detection methods. PD characteristics at AC and DC are different, and the related knowledge is therefore introduced separately.

2.1 Basic Gas Breakdown Theory

Important definitions and processes are introduced in this part by helping in a better understanding of the physical mechanism behind partial discharges.

2.1.1 Sources of Electron Amount Variation

There can be several sources to the variation in the amount of electrons inside the cavity, and the charge flow or the current can be detected [52]. The amount of electron can vary under no field condition due to the effect of background radioactivity or cosmic radiation. It is stated in [53] that the typical lag time, the gap between the time point when the cavity field exceeds the inception field and the point when the discharge happens, caused by these two phenomena is in the order of milliseconds, which is much longer than the avalanche formation time. They are not considered to be the key factors affecting the electron amount variation.

The number of electrons may vary in four possible ways. The first process, namely the collisional ionization, occurs when electrons with a kinetic energy level higher than the ionisation energy level of the molecules collide with a neutral gas molecule.

$$M + e^- \rightarrow M^+ + 2e^- \tag{2.1}$$

The number of electrons raises by one with each collision ionisation process.

The second process is called photoionisation. The photon with the energy exceeding the gas molecule ionisation energy can possibly ionise the molecule, and the number of electron raises by one from each photoionisation process

$$M + h\nu \rightarrow M^+ + e^- \tag{2.2}$$

where h is Planck's constant and ν is the photon frequency.

The third and final methods are attachment and detachment. Neutral molecules are converted to negative particles with an electron attached in the attachment process. Negative ions become neutral as the

electron is detached in the detachment process.

$$M + e^- \rightarrow M^- \qquad\qquad\qquad (2.3)$$

$$M^- \rightarrow M + e^- \qquad\qquad\qquad (2.4)$$

The number of electrons in the cavity increases by one from each detachment process while the opposite effect can be detected in the attachment process.

2.1.2 Electron Avalanche

Electron avalanche was studied by Sparks et al. in 1975 via the comparison between experiment and theory results [54]. R. J. Van Brunt defined the electron avalanche as the phenomenon where the total number of electrons keeps increasing due to continuous collision ionisation under high field strength [36]. Molecules involved in electron avalanche are collided by highly energised electrons, and the collision results in the rise in the number of electrons and the appearance of positive ions.

The electron that triggers electron avalanche is defined as the initiators electron. It comes in two ways. First, electron emission from the cavity surface can possibly happen at a high field. This method is defined as 'surface emission'. Second, new electrons can be introduced via the collision ionisation process, photoionisation process, and detachment process, and they are together defined as the 'volume generation' process [37, 38, 48].

Fig. 2.1 graphically represents the electron avalanche process. Positive ions and electrons are separated in the avalanche propagation: positive ions and electrons move towards the cathode and the anode respectively. The local electric field is enhanced at the avalanche head (close to the electrodes) while the field reduction happens in the region between positive ions and electrons.
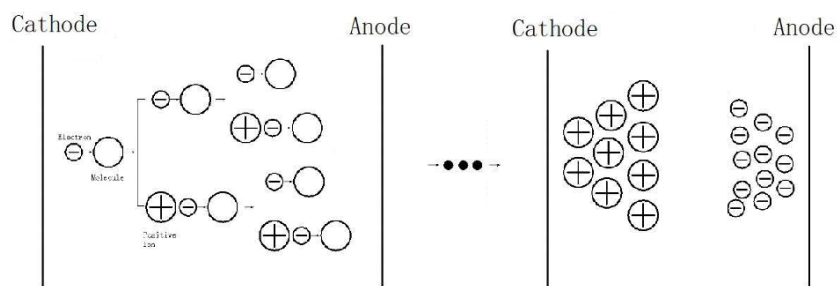
Fig. 2.1. Electron avalanche process [52, 55].

Three conditions should be satisfied in obtaining the continuous electron avalanche across the cavity [52]. First, starting electrons are available while triggering the avalanche. Second, the field strength should be high enough in providing electrons involved in the avalanche with a kinetic energy level

exceeding the molecule ionisation energy. Electron avalanche possibly extinguishes in the low field region as the energy of electron is weak in triggering the collision ionisation. Third, the effect of attachment is not dominant as the number of electrons is reduced by the attachment process.

2.1.3 Townsend Breakdown Theory

In the early 1900s, J. S. Townsend proposed a gas breakdown theory based on the gas ionisation mechanism under the uniform field [52, 56–58]. Each second, it is assumed that n number of electrons are injected from the cathode, and the number of electrons arriving at the anode is Mn. The amount of electrons generated via ionisation is $(M - 1)n$, and the same number of positive ions moves towards the cathode.

A parameter describing an increase in the number of electrons in each single secondary avalanche is defined as the Townsend 2nd coefficient γ. The number of charges increases by the first secondary avalanche in each second is therefore expressed as

$$N = \gamma(M - 1)n \tag{2.5}$$

$\gamma(M - 1)$ is replaced by μ for simplification. Considering the continuous secondary avalanche processes, the total amount of electrons arriving at the anode is expressed as

$$N\_e = n(1 + \mu + \mu^2 + \mu^3 + \cdots) \tag{2.6}$$

The μ value in Equation (2.6) has to be equal to unity: if the condition is not satisfied, N_e can be infinite ($\mu > 1$) or the avalanche may cease to grow ($\mu < 1$). It means

$$\gamma(M - 1) = 1 \tag{2.7}$$

α is the Townsend 1st coefficient [52, 57]. In a unit distance dx, the amount of electrons increases by αdx through collision ionisation. The variation is expressed as

$$dn_e = \alpha n_e(x)dx \tag{2.8}$$

x is the location for calculation, and $n_e(x)$ is the number of electrons at the position x. Applying Equation (2.8) to the whole region between two electrodes (with d in distance), the number of electrons available for collision is

$$n_e = n \cdot \exp \int_0^d \alpha dx = Mn \tag{2.9}$$

$$M = \exp(\alpha d) \tag{2.10}$$

11

Equations (2.7) and (2.10) are combined, and the Townsend breakdown criteria is

$$\gamma(\exp(\alpha d) - 1) = 1 \qquad (2.11)$$

Townsend breakdown theory is proved to be reliable under various pressure levels [59] and under the conditions when attachment and detachment are considered [52]. The weakness of the theory is that it is limited in the uniform electric field, and is not applicable to a system when the influence of space charge is significant [58, 60].

2.1.4 Paschen's Law

Paschen's law is based on Townsend's breakdown theory, and it indicates the relationship between the breakdown voltage and the product value of gas pressure and distance between electrodes [57]. The ionisation coefficient is generally determined by the electric field strength for a given non-attaching gas under the uniform field [52]. Define N as the gas number density and E is the strength of the uniform field. Townsend's 1st and 2nd coefficients can therefore be written as [52]

$$\frac{\alpha}{N} = f(E/N) \qquad (2.12)$$

$$\gamma = g(E/N) \qquad (2.13)$$

Substitute Equations (2.12) and (2.13) into Equation (2.11), and the expression is transformed into

$$g\left(\frac{V_s}{Nd}\right) * \left\{\exp\left[Nd \cdot f\left(\frac{V_s}{Nd}\right)\right] - 1\right\} = 1 \qquad (2.14)$$

V_s is the breakdown voltage. Paschen's law indicates that the breakdown voltage uniquely depends on the product of the gas number density and the gap length, and as for any specific value of Nd, there is only one breakdown voltage level satisfying Equation (2.14).

Gas pressure can be a parameter indicating the gas number density, and Paschen's law can be further expressed as [61]

$$V_s = \frac{a(pd)}{\ln(pd) + b} \qquad (2.15)$$

where a and b are two constants depending on gas composition. The Paschen's curve for dry air is illustrated in Fig. 2.2 [61]. The curve in the figure represents the critical pd value at a given potential, and gas breakdown tends to happen when the practical pd value is in the region above.
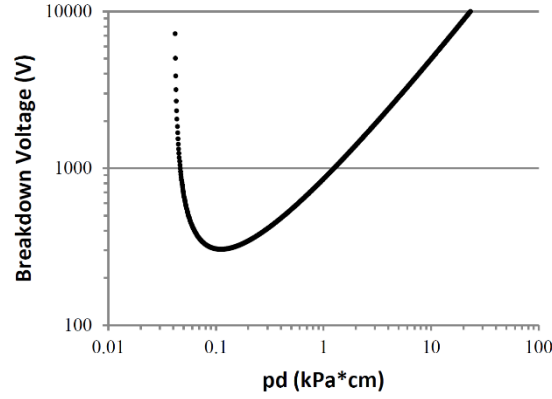
Fig. 2.2. Paschen's curve for air [61].

The breakdown potential is expressed as [57, 58]

$$V_s = Bpd/\ln\{Apd/[\ln(1 + 1/\gamma)]\} \qquad (2.16)$$

where A and B are experimental constants from Townsend equations when E/p ranges between 450 and 7500 $V.kPa^{-1}$ [58]. A indicates the gas saturation ionisation at the specific condition and B is related to the ionisation and excitation energies [58, 62, 63].

2.2 Types of Partial Discharge

There are four types of partial discharge, namely corona, surface discharge, internal discharge, and electrical treeing [64] (as shown in Fig. 2.3). Corona can be detected at the sharp needle or conductor edge, or conducting particles with high field strength. Surface discharge occurs at the insulator surface.

Internal discharge, which is the type of discharge to be researched in the project, is the discharge occurring inside the defect presented in the dielectric. Defects and cavities can be present in polymeric cable insulation via two processes. First, the cavity or defect can possibly appear in the XLPE manufacturing or fabrication process [65]. Second, new defects can possibly be generated during operation. Under high field (over 15 $kV.mm^{-1}$ for polyethylene [66]), electrons injected into the insulation obtain energy from the applied field. When these electrons have energy exceeding a critical level high enough in vaporising the Van der Waals bonds, submicrocavities with diameter λ appear in the insulation. The cavity diameter depends on the travel length of the injected electron without scattering. The critical energy level for bond vaporisation is $1.9 \times 10^{-20}J^{-1}$ (0.12eV) for XLPE at 22°C, and the diameter of the submicrocavity is empirically given as around 8.5 nm at 20 $kV.mm^{-1}$[67]. The presented submicrocavities tend to coalesce, and microcavities eventually appear: inside the microcavity, electrons can possibly obtain the kinetic energy which is strong enough to break the intermolecular bond [66] and produce deteriozation [68]. Presence of a microcavity is harmful to the insulation, and it can finally result in insulation failure.
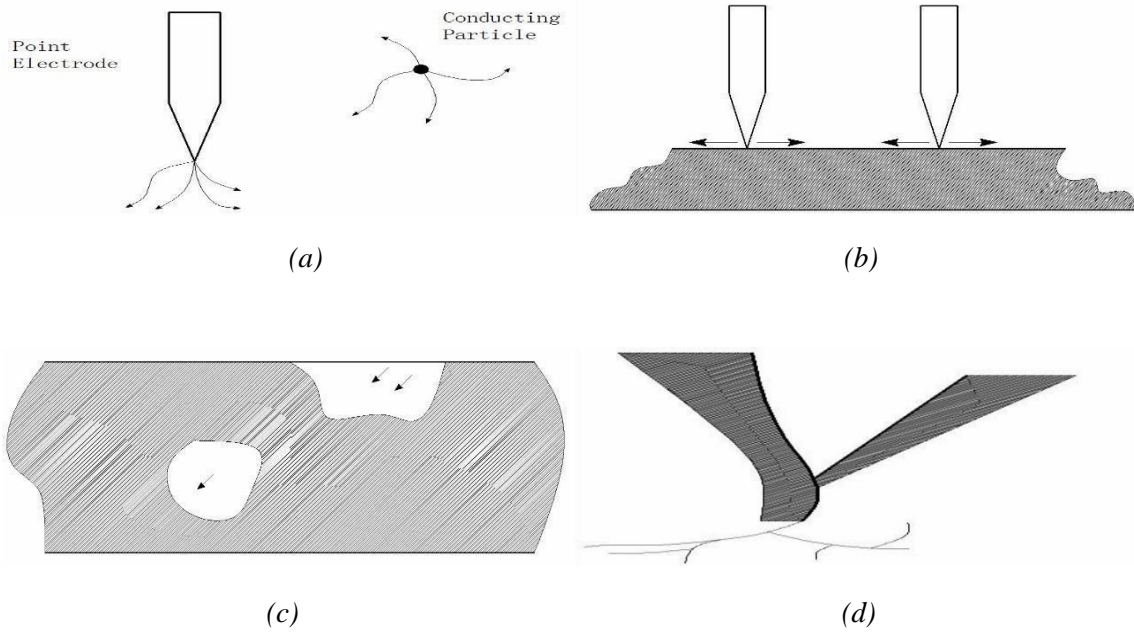
Fig. 2.3. Four types of PD (a) corona, (b) surface discharge, (c) internal discharge, and (d) electrical treeing [64].

The presence of defects in XLPE cables can affect the electrical performance by disturbing the electric field distribution. The appearance of the air-filled void or cavity enhances the local field at the AC field, and the field inside the cavity is stronger than that of the surrounding material [12–15]. The dielectric strength of air, however, is much lower than that of the surrounding dielectric: the breakdown strength of air is $3\,kV.mm^{-1}$ at atmospheric pressure [57], while the breakdown strength of XLPE can be over $60\,kV.mm^{-1}$ and reaches nearly $100\,kV.mm^{-1}$ with proper additive manufacturing and cooling [69]. Therefore, the higher local field strength and weaker breakdown strength lead the partial discharge to happen inside the defect. Internal discharge can also occur in low-density domains or channels [64, 70].

Electrical treeing tends to occur in the inhomogeneous place in the insulation where the material is impure, or the insulation has mechanical defects or gas voids [71, 72]. It is a main cause of the long term degradation of polymeric material and therefore in-service XLPE power cable failure [72, 73].

2.3 Partial Discharge Occurrence Conditions

In triggering partial discharge inside the air-filled cavity, three conditions have to be. First, there has to be at least one starting electron available inside the cavity in triggering the electron avalanche occurrence. Second, the cavity field that is higher than a critical electric field which is defined as the inception field. The level is at a specific strength above which self-sustaining electron avalanche across the cavity can be maintained [20, 21, 37].

Third, the ionisation coefficient value is higher than the attachment value. Assume that there is no

energy loss. The electron density changes via ionisation and attachment.

$$\frac{dn_e}{dt}\bigg|_i = \int_l^\infty N v \sigma_i(\varepsilon) n_e(\varepsilon) = v_i n_e \tag{2.17}$$

$$\frac{dn_e}{dt}\bigg|_a = -v_a n_e \tag{2.18}$$

$$\frac{dn_e}{dt} = (v_i - v_a) n_e \tag{2.19}$$

where $\sigma_i(\varepsilon)$ is the ionisation cross section by electron with energy ε. v_a and v_i are the attachment and ionisation coefficient respectively [74]. According to Equation (2.19), if the attachment process is dominant ($v_i - v_a < 0$), the electron density keeps decreasing with time. The number of electrons decreases, and it is hard to maintain the self-sustaining electron avalanche. Therefore, v_i has to be higher than v_a in ensuring the PD occurrence.

2.4 Partial Discharge Randomness

Internal PD activity is considered to be random because

- The size and the position of a defect in insulation are hard to predict. In a multiple-void system, the sequence and number of voids with PD occurrence are also difficult to determine;

- The PD occurrence position inside the cavity is random;

- Starting electron generation is random;

- Electron collision with molecules is stochastic;

- Other reasons, such as the complex gas conditions (gas composition, gas pressure and temperature) inside the cavity.

Therefore, PD characteristics should be analysed in a stochastic way.

2.5 Partial Discharge Processes

In this section, partial discharge processes at AC and DC voltage are introduced, and the difference between the two conditions is stated.

2.5.1 Process of Partial Discharge under AC Voltage

The research on PD has been carried out mostly with respect to its characteristics, and it helps understand the physical mechanism better if AC PD processes are introduced first. The relationship of the electric field associated with partial discharge is introduced, together with the amount of charge involved in discharge and the discharge occurrence probability.

Cavity Field Calculation

Partial discharge activity is a stochastic phenomenon [35, 36]. The cavity field is significant in partial discharge as it determines the occurrence of partial discharge. Cavity field is determined by two components [37, 48]: one is produced by the externally applied voltage, and the other one is induced by charges on the cavity wall. Generally, the cavity field $\overrightarrow{E_c}$ is represented by the stress at the cavity centre, and it is expressed as

$$\overrightarrow{E_c} = f\overrightarrow{E_{app}} + \overrightarrow{E_q} \qquad (2.20)$$

where $\overrightarrow{E_{app}}$ is the field vector produced by the externally applied field at the cavity centre when there is no cavity. The positive direction of the vector is set in the direction similar to $\overrightarrow{E_{app}}$ when the applied voltage is positive. $\overrightarrow{E_q}$ is the field vector induced by charge on the cavity surface. It equals zero prior to the occurrence of the first ever discharge activity. The absolute magnitude $\overrightarrow{E_q}$ is related to the amount of charge on the cavity surface [48, 49], while the polarity is determined by the distribution of positive and negative charges. f is defined as the geometry factor which is determined by the cavity shape. Actually, f can be calculated as the field enhancement coefficient by the air-filled cavity [47, 49].

The reason for having a lag time where discharge cannot happen instantly when the cavity field exceeds the inception level is related to the starting electron generation. When partial discharge extinguishes, cavity field drops to the residual field [75] below which self-sustaining avalanche disappears. It helps determine the strength of $\overrightarrow{E_q}$ at the end of discharge and the discharge magnitude.

Important Phenomena involved in AC PD

Both the phenomena involved in the AC PD are important and can be different from DC PD. The first one is the polarity reversal of $\overrightarrow{E_{app}}$ by the applied voltage. It makes the complexity of the impact of $\overrightarrow{E_q}$ on the cavity field. Prior to the field polarity reversal, $\overrightarrow{E_q}$ keeps reducing the cavity field when the absolute magnitude of $f\overrightarrow{E_{app}}$ is stronger than $\overrightarrow{E_q}$. There is an absolute magnitude decreasing stage. When the absolute magnitude of $f\overrightarrow{E_{app}}$ equals to $\overrightarrow{E_q}$, the cavity field is zero, and the field due to the deposited surface charge has an enhancement effect on the cavity field starting between this time point

and the occurrence of the following discharge activity. Therefore, the first discharge after the field polarity reversal can possibly happen at a lower applied voltage level [75].

The second phenomenon is charge decay between two consecutive activities. The number of surface charges decrease due to the decay process, resulting in a drop of the absolute magnitude of $\overrightarrow{E_q}$. There are three ways through which charges inside the cavity can possibly disappear [38]. First, when the $\overrightarrow{E_c}$ is in the same direction as $\overrightarrow{E_q}$, positive and negative charges tend to propagate along the cavity wall, and charge recombination occurs (as given in Fig. 2.4). The influence of the recombined charges disappears, and the absolute magnitude of $\overrightarrow{E_q}$ drops. Charge recombination is the main source of charge decay at the AC voltage.

(a) *(b)*
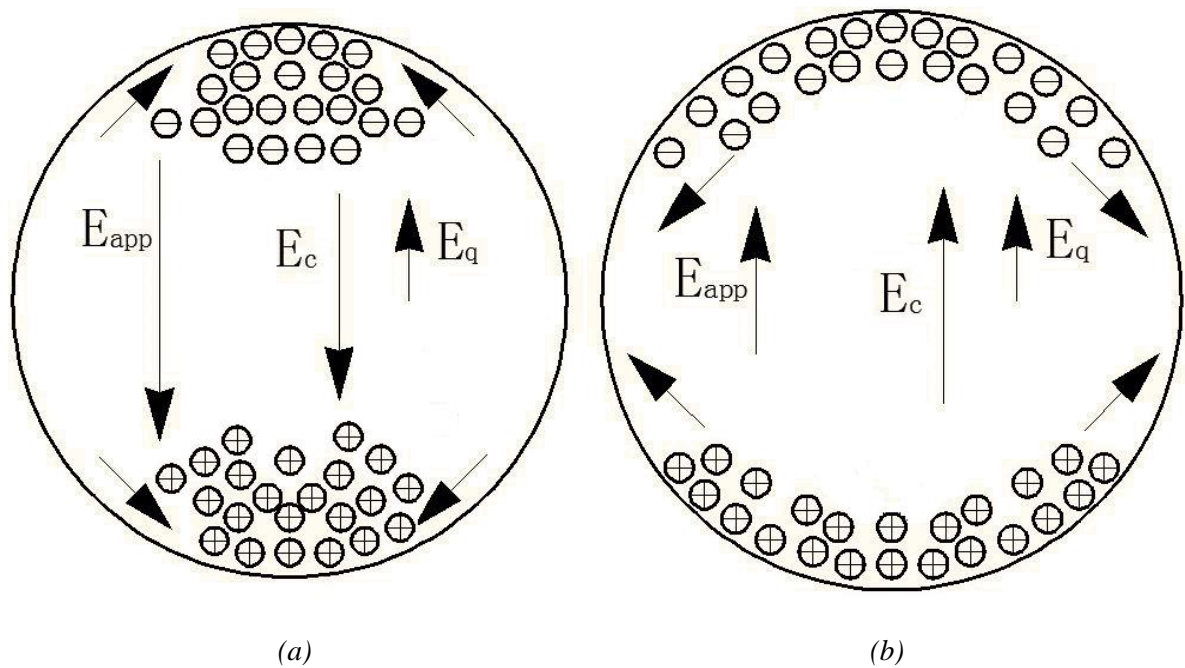
Fig. 2.4. Charge propagation along the surface (a) cavity field is in opposite direction to charge field, and (b) cavity field is in the same direction to charge field.

Second, charges can be trapped on the surface in shallow or deep traps, and these trapped charges cannot be the source of generation of the starting electron in the following activity, especially when they are deeply trapped. Deeply trapped charges have little effect on $\overrightarrow{E_q}$.

Third, charges can possibly enter the insulation bulk according to the bulk conduction. The speed of charge decays in this way increases with the bulk conductivity, and charge migration through the bulk can lead to a longer lag time and lower repetition rate as the amount of charges for the starting electron generation decreases [34].

Accordingly, charge decay is important as it has an effect on charge recovery after the previous discharge and the starting electron generation, and therefore, the discharge occurrence probability.

17

Unlike the sharp change across the discharge event, the speed of charge decay is gradual.

Charge Amount Calculation

According to the previous discussion, the amount of charge varies in two processes. The first process is the partial discharge, and the amount of induced charge is relative to the field drop across the discharge process [48, 49]. Equation (2.20) is referred to while calculating the cavity surface charge when the discharge stops. $\overrightarrow{E_{app}}$ can be calculated according to the cable geometry, material properties and the voltage level at the discharge occurrence. $\overrightarrow{E_c}$ is set to be the residual field level [75]. $\overrightarrow{E_q}$ is therefore obtained, and the amount of charge on the cavity surface can be calculated [48, 49].

The amount of charge induced in the discharge process is defined as the discharge magnitude. It is a significant parameter in describing discharge characteristics. The maximum discharge magnitude depends on the maximum possible collapsed cavity field. When the amount of charge for the following discharge is numerous, a discharge tends to happen instantly when the cavity field exceeds the inception level. The minimum discharge magnitude appears under this condition, and the level is determined by the difference between inception and residual field. The average discharge magnitude is the sum of all discharge magnitudes divided by the amount of discharge pulses in a given period of time [37], and it describes the destructive effect of partial discharge on insulation.

The second process through which the amount of charge varies is the charge decay, especially when charge recombination occurs at the cavity wall. Equations describing the amount of charge decayed between two activities are listed in [48, 49].

PD Occurrence Probability

Partial discharge can be separated into two types, namely fast PD and slow PD. The former is with a higher repetition rate, shorter lag time and lower discharge magnitude, while the latter one has a lower repetition rate, with long lag time and higher discharge magnitude [34]. In a time interval $[t, t + dt]$, the PD occurrence probability is calculated as

$$probability = c \cdot dt \tag{2.21}$$

for fast discharge and

$$probability = 1 - c \cdot dt \tag{2.22}$$

for slow discharge [75]. c is defined as the rate constant. If the cavity field is lower than the inception level, c equals to zero for fast PD and is infinite for slow PD. When the cavity field exceeds the inception field, c is a constant which is dynamically determined by volume generation and surface emission [48, 49, 75].

Under 50Hz AC voltage, the cavity field variation with time is graphically shown in Fig. 2.5. Red and blue lines represent the cavity field with and without PD occurrence respectively. Black lines represent the inception and residual field [37]. The reason for phase shift is a variation of the effect of the charge field $\overrightarrow{E_q}$ on cavity field due to field polarity reversal.
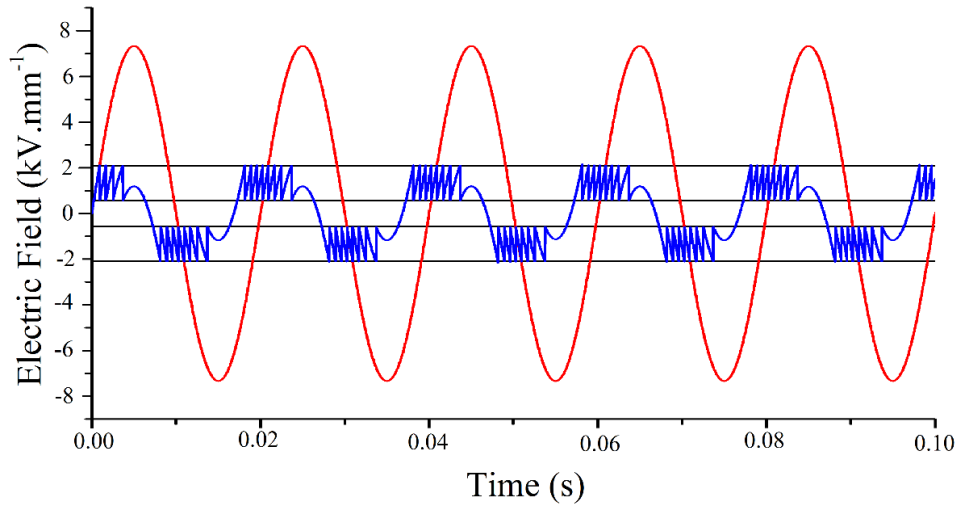
Fig. 2.5. Cavity field variation with time with discharge consideration.

2.5.2 Process of Partial Discharge under DC Voltage

Unlike PD activities at AC voltage that have been greatly researched and published, the knowledge of PD characteristics at DC is still at an early stage [76, 77]. As it is defined as 'DC PD', the research concentrates on the condition that partial discharge events are triggered under the direct voltage with constant magnitude and polarity. Discharge occurrence conditions are the same as that under AC voltage [21]. At DC voltage, the discharge occurrence probability is also calculated as the comparison between the starting electron generation probability and a random number between 0 and 1. In this part, the mechanism which is different from that of AC PD is to be outlined.

Model in DC PD description

P. H. F. Morshuis and J. J. Smit explained the partial discharge at DC voltage in an easy way via the charging and discharging of the capacitor [21]. The equivalent circuit for insulation containing a single cavity inside at DC voltage is given in Fig. 2.6. R_a, R_b and R_c are the resistance values of the entire insulation, the dielectric in series to the cavity and the cavity itself. C_a, C_b and C_c are the associated capacitance values. The gap S indicates the place where discharge occurs: ignition of partial discharge shorts the R_c and C_c due to high conductivity across the PD activity [38].

19
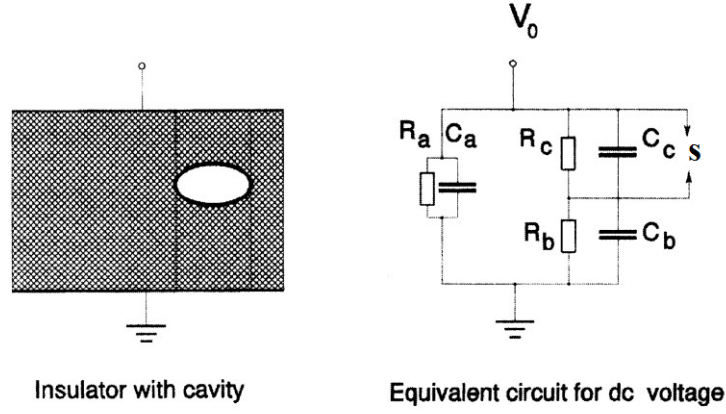
Fig. 2.6. Equivalent circuit describing PD at DC voltage [21].

Reoccurrence of PD at DC voltage is due to the finite resistivity value of the dielectric and the infinite impedance value of the capacitor at the DC voltage [21]. Prior to the occurrence of the next discharge, capacitor charging first occurs after the end of the event. Assuming that the capacitance value is constant, the cavity voltage, and therefore, the cavity field keeps increasing in the charging process. PD happens when the cavity field recovers back to the stress exceeding the inception level with starting electrons available in triggering electron avalanche [21]. However, the model is not that applicable for the HVDC cable, as the resistance value varies with the temperature.

Two time parameters are used in describing the discharge process at the DC voltage. The recovery time constant (t_R) describes the time for the cavity field strength to recover back to the inception field since the previous event. Lag time (t_l) represents the time between the point when the cavity field reaches the inception field and the point when discharge happens. The time interval between two events is expressed as the sum of t_R and t_l.

Cavity Field Enhancement

Electric field tends to be resistively graded at DC steady state. Therefore, instead of the relative permittivity at AC voltage, the electrical conductivity of gas inside the cavity and that of the surrounding dielectric is important in field enhancement under the condition. Therefore, the value of f in Equation (2.20) should be modified while calculating cavity field at DC voltage.

PD Repetition Rate

PD repetition rate at DC is expressed as

$$V_{c,\infty} = V \frac{R_c}{R_b + R_c} \tag{2.23}$$

20

$$n = \frac{1}{\tau}\left(\frac{V_{c,\infty}}{V_{min} - V_r}\right) \qquad (2.24)$$

where $V_{c,\infty}$ and τ are the voltage across the cavity without PD consideration and the DC PD repetition rate respectively. V is the external applied voltage. V_{min} and V_r are defined as the inception and the residual voltage [21]. The lowest repetition rate appears at the inception voltage. The minimum rate is empirically less than one event per minute, which is much lower than the repetition rate at the AC voltage. Inception field determination is more suitable for fresh solid samples because of no space charge injection [78].

Charge Decay

The difference between charge decay at DC voltage and that at AC voltage is significant. When the voltage with a constant magnitude and polarity is applied, $\overrightarrow{E_{app}}$ magnitude is constant at the DC steady state. Field polarity reversal of the applied field does not happen, and charge decay which results in a decrease in the absolute magnitude of $\overrightarrow{E_q}$ is the only way that cavity field recovers back to the level exceeding the inception field.

Besides, charge recombination due to charge propagation along the cavity wall can hardly happen between two discharge activities. Charge movement on the cavity wall happens when the cavity field is in the same direction as that of the field produced by the surface charge. The phenomenon can hardly appear at the constant voltage stage due to no field polarity reversal, and the field produced by surface charge keeps reducing the cavity field.

Charge migration through the insulation bulk is therefore the main source of charge decay. The total number of charges changes slightly: though the amount inside the cavity decreases, the amount of charges accumulated in the bulk increases. The field strength produced by the charge is inversely related to the square of distance of the charge from the cavity centre, and the distance increases with the charge movement in the insulation bulk. Therefore, absolute electric field strength produced by charge decreases. Repetition rate of partial discharge at DC voltage is much slower than that at AC voltage due to the constant applied voltage and the slower charge decay through the bulk.

2.6 Descriptive Parameters

Several parameters are important in describing PD characteristics [79]:

- Inception field: the cavity field threshold exceeding which PD can occur. It is a level high enough in triggering sustainable avalanche;

- Residual field: cavity field value level to which cavity field is reset by PD. Sustainable avalanche cannot be kept below this level;

- Lag time and recovery time: they together describe the time interval between two consecutive activities, and reflect the discharge repetition rate [21, 54];

- Over-voltage: voltage difference between PD occurrence voltage and the inception voltage. It relates to the length of lag time, and determines the discharge magnitude;

- Real and apparent charges: real charges are charges that are actually induced across the discharge event, and they can hardly be externally measured [34]. Apparent charges are the ones going through the ground and influencing the voltage between terminals. Magnitude of real and apparent charges is related to the same parameters, namely field drop across the discharge, cavity size and shape, and the material properties of the dielectric surrounding the air-filled cavity [48]. Apparent charges can therefore be used to indicate the discharge magnitude [80].

- Occurrence time: it indicates the cycle numbers and PD occurrence phase angle at AC voltage, and represents the actual time point of discharge occurrence at DC voltage.

2.7 Potential Influencing Factors

Partial discharge characteristics, such as discharge repetition rate and discharge magnitude, vary with several factors because of their effects on [37]:

- number of charges available for the PD occurrence;

- externally applied voltage conditions;

- physical parameters associated with PD.

At AC voltage, three main factors with a potential influence on the discharge characteristics are the applied voltage, cavity conditions, and insulation material properties [35].

2.7.1 Applied Voltage

The applied voltage affects PD characteristics significantly via determining the absolute magnitude of $\overrightarrow{E_{app}}$, and therefore, the cavity field. Cavity field is an important factor in influencing PD occurrence and determining discharge repetition rate. Besides, the level of field possibly collapsed across the discharge process increases with the applied voltage as well. Therefore, a higher applied voltage

increases the PD repetition rate and the peak and average discharge magnitude.

2.7.2 Cavity Conditions

When the cavity conditions are referred to, the cavity geometry (size, location and shape), temperature, pressure and surface conductivity are included. At the AC voltage, the cavity field varies with the cavity location and shape, and a higher cavity field can result in a higher repetition rate and a higher discharge magnitude. Larger cavity size enhances the discharge magnitude. More charges are available for electron avalanche in the following event [48, 49], and discharge repetition rate increases with cavity size.

High temperature enhances the starting electron generation probability, and therefore, increases the PD repetition rate [40]. The inception field also increases with temperature, and the minimum discharge magnitude is higher. High surface conductivity results in faster charge decay, and it results in the reduction of the starting electron, and therefore, reduces the PD repetition rate (though the phenomenon is not apparent at AC voltage). In the long term, because of degradation by an accumulated effect of continuous PD activities, the cavity surface keeps becoming less smooth due to the continuous bombardment of electrons with high energy (over 10 eV) [44]. A microscopic detection indicates that material is removed from the cavity surface [44]. Partial discharge characteristics change with this deterioration of the cavity surface [75, 81].

2.7.3 Insulation Material Properties

At AC voltage, the relationship between the air permittivity and the surrounding material permittivity determines the cavity field. The higher the material permittivity than that of air, the higher the cavity field will be when the cavity size, location and shape do not change. Both discharge magnitude and repetition rate rise.

2.8 Partial Discharge Detection

Partial discharge detection and measurement are important in assessing the condition of HV equipment [82]. The detection and measurement methods have to be non-destructive [17], where the methods are harmless on the specimen under examination and no PD characteristics are disturbed. In detecting and recording PD signals, various systems are designed and developed in monitoring a discharge or a failure in the insulation [34]. Four popular detection methods, namely electrical detection, chemical detection, acoustic detection and optical detection, are introduced in this section.

2.8.1 Electrical Detection

Electrical detection is the method through which the short current impulse (can be as short as 10 nanoseconds) induced in discharge through the defect can be recorded [26, 75, 83]. This detection method can be realised via either an externally-placed PD detector and circuit, or internal resonances detection and measurement [83].

The external detection circuit is set based on the IEC 60270 Standard. As the discharge pulse duration is extremely short, and multiple reflections are in association with the pulse propagation, the external circuit cannot collect impulses immediately after discharge. Actually, signals are collected after pluses die away from the capacitor discharge in the circuit [83]. Detecting PD signals via the external circuits is conventional as the circuit is simple and widely used.

PD signals consist of components ranging from zero hertz to megahertz in frequency [83], and resonance is possibly induced in the equipment. Resonance detection and measurement are widely used in gas-insulated substations.

2.8.2 Chemical Detection

PD activities can be detected chemically because of the generation of new products resulting from the chemical reaction involved in partial discharge. Dissolve gas analysis (DGA) and high performance liquid chromatography (HPLC) are two popular methods. The former reflects PD characteristics according to the change in gas volume, and the latter relies on the by-products resulting from the chemical reaction involved in PD activities [82].

However, chemical detection can hardly indicate PD characteristics, such as the defect location and discharge intensity, accurately. Moreover, it is not flexible enough for online detection because of the complicated signal processing work [82].

2.8.3 Acoustic and Optical Detection

Acoustic signals are associated with PD activities. In acoustic PD detection, sensors are placed outside the equipment for testing. The significant advantage of acoustic detection is the elimination of electro-magnetic interference (EMI) disturbance as no electrical elements are involved [82, 84]. One limitation of acoustic detection is that the acoustic wave propagation is complex, and the wave does not travel in perfect spherical wave fronts as the high voltage equipment is generally not homogeneous. Besides, acoustic signals of partial discharge and background noise are collected together, and the denoising work is essential [82, 85].

Optical signal is another signal involved in partial discharge. The method called the direct optical partial

24

discharge detection (DOPDD) is applied in detecting PD signals optically. Similar to the acoustic detection, EMI disturbance is eliminated. In contrast to the acoustic detection, an optical sensor is placed inside the apparatus under test, and the disturbance of the background noise is consequently reduced. The defect location can be accurately determined, and the optical detection is highly sensitive in detecting small signals [82]. Limitations of the technology include the expense of installing the sensor in the equipment, and the optical detection is not applicable for material or equipment that is not transparent [86].

2.9 Partial Discharge Pattern Analysis

With the help of advanced digital processing technique, PD patterns are helpful in identifying PD characteristics, as it is believed that each type of discharge has its unique pattern [20, 26, 87]. PD categories can therefore be distinguished and determined.

2.9.1 Partial Discharge Analysis at AC Voltage

Despite the development of digital analysis of partial discharge [88], PD patterns and characteristics analysis is still a key issue [34]. This issue can be addressed by two methods. First, PD characteristic parameters, such as repetition rate, discharge magnitude and phase angle can be interpreted and analysed from the empirically recorded data to draw conclusions [89–91]. Second, simulation work according to the accepted numerical model can be an effective tool in solving the issue. The value of parameters used should be practical and reasonable [34]. The former method should be more practical as the results are empirical, and several assumptions or simplifications are made in solving the problem via the modelling work. In understanding PD patterns at AC voltage, two analysis methods are widely accepted, namely the phase-resolved partial discharge pattern analysis (PRPD) and pulse-sequence analysis (PSA).

PRPD method

PRPD pattern analysis is a basic and popular method in analysing PD pattern at AC voltage according to the PD stochastic theory [87]. Discharge characteristics involved in the PRPD analysis are the apparent discharge magnitude (q), PD occurrence phase angle (φ), and the discharge pulse number (n) [87]. Descriptive patterns are q$\sim\varphi$, q$\sim$n and $\varphi\sim$n, and they indicate the discharge magnitude at each phase angle, the number of discharge with the same discharge magnitude, and the discharge repetition rate at each phase angle [20].

Two statistical factors are used in expressing the distribution, namely skewness and kurtosis.

$$S_k = \frac{\sum_{i=1}^{N}(X_i - \mu)^3 f(X_i)}{\sigma^3 \sum_{i=1}^{N} f(X_i)} \tag{2.25}$$

$$K_u = \frac{\sum_{i=1}^{N}(X_i - \mu)^4 f(X_i)}{\sigma^4 \sum_{i=1}^{N} f(X_i)} - 3 \tag{2.26}$$

where N is the number of discharge activities, and $f(X_i)$ is the discharge magnitude. μ is the average discharge magnitude, and σ is the discharge variance. These two factors are expressed as

$$\mu = \frac{\sum_{i=1}^{N} f(X_i) X_i}{\sum_{i=1}^{N} f(X_i)} \tag{2.27}$$

$$\sigma = \sqrt{\frac{\sum_{i=1}^{N}(X_i - \mu)^2 f(X_i)}{\sum_{i=1}^{N} f(X_i)}} \tag{2.28}$$

Skewness and kurtosis are gained via comparing the practical PRPD data with the normal distribution: S_k equals zero for symmetric distribution, is positive for asymmetric distribution to the left, and is negative for asymmetric distribution to the right; K_u equals zero if the practical distribution has the same sharpness as the reference, and the sharpness increases the kurtosis value [20].

Typical PRPD patterns of cavity discharge, surface discharge and corona are given in Fig. 2.7. For cavity discharge, the PRPD pattern is nearly symmetric if the cavity is located in the middle of the insulation. Phase variation occurs due to the field polarity reversal. Many more discharges are detected in the negative half cycle than those at a positive half cycle in surface discharge and corona. The reason is that they both occur when the local electric field exceeds the breakdown strength of air, and air is ionised near the electrode. Many more electrons can be involved in the discharge activity from the electrode in the negative half cycle than the positive charge carriers involved in the positive one [92]. Corona is more concentrated in the phase angle of the PRPD pattern.

Advantages exist in PRPD pattern analysis. It is reliable in analysing the pattern of different types of partial discharge at AC voltage. Moreover, data applied to PRPD analysis may be gained from the laboratory, and this pattern method is applicable to the engineering work as well [34]. However, discharge sequence is hardly reflected in this method.
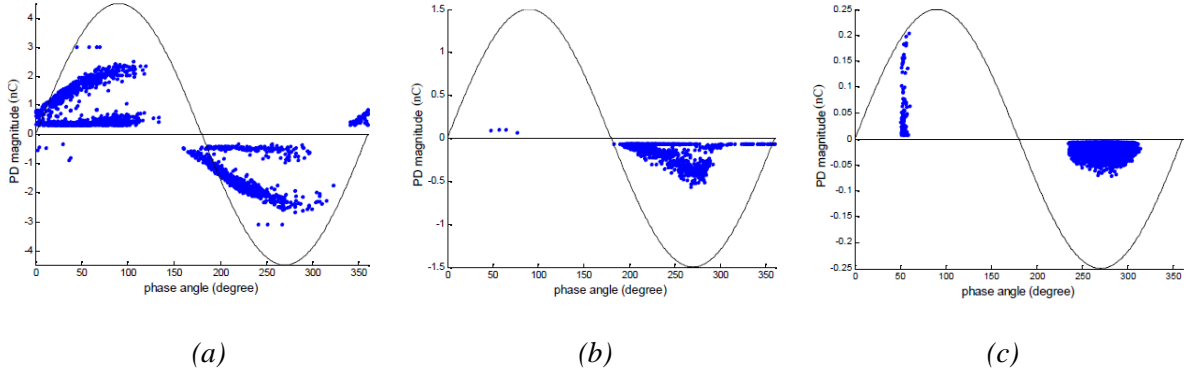
Fig. 2.7. PRPD q~φ patterns of (a) cavity discharge (24kV), (b) surface discharge (6kV), and (c) corona (14kV) [92].

PSA method

In 1993, the PSA method was published in [75, 93, 94], and the detail of pulse-pulse correlations were discussed in detail in [95–98]. It was revealed that there is a specific sequence between two consecutive events. The reason can be that the 'Memory Effect' that the charges left from the previous discharge can possibly influence the occurrence of the following event. PSA technique reveals the PD occurrence sequence and reflects the correlation between two consecutive events [75, 92]. The waveform of electric field with partial discharge is illusrtrated in Fig. 2.8. ΔU_n and ΔU_{n-1} represents the external voltage difference between the recent discharge and the following one, and the external voltage difference between the recent discharge and the previous one respectively. Δt_n and Δt_{n-1} represents the time interval between the recent discharge and the following one, and the time interval between the recent discharge and the previous one respectively.
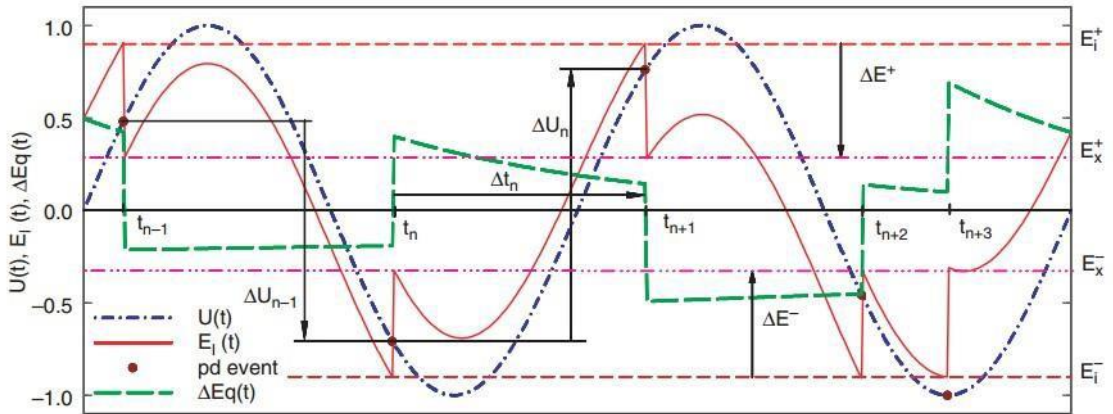
Fig. 2.8. Partial discharge pulse sequences analysis and electric field variation situation with PD consideration [75].

Typical PSA patterns of cavity discharge, surface discharge and corona are given in Figs 2.9 and 2.10. High voltage expands the PSA voltage difference pattern. The rise in field strength is faster under higher voltage. The PSA time difference pattern is concentrated. The lag time of each event is not long, and a

longer lag time of the last event can possibly reduce the lag time of the next discharge due to more charge for the starting electron generation.

PSA helps enrich knowledge of the discharge sequence. In Fig. 2.9 (c), the pattern in the middle of the figure, for example, means that no voltage polarity reversal appears in the period between the recent discharge and the previous one, and the recent discharge and the following one: both voltage difference value, namely ΔU_n and ΔU_{n-1}, are positively low. For other three parts, either the ΔU_n or ΔU_{n-1} is with high absolute magnitude (as high as 20kV), and it means voltage polarity reversal happens. However, stochastic parameters, such as discharge magnitude and repetition rate, cannot be reflected from the method.
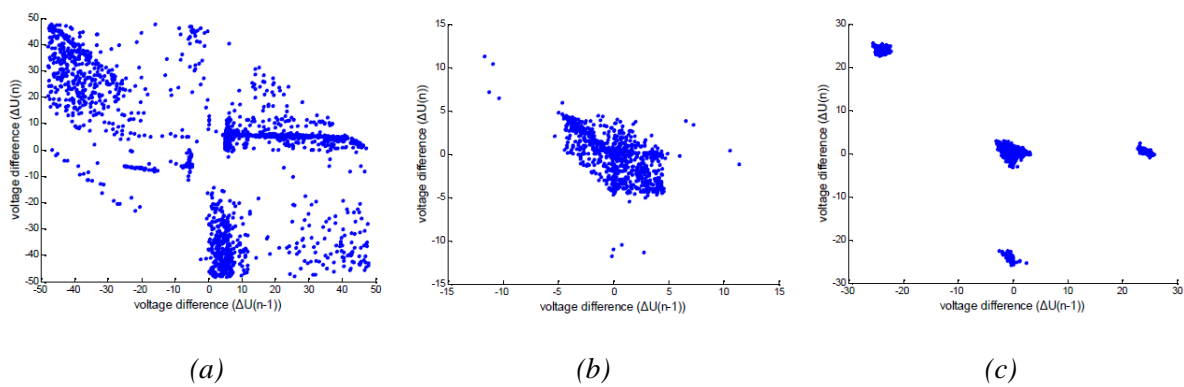
Fig. 2.9. PSA voltage difference patterns of (a) cavity discharge (24kV), (b) surface discharge (6kV), and (c) corona (14kV) [92].
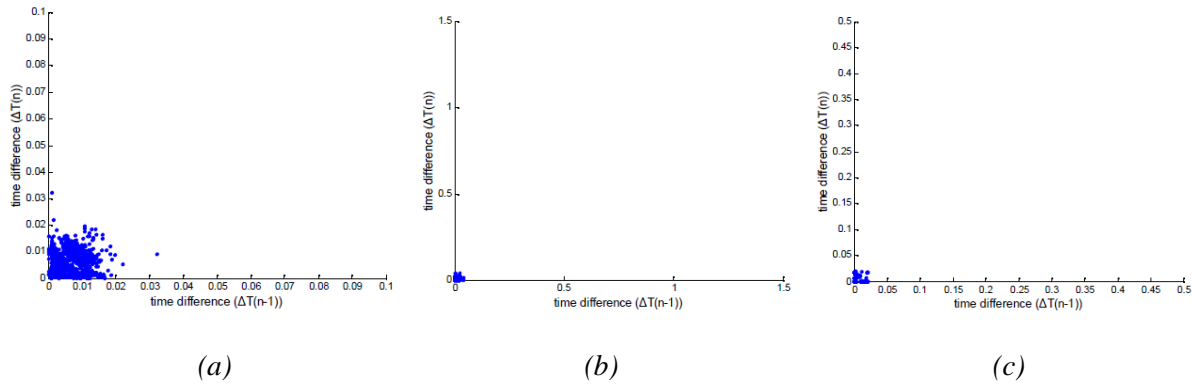
Fig. 2.10. PSA time difference patterns of (a) cavity discharge (24kV), (b) surface discharge (6kV), and (c) corona (14kV) [92].

2.9.2 Partial Discharge Analysis at DC Voltage

The method in which DC PD is studied is different from those popular in AC analysis. PRPD is not available as the term 'phase angle' is meaningless at DC voltage. PSA is not applicable due to the constant applied voltage. ΔU always equals zero. Therefore, exploring a reasonable method of analysing

DC PD is necessary.

There are two important parameters in DC PD analysis, namely the discharge occurrence time (t) and the discharge magnitude (q) [99]. Two partial discharge patterns are analysed in time-resolved partial discharge analysis, being the discharge magnitude to the occurrence time [q(t)] and PD occurrence probability density to discharge magnitude [H(q)]. Fig. 2.11 graphically show the typical time-resolved PD pattern at DC voltage. Considering the influence of voltage magnitude on PD characteristics, the relationship between PD properties and voltage magnitude is studied in [21].
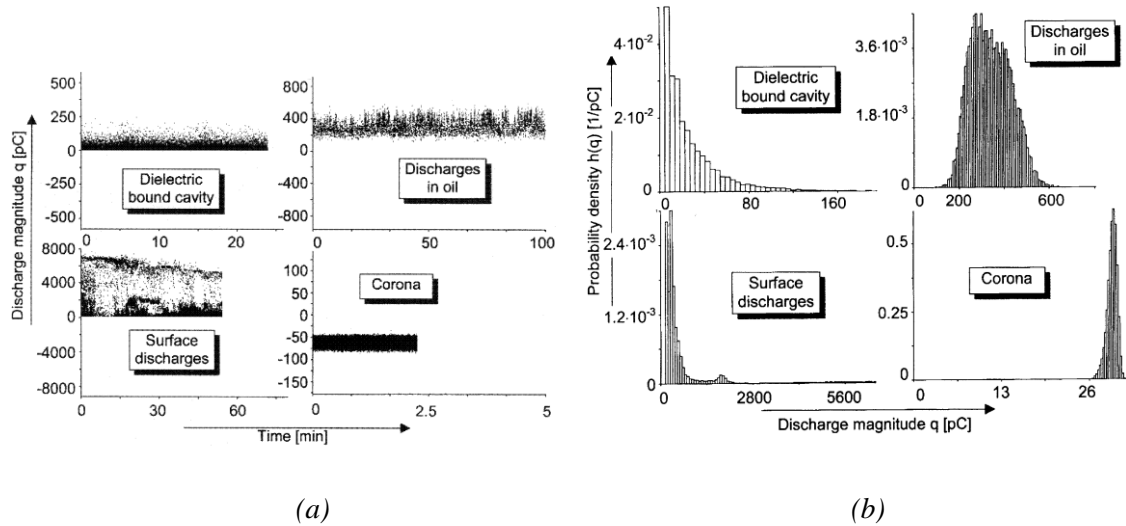
Fig. 2.11. Time-resolved PD analysis (a) $q(t)$ function, and (b) $H(q)$ function [21].

q(t) is most commonly used in describing DC PD characteristics. The discharge repletion rate, time interval between two events, and some other stochastic parameters can be calculated. H(q) relates to the total magnitude of PD, and it reflects the negative effect of discharge on the insulation. Researchers [21, 100] studied and stated that 'Memory Effect' in cavity discharge at DC is low because of the lengthy time interval between two activities: the following activity is relatively independent of the previous one.

2.10 Summary

The amount of charge can possibly change in four processes, namely collision ionisation, photonionisation, attachment and detachment. There are four types of discharge: corona, surface discharge, cavity discharge and electric tree. Cavity discharge can occur in polyethylene in two processes. The first one is across manufacture or fabrication work. The second one is across the operation when the injected electrons have an energy level high enough to vaporise the Van der Waal bond. Submicrocavities appear first, and they tend to coalesce to form the microcavities, which are destructive to the insulation and finally result in insulation failure.

The random cavity discharge activities happen under the conditions that the cavity field exceeds the inception value, starting electrons are available in triggering the electron avalanche, and the ionisation coefficient is higher than the attachment coefficient value.

Cavity field vector is the sum of vectors induced by the external applied voltage and the vector induced by charge on the cavity surface. Discharge happens at the occurrence field strength which is stronger than the inception level due to waiting for starting electron generation, and the event drops the cavity field to the residual level. The charge induced in the activity or the discharge magnitude is determined by the field collapsed across the event.

There are two important phenomena associated with PD at AC voltage which are different from PD at DC voltage. The first one is the field polarity reversal of the applied voltage. It increases the complexity of the field induced by charge on the cavity surface, and leads the first event after the polarity reversal to happen at a lower applied voltage. Phase shift therefore can be detected. The second phenomenon is the charge decay process. Charge recombination due to charge propagation on the cavity wall is the main source, and the decrease in the absolute charge field is mainly due to the decrease in the charge amount.

At DC voltage, charge decay occurs mainly due to the phenomenon of charge migration into the insulation bulk. The total amount of charge slightly changes. The absolute magnitude of field induced by charges in the insulation bulk drops due to the increase in the distance from the cavity centre. The discharge repetition rate at DC voltage is much lower due to the constant applied voltage or field and the slow charge decay depending on the bulk conductivity.

At AC voltage, discharge characteristics, including the discharge repetition rate and discharge magnitude, are influenced by the magnitude of the applied voltage, cavity conditions and the insulation properties. Partial discharge can be detected by four methods: electrical detection, chemical detection, acoustic detection and optical detection. Electrical detection is the most popular method in measuring short current impulse from the discharge via the external circuit.

At AC voltage, the discharge pattern can be analysed in PRPD or PSA method. Stochastic parameters can be reflected and calculated from the PRPD pattern analysis, while the PSA analysis indicates the sequence of discharge and the 'Memory Effect' of the previous event on the following one. At DC voltage, time-resolved partial discharge analysis is used, and the relationship between discharge magnitude and time is indicated.

The electric field is distorted by the presence of a cavity due to its effect on the electric field lines distribution. In the air-filled cavity, the electric field seems to be uniformly distributed. In the region surrounding the cavity, the electric field tends to be enhanced in one part of the region and reduced in

the remaining part. Field enhancement in the region surrounding the cavity can accelerate the degradation and tends to change the cavity shape.

The contribution to the project starts from the following chapter: equations describing the critical temperature difference for field reversal occurrence, and temperature and electric field distribution across the inslation are derived and proposed, 2D and 3D models are compared to provide the reference for model selection, field enhancement inside the cavity, and field distortion in the region surrounding the cavity are researched, and a preliminary modelling work on partial discharge in HVDC polymeric cable applied with the constant voltage is studied.

Chapter 3. HVDC XLPE Cable Analysis at Steady State

In this chapter, the HVDC cable is analysed at the steady state. Equations describing electric field and temperature distribution across the insulation at DC steady state are derived and proposed. Referring to the equation describing field enhancement by a single air-filled cavity at AC voltage, a speculation is stated to describe the same condition at DC steady state. Field distortion by the cavity in the surrounding region is studied in the project, and the method through which data are extracted from the FEA in understanding the conditions across the insulation and at or surrounding the cavity is introduced in this chapter. In the final section of this chapter, the value setting of the parameters in the simulation work is listed.

3.1 Equations Derivation

In this part, equations describing the critical temperature difference for field reversal occurrence and temperature and electric field distribution across the insulation at DC steady state are derived. Prior to the equation derivation, assumptions are introduced.

3.1.1 Equation Derivation Assumption

First, it is assumed that temperature at the outermost insulation layer is constant. It is practical to the HVDC submarine cable: the cable is buried under the seabed, and the soil temperature is constant. In understanding the effect of temperature on the electric field across the insulation or at the cavity, temperature difference across the insulation is manually set in indicating the value of the conductor. Second, electrical conductivity of the dielectric is a field- and temperature-dependent factor in the HVDC cable [101]. Third, the analysis given in this chapter concentrates on the HVDC cable at steady state, and the transition process is not considered, as well as the discharge occurrence inside the cavity. To understand PD characteristics in HVDC cables, the cable is mainly at steady state, and results obtained in this part can help understand the mechanism behind the discharge.

3.1.2 Equation Derivation Processes

The part of cable selected for analysis is graphically given in Fig. 3.1. The central angle θ is extremely small, and the distance between the two points (X_1 and X_2) selected for analysis is extremely short. Therefore, it can be believed that the leakage current flowing through the part at DC steady state is all in the direction parallel to the line crossing these two points.
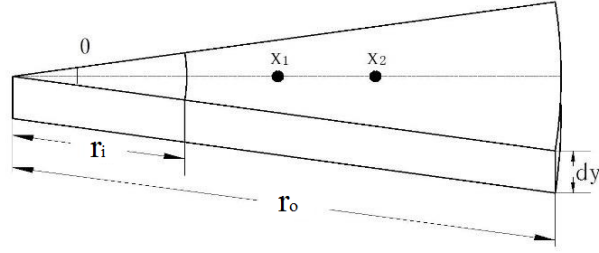
Fig. 3.1. Part of cable selected for analysis.

Under the condition,

$$I_1 = I_2 \tag{3.1}$$

$$I = J * S \tag{3.2}$$

where I_1 and I_2 represent the leakage current through the point X_1 and X_2 respectively, J represents the current density, and S is the area through which current flows.

$$J = E \cdot \sigma \tag{3.3}$$

$$S = \theta \cdot x \cdot dy \tag{3.4}$$

The electrical conductivity of XLPE at DC voltage is expressed as [102]

$$\sigma(E, T) = A\exp(\frac{-\varphi q}{k_b T})\frac{\sinh(B|E|)}{E} \tag{3.5}$$

where A and B are constants in the units of $A.\,m^{-2}$ and $m.\,V^{-1}$, φ is the thermal activation energy in eV, and q is the elementary charge. T is the local temperature (K) and E is the field strength ($V.\,m^{-1}$). x is the distance from the cable centre, and dy is the thickness of the selected cable part.

Merge Equations (3.3) to (3.5) into Equation (3.3),

$$A\exp\left(\frac{-\varphi q}{k_b T}\right) \sinh(B|E|)\, x = k \; (r_i \le x \le r_o) \tag{3.6}$$

where r_i and r_o represent the inner radius and the outer radius of the insulation layer. Equation (3.6) indicates that the product value of the electric field strength, DC electrical conductivity and the distance of the analysed point from the cable centre is a constant at DC steady state with the given applied voltage and temperature difference level. The expression is applicable for any location at the insulation.

At the initial stage when the cable is put into operation, the electric field strength at the insulation layer closer to the cable centre is higher. A phenomenon defined as field reversal can possibly happen, and

34

the region further away from the conductor will have stronger stress. It is different from the field polarity reversal stated in Chapter 2 where the polarity of the applied voltage varies. The reason is that the electrical conductivity which determines the electric field distribution at DC steady state is determined by the local temperature and the electric field strength [101].

A critical condition is that the field stress at the innermost insulation layer E_i equals the level at the outermost layer E_o. Equation (3.6) is therefore rewritten as

$$A\exp\left(\frac{-\varphi q}{k_b T_i}\right)\sinh(B|E_i|)\, r_i = A\exp\left(\frac{-\varphi q}{k_b T_o}\right)\sinh(B|E_o|)\, r_o \tag{3.7}$$

as the equation is available for any location of the insulation layer. The temperature difference across the HVDC cable ΔT and the field difference across the insulation ΔE are defined as

$$\Delta T = T_i - T_o \tag{3.8}$$

$$\Delta E = E_i - E_o \tag{3.9}$$

where i and o in the script represent the innermost and outermost layer respectively. The critical condition occurs when $E_i = E_o$. Merging Equations (3.8) and (3.9) into Equation (3.7), Equation (3.7) is developed as

$$-\frac{\varphi q}{k_b T_i} + \ln r_i = -\frac{\varphi q}{k_b T_o} + \ln r_o \tag{3.10}$$

$$M = \frac{\varphi q}{k_b} \tag{3.11}$$

$$\Delta T_{cri} = T_i - T_o = \frac{T_o^2 \ln(r_o/r_i)}{M - T_o \ln(r_o/r_i)} \tag{3.12}$$

where M is a factor used for simplification. Therefore, the critical temperature difference level for field reversal occurrence is determined by the radius ratio of the outermost layer to the innermost layer, the outermost layer temperature and the material properties.

An interesting and important phenomenon is that even though field reversal can possibly happen, the electric field strength in the middle of the insulation is more or less constant [103, 104]. Under the special condition that electric field reversal is about to happen ($\Delta T = \Delta T_{cri}$), the electric field distribution is uniform across the HVDC cable insulation at the steady state.

$$\int_{r_i}^{r_o} E\,dx = E_c(r_o - r_i) \tag{3.13}$$

$$E_c = \frac{V}{R_o - R_i} \tag{3.14}$$

E_c is the stress in the middle of insulation under this specific condition. V is the level of the external applied voltage on the HVDC cable. To obtain the temperature distribution across the insulation at DC steady state, the temperature in the middle of the insulation is analysed first. Replace the temperature at the innermost layer and the associated distance from the cable centre in Equation (3.10) with the temperature in the middle of the insulation and the corresponding distance to the cable centre,

$$-\frac{\varphi q}{k_b T_c} + \ln r_m = -\frac{\varphi q}{k_b T_o} + \ln r_o \tag{3.15}$$

$$T_c = \frac{1}{\dfrac{1}{T_o} - \dfrac{\ln r_o - \ln r_m}{M}} \tag{3.16}$$

where T_c is the temperature in the middle of the insulation r_m. To propose a general temperature distribution equation, Equation (3.16) is rewritten as

$$T_x = \frac{1}{\dfrac{1}{T_o} - f\dfrac{\ln r_o - \ln r_x}{M}} \tag{3.17}$$

where T_x is the temperature at r_x ($r_i \leq r_x \leq r_o$), and f is a modification factor. When r_x is set to equal r_i,

$$T_i = \frac{1}{\dfrac{1}{T_o} - f\dfrac{\ln r_o - \ln r_i}{M}} \tag{3.18}$$

$$f = \frac{M\Delta T}{T_i T_o (\ln r_o - \ln r_i)} \tag{3.19}$$

Therefore,

$$T_x = \frac{T_o * (T_o + \Delta T)}{T_o + \Delta T * \dfrac{\ln r_x - \ln r_i}{\ln r_o - \ln r_i}} \tag{3.20}$$

The temperature distribution at DC steady state is determined by the outermost layer temperature, temperature difference across the cable, cable geometry and the distance from the cable centre. It seems that material properties do have little influence on temperature distribution across HVDC cables at steady state.

It has been proposed in some previous research that for the isotropic material, temperature distribution across the insulation at DC steady state can be derived from the thermal Ohm's law, as [34, 35]

$$T_x = T_o + \Delta T * \frac{\ln r_o - \ln r_x}{\ln r_o - \ln r_i} \tag{3.21}$$

Having known the temperature distribution expression, Equation (3.6) is developed to be

$$k = A \exp\left(\frac{-\varphi q}{k_b T_c}\right) \sinh(B|E_c|) \, r_m \tag{3.22}$$

in the middle of the insulation. The temperature in the middle of the insulation can be calculated according to Equation (3.16). When a DC voltage with constant magnitude and polarity is applied on the HVDC cable, the k value varies with the temperature in the middle of the insulation (T_c) and the material properties (φ).

It is stated in [103] that the electric field distribution can be calculated via the Gauss-Seidel iterative method. Under the known value of T_o and ΔT,

$$A \exp\left(\frac{-\varphi q}{k_b T_x}\right) \sinh(B|E_x|) \, r_x = k \tag{3.23}$$

$$P = \ln \frac{2k}{A r_x} + \frac{M}{T_x} \tag{3.24}$$

$$E_x = \frac{1}{B} \ln \frac{\exp(P) + \sqrt{\exp(2P) + 4}}{2} \tag{3.25}$$

Similar to M in Equation (3.11), the factor P in Equation (3.24) is defined for simplification. The electric field stress at any position on the insulation layer can be calculated via solving Equation (3.25).

In summary, due to the constant leakage current at DC steady state at the given voltage and temperature difference level, the product value of the local electric field strength, electrical conductivity and the distance from the cable centre is a constant for any location at the insulation layer. Proposed and derived equations indicate the calculation of the value, the critical temperature difference level for field reversal occurrence, and temperature and electric field distribution across the insulation without cavity presence.

3.2 The Comparison in Equation Derivation via Different Conductivity Expressions

In Section 3.1, the equations were derived under the condition that the electrical conductivity of XLPE at DC voltage is expressed as Equation (3.5). In describing the dependence of electrical conductivity on

the electric field and temperature, there is another expression as [103]

$$\sigma(E, T) = \sigma_0 \exp[\alpha(T - T_{ref}) + \beta(E - E_{ref})] \tag{3.26}$$

where σ_0 is the empirical value of material electrical conductivity when the measuring temperature is T_{ref} and the measuring field level is E_{ref}. α and β are the temperature and field coefficients in the unit of K^{-1} and $m.V^{-1}$ respectively. The equation and parameter value given in [103] are for the condition when $T_{ref} = 273.15K$ and $E_{ref} = 0V.m^{-1}$

Equation (3.26) is widely accepted in describing the electrical conductivity of the mass-impregnated cable at DC voltage, and it is applicable for XLPE cable under the specific temperature conditions [103, 105]. If electrical conductivity is described via Equation (3.26), and the basic theory (continuity of the leakage current through the insulation layer under steady state) and equation deviation processes are the same as that in Section 3.1, the proposed equations can now be presented as

$$\Delta T_{cri} = \frac{\ln(r_o/r_i)}{\alpha} \tag{3.27}$$

$$T_x = T_o + \Delta T * \frac{\ln r_o - \ln r_x}{\ln r_o - \ln r_i} \tag{3.28}$$

$$k = \frac{U(R_o + R_i)}{2(R_o - R_i)} \sigma_0 \exp(\alpha T_c + \beta E_c) \tag{3.29}$$

$$E_x \exp(\alpha T_x + \beta E_x) = \frac{k}{\sigma_0 r_x} \tag{3.30}$$

$$W = \ln \frac{k}{\sigma_0 r_x} - \alpha T_x \tag{3.31}$$

$$E_x + \beta \ln E_x = W \tag{3.32}$$

The factor W in Equation (3.31) is defined as well for simplification. Field distribution at steady state can be obtained from Equation (3.32) via the simulation method as the equation can hardly be solved via the traditional method.

Even though it is stated that Equations (3.26) and (3.5) can describe the characteristics of XLPE under some specific conditions [103, 105] in a somewhat similar manner, they cannot be exactly similar to each other precisely due to different forms in relationship to field and temperature. Consequently, the field or temperature calculated from them are probably different. In the next chapter, FEA is used to understand the suitability of Equations (3.27) to (3.32). Results obtained based on Equation (3.5) are to be compared with those obtained based on Equation (3.26) to see whether these two equations can be

replaced by each other in reflecting the electric field distribution across the insulation in HVDC cable at steady state under the specific thermal conditions.

3.3 Field Enhancement Percentage under DC Voltage

The presence of an air-filled cavity, regardless of its shape, size, location or number of cavities, can distort the local field distribution, and enhance the field to a level destructive to the insulation. Electric field is capacitively graded at AC voltage, and the capacitance or permittivity value is important in determining the field enhancement level. The field enhancement at AC voltage η_{AC} is expressed as [49]

$$\eta_{AC} = \frac{K\varepsilon_0\varepsilon_r}{\varepsilon_0 + (K-1)\varepsilon_0\varepsilon_r} \tag{3.33}$$

where ε_r and ε_0 are the relative permittivity of the surrounding dielectric and the vacuum permittivity value. K is a coefficient with the value determined by the cavity shape [47]. According to the equation, η_{AC} is related to the material type and the cavity shape, but is hardly dependent to the cavity size, location, or temperature distribution.

At DC steady state, the electric field is resistively graded, and electrical conductivity is important in determining field distribution instead of the permittivity. It is speculated and expected that the field enhancement by a single air-filled cavity at DC steady state can be expressed as [106]

$$\eta_{DC} = \frac{K\sigma_{XLPE}}{\sigma_{air} + (K-1)\sigma_{XLPE}} \tag{3.34}$$

where only the permittivity value (ε_0 for air and $\varepsilon_0\varepsilon_r$ for XLPE) in Equation (3.33) is replaced by the corresponding electrical conductivity value. σ_{XLPE} is the electrical conductivity of XLPE, and σ_{air} is the conductivity of air inside the cavity.

The calculation of η_{DC} should be more complex than the η_{AC} calculation. The relative permittivity value is regarded to be constant at the mains frequency. The electrical conductivity of XLPE at DC voltage is determined by the local electric field strength and temperature [as expressed in Equation (3.5) or Equation (3.26)]. Electrical conductivity can possibly vary with cavity location under a given temperature difference, or differ with the loading level or temperature difference even if the cavity location does not change. In the next chapter, FEA is used to understand the suitability of this speculation, taking the effect of cavity size, location, shape, temperature gradient across the insulation, and material properties into consideration.

3.4 2D and 3D Model Comparison

The mechanism behind the field distortion by the cavity presence is the variation in electric field line distribution, especially at the cavity. The local field is physically determined by the density of local electric field lines. The electric field strength is stronger when the electric field line density is more intensive.

The effect of the cavity on the electric field line distribution at the cavity at DC steady state is illustrated in Fig. 3.2. Electric field lines tend to distribute along the cable radius when there is no cavity present in the insulation. The appearance of a cavity distorts the distribution in the region, and it turns from flowing through the cable radius to surrounding the cavity. At AC voltage, the reason can be the difference in relative permittivity value inside and outside the cavity. At DC steady state, it is due to the difference in electrical conductivity.

(a)   *(b)*
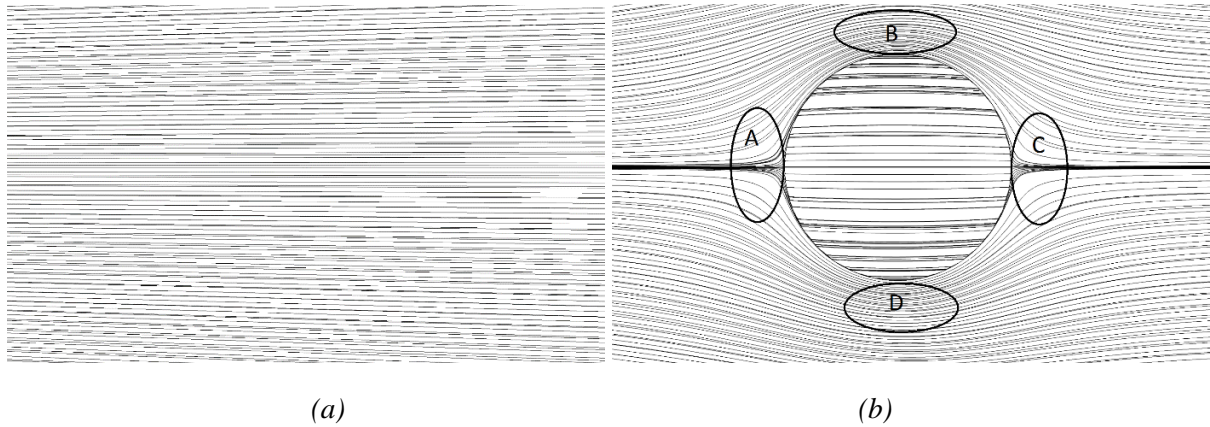
Fig. 3.2. Electric field lines distribution at the cavity (a) before cavity presence, and (b) with cavity presence.

Distortion on electric field lines density results in local field variation and therefore the field enhancement at or in the region close to the cavity. In Fig. 3.2 (b), the density of electric field lines in region A and C decrease because few lines can possibly enter into the region. On the contrary, the density becomes more intense in regions B and D. Field strength therefore is enhanced in regions B and D, while the field reduction phenomenon happens in A and C. Field enhancement happens inside the air-filled cavity at AC or DC voltage, and electric field line becomes more intensive. Electric field lines seem to be parallel in the cavity, which shows understand that the field inside the cavity is more or less uniform.

Field enhancement can accelerate the insulation degradation, and it has a negative effect on the insulation. Besides, the spherical cavity tends to be ellipsoidal due to the ease in breaking the Van der Waals bonds. The cavity size tends to be larger in the region with a stronger field strength [66, 67], and therefore a spherical cavity tends to be ellipsoidal.

To reduce the simulation time, the 2D model was used in several published papers [12, 13]. However, the 2D model has a physical weakness – a single spherical cavity described in this model is actually a cylindrical one in practice. The reason is that the model length is not considered in the 2D model. Therefore, the electric field line distribution, or therefore electric field distortion, calculated from this model cannot be precisely agree with the real condition.

The advantage of the 3D model over the 2D model is that the geometry of the cable and the cavity presented in cable insulation can be practically described. The cavity size, location, and shape can be accurately and practically reflected in the 3D model. The only problem with the 3D model is that it takes much longer in calculation as there are many more elements for which the value should be analysed and calculated than those in the 2D model. In the following chapter, simulation results from the 2D and the 3D model are compared, and recommendations on proper model selection are provided.

3.5 Data Selection Methods

In this project, COMSOL is used as the tool-building software and also for solving the model, and MATLAB is the software extracting the expected parameters, including the electric field, electrical conductivity, temperature, and distance from the cable centre, from COMSOL for analysis and data processing. COMSOL is a software package used for solving the model via finite element analysis. Partial differential equation (PDE) solutions are first found, and the solutions are rendered into equivalent ordinary differential equations to be solved via standard techniques, such as the Newton-Raphson iteration method [107, 108]. MATLAB combines the numerical computing environment to the programming language. The software increases the flexibility of research as it is easy to plot data or function, implement algorithms or create graphical user interfaces [107], and results across the insulation or inside the cavity can be analysed more precisely.

To understand the electric field and the temperature distribution across the cable at DC steady state and the field distortion inside or surrounding the cavity, the method through which data were extracted from the 3D model is introduced in this part.

3.5.1 Data Selection for Research on Field Enhancement across the Insulation and inside the Cavity

The 3D model with the cavity presence is illustrated in Fig. 3.3. In studying the condition across the insulation and inside the cavity, for example, electric field strength and temperature distribution, model division is illustrated in Fig. 3.4 (a). Points 'O' and 'C' are the centre of the cable and the cavity. 'A' and 'B' are the two intersection points by the line OC and the insulation layer. 'M' and 'N' are the two intersection points by line OC and the cavity wall. Points with superscript are the mirror points

indicating the conditions without cavity presence. The setting is regarded to be acceptable as the field or temperature distortion by cavity is a local phenomenon.
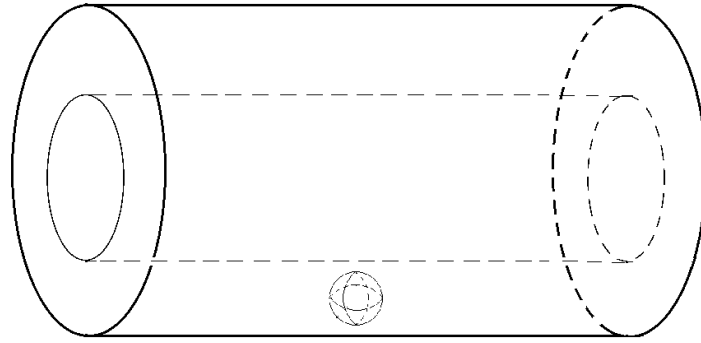
Fig. 3.3. 3D model with the cavity presence.

| (a) | (b) |
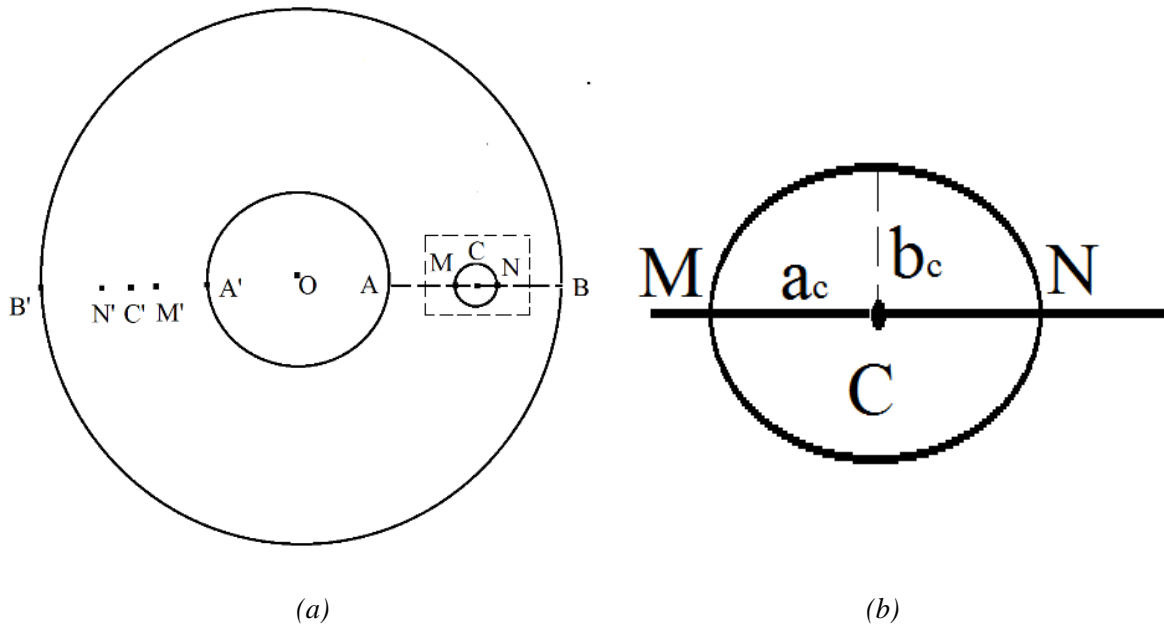
Fig. 3.4. (a) Data selection method in studying field in cavity and across the insulation. (b) Cavity shape indication.

Cavity location is one of the factors considered in the cavity distortion on the local field at DC steady state. The distance of point C from the cable centre is expressed as

$$X = R_i + a(r_o - r_i) \tag{3.35}$$

where a is the distance coefficient: smaller value means that the cavity is closer to the conductor. Although the value varies between 0 and 1, the cavity wall cannot be located outside the insulation when the value of a is set.

The cavity shape is illustrated in Fig. 3.4 (b), which indicates the situation in the region surrounded by the dashed lines in Fig. 3.4 (a). The cavity axis ratio, which is calculated as a_c/b_c, depends on the cavity shape: if the value equals to 1, the cavity is a spherical one. Field enhancement, or distortion, is calculated as

$$\eta = E/E_0 \times 100\% \tag{3.36}$$

where E and E_0 are the average electric field strength of the region with the cavity presence and that on the associated mirror section. To study the field and temperature across the insulation, lines AB and A'B' are uniformly divided into 500 small sections with the same length, and the field stress and temperature value of each element are extracted and processed. To study the magnitude of cavity field, and therefore, field enhancement by the cavity, lines MN and M'N' are uniformly divided into 100 small sections with the same length, and the field stress of each element is extracted and processed. The average cavity field level is calculated via the sum of electric field strength of each section over the number of sections (100).

3.5.2 Data Selection for Research on Field Distortion surrounding the Cavity

In understanding the field distortion in the region surrounding the cavity, the shape of the cavity is spherical and the ellipsoidal one is not considered in the project. The coordinate system of the 3D model is illustrated in Fig. 3.5. The origin 'O' represents the cavity centre. Electric field distribution and field distortion on three planes can be different: the normal line of xy plane is parallel to the cable axis while the line of xz or yz plane is vertical to the cable axis. Elements on the yz plane are almost of the same distance from the cable centre, while those on xy and xz planes vary in the distance from the cable centre. When the distance from the cable centre does not change, the electric field on the yz plane should possibly be similarly enhanced (as shown in Fig. 3.2). Field enhancement and reduction appear on the xy or xz planes.

Fig. 3.6 indicates the method through which data is extracted out for the research in distortion in the region surrounding the cavity at DC steady state. R_c is the cavity radius. b is the radius ratio (b>1), and the location of the point for analysis is together determined by b and angle θ. Therefore, the coordinate setting of points on xy, xz and yz planes is

$$X_{xy} = X + bR_c \cos\theta, Y_{xy} = bR_c \sin\theta, Z_{xy} = 0 \tag{3.37}$$

$$X_{xz} = X + bR_c \cos\theta, Y_{xz} = 0, Z_{xz} = bR_c \sin\theta \tag{3.38}$$

$$X_{yz} = X, Y_{yz} = bR_c \cos\theta, Z_{yz} = bR_c \sin\theta \tag{3.39}$$

X equals the distance of the cavity centre from the cable centre [refer to Equation (3.35)].
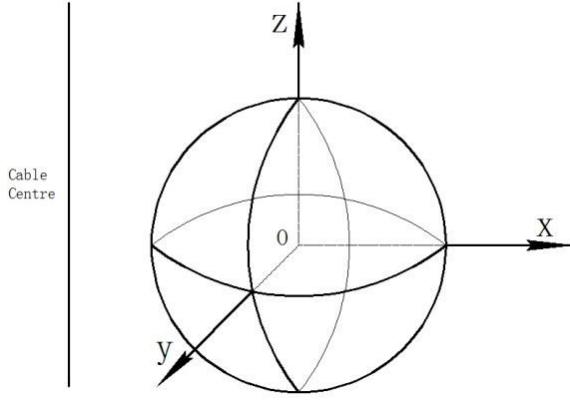
Fig. 3.5. Coordinate system.   *Fig. 3.6. Data selection in example of xy plane.*
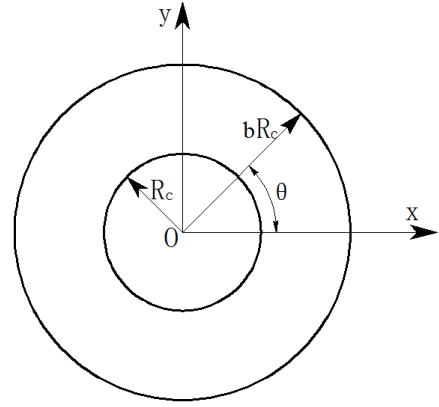
Similar to Equation (3.36), electric field distortion in the region surrounding the cavity is calculated via the electric field in the region surrounding the cavity over its mirror section. If the value is higher than 100%, cavity presence enhances the field at the region; if the value is lower than 100%, the local field is reduced by the cavity presence. If the absolute difference between the distortion percentage and 100% is not higher than 1%, it can be believed in this project that the influence of the cavity is small enough. Cavity distortion is therefore neglected beyond the region.

To indicate the volume of the region possibly distorted by the cavity, the value of b first increases from 1.001 to 5. If the electric field distortion can be small enough to be neglected before b reaches 5, the value is large enough, and the region volume is thus obtained. Otherwise, the value of b keeps increasing further until the entire potentially-distorted region can be explored. θ increases from 0 to $360°$ with a step angle of $2°$.

3.6 Parameter Value Setting

Cable geometry and other parameters used in researching the electric field and temperature distribution across the insulation and electric field inside the air-filled cavity or in the surrounding region are listed in Table. 3.1 [7, 101]. First, values of A, B and φ are determined by material properties, and two value groups are listed in the table describing the fresh and aged material respectively. The qualities are defined according to [102].

Table. 3.1. Parameters used for DC steady state simulation [7, 101-103].

Parameter Name	Value	Unit	Explanation
V	150	kV	Applied voltage
r_i	29.854	mm	Inner insulation radius
r_o	63	mm	Outer insulation radius
R_c	0.5,1,1.5	mm	Cavity radius
L	0.5	m	Cable length
ε_r	2.3		Relative permittivity
σ_{air}	1×10^{-16}	$S.m^{-1}$	Conductivity of air
a	0.25,0.5,0.75		Distance coefficient
T_O	301.15	K	Outer cable temperature
ΔT	3; 7; 12; 20	K	Temperature difference across cable
A	3.2781	$A.m^{-2}$	Constant of fresh material
	3.6782×10^7	$A.m^{-2}$	Constant of aged material
B	2.7756×10^{-7}	$m.V^{-1}$	Constant of fresh material
	1.086×10^{-7}	$m.V^{-1}$	Constant of aged material
φ	0.56	eV	Thermal activation energy of fresh material
	0.98	eV	Thermal activation energy of aged material
σ_0	0.91×10^{-16}	$S.m^{-1}$	Electrical conductivity at 273.15K and 0 $kV.mm^{-1}$
α	0.11	K^{-1}	Temperature coefficient
β	0.24×10^{-6}	$m.V^{-1}$	Electric field coefficient

Second, to draw a better conclusion, the effect of the cavity size, the distance coefficient (a) and the temperature difference is researched via selecting data from the following table. According to Equation (3.12), the critical temperature difference for field reversal occurrence in fresh material at DC steady state is between 10.7 K and 10.8 K. Therefore, field reversal does not happen at $\Delta T = 3K$ and $\Delta T = 7K$, but occurs at the other two difference levels.

Third, the air conductivity is set to be zero without the occurrence of discharge in [109, 110]. However, the setting clears all electrical conductivity parameters in Equation (3.34), and cavity distortion under the DC voltage at steady state consequently tends to only be decided by the cavity shape. In [111], air conductivity can be with a level in the order of 10^{-6} $S.m^{-1}$.

3.7 Summary

In this chapter, based on the theory that the leakage current through the insulation at DC steady state is constant, equations describing the critical temperature difference for field reversal occurrence and the temperature and electric field distribution across the insulation are derived and proposed. The product of the local field, electrical conductivity and distance to the cable centre is almost constant at any location across the insulation under the given voltage and temperature difference. The method in

calculating the product value is provided as well.

Field enhancement by air-filled cavity at AC voltage can be calculated according to a widely accepted equation [Equation (3.33)]. It is speculated that field enhancement at DC voltage can be calculated with a similar equation with the replacement of permittivity value by the corresponding electrical conductivity [Equation (3.34)]. Calculation of electrical conductivity is more complicated than relative permittivity, and cavity shape, location, temperature distribution across the insulation and material properties can influence the enhancement percentage.

Even though the simulation time is much longer, the 3D model has an inherent advantage over the 2D model as the length of the cable and the cavity height are not considered in the 2D model: the spherical cavity built in the 2D model is a cylindrical one in reality. A 3D model can be the solution even though the simulation time may be significantly longer. The data selection method in understanding the electric field and temperature distribution across the cable at DC steady state, and the field distortion inside or surrounding the cavity, the method through which data are extracted from the 3D model were introduced in this part.

In the final section of this chapter, the cable geometry and the value of other key factors were listed. In the following chapters, the suitability of the proposed equations will be proved via the comparison between simulation results and calculation results from the corresponding equations. With the help of FEA, the reference for the model selection, the field enhancement at DC steady state, and the field distortion in the region surrounding the cavity is to be given in the next chapter.

Chapter 4. HVDC XLPE Cable Simulation Results at Steady State

In this chapter, the suitability of the equations proposed in the previous chapter is to be proved via the comparison between results from COMSOL and those from calculation according to the corresponding equation. 2D and 3D models are compared to provide the reference in model selection. Field distortion in the region surrounding a single spherical air-filled cavity is researched in this chapter, and the volume of the region with potential to be distorted is given, with the effect of cavity size and location, temperature difference across the insulation and material properties taken into consideration.

4.1 Model Reliability

It is important to ensure that the results, especially in the electric field distribution, from modelling and simulation work are accurate. In [112], the electric field distribution inside and outside the spherical cavity presented in high voltage cable at AC voltage is expressed as

$$E = E_0 \left(\frac{3\varepsilon_r}{\varepsilon_0 + 2\varepsilon_r}\right)(-(i_r\cos\theta - i_\theta\sin\theta)) \tag{4.1}$$

$$E = E_0(i_r\left(-1 - \left(\frac{\varepsilon_0 - \varepsilon_r}{\varepsilon_0 + 2\varepsilon_r}\right)\frac{2R_c^3}{r^3}\right)\cos\theta + i_\theta\left(1 - \left(\frac{\varepsilon_0 - \varepsilon_r}{\varepsilon_0 + 2\varepsilon_r}\right)\frac{R_c^3}{r^3}\right)\sin\theta) \tag{4.2}$$

respectively. E_0 is the field when no cavity is present, and r is the distance from the cavity centre. i_r and i_θ are the unit vectors of the insulation coordinate system. θ is the angle value which determines the location.

When a 1 mm radius spherical cavity is located in the middle of the insulation (a = 0.5), the comparison between calculation results from Equations (4.1) and (4.2) and those from simulation are illustrated in Figs 4.1 and 4.2. The location ratio in Fig. 4.1 is calculated as the value of r in Equation (4.2) to the cavity radius. Cable geometry and the peak applied voltage are listed in Table. 3.1. Fig. 4.1 indicates the electric field distribution across the cable insulation starting from the cavity centre, and Fig. 4.2 shows the electric field distribution closely surrounding the cavity.

The similarities between calculation and simulation results show that simulation results can be believed to be accurate enough in indicating the results across the insulation and at the cavity. Having proved that simulation results are satisfactorily accurate, situations that are more complicated can be evaluated based on the simulation results.
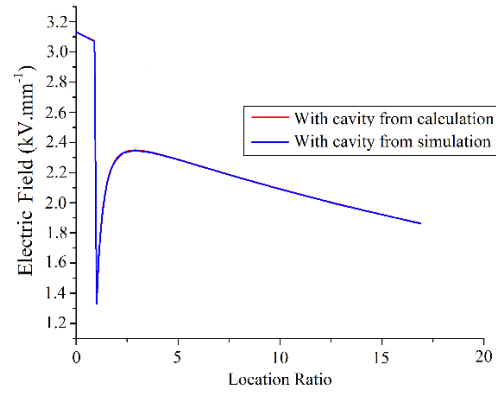
Fig. 4.1. Electric field comparison between calculation and simulation results in field distribution across cable at t=0.002s (1/10 cycle time).

(a)   *(b)*
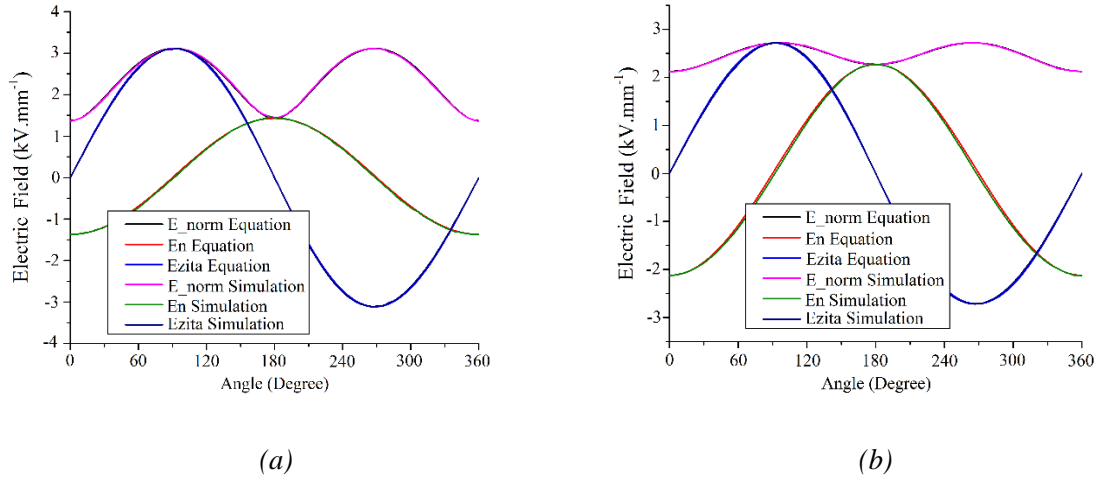
Fig. 4.2. Electric field comparison between calculation and simulation results in field distribution (a) at the cavity surface at t=0.002s (1/10 cycle time, $r = 1.01R_c$), and (b) surrounding the cavity at t=0.002s (1/10 cycle time, $r = 1.5R_c$).

4.2 Reliability of the Proposed Equations

In this section, the reliability of the equations proposed in Chapter 3 is illustrated. As there are two groups of equations describing the electrical conductivity at DC voltage, the reliability of equations describing the critical temperature difference for field reversal occurrence, temperature and electric field distribution and the k value calculation are provided in this section for the two conditions separately. A comparison between the two groups of conductivity equations in the electrical field distribution are illustrated.

4.2.1 Equations Derived from Equation (3.5)

The k value across the cable insulation from the simulation under four temperature levels studied in the project is illustrated in Fig. 4.3. First, the k value across the insulation is fairly uniform at any location across the insulation under a given temperature difference level. The reason is that the leakage current through the insulation at steady state is continuous. Second, the k value increases with the temperature difference value.

(a)   *(b)*
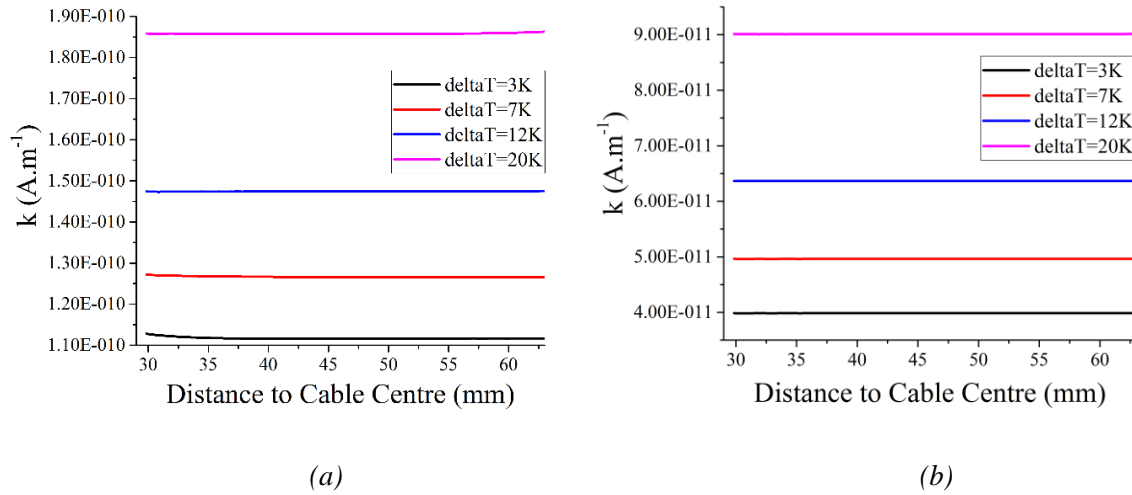
Fig. 4.3. k value across the insulation from simulation under different temperature difference levels in (a) fresh material, and (b) aged material.

It seems that the k value across fresh material insulation at a low temperature difference ($\Delta T = 3K$) is not as stable as that at a high difference level. Error for the k value is listed in Tables 4.1 and 4.2. The average value is calculated as the sum of k value of in each section over the total number of sections (500). The error value is calculated as the difference between the maximum and the minimum value over the maximum value. It is never higher than 1.1% across all the temperature difference levels and material properties studied in this project. The k value across the insulation can be believed to be constant under the given temperature difference level.

Table. 4.1. k value across the fresh material insulation.

ΔT (K)	k value–Max ($A.m^{-1}$)	k value–Min ($A.m^{-1}$)	k value–Average ($A.m^{-1}$)	Error (%)
3	1.13E-10	1.12E-10	1.12E-10	1.07
7	1.27E-10	1.27E-10	1.27E-10	0.46
12	1.48E-10	1.47E-10	1.47E-10	0.13
20	1.86E-10	1.86E-10	1.86E-10	0.28

Table. 4.2. k value across the aged material insulation.

ΔT (K)	k value–Max (A. m^{-1})	k value–Min (A. m^{-1})	k value–Average (A. m^{-1})	Error (%)
3	3.99E-11	3.98E-11	3.99E-11	0.06
7	4.96E-11	4.96E-11	4.97E-11	0.05
12	6.37E-11	6.37E-11	6.37E-11	0.02
20	9.01E-11	9.01E-11	9.01E-11	0.06

The comparison between the simulation results and the results from Equation (3.22) is plotted in Fig. 4.4, and the difference between the simulation and calculation results is listed in Tables 4.3 and 4.4. Errors in Tables 4.3 and 4.4 are calculated as the absolute difference between simulation and calculation results over the simulation value. The line labelled as 'Simulation' is the average k value listed in Tables 4.1 or 4.2: k value across the insulation does not change much, and the average value is taken in the thesis. Fig. 4.4, Table. 4.3 and Table. 4.4 together indicate that the simulation and calculation results match with each other with a low error (never higher than 5%), and it accordingly can be believed that the k value can be calculated according to Equation (3.22). It helps explain the variation of k value with temperature difference: temperature in the middle of the insulation increases with the temperature difference level when the outer temperature is set to be constant.

(a)   (b)
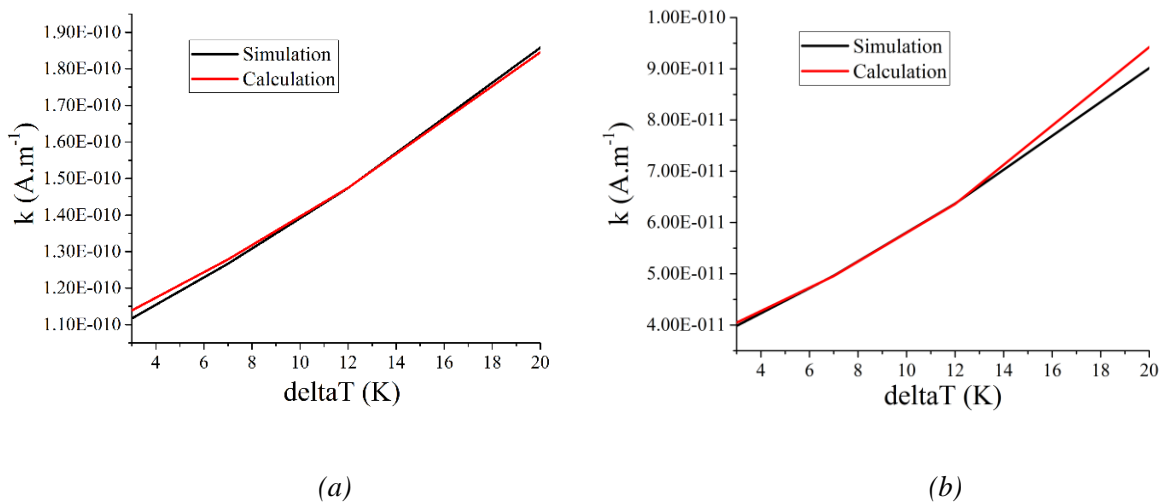
Fig. 4.4. Comparison between simulation and calculation value on k value across the insulation under different temperature difference levels in (a) fresh material, and (b) aged material.

Table. 4.3. Comparison between simulation and calculation results on k value across the fresh material insulation.

ΔT (K)	k value–Simulation(A. m^{-1})	k value–Calculation(A. m^{-1})	Error (%)
3	1.12E-10	1.14E-10	1.93
7	1.27E-10	1.28E-10	0.92
12	1.47E-10	1.47E-10	0.01
20	1.86E-10	1.85E-10	0.69

Table. 4.4. Comparison between simulation and calculation results on k value across the aged material insulation.

ΔT (K)	k value–Simulation($A.m^{-1}$)	k value–Calculation($A.m^{-1}$)	Error (%)
3	3.99E-11	4.05E-11	1.58
7	4.96E-11	4.96E-11	0.15
12	6.37E-11	6.36E-11	0.078
20	9.01E-11	9.42E-11	4.57

Another thing is that the k value from fresh material is higher than that from aged material. It can be explained from the electrical conductivity value. The ratio of electrical conductivity of fresh material to the level of aged material at the same electric field and temperature, η_{cond}, is calculated as

$$\eta_{cond} = \frac{A_{fresh}}{A_{aged}} \exp(\frac{\varphi_{aged} - \varphi_{fresh}}{k_b T} q) \frac{\sinh(B_{fresh}E)}{\sinh(B_{aged}E)} \tag{4.3}$$

It means that when η_{cond} is higher than 1, fresh material has a higher electrical conductivity value. When η_{cond} is lower than 1, aged material has a higher electrical conductivity value.

According to Equation (4.3), the condition where aged material has a higher electrical conductivity value is listed in Table. 4.5. The maximum ΔT value is 62 K, and the insulation with the highest temperature reaches the maximum operation temperature value (363.15 K, 90℃) at this temperature difference value. The location where the electrical conductivity value of fresh material equals to that of aged material is indicated by the value of a. Beyond the values of a listed in the table, the electrical conductivity value of fresh material is higher. The electric field strength E in the table represents the stress at the location when the electrical conductivity values of different materials are equal. The value of E is different in different materials, and it is due to the properties of the material.

To help understand the phenomenon that aged material has a higher electrical conductivity value, the electrical conductivity of fresh and aged material is illustrated in Fig. 4.5. Therefore, the situation that aged material has a higher electrical conductivity value generally occurs in the region closer to the conductor with the occurrence of field reversal. Higher electrical conductivity leads to higher value of k.

Table. 4.5. The condition where electrical conductivity of aged material is higher.

ΔT (K)	E ($kV.mm^{-1}$)		a
	Fresh	Aged	
20	N.A.	N.A.	N.A.
25	3.57	2.10	0.14
30	3.71	2.45	0.24
40	4.14	3.45	0.38
62	5.49	7.41	0.55
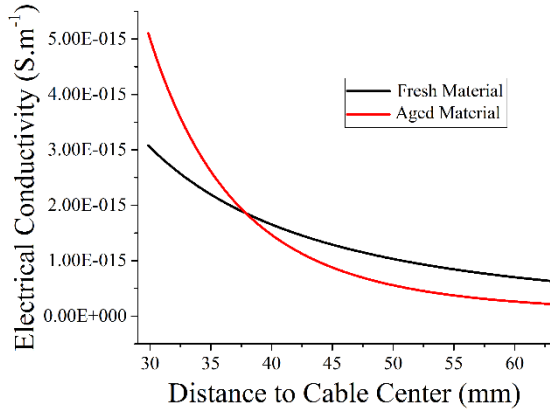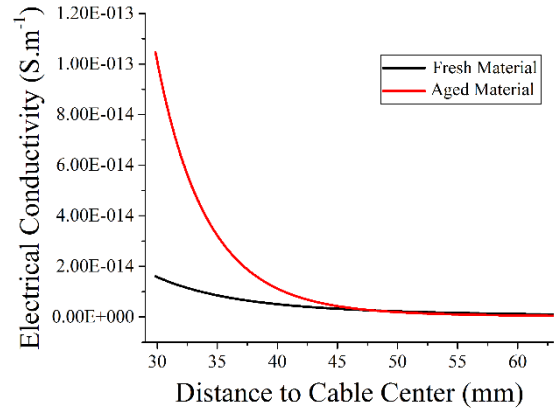
(a)   (b)

Fig. 4.5. Electrical conductivity across different material insulation without cavity when (a) $\Delta T = 30K$, and (b) $\Delta T = 62K$.

The comparison between simulation and calculation results in critical temperature difference for field reversal occurrence at DC steady state is illustrated in Fig. 4.6 and the error is given in Table. 4.6. The error value is calculated as the absolute difference between the simulation and calculation value, and the error percentage is calculated as the error value over the simulation result. It can be seen from the figure and the table that the similarity of simulation results with the calculation results from Equation (3.12) is low in both the error values (never higher than 0.05 K) and error percentage (never higher than 1%). It can therefore be believed that the critical temperature difference for field reversal occurrence can be calculated according to Equation (3.12).
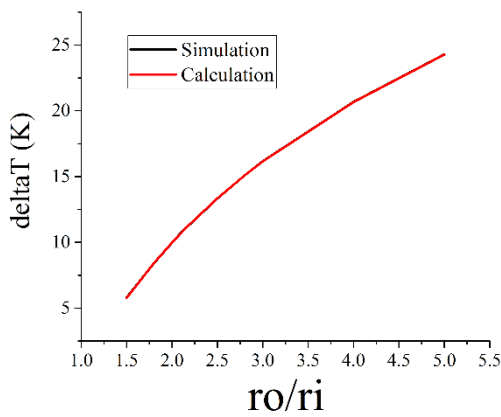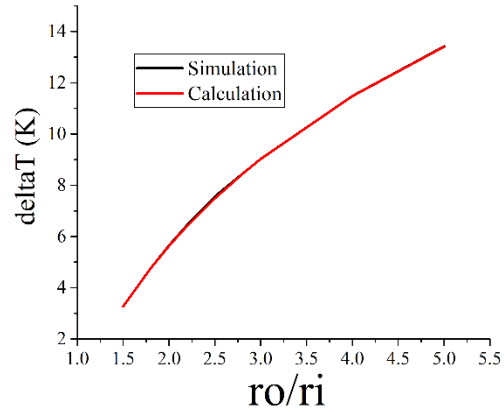
(a)   (b)

Fig. 4.6. Comparison between simulation and calculation value on critical temperature difference for field reversal occurrence in (a) fresh material, and (b) aged material.

52

Table. 4.6. Comparison between simulation and calculation results on critical temperature difference for field reversal ocurrence.

R_o/R_i	ΔT_{cri} simulation fresh (K)	ΔT_{cri} calculation fresh (K)	ΔT_{cri} simulation aged (K)	ΔT_{cri} calculation aged (K)	Error-Fresh		Error-Aged	
					Value (K)	Percentage (%)	Value (K)	Percentage (%)
1.5	5.81	5.77	3.28	3.27	0.04	0.71	0.01	0.28
1.8	8.42	8.43	4.77	4.76	0.01	0.13	0.00	0.08
2	9.97	9.99	5.65	5.63	0.03	0.27	0.02	0.32
2.11	10.84	10.80	6.10	6.08	0.04	0.38	0.03	0.43
2.2	11.40	11.42	6.46	6.42	0.03	0.22	0.04	0.56
2.5	13.34	13.35	7.56	7.49	0.02	0.13	0.07	0.95
2.8	15.09	15.09	8.44	8.44	0.00	0.01	0.00	0.04
3	16.17	16.15	9.03	9.02	0.02	0.12	0.00	0.03
4	20.69	20.68	11.48	11.48	0.01	0.07	0.01	0.06
5	24.29	24.27	13.42	13.41	0.02	0.07	0.01	0.08

Comparison between simulation results and calculation results from Equations (3.20) and (3.21) in describing temperature distribution across the insulation at DC steady state is illustrated in Fig. 4.7, and the error is listed in Table. 4.7. The error value is the absolute difference between simulation and calculation according to the corresponding equation, and the error percentage is the error value over the simulation results. The figure and table together indicate that both of these equations are suitable for calculating the temperature distribution across the insulation due to low error value (never higher than 0.15 K) and low error percentage (never higher than 0.15%). Besides, Equation (3.21) seems to be more precise in describing temperature distribution because of the relatively lower error value and error percentage.
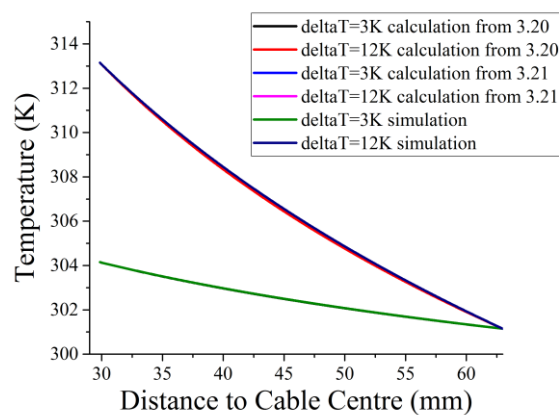
Fig. 4.7. Comparison between simulation and calculation value on temperature distribution across fresh material insulation.

Table. 4.7. Error in temperature distribution across fresh material insulation at DC steady state.

ΔT (K)	Max Error-Equation 3.20		Max Error-Equation 3.21	
	Value (K)	Percentage (%)	Value (K)	Percentage (%)
3	0.01	0.00	1.09E-05	3.59E-08
7	0.04	0.01	2.24E-05	7.28E-08
12	0.12	0.04	3.67E-05	1.18E-07
20	0.32	0.10	5.99E-05	1.88E-07

No material property parameters appear in any of the two equations. Therefore, material properties have little influence over temperature distribution across the insulation at DC steady state. Consequently, the situation in the aged material is not presented in this section, and the conclusion is similar to that of the fresh material.

Field distribution across the insulation without cavity at DC steady state is illustrated in Fig. 4.8, and the error is listed in Table. 4.8. First, field reversal happens at a high temperature difference level: the electric field in the region closer to the conductor is higher at a lower temperature difference value, while the electric field in the region further away from the conductor tends to be higher at a higher temperature difference level. Second, the field in the middle of the insulation tends to be nearly constant with a slight fluctuation. The field level can be calculated according to Equation (3.14). Third, the maximum error between simulation and calculation from Equation (3.25) is acceptably low (never higher than $0.5 \, \mathrm{kV. mm^{-1}}$), while the error percentage can possibly reach a level over 5%. The error can be due to three reasons. In proposing the electric field distribution, the strength in the middle of the insulation is important. It is believed that the electric field strength in the middle of the insulation is constant under the given applied voltage, but the level actually slightly fluctuates. Besides, the accuracy of meshing in FEA can influence simulation results as well. The precise meshing leads to accurate results, but the time for simulation increases greatly. Furthermore, the average field is used in indicating the field inside cavity as the field is regarded to be uniformly distributed. It can possibly raise the error level. As the maximum error value and error percentage are acceptably low, electric field distribution across the insulation at DC steady state can possibly be calculated from Equation (3.25). Among them, the usage of the average field value is the main reason.
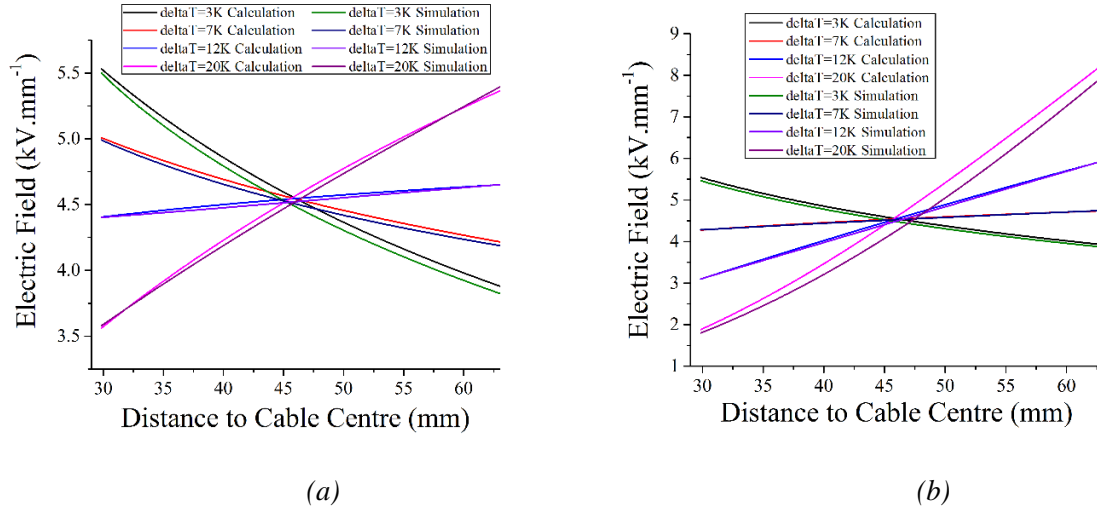
Fig. 4.8. Comparison between simulation and calculation on field distribution across the insulation at DC steady state for (a) fresh material, and (b) aged material.

Table. 4.8. Error in field distribution across the insulation at DC steady state.

ΔT (K)	Max Error-Fresh		Max Error-Aged	
	Value (kV. mm^{-1})	Percentage (%)	Value (kV. mm^{-1})	Percentage (%)
3	0.065	1.46	0.08	1.57
7	0.039	0.85	0.02	0.33
12	0.026	0.57	0.06	1.27
20	0.046	1.04	0.37	8.13

In summary, the suitability of equations derived in Chapter 3.1 when the electrical conductivity of XLPE at DC voltage was described as Equation (3.5) is proved via the comparison between simulation and calculation results. The product value k of electrical conductivity, electric field and distance from the cable centre is almost constant under the given temperature difference and applied voltage level due to the continuous leakage current at DC steady state. Equations describing the calculation of k value, critical temperature difference for field reversal occurrence, and temperature and electric field distribution across the insulation without cavity presence at DC steady state are proved to be with acceptable error values or error percentages. The conclusion is applicable for both fresh and aged material.

4.2.2 Equations Derived from Equation (3.26)

In this part, simulation and calculation results are compared to indicate whether the equations derived are reasonable when the electrical conductivity of XLPE at DC voltage is described as Equation (3.26). The k value and its corresponding error are given in Fig. 4.9 and Table. 4.9. In Table. 4.9, 'Error-simulation' describes the fluctuation in k value from the simulation, and 'Error-calculation' describes the absolute difference between simulation and calculation from Equation (3.29).
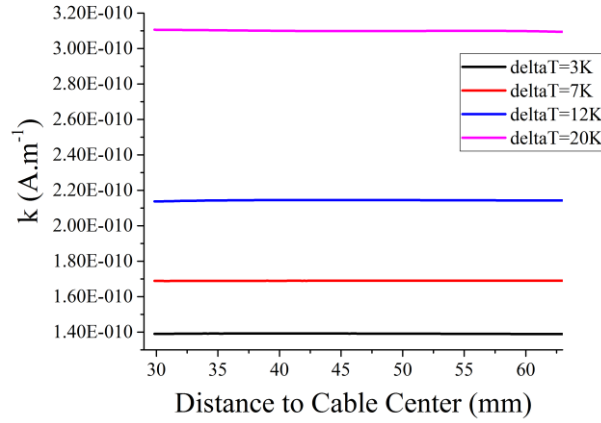
Fig. 4.9. k value across the insulation from simulation under different temperature difference levels.

Table. 4.9. Error in k value across the insulation.

ΔT (K)	k simulation– Max (A. m^{-1})	k simulation– Min (A. m^{-1})	k simulation– Average (A. m^{-1})	k calculation (A. m^{-1})	Error-simulation (%)	Error-calculation (%)
3	1.39E-10	1.39E-10	1.39E-10	1.41E-10	1.07	1.41
7	1.69E-10	1.69E-10	1.69E-10	1.69E-10	0.46	0.07
12	2.15E-10	2.14E-10	2.14E-10	2.11E-10	0.13	1.38
20	3.11E-10	3.09E-10	3.10E-10	3.03E-10	0.28	2.28

Similar to the conclusion drawn in Section 4.2.1, k value can be believed to be constant across the insulation under the given temperature difference and applied voltage, and the value increases with the temperature difference value. Besides, the difference between simulation and calculation value is acceptably low (not higher than 2.3%), and it therefore can be believed that Equation (3.29) is applicable in calculating k value across the insulation at DC steady state.

The comparison between simulation and calculation in the critical temperature difference for field reversal occurrence, k value calculation, and temperature and electric field distribution across the insulation without cavity at DC steady state is given in Fig. 4.10. The error is listed in Tables 4.10 and 4.11. They together indicate that simulation and the corresponding calculation results are similar due to a low error value and a low error percentage (never higher than 1.5%). Therefore, it can be believed that Equations (3.27), (3.28), (3.29) and (3.32) are valid for calculating the critical temperature difference for field reversal occurrence, temperature distribution, k value calculation and electric field distribution at DC steady state when the electrical conductivity of XLPE at DC voltage is expressed by Equation (3.26).
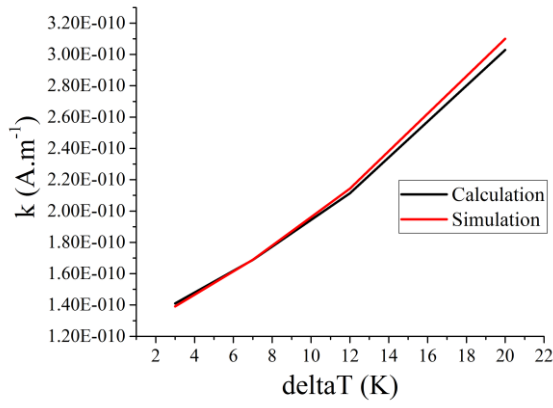
(a)
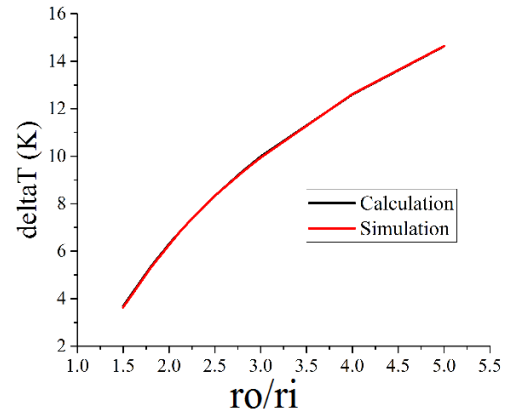
(b)
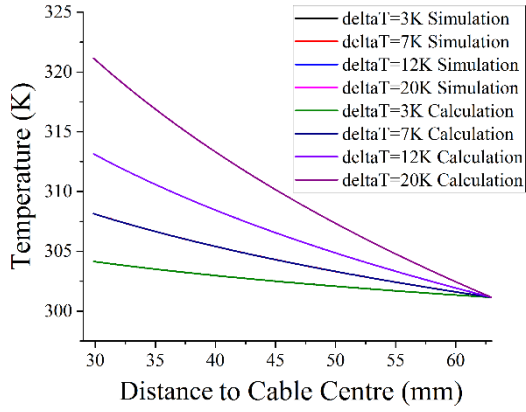
(c)
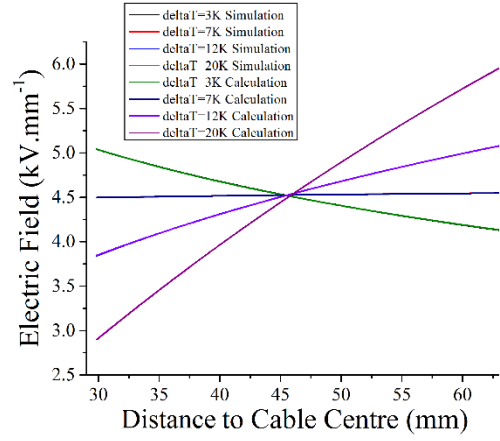
(d)

Fig. 4.10. Comparison between simulation and calculation at DC steady state on (a) k value, (b) critical temperature difference for field reversal, (c) temperature distribution across the insulation without cavity, and (d) field distribution across the insulation without cavity.

Table. 4.10. Comparison between simulation and calculation results on critical temperature for field reversal occurrence.

R_o/R_i	ΔT_{cri} simulation (K)	ΔT_{cri} calculation (K)	Error	
			Value(K)	Percentage (%)
1.5	3.69	3.63	0.05	1.43
1.8	5.34	5.31	0.03	0.65
2	6.30	6.27	0.03	0.55
2.11	6.79	6.78	0.01	0.08
2.2	7.17	7.17	0.00	0.04
2.5	8.33	8.34	0.01	0.11
2.8	9.36	9.33	0.03	0.33
3	9.99	9.94	0.05	0.47
4	12.60	12.62	0.02	0.13
5	14.63	14.64	0.01	0.08

Table. 4.11. Error in temperature and electric field distribution across the insulation at DC steady state.

ΔT (K)	Max Error - Temperature		Max Error - Electric Field	
	Value (K)	Percentage (%)	Value (kV.mm^{-1})	Percentage (%)
3	0.01	0.00	0.09	0.00
7	0.04	0.00	0.04	0.01
12	0.12	0.01	0.15	0.04
20	0.32	0.00	0.11	0.10

4.2.3 Comparison on the Influence of Material Properties and Conductivity Equations

In this part, the results from fresh material and aged material are to be compared, and an issue that can possibly appear in long-term continuous cable operation is discussed. Besides, the results from different electrical conductivity expressions are compared, indicating whether the two equations are interchangable.

Comparison of the Results from Different Material Properties

Field distribution across the insulation at DC steady state varies with material properties due to the electrical conductivity value. The critical temperature difference for field reversal occurrence in fresh and aged material is illustrated in Fig. 4.11. Under the same cable geometry or even the same radius ratio, the level from fresh material becomes higher than that from the aged material.
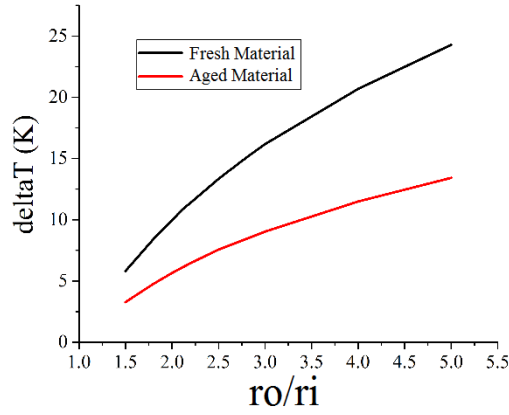
Fig. 4.11. Critical temperature difference level for field reversal occurrence in different materials.

Accordingly, an issue can possibly be detected in HVDC cable which is continuously under operation for a long period of time: when the cable is put into service at an early stage, field reversal may not happen under steady state due to the higher critical temperature difference level required in fresh material. Though the load and applied voltage is stable across the service life, the insulation keeps being degraded, and field reversal can possibly happen due to the variation in material properties. For example, in the cable with a geometry listed in Table. 3.1, ΔT_{cri} decreases from 10.8 K to 6.08 K across the lifetime. If the level of temperature difference is between these two levels (8 K, for example) at steady state, field reversal can possibly happen across the operation.

Comparison of Results from Two Electrical Conductivity Expressions

In [103, 105, 113], it was stated that Equations (3.5) and (3.26) could be used to represent electrical conductivity of XLPE between 20℃ and 60℃. Under high temperature, between 70℃ and 90℃, the microstructure and molecular chain change, and there can possibly be an aberration in describing electrical conductivity via Equation (3.26). Equation (3.5) has been derived from the experiment, and it has a high reliability.

When the electric field across the insulation based on Equation (3.26) is always between the one based on Equation (3.5) for fresh material and the one based on Equation (3.5) for aged material, it can be believed that these two equations can be replaced between each other in describing the electric field distribution across the HVDC cable operation process. These two equations cannot match each other at the start of operation and long-term degradation: in Equation (3.5), the dependence of electrical conductivity to electric field is hyperbolic function, while the electrical conductivity depends on electric field in an exponential form in Equation (3.26). They cannot be precisely matched.

The comparison in electric field distribution across the insulation is illustrated in Fig. 4.12. The outer temperature is set at 293.15K (20℃), and four temperature difference levels are applied. Electric field

distribution when the electrical conductivity is derived from Equation (3.26) seems to always be between the other two lines when Equation (3.5) is applied. It means that if a proper value of σ_0, α and β are used, Equation (3.26) is acceptable in describing the value of XLPE between 20℃ and 60℃.
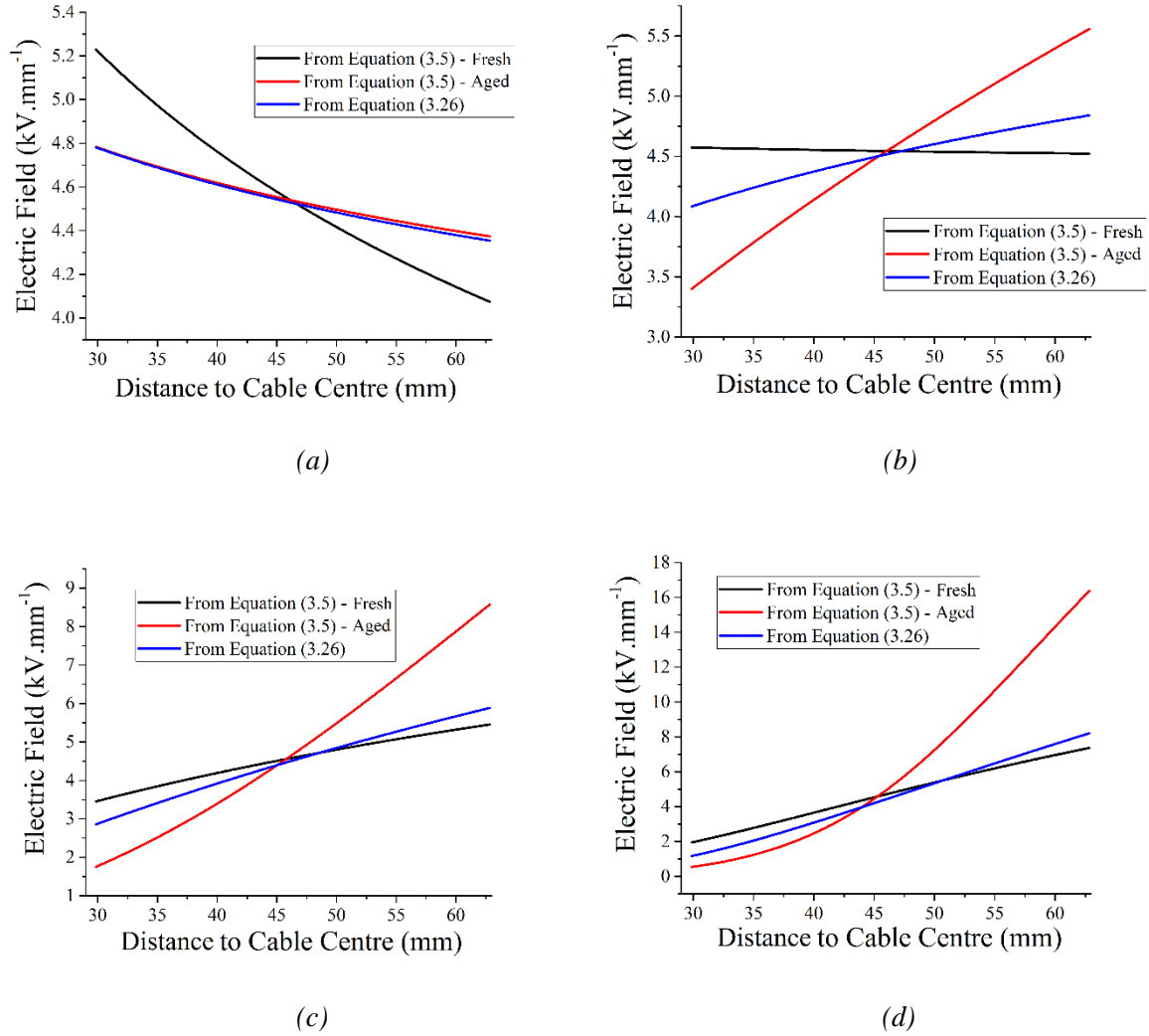
Fig. 4.12. Electric field across the insulation from two groups of electrical conductivity expressions when (a) $\Delta T = 5K$, (b) $\Delta T = 10K$, (c) $\Delta T = 20K$, and (d) $\Delta T = 40K$.

4.3 2D and 3D Model Comparison

2D and 3D models have different ways of describing the cavity, and the electric field or temperature distribution with the cavity presence from 2D model can be different from that of the 3D model. Electric field and temperature distribution across the insulation without cavity at DC steady state is illustrated in Figs 4.13 and 4.14. When no cavity exists in the insulation, results from 2D and 3D models are the same. A comparison in the solution time between two models is listed in Table. 4.12. 'Extra fine mesh' and 'Extremely fine mesh' are two meshing work predefined in the software, and the meshing precision is not manually set. 'Custom mesh' is the meshing work with the precision manually set. The solution

time of the 3D model can be at least 6 times longer than that of the 2D model, and the shortcoming in the solution time of the 3D model can be much more significant if the meshing work is precise to obtain more accurate results. The 2D model is, therefore, a better choice in electric field or temperature analysis without the cavity presence: much less elements are to be calculated in the FEA, and the simulation time is greatly reduced.

(a)   *(b)*
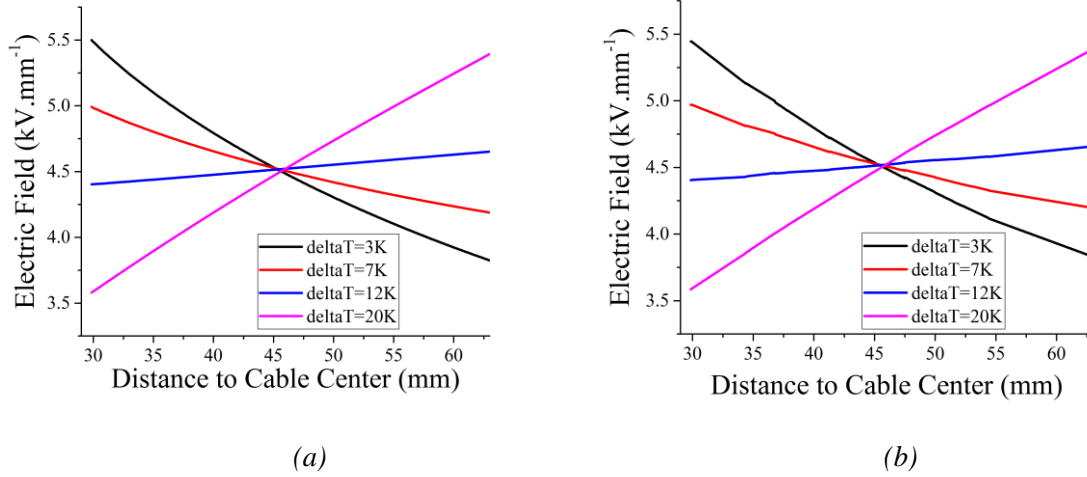
Fig. 4.13. Electric field across the insulation without cavity appearance at DC steady state (a) 2D model, and (b) 3Dmodel.

(a)   *(b)*
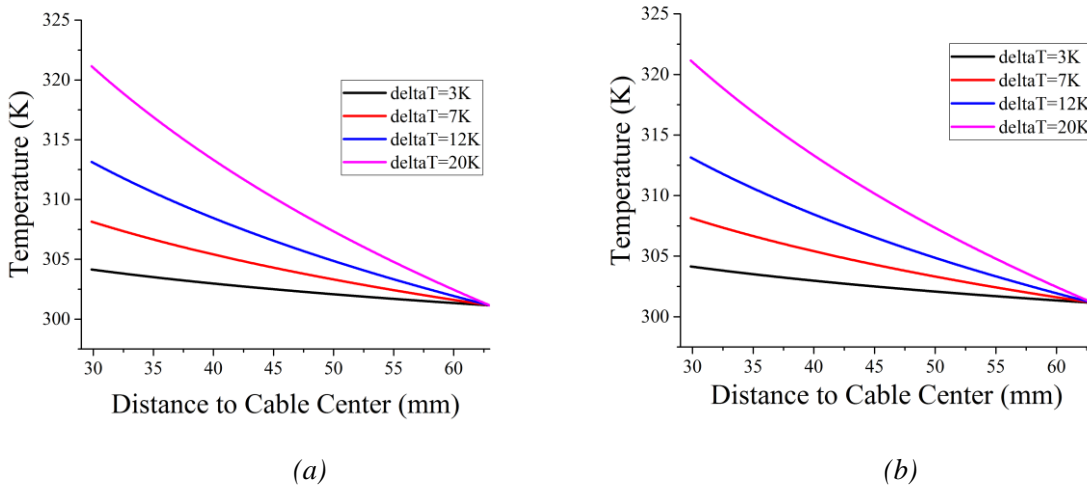
Fig. 4.14. Temperature across the insulation without cavity appearance at DC steady state (a) 2D model, and (b) 3D model.

Table. 4.12. Model solution time comparison between two models.

	Maximum Element Size (m)	Minimum Element Size (m)	2D Model Solution Time (s)	3D Model Solution Time (s)
Extra fine mesh	0.0044	1.89E-4	3	19
Extremely fine mesh	0.0025	2.52E-5	5	59
Custom mesh	0.0010	2.52E-5	23	886

The presence of a single air-filled cavity can distort the local electric field and temperature distribution. Assume that a 1 mm radius spherical air-filled cavity is located in the middle of the insulation. Comparison in the electric field across the insulation with the cavity presence from 2D and 3D models is plotted in Fig. 4.15. First, the field inside the cavity tends to be uniformly distributed. The reason can be that the electrical conductivity in the cavity is set to be equal to air conductivity at any location, and the density of electric field lines seems to be uniformly distributed (as shown in Fig. 3.2).

Second, the electric field in the 2D model is higher than that in the 3D model. Field enhancement from the 2D model should be higher as well because electric field distribution without cavity from the 2D and the 3D model is the same.
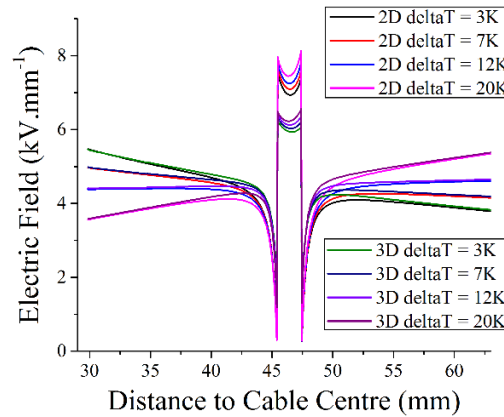
Fig. 4.15. 2D and 3D model comparison in electric field distribution across the insulation with a single spherical cavity ($R_c=1mm$, a=0.5) appearance at DC steady state.

Finally, in describing the electric field in the insulation far from the cavity, the results from the 2D and the 3D models are almost the same. It means that the electric field distortion by the cavity is a local phenomenon at the cavity. The volume of the potentially distorted region is investigated and discussed in a later section of this chapter.

The maximum, minimum and average electric field strength inside the cavity is given in Fig. 4.16 when a 1 mm radius spherical cavity is located in the middle of the insulation. 'Max' and 'Min' represent the peak and weakest field strength in the cavity field, and 'Average' is the average field strength of the cavity field. The difference between the maximum and minimum value is not higher

than 5% of the maximum field strength. Therefore, the electric field tends to be uniformly distributed inside the cavity. To simplify the analysis, the average strength is used in indicating the cavity field.
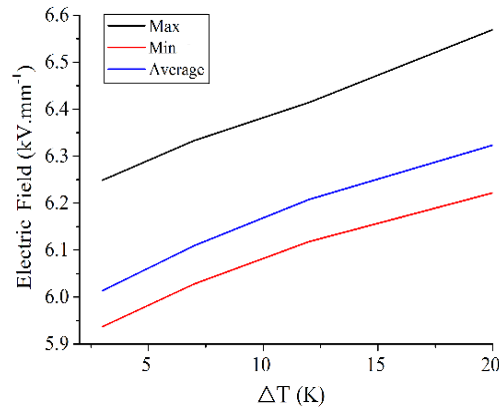
Fig. 4.16. Electric field inside the cavity across temperature difference level studied in the project.

A model comparison in electric field strength and field enhancement is listed in Table. 4.13. Field enhancement from the 2D model can be 25% and even nearly 30% higher than that of the 3D model. When the cavity field is the key parameter in research, for example, cavity discharge in HVDC cable, the 2D model cannot be the choice as the value obtained is not accurate. In this case, the 3D model is the only choice.

Table. 4.13. Model comparison on field inside the cavity.

ΔT (K)	Electric Field (kV. mm^{-1})		η_{DC} (%)	
	2D model	3D model	2D model	3D model
3	7.11	6.01	159.31	134.72
7	7.27	6.11	161.73	135.91
12	7.43	6.21	164.43	137.22
20	7.64	6.32	168.05	139.14

A comparison in temperature distribution across the insulation with the cavity presence from the 2D and the 3D models is plotted in Fig. 4.17, and the data is given in Table. 4.14. It can be seen that the difference between the two models in describing the temperature distribution with the cavity presence is acceptably low (not higher than 0.3 K). Therefore, when the focus is on the temperature inside the cavity or in the region close to the cavity, the 2D model is still reasonable even if air-filled cavities are present in the insulation.
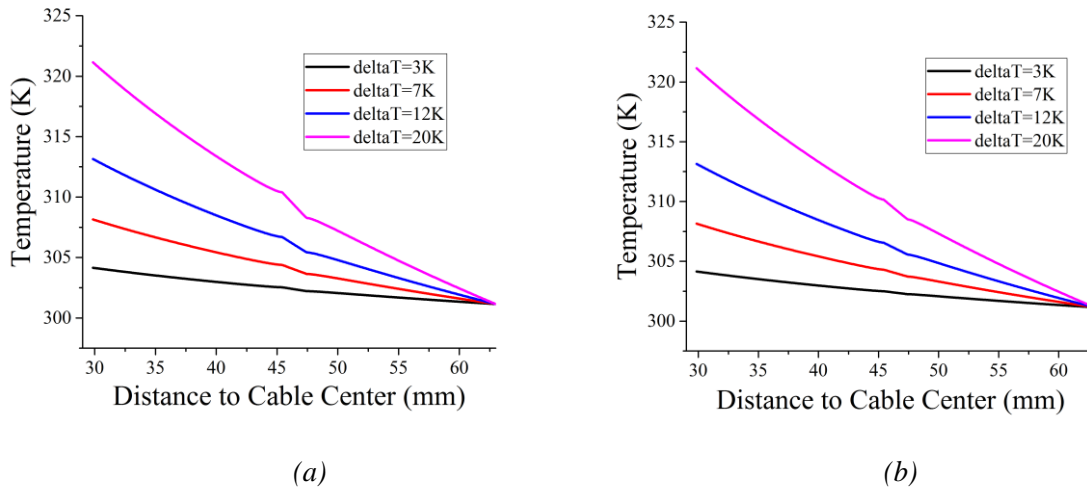
Fig. 4.17. Temperature across the insulation with cavity appearance at DC steady state (a) 2D model, and (b) 3D model.

Table. 4.14. Model comparison on temperature at the cavity.

ΔT (K)	Temperature gap between models (K)
3	0.04
7	0.08
12	0.14
20	0.23

In summary, 2D and 3D models are compared, and the reference for model selection is provided in this section. A 2D model can be the better choice in electric field and temperature analysis at DC steady state when there is no cavity in the insulation. When the air-filled cavity appears, a 2D model can still be applicable when the cable temperature across the insulation or at the cavity is researched due to a small difference between the results from the 3D model. When the field at or near the cavity is the key factor involved in the phenomenon to be studied, the 3D model is the only choice as results from the 2D model are not accurate. However, if the electric field in the region 'far' from the cavity is to be studied, 2D model can be the choice as the electric field distortion by the cavity is a local phenomenon.

4.4 Cavity Field Enhancement at DC Steady State

It is speculated that field enhancement by a single air-filled cavity can be expressed as Equation (3.34) at DC steady state: cavity shape and electrical conductivity are the two factors with potential effect on the field enhancement. The relationship between electrical conductivity of XLPE and cavity location, temperature difference and material properties is illustrated in Fig. 4.18. Electrical conductivity increases with the temperature difference when the outer temperature does not change. The region closer to the conductor has a higher electrical conductivity value, and this trend is

independent of temperature difference or material properties. The electrical conductivity of fresh material is higher than that of aged material, and it has been explained in Fig. 4.5 and Table. 4.5.

(a)   *(b)*
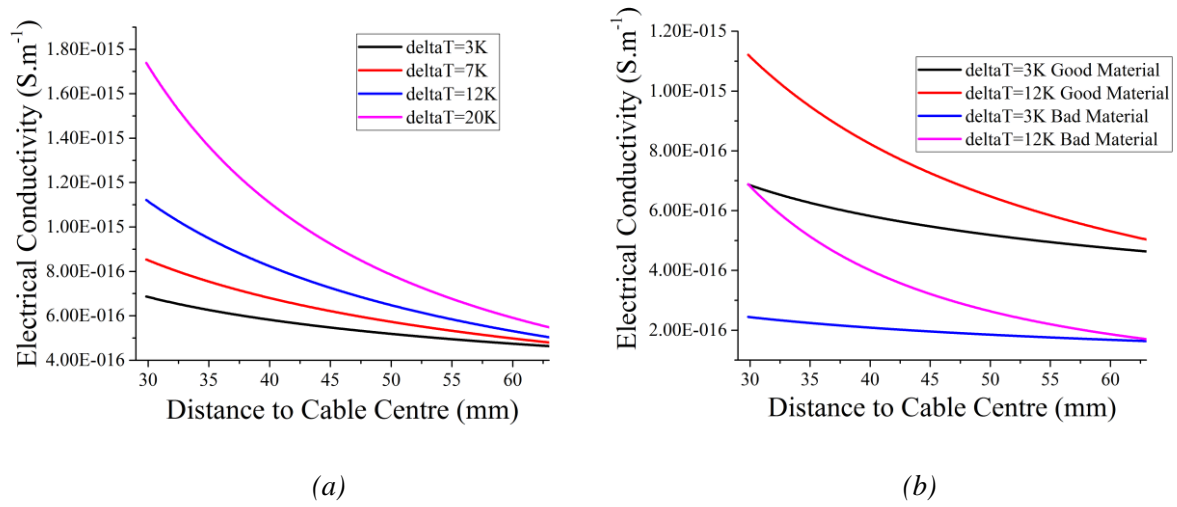
Fig. 4.18. Electric conductivity across fresh material insulation without cavity under (a) different temperature difference in fresh material, and (b) different material properties.

The relationship between the value of axis ratio [a_c/b_c in Fig. 3.4 (b)] of the cavity and the value of K is listed in Table. 4.15 [47]. In calculating the enhancement value at DC steady state η_{DC}, the average field strength is used in indicating the cavity field and the reference field due to the uniform field distribution in the cavity (as shown in Fig. 4.15). Electrical conductivity value of XLPE in the reference region corresponding to the cavity is also calculated as the average value. To completely eliminate the influence of cavity size, the volume of the cavity needs to be constant even though the ratios vary in order to understand the influence of the cavity shape: the volume is kept similar to the spherical one with 1 mm radius.

Table. 4.15. Dependency of K value on the axis ratio [47].

Axis Ratio	K	Axis Ratio	K
0.2	1.333	2	5.762
0.33	1.574	3	9.313
0.5	1.897	5	17.914
1	3.000		

The results of the match between simulation and calculation for fresh material are given in Fig. 4.19. The errors are given in Table 4.16. Error percentage is calculated as the error value, which is the absolute difference between simulation and calculation, over the simulation value. The results of the match between simulation and calculation are ok as the error percentage is acceptably low (not higher than 4%) under most conditions. However, when the cavity is close to the cable conductor at a low temperature difference level (a = 0.25, ΔT = 3K), the error percentage value can be higher than 5%, but never exceed 5.3%. The error level can possibly occur due to the imprecision of the meshing work and the way in indicating the cavity field that it is represented by the average strength inside the cavity.

(a)   *(b)*
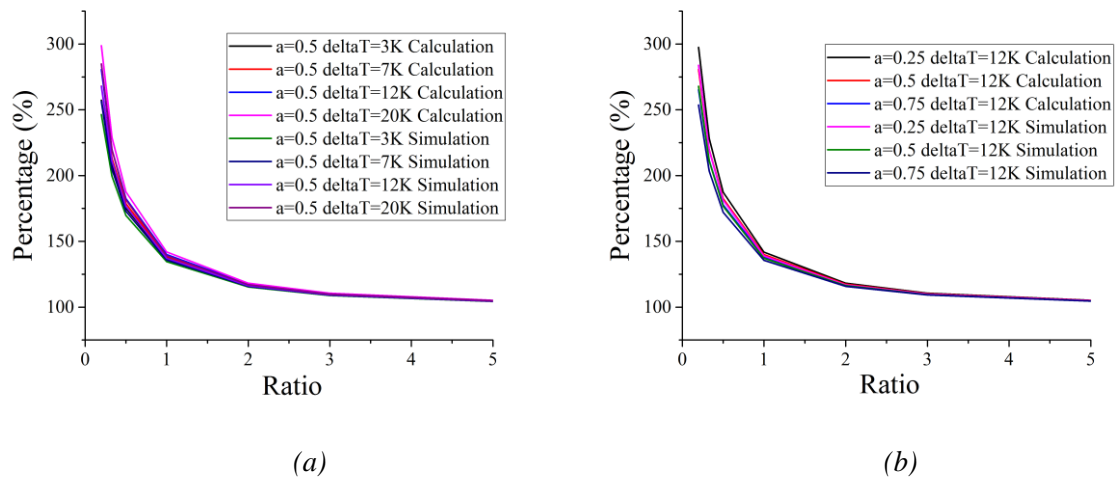
Fig. 4.19. Comparison between simulation and calculation results in field enhancement by single air-filled cavity at DC steady state in fresh material under (a) different temperature difference ($a = 0.5$), and (b) different cavity location ($\Delta T = 12K$).

Table. 4.16. Error in simulation and calculation comparison of η_{DC} in fresh material (Error percentage, %)

Axis Ratio	ΔT = 3K			ΔT = 7K			ΔT = 12K			ΔT = 20K		
	a=0.25	a=0.5	a=0.75	a=0.25	a=0.5	a=0.75	a=0.25	a=0.5	a=0.75	a=0.25	a=0.5	a=0.75
0.2	5.28	4.40	3.47	5.09	4.57	3.97	4.79	4.72	4.57	4.26	4.88	2.48
0.33	4.61	3.88	3.06	4.41	3.98	3.47	4.11	4.07	3.96	3.61	4.14	0.41
0.5	3.84	3.24	2.58	3.65	3.30	2.93	3.38	3.35	3.31	2.94	3.38	0.61
1	2.40	2.02	1.52	2.26	2.04	1.74	2.07	2.06	1.98	1.77	2.05	0.86
2	1.27	1.00	0.67	1.20	1.00	0.80	1.10	1.00	0.94	0.93	0.98	0.56
3	0.77	0.62	0.34	0.72	0.61	0.42	0.64	0.61	0.52	0.52	0.59	0.34
5	0.44	0.39	0.09	0.40	0.37	0.14	0.34	0.35	0.19	0.25	0.32	0.25

The results of the match between simulation and calculation for aged material is given in Fig. 4.20. The errors are given in Table 4.17. The results of the match between simulation and calculation tends to be much more satisfactory, as the maximum error percentage level is never higher than 1%, regardless of the temperature difference value, cavity location and cavity axis ratio. Accordingly, field enhancement by a single air-filled cavity at DC steady state can be calculated according to Equation (3.34).


(a)   *(b)*
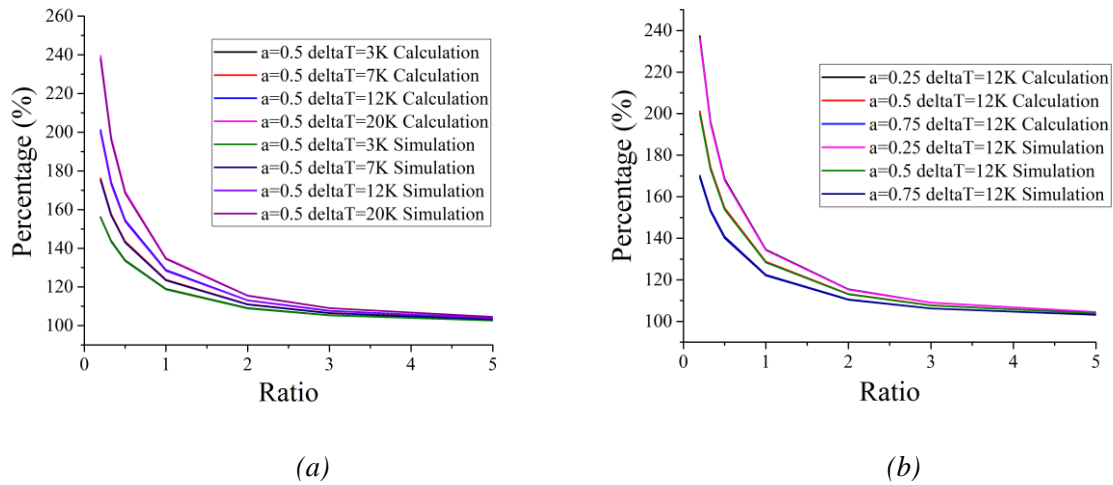
Fig. 4.20. Comparison between simulation and calculation results in field enhancement by single air-filled cavity at DC steady state in aged material under (a) different temperature difference ($a = 0.5$), and (b) different cavity location ($\Delta T = 12K$).

Table. 4.17. Error in simulation and calculation comparison of η_{DC} in aged material (Error percentage, %)

Axis Ratio	$\Delta T = 3K$			$\Delta T = 7K$			$\Delta T = 12K$			$\Delta T = 20K$		
	a=0.25	a=0.5	a=0.75	a=0.25	a=0.5	a=0.75	a=0.25	a=0.5	a=0.75	a=0.25	a=0.5	a=0.75
0.2	0.65	0.28	0.05	0.71	0.58	0.22	0.53	0.67	0.54	0.24	0.73	0.97
0.33	0.65	0.33	0.01	0.68	0.56	0.25	0.49	0.62	0.54	0.14	0.64	0.89
0.5	0.59	0.32	0.00	0.59	0.49	0.25	0.41	0.53	0.51	0.05	0.52	0.77
1	0.43	0.24	0.05	0.40	0.34	0.15	0.26	0.35	0.32	0.03	0.32	0.44
2	0.28	0.14	0.11	0.24	0.17	0.03	0.14	0.15	0.13	0.11	0.11	0.14
3	0.19	0.11	0.13	0.13	0.11	0.03	0.03	0.08	0.03	0.18	0.02	0.01
5	0.15	0.12	0.16	0.08	0.09	0.09	0.02	0.04	0.02	0.21	0.06	0.07

4.5 Field Distortion in the Region Surrounding the Cavity

This section discusses the field distortion in the region surrounding the cavity. A 3D model is used and the results on the three planes are illustrated separately. With the help of the field distortion data in the

region surrounding the cavity, the volume of the region, possibly distorted by the cavity, is presented in this section.

Change in the cavity shape is not considered here, and only the spherical cavity in the insulation is studied. The distortion condition is possibly influenced by cavity location, temperature difference across the cavity and material properties, as they can vary the electrical conductivity of dielectric at DC voltage. To see the possible extent of the electric field distribution, three levels of cavity sizes are studied to observe the region.

4.5.1 Electric Field Distribution and Distortion on Three Planes

The field distribution and field distortion percentages on three planes are first indicated and compared. A single spherical cavity is located in the middle of the fresh material insulation, where the cavity radius is 1mm. The temperature difference is set at 12K.

Electric Field and Field Distortion on xy Plane

Distribution of electric field in the region around the cavity on xy plane is given in Fig. 4.21 (a). Field around the cavity peaks at $\theta = 90°$ and $\theta = 270°$, where it is at the top and bottom part of the cavity (as shown in Fig. 3.6), and it drops to the lowest at $\theta = 0°$ (or $\theta = 360°$) and $\theta = 180°$, where the coordinate y equals to zero. The reason is that according to Fig. 3.2, the electric field lines distribution at $\theta = 90°$ and $\theta = 270°$ is denser, while the electric field lines are difficult to reach the region where $\theta = 0°$ and $\theta = 180°$.

*(a)*   *(b)*
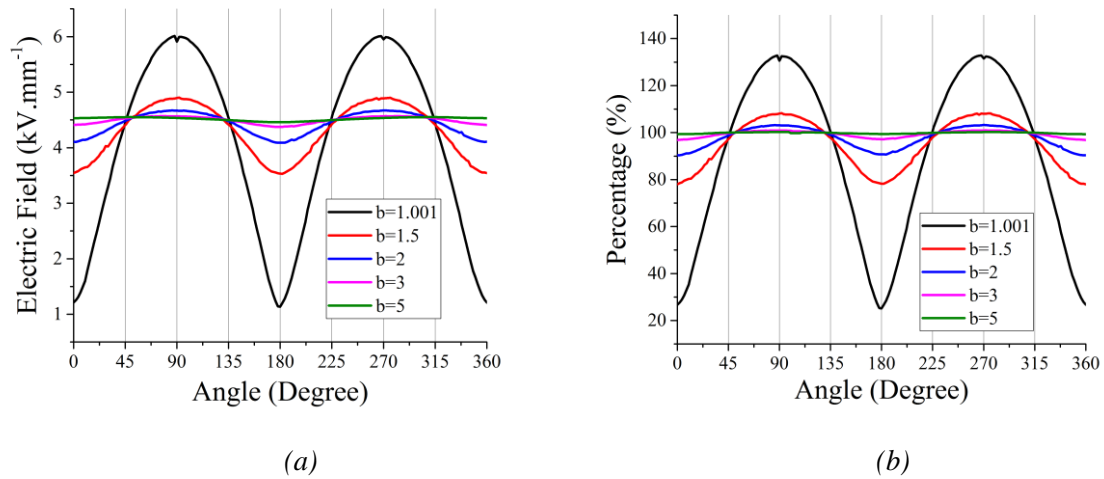
Fig. 4.21. (a) Electric field, and (b) Field distortion around the cavity on xy plane (fresh material, $R_c = 1mm$, $a = 0.5$, $\Delta T = 12K$).

The field distortion value is calculated as the field strength in the region surrounding the cavity over the corresponding reference field strength. The closer the distortion value is to the unit value (100%), the

less distortion is on the field around the cavity. If the distortion percentage is lower than 100%, it seems that the field is reduced by the cavity. Similarly, if the distortion percentage is higher than 100%, the cavity enhances the surrounding field.

According to Equation (3.37), the distance of the points on xy plane from the cable centre is calculated as follows:

$$D = \sqrt{X_{xy}^2 + Y_{xy}^2} = \sqrt{(X + bR_c)^2 + 2bR_cX(\cos\theta - 1)} \qquad (4.4)$$

It can be seen that the value of D varies slightly. Compared to $X + bR_c$, the value of $2bR_cX$ is smaller. The variation in the value of D means the reference field changes slightly. Accordingly, the relationship between field distortion and angle, which is illustrated in Fig. 4.21 (b), should be similar to the relationship between electric field and angle.

Fig. 4.21 (b) shows that field enhancement happens in the region between $45°$ and $135°$, and the region between $225°$ and $315°$. In the remaining region, the electric field tends to be reduced by the cavity. It means that the volume of the field reduction region (region A and C in Fig. 3.2) equals to the field enhancement region (region B and D in Fig. 3.2). The maximum negative difference between the distortion and 100% is obtained at $\theta = 0°$ (or $\theta = 360°$) and $\theta = 180°$, while the maximum positibe difference between the distortion and 100% is obtained at $\theta = 90°$ and $\theta = 270°$.

The field distortion data is listed in Table. 4.18. It has been stated in Chapter 3 that if the absolute difference between field distortion and 100% is not higher than 1%, the influence of cavity can be neglected. Table. 4.18 indicates that in the region at the cavity's outer surface, the field can be reduced even to a value as low as a quarter of the initial strength. In the region where $b \geq 5$, the influence of cavity on the electric field can be neglected as the variation in field strength caused by the cavity presence is not apparent (not higher than 0.7%). It can therefore be concluded that when a 1mm spherical cavity is located in the middle of fresh insulation ($\Delta T = 12K$), the region that is possibly distorted is spherical with the same centre to the cavity, and the radius of the region is five times the cavity radius.

There are two other points that should be introduced. First, though the degree of field distortion decreases with the distance to the cavity centre, influence of cavity at $45°$ or $135°$ is never significant (never higher than 3%). It further indicates that volume of the field enhancement region arguably equals to that of the field reduction region. Second, field enhancement by the cavity, η_{DC}, under the same condition is 137.21% from simulation. It is slightly higher than the maximum distortion level. It is possible, as the point is actually not at the cavity wall when $b = 1.001$. It can be further researched whether there is any co-relationship between field enhancement in the cavity and in the region

surrounding the cavity.

Table. 4.18. Field distortion around the cavity on xy plane (fresh material, $R_c = 1mm$, $a = 0.5$, $\Delta T = 12K$).

b	Distortion – at 45° and 135° (%)		Distortion - whole (%)	
	at 45°	at 135°	Max	Min
1.001	98.03	100.39	132.81	25.17
1.5	97.19	97.77	108.28	78.03
2	98.81	99.10	103.25	90.32
3	99.73	99.87	100.95	96.89
5	100.02	99.94	100.26	99.35

Electric Field and Field Distortion on xz Plane

The common point between xy and xz planes is that elements to be analysed on the plane vary in distance from the cable centre. However, the difference is that the normal line of the xy plane is parallel to the cable axis, while the one of the xz plane is vertical to the cable axis. Distribution of the electric field and the field distortion around the cavity on xz plane are given in Fig. 4.22. When Fig. 4.22 is compared with Fig. 4.21, it seems that field distribution and field distortion conditions in the region surrounding the cavity on xz plane are similar to those on xy plane.

(a) *(b)*
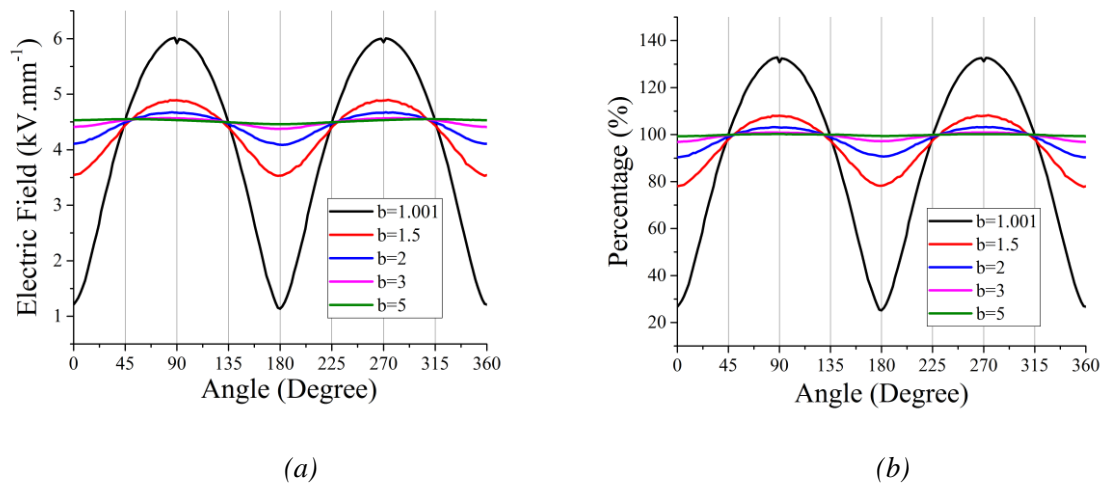
Fig. 4.22. (a) Electric field, and (b) Field distortion around the cavity on xz plane (fresh material, $R_c = 1mm$, $a = 0.5$, $\Delta T = 12K$).

The comparison between field distribution and field distortion on xy and xz planes is listed in Table. 4.19. Error is calculated as the absolute difference between the value on xz plane and the associated value on xy plane at the same angle value. Error value indicates that the difference between electric field and field distortion on xy plane and those on xz plane is small. The maximum and

70

minimum field distortion on xz plane when b = 5 are 100.24% and 99.34% respectively. Therefore, conclusions drawn from the xy plane can be applied on the xz plane.

Table. 4.19. Comparison between xy and xz planes on field distribution and field distortion (fresh material, $R_c = 1mm$, $a = 0.5$, $\Delta T = 12K$).

b	Max Error - Field distribution (kV.mm^{-1})	Max Error – Field distortion (%)
1.001	0.10	2.18
1.5	0.05	1.23
2	0.03	0.66
3	0.01	0.28
5	0.00	0.33

Electric Field and Field Distortion on yz Plane

According to Equation (3.39), the distance of the elements on the yz plane from the cable centre is expressed as follows:

$$D = \sqrt{X_{yz}{}^2 + Y_{yz}{}^2} = \sqrt{X^2 + (bR_c\cos\theta)^2} \qquad (4.5)$$

The value of bR_c can be neglected as it is much smaller than X, and the D value is nearly constant with slight variation. Therefore, though the normal line is vertical to the cable axis, which is the same as for xz plane, electric field distribution and field distortion on yz plane should be different from that on xz plane.

Electric field distribution and field distortion in the region surrounding the cavity on yz plane are illustrated in Fig. 4.23. Field around the cavity tends to be constant with slight variation under the same value of b. The precision for Fig. 4.23 is 'Extremely fine mesh', which can be referred to in Table. 4.11. To explain the influence or the improvement on the results' accuracy if the more precise meshing is applied, the comparison is listed in Table. 4.20. The increase in the meshing work precision reduces the fluctuation of electric field and field distortion for b = 1.001. Therefore, the slight fluctuation can occur from the precision of the meshing work. The solution time is much longer when more precise meshing is applied (as shown in Table. 4.11) and the accuracy of the results is acceptably high (as shown in Fig. 4.23). Therefore, the meshing accuracy for Fig. 4.23 is reasonable.
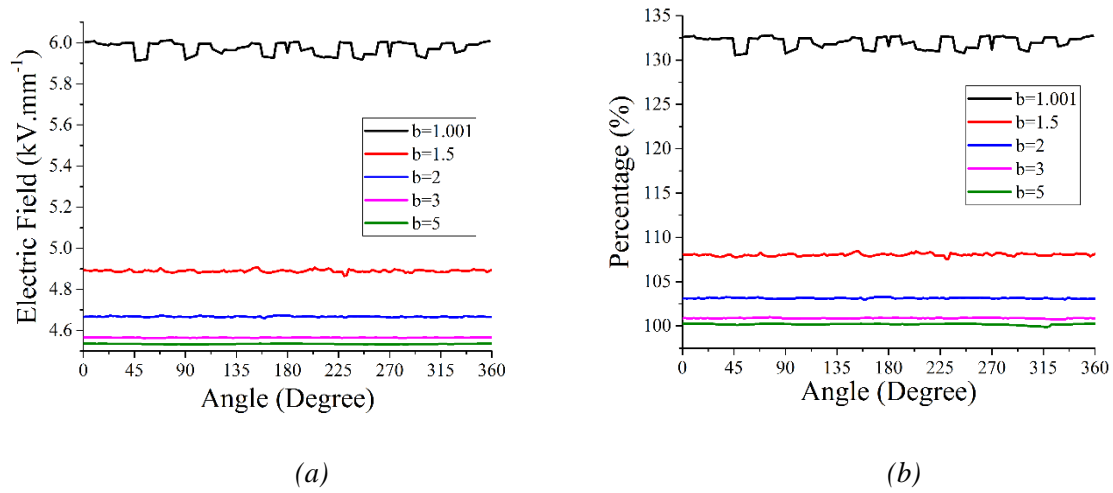
Fig. 4.23. (a) Electric field and (b) Field distortion around the cavity on yz plane (fresh material, $R_c = 1mm$, $a = 0.5$, $\Delta T = 12K$).

Table. 4.20. Comparison in field distortion percentage between two meshing work precision levels.

		Electric Field Fluctuation $(kV.mm^{-1})$	Field Distortion Fluctuation (%)
Extremely fine mesh	b = 1.001	0.13	2.26
	b = 1.5	0.05	0.89
	b = 2	0.02	0.31
	b = 3	0.01	0.24
	b = 5	0.01	0.38
Custom mesh	b = 1.001	0.11	2.01
	b = 1.5	0.05	0.89
	b = 2	0.02	0.31
	b = 3	0.01	0.24
	b = 5	0.01	0.38

Similar to the field distribution, field distortion value is more or less constant across the whole angle values. Distortion level remains higher than 100%, and the reason is it reflects the conditions where $\theta = 90°$ and $\theta = 270°$, such that the electric field lines are densely distributed (shown as regions B and D in Fig. 3.2).

Error in the fluctuation on field and field distortion on yz plane is given in Tables 4.21 and 4.22. The difference between the maximum and minimum electric field is not high (never higher than 0.1 kV.mm^{-1}) and the difference between the maximum and minimum distortion percentage is acceptably low (not higher than 2.5%). Therefore, it can be believed that electric field and field distortion on yz plane are both constant under the same b value.

Table. 4.21. Error in field distribution on yz plane (fresh material, $R_c = 1mm$, $a = 0.5$, $\Delta T = 12K$).

B	Electric field - max (kV. mm^{-1})	Electric field - min (kV. mm^{-1})	Error (kV. mm^{-1})
1.001	6.01	5.91	0.10
1.5	4.91	4.87	0.04
2	4.67	4.66	0.01
3	4.57	4.56	0.01
5	4.54	4.53	0.00

Table. 4.22. Error in field distortion on yz plane (fresh material, $R_c = 1mm$, $a = 0.5$, $\Delta T = 12K$).

b	Field distortion - max (%)	Field distortion - min (%)	Error (%)
1.001	132.80	130.54	2.26
1.5	108.42	107.54	0.89
2	103.29	102.98	0.31
3	101.00	100.75	0.24
5	100.28	99.89	0.38

Under the condition that $b = 3$, the influence of the cavity can be neglected, as the maximum distortion is 1% higher than 100%. However, considering the distortion condition on xy and xz planes, the region possibly distorted by the spherical cavity is not larger than five times the cavity radius. This conclusion is applicable for the condition that $R_c = 1mm$, $a = 0.5$, and $\Delta T = 12K$ in fresh material. Further research in this section indicates whether it is reasonable in case of the other temperature differences, cavity sizes, cavity locations and material properties.

To help understand the electric field distribution in the region surrounding the cavity, simulation results from COMSOL on the xy and yz planes are illustrated in Fig. 4.24. Fig. 4.24(a) indicates that on the xy plane, there are field enhancement regions and field reduction regions surrounding the cavity. Fig. 4.24(b) shows that on the yz plane, when the distance from the cavity centre is the same, electric field, and therefore, field distortion in the region surrounding the cavity, are nearly constant.

(a)   *(b)*
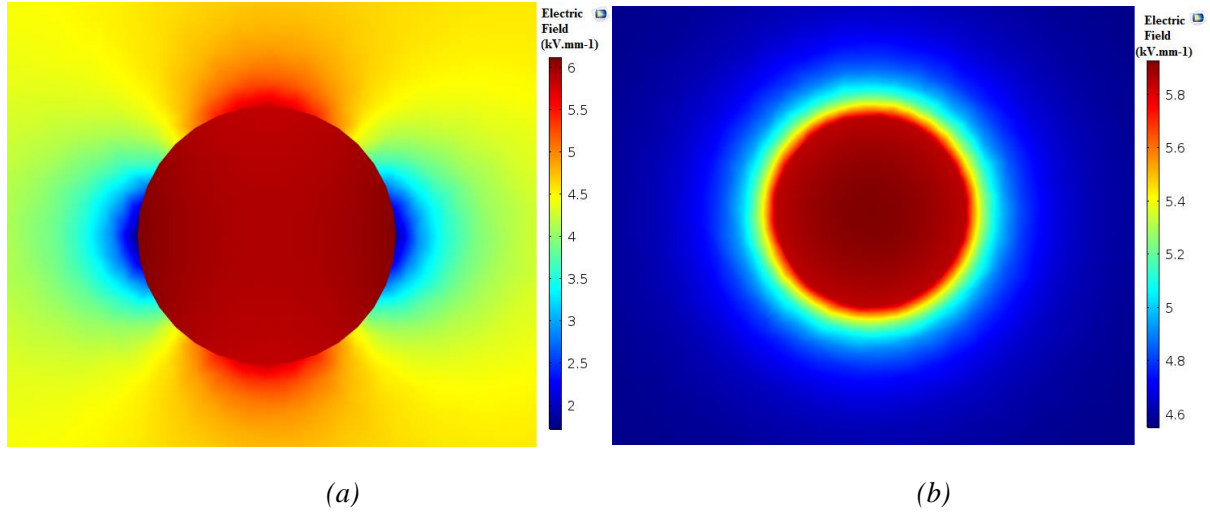
Fig. 4.24. COMSOL results of electric field on (a) xy plane, and (b) yz plane.

4.5.2 Potentially Influential Factors

The effect of cavity location, temperature difference across the insulation and material properties on field distortion in the region surrounding the spherical cavity at DC steady state is illustrated in this section. To understand the volume of the region possibly distorted by the cavity, cavity size is also considered. It has been indicated in Section 4.5.1 that both electric field distribution and electric field distortion on xy and xz planes are similar. Therefore, conditions on the xy and yz planes are presented.

Cavity Location

In understanding the variation of electric field distortion in the region surrounding the cavity with cavity location on the xy and yz planes, it is assumed that a 1mm radius air-filled cavity varies its position in fresh material insulation. The temperature difference across the insulation is 12K, and field reversal occurs under the condition.

The relationship between field distortion and cavity location on the xy and yz planes are given in Figs 4.25 and 4.26 respectively. Field distortion tends to be more serious when the cavity is closer to the conductor: the absolute value of maximum positive or negative difference between distortion percentage and 100% is higher when the cavity is closer to the conductor. The trend is due to the electrical conductivity of XLPE surrounding the cavity, and it matches the results given in Fig. 4.17 (a): material electrical conductivity is higher in the region closer to the conductor, regardless of the occurrence of field reversal.
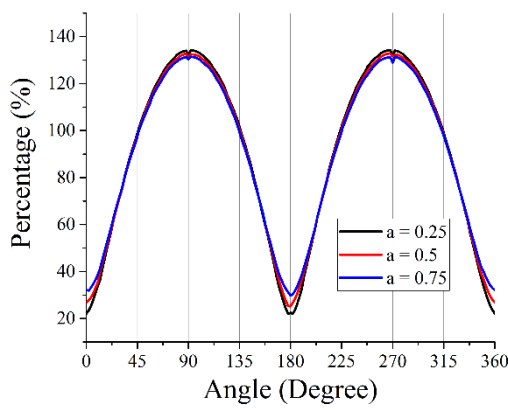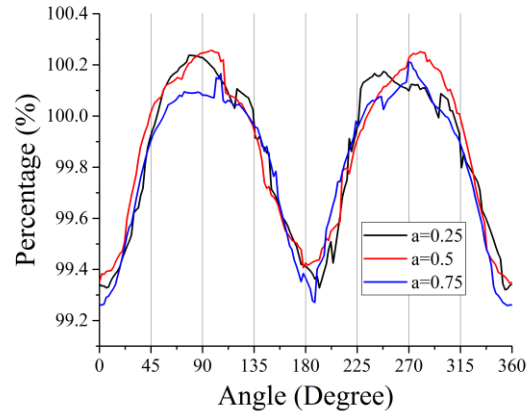
(a)   *(b)*

Fig. 4.25. Field distortion on xy plane under various cavity location ($R_c = 1mm$, $\Delta T = 12K$, fresh material) for (a) b=1.001, and (b) b=5.
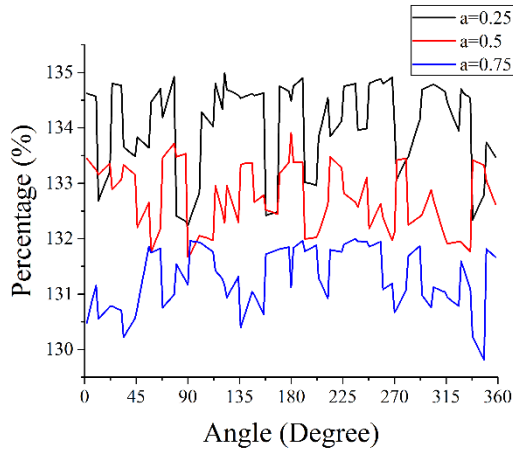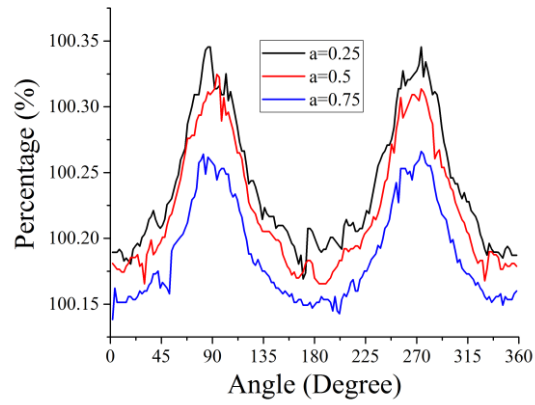
(a)   *(b)*

Fig. 4.26. Field distortion on yz plane under various cavity location ($R_c = 1mm$, $\Delta T = 12K$, fresh material) for (a) b=1.001, and (b) b=5.

Similar to the discussion in the previous section, the region possibly distorted by the cavity is five times the cavity radius, as the influence of cavity presence on the field is small enough. The trend is applicable for the three-cavity locations studied in this project.

To understand the influence of cavity location on field distortion, data are listed in Table. 4.23. Electric field distortion on yz planes fluctuates in a small region and the most serious fluctuation region is 2.72%, which appears under the condition where the cavity is closer to the conductor. The corresponding maximum distortion percentage is as high as 134.15% and the fluctuation degree is accordingly small. It means that field distortion on yz planes is nearly constant. Besides, for the condition where b = 5, the maximum absolute difference between field distortion and 100% is

0.95%. Accordingly, the volume of the influenced region is obtained.

Table. 4.23. Error in field distortion on xy and yz planes with different cavity location (fresh material, $R_c = 1mm$, $\Delta T = 12K$).

		xy plane		yz plane	
		Distortion - max (%)	Distortion - min (%)	Distortion - max (%)	Distortion - min (%)
b=1.001	a = 0.25	134.22	21.99	134.99	132.24
	a = 0.5	132.81	25.17	133.91	131.67
	a = 0.75	131.49	29.77	132.00	129.81
b=3	a = 0.25	100.97	96.89	101.09	100.71
	a = 0.5	100.95	96.89	101.00	100.75
	a = 0.75	100.89	97.17	100.94	100.76
b=5	a = 0.25	100.24	99.32	100.35	100.17
	a = 0.5	100.95	99.35	100.32	100.17
	a = 0.75	100.21	99.26	100.32	100.17

Temperature Difference

To understand the influence of temperature difference, i.e. the occurrence of field reversal on field distortion, it is assumed that a 1mm radius air-filled cavity is located in the middle of fresh material insulation. The relationship between electric field distortion and temperature difference on xy and yz planes are given in Figs 4.27 and 4.28. The field tends to be more seriously distorted at a higher temperature difference value. The reason is that electrical conductivity is higher at higher ΔT value. Similar to the phenomenon obtained in the effect of cavity location, field distortion is nearly constant on yz plane with slight fluctuation.

(a)   (b)
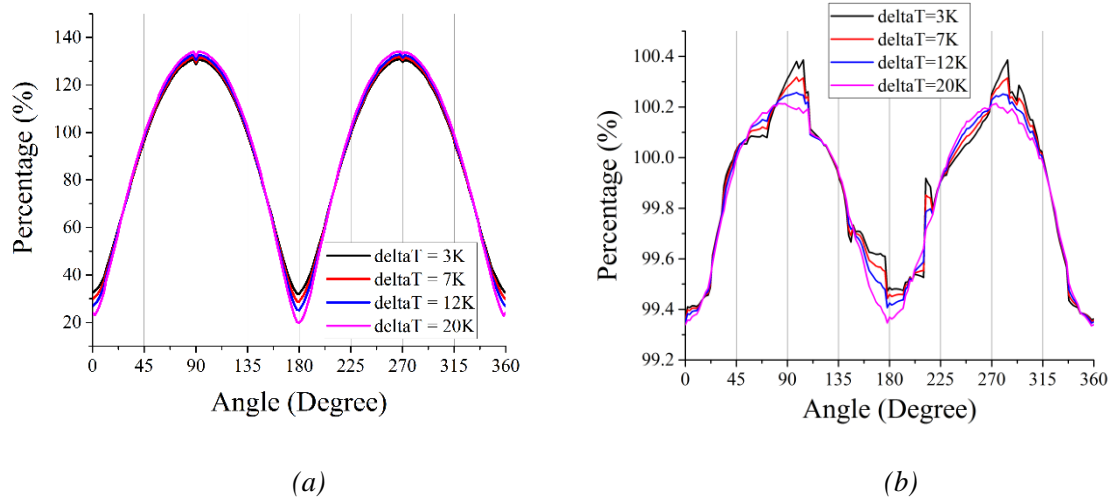
Fig. 4.27. Field distortion on xy plane under various temperature difference ($R_c = 1mm$, $a = 0.5$, fresh material) for (a) b=1.001, and (b) b=5.

(a)   *(b)*
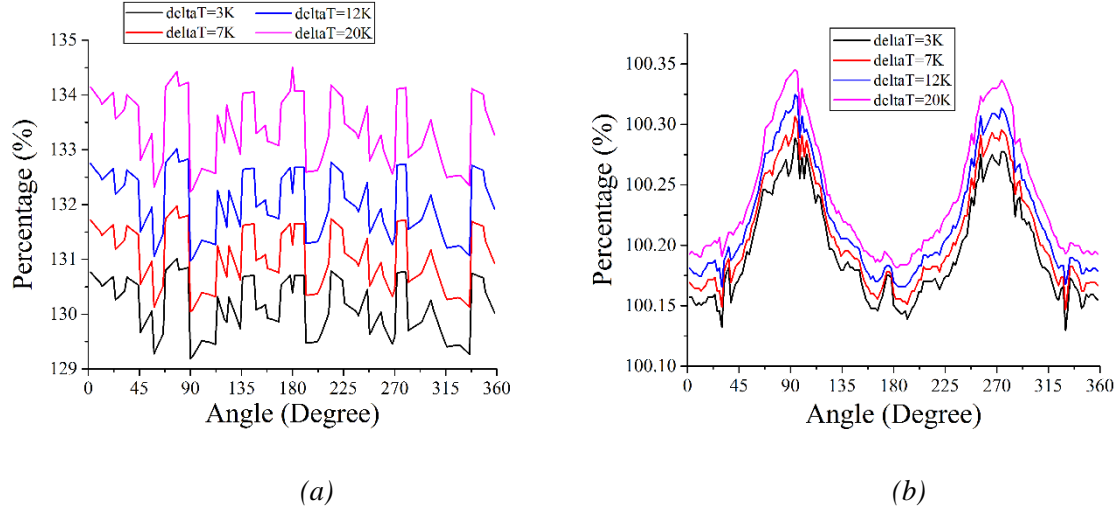
*Fig. 4.28. Field distortion on yz plane under various temperature difference ($R_c = 1mm$, $a = 0.5$, fresh material) for (a) b=1.001, and (b) b=5.*

Error is listed in Table. 4.24 for better understanding. The region distorted by the cavity is five times the cavity radius and it is applicable for all temperature difference levels studied in this project (the maximum absolute difference between distortion percentage and 100% is 0.67%). Besides, the maximum fluctuation percentage on yz plane is 2.32%, when the corresponding maximum distortion percentage is 134.2%. Therefore, field distortion on yz planes tends to be nearly constant.

Table. 4.24. Error in field distortion on xy and yz planes with different temperature difference (fresh material, $R_c = 1mm$, $a = 0.5$).

		xy plane		yz plane	
		Distortion - max (%)	Distortion - min (%)	Distortion - max (%)	Distortion - min (%)
ΔT = 3K	b = 1.001	130.88	32.07	131.01	129.19
	b = 3	100.91	96.97	101.05	100.64
	b = 5	100.39	99.36	100.29	100.13
ΔT = 7K	b = 1.001	131.81	28.81	131.97	130.05
	b = 3	100.93	96.93	101.02	100.69
	b = 5	100.32	99.35	100.31	100.15
ΔT = 12K	b = 1.001	132.81	25.17	133.02	130.97
	b = 3	100.95	96.89	101.00	100.75
	b = 5	100.26	99.35	100.32	100.17
ΔT = 20K	b = 1.001	134.21	20.28	134.50	132.23
	b = 3	100.97	96.86	100.98	100.85
	b = 5	100.21	99.33	100.35	100.18

Material Properties

To study the influence of material properties on field distortion, four groups of cavity conditions are considered in each type of material. The first condition is that a 1mm spherical cavity is located in the middle of the insulation when $\Delta T = 3K$ (condition A) and the second is that a 1mm spherical cavity is located in the middle of the insulation when $\Delta T = 12K$ (condition B). In the third case, a 1mm spherical cavity is located closer to the conductor when $\Delta T = 3K$ (condition C) and the fourth condition is that a 0.5mm spherical cavity is located in the middle of the insulation when $\Delta T = 12K$ (condition D).

The setting can possibly seperate the influence of cavity location (comparison of A with C), temperature difference (comparison of A with B) and cavity size (comparison of B with D) on field distortion. When the influence of material properties is to be researched, the corresponding conditions in each material, e.g. condition A in fresh material and condition A in aged material, are compared.

Field distortions on xy and yz planes are given in Figs 4.29 and 4.30 respectively. For the aged material, the trend is similar to that in fresh material. The field distortion is more serious when the cavity is closer to the conductor. It is also more serious under higher temperature difference level. Cavity size is of little influence on the electric field distortion surrounding the cavity. Besides, the variation in cavity location or temperature difference has more significant influence on field in aged material than in fresh material. The reason for this is that the temperature coefficient of electrical conductivity, A of aged material is much larger than that of fresh material (see Table. 3.1).


(a)   *(b)*
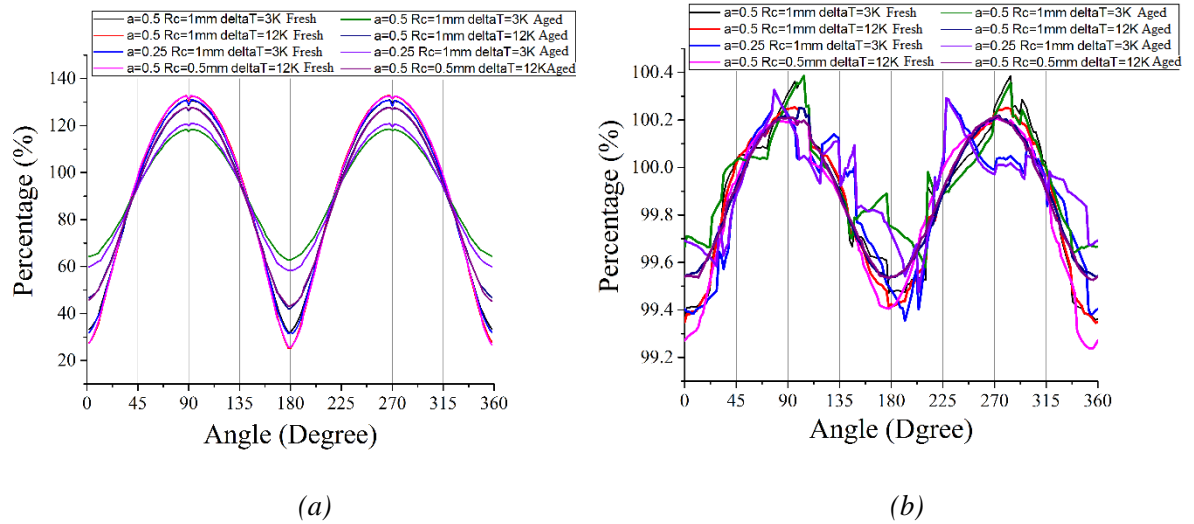
Fig. 4.29. Field distortion on xy plane under different material properties (a) b=1.001, and (b) b=5.
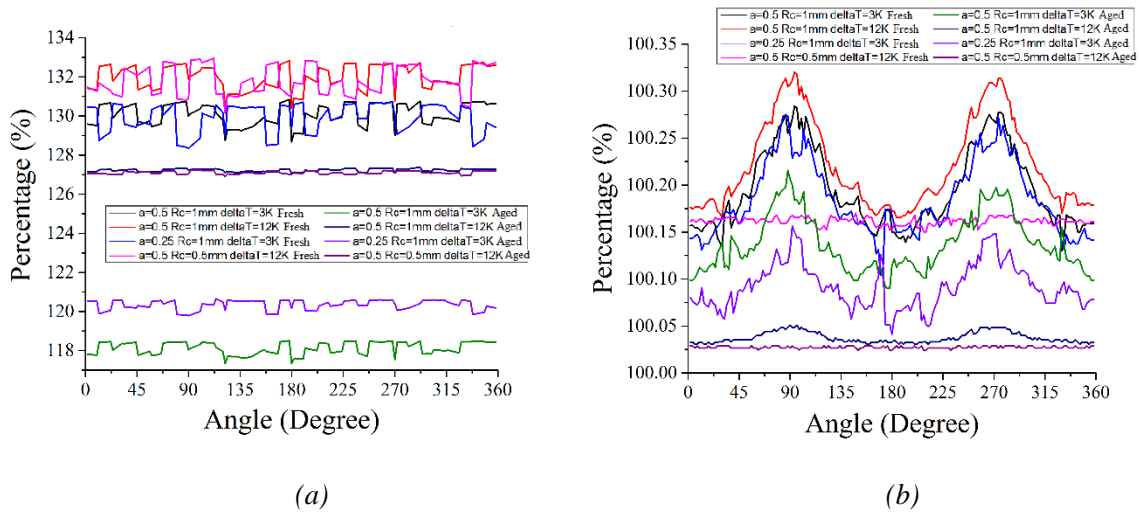
Fig. 4.30. Field distortion on yz plane under different material properties (a) b=1.001, and (b) b=5.

Another point is that at the same temperature difference, cavity location and cavity size, field distortion in fresh material is more serious than in aged material. It is also related to the electrical conductivity: electrical conductivity value of fresh material is higher than that of aged material at the same position in the insulation layer and temperature difference level [as shown in Fig. 4.17(b)].

Table. 4.25 lists the field distortion data for better understanding. Field distortion on yz plane is acceptably constant with slight fluctuation. Besides, the region possibly distorted by the spherical cavity is limited to five times cavity radius and the conclusion is applicable for aged material as well.

Cavity Size

Electrical conductivity is the key factor determining the distortion condition by the single spherical cavity, and therefore cavity size is not regarded as the parameter influencing the field distortion. However, it can influence the volume of the region where the field can possibly be distorted.

It is assumed that the spherical cavity is located in the middle of g fresh material insulation when $\Delta T = 12K$. Field distortion on xy and xz planes is listed in Table. 4.26. Though cavity radius varies, the region possibly distorted by the cavity is limited to five times the cavity radius: volume of the region changes, while the radius ratio to the cavity radius seems to be constant. Data listed in the table indicates that similar conclusions can be drawn, i.e. field distortion on yz plane is stable and the fluctuation region is less than 3%.

4.5.3 Summary

Field distribution and field distortion in the region surrounding the cavity has been researched. A 3D model is used in the research and field distortion condition on three planes is studied separately. Both

field distribution and field distortion on xy and xz planes are similar, while they are different on the yz plane.

On xy and xz planes, the cavity enhances the field in the region from $45° \leq \theta \leq 135°$ and $225° \leq \theta \leq 315°$, and it reduces the field in the remaining regions. Therefore, the volume of the field enhancement region (region A and C in Fig. 3.2) is equal to that of the field reduction region (region B and D in Fig. 3.2). Field strength and field distortion are nearly constant with slight fluctuation on the yz plane. This is due to the slight variation in distance from the cable centre and the precision of meshing used in the simulation.

Table. 4.25. Error in field distortion on xy and yz planes with different material properties.

		xy plane		yz plane	
		Distortion - max (%)	Distortion - min (%)	Distortion - max (%)	Distortion - min (%)
$R_c = 1mm, a = 0.5, \Delta T = 3K$ Fresh	b = 1.001	130.88	32.07	130.84	128.68
	b = 3	100.91	96.97	100.74	100.64
	b = 5	100.39	99.36	100.28	100.13
$R_c = 1mm, a = 0.5, \Delta T = 12K$ Fresh	b = 1.001	132.81	25.17	132.83	130.39
	b = 3	100.95	96.89	100.83	100.73
	b = 5	100.26	99.35	100.32	100.17
$R_c = 1mm, a = 0.25, \Delta T = 3K$ Fresh	b = 1.001	130.87	30.91	130.71	128.34
	b = 3	100.93	97.12	100.75	100.62
	b = 5	100.32	99.35	100.27	100.10
$R_c = 0.5mm, a = 0.5, \Delta T = 12K$ Fresh	b = 1.001	132.75	25.66	132.95	130.13
	b = 3	100.90	96.90	100.79	100.68
	b = 5	100.21	99.24	100.17	100.15
$R_c = 1mm, a = 0.5, \Delta T = 3K$ Aged	b = 1.001	118.53	62.73	118.50	117.33
	b = 3	100.72	98.36	100.52	100.44
	b = 5	100.36	99.58	100.22	100.09
$R_c = 1mm, a = 0.5, \Delta T = 12K$ Aged	b = 1.001	127.75	42.12	127.37	127.05
	b = 3	101.00	97.83	100.14	100.12
	b = 5	100.22	99.53	100.05	100.03
$R_c = 1mm, a = 0.25, \Delta T = 3K$ Aged	b = 1.001	120.95	58.33	120.66	119.80
	b = 3	100.84	98.39	100.36	100.28
	b = 5	100.33	99.48	100.16	100.04
$R_c = 0.5mm, a = 0.5, \Delta T = 12K$ Aged	b = 1.001	127.73	43.22	127.22	126.90
	b = 3	101.00	97.81	100.13	100.11
	b = 5	100.22	99.53	100.03	100.02

Table. 4.26. Error in field distortion on xy and yz planes with different cavity size (fresh material, $a = 0.5$, $\Delta T = 12K$).

		xy plane		yz plane	
		Distortion - max (%)	Distortion - min (%)	Distortion - max (%)	Distortion - min (%)
$R_c = 0.5$mm	b = 1.001	132.75	25.66	132.69	130.45
	b = 3	100.90	96.90	100.95	100.72
	b = 5	100.21	99.24	100.25	100.08
$R_c = 1$mm	b = 1.001	132.81	25.17	132.80	130.54
	b = 3	100.95	96.89	101.00	100.75
	b = 5	100.26	99.35	100.28	99.89
$R_c = 1.5$mm	b = 1.001	132.70	24.95	134.32	131.53
	b = 3	100.95	96.99	101.07	100.50
	b = 5	100.23	99.36	100.38	99.93

Electric field distortion conditions on xy and yz planes under different cavity locations, temperature differences and material properties are researched. Electric field tends to be more seriously distorted when the cavity is closer to the conductor and higher temperature difference. Besides, under the same cavity location and temperature difference condition, field distortion is more serious in fresh material. The trend follows the value of electrical conductivity of the insulation.

Together with the results from the field distortion value under different cavity size, it can be concluded that the region possibly distorted is also spherical and the size is not higher than five times the cavity radius: the volume of the affected region can possibly change with cavity size, while the radius ratio remains constant.

4.6 Conclusions

In this chapter, equations describing the k value across the insulation at a given temperature difference and applied voltage, the critical temperature difference level for field reversal occurrence and temperature distribution across the insulation at DC steady are believed to be reasonable due to the small difference between the simulation and calculation from the corresponding equation. In calculating the electric field distribution across the insulation at DC steady state, the error value can be over 5% and the condition can possibly be improved by increasing the accuracy of meshing work. This conclusion is applicable for both groups of material properties and both groups of electrical conductivity expressions.

The critical temperature difference level for field reversal occurrence of aged material, which is highly degraded, is lower than that of fresh material under the same cable geometry. Accordingly, field reversal can possibly happen over years of cable operation, even though the phenomenon does not appear at the

beginning of the cable's operating life. The comparison in electric field distribution across the insulation indicates that the replacement in electrical conductivity expression is acceptable in describing the cable condition across its lifetime.

The 2D and 3D models are compared to provide reference for the correct model selection. 2D model helps reduce the length of simulation time, and it has been shown that the 2D model is a better choice in understanding electric field and temperature distribution when no cavity appears inside the cable, and understanding temperature distribution even though cavity appears, or the electric field in the region not close enough to the cavity. When the electric field in the cavity is researched and cavity field is the key factor influencing the phenomenon involved in the research, 3D model is the only choice, though the solution time of the 3D model can be at least six times longer than the 2D model when the same meshing work precision is applied.

Research in field enhancement by a single spherical or ellipsoidal air-filled cavity at DC steady state shows that Equation (3.34) is acceptable in describing field enhancement with the error percentage level between simulation and calculation results not higher than 5.5% (lower than 4% under most conditions). Reasons for the error can be the assumptions that the average field inside the cavity is used as the strength describing cavity field, and the accuracy of meshing work.

Having finished the model comparison and research in field enhancement in the cavity, field distortion by the cavity in region surrounding the cavity is studied. It is found that electric field strength and field distortion on xy and xz planes are similar and volume of field enhancement region tends to equal to that of the field reduction region. When peak error is set at 1%, the radius ratio of possibly distorted region to the cavity seems to be constant (being 5), though the volume of the region increases with cavity radius. This conclusion is applicable across the cavity locations, cavity sizes, temperature difference levels and material properties studied in this project.

Chapter 5. Partial Discharge Modelling Work in HVDC XLPE Cable

This chapter discusses and introduces the assumptions and important equations in time-dependent modelling work. Flow chart and parameters used in the modelling work of DC PD in HVDC XLPE cable are listed in this chapter.

5.1 Assumptions for Modelling Work

Characteristics of partial discharge, including the discharge magnitude and repetition rate in HVDC XLPE cable are studied via the modelling work. The assumptions are as follows:

- The cavity geometry is independent of discharge activities. Shape and volume of the cavity do not change over the whole simulation process;

- There is a ramping stage before the applied voltage reaches the constant value. Both level and polarity of the voltage do not change over the period of the study;

- The change in pressure and temperature during the discharge is ignored. The reason is that the time interval between two events at DC voltage can be as long as several minutes and the number of events is seldom;

- The electric field component induced by the applied voltage in the cavity is assumed unchangeable across the partial discharge activity. The reason is that the time length of discharge is short (in several nano-seconds) and the variation of field induced by the applied voltage is narrow;

- In calculating the charge decay, it is assumed that charges are not trapped in the insulation and the effect on the electrical conductivity by the charge accumulation is ignored. The assumption is set to simplify the simulation;

- The region for the streamer-like discharge occurrence is assumed cylindrical. It helps calculate the area for charge accumulation on the cavity surface;

- Simulation time step varies across the whole process according to the situation of applied voltage and the occurrence of partial discharge. In the ramping stage, time step is set to be 10ms, as partial discharge tends to be more frequent at the stage. In the constant stage, time step is set to be 1s. Time interval across the discharge occurrence is set to be 10 nano-seconds. Total length of simulation is set to be 10 hours to ensure that the HVDC cable stays at steady state for long;

- Finally, cavity field strength is represented by the electric field strength at the cavity centre. Electric field strength distribution in the cavity tends to be somewhat uniform (as given in Fig. 4.15). Modelling work is simplified accordingly and the corresponding error level should not be high.

5.2 Partial Discharge Processes

Referring to the PD processes discussed in Chapter 2, cavity field follows the component induced by the applied field before discharge ever happens as the amount of charge and field produced by the charges on the cavity surface and inside the insulation bulk are both zero.

When the condition to discharge is satisfied, i.e. the cavity field exceeds the inception field and there is at least one starting electron available in triggering the electron avalanche, partial discharge happens: the cavity field drops to a low level defined as the residual field; the cavity becomes conductive during the discharge and nonconductive at the end of the PD activity; at first current through the cavity increases and then drops to zero at the end of discharge; charges are induced inside the cavity and the number is related to the electric field strength collapsed during the activity.

It is possible for charge decay to happen across the process between two consecutive activities. When a voltage with constant magnitude and polarity is applied on the high voltage cable, the cavity field and component caused by the applied field are always in the same direction. There is a possibility of charge recombination happening on cavity wall at AC voltage due to charge movement along the surface. At DC voltage, however, charge migration along the cavity wall is hard due to the polarity of cavity field. The phenomenon that charges transport through the bulk of insulation, which is not significant at AC voltage, is the key reason for the charge decay. The phenomenon is illustrated in Fig. 5.1.

Under AC voltage, the effect of decayed charges by charge recombination is not considered because they disappear. Under DC voltage, the total amount of charge in insulation does not change across the charge decay process because charges migrate through the bulk of insulation, and they are then accumulated in the bulk. Charges accumulated in the insulation can influence the cavity field. Electric field induced by charge is inversely related to the square of distance of charge from the cavity centre, and the contribution of accumulated charges to the cavity field keeps decreasing.

(a)   *(b)*
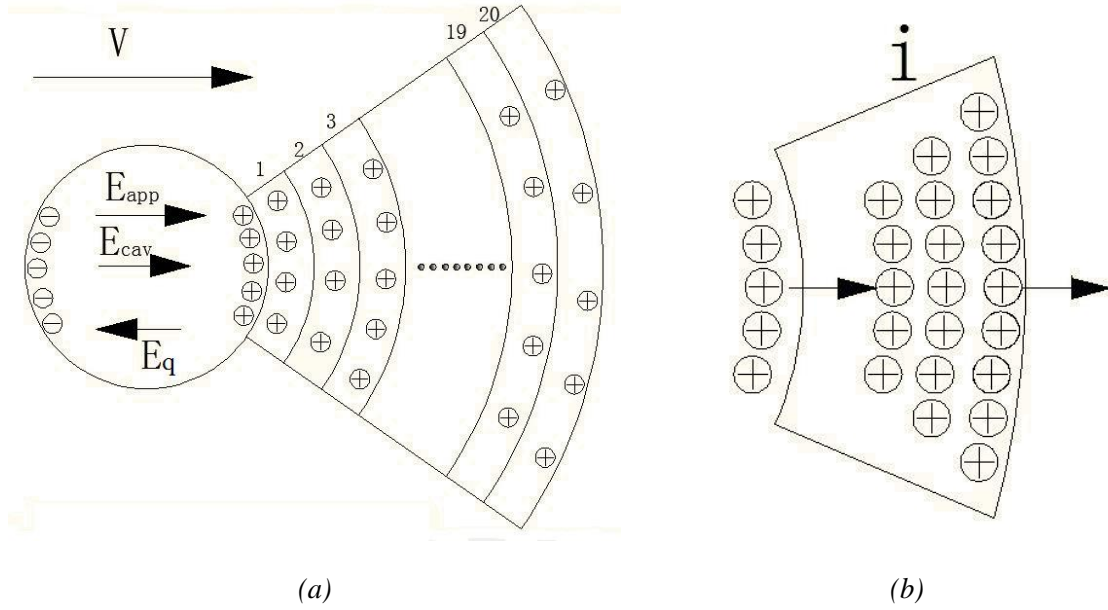
Fig. 5.1. (a) Charge migration into bulk of insulation. (b) Charge accumulation at a single layer.

Charge decay or the decay in field produced by the charges on the cavity surface and charges accumulated in the insulation bulk is important for the DC PD characteristics, especially at the DC steady state. During the ramping stage, increase in the applied voltage is the main reason in the variation or recovery of cavity field. The reason is that no charges are present in the cavity before the occurrence of the first event and the rise in the applied field is much faster than the variation of field produced by charges on the cavity surface and charges inside the insulation bulk due to charge decay starting from the end of the first PD activity. When the applied voltage is constant but the cable is under transition stage, field variation is related to electrical conductivity value, and therefore, the cavity location and the cable loading level can influence the cavity field variation. When the HVDC cable is at a steady state, the decay in field produced by charges on the cavity surface and charges inside the insulation bulk is the only way that cavity field recovers to the level exceeding the inception field after the previous event extinguishes.

The equation describing the cavity field [Equation (2.20)] is as follows:

$$\overrightarrow{E_{cav}} = \overrightarrow{E_{app}} + \overrightarrow{E_q} \tag{5.1}$$

$\overrightarrow{E_{app}}$ is the component created by the externally applied voltage, and $\overrightarrow{E_q}$ is the field produced by charges on the cavity surface and those migrated into the insulation. The geometry determined factor, f, does not appear in the equation, as $\overrightarrow{E_{app}}$ is extracted from simulation for the cavity field without PD occurrence and the field enhancement by the cavity has been considered. The previously discussed processes repeats across the whole simulation process: discharge happens once the occurrence conditions are satisfied, and charges are induced in the activity and decay between two consecutive activities through the bulk of the insulation.

5.3 Numerical Calculation

Until now, there has been no model available in describing DC PD numerically. Therefore, the research on PD characteristics is preliminary. For the AC voltage, when Niemeyer's model was published, it was widely accepted because the match between simulation and experiment results on PD pattern and repetition rate was good. Niemeyer's model is used in this study as well. Though the cable is at the DC steady state, the cavity is always under transition: the amount of surface charge and cavity field keep varying across the simulation process. Therefore, Niemeyer's model is expected to be applicable in describing the DC PD characteristics, along with the modification in the description of the charge decay process.

Equations used in the modelling work are listed in this section, including the level of specific field strength, charge associated with discharge and PD occurrence probability.

5.3.1 Electric Field Calculation

The key factor in determining the discharge characteristics is the cavity field. $\overrightarrow{E_{app}}$ is calculated as the cavity field when no discharge occurs and it is extracted from the time-dependent simulation. Field produced by charges on the cavity surface is calculated as [49]

$$E_q = \frac{q}{\varepsilon_0 \pi R_c{}^2 [1 + \varepsilon_r(K - 1)]} \qquad (5.2)$$

where q is the amount of surface charge and K is the geometry coefficient, which equals 3 for the spherical cavity. When the electric field induced by the charge accumulated in the bulk of the insulation is calculated, the cavity radius, R_c, is replaced by the associated distance from the cavity centre.

Inception field is given as [49]

$$E_{inc} = (E/p)_{cr} p [1 + \frac{B}{(2pR_c)^n}] \qquad (5.3)$$

where $(E/p)_{cr}$ is the critical value of pressure reduced electric field, p is the gas pressure, and B and n are parameters in streamer criterium [48]. Any gas pressure variation is ignored across the whole process and the value of all parameters in Equation (5.2) is constant at DC voltage. Breakdown strength of air is $3kV. mm^{-1}$ at atmospheric pressure [57] and the inception field is set to be equal to this level.

Residual field at the end of the discharge should be closely related to the over-voltage (Δv), the difference between the occurrence field and the inception field.

$$\Delta v = v(\theta) - v_{s\infty} \qquad (5.4)$$

$$v_r = v_{rmin} + (v_{s\infty} - v_{rmin})\exp(\frac{-\Delta v}{v_{s\infty} - v_{rmin}}) \tag{5.5}$$

Δv and v_r represent over-voltage and dynamic residual voltage. $v(\theta)$ is the cavity voltage at the phase angel θ, $v_{s\infty}$ is the inception voltage and v_{rmin} is the minimum residual voltage [79]. As the electric field strength inside the cavity is nearly uniformly distributed and the cavity geometry is assumed unchangeable, all voltage parameters in Equation (5.5) can be replaced by the associated electric field factor:

$$E_r = E_{rmin} + (E_{s\infty} - E_{rmin})\exp(\frac{-E_{over}}{E_{s\infty} - E_{rmin}}) \tag{5.6}$$

where all subscripts in the equation have the same meaning as the corresponding ones in Equation (5.5).

5.3.2 Charge Amount Associated with Discharge Calculation

Real charge induced inside the cavity across the discharge event is calculated as follows:

$$q = \pi\varepsilon_0 R_c{}^2[1 + \varepsilon_r(K - 1)]\Delta E \tag{5.7}$$

ΔE is the electric field collapsed in discharge

$$\Delta E = E_{occ} - E_r \tag{5.8}$$

E_{occ} is the cavity field strength at PD occurrence. Charge decay happens between two consecutive PD activities. There can be a special condition: when the loading level is high and the cavity is close to the conductor, $\overrightarrow{E_{app}}$ in Equation (5.1) keeps decreasing in the transition stage and the reversal of the cavity field polarity may possibly happen. Under this condition, charge recombination on the cavity surface happens, and it is calculated as [49]

$$dq = \frac{\pi}{2}(\sigma_s E_{cav} 2R_c{}^2)dt \tag{5.9}$$

where σ_s is the electrical conductivity of cavity surface and dt is the time step in calculating the charge decay.

When the cavity field polarity does not change, charges decay through the bulk. In calculating the charge distribution in the bulk, the region surrounding the cavity is uniformly divided into 20 layers with the same thickness. Influence of charges in the bulk of insulation on electric field at the cavity centre is calculated according to Equation (5.2) and it decreases with the square of distance to the cavity centre.

The region with two times the cavity radius is considered and the effect of charges in the remaining part is not considered due to the distance and the amount of charge accumulated. According to

Equation (5.2), the field produced by the charge inside the insulation bulk is inversely related to the square of distance from the cavity centre. Therefore, compared to the charge on the cavity surface, if the amount of charge is equal, field produced by the charge on two times cavity radius is one quarter of those on the cavity surface. Effect of charges on further region is smaller and it can be believed that two times cavity radius is large enough to consider the effect of charges inside the insulation bulk.

The number of charges on each layer is the sum of charges accumulated on the layer before the charge decay process at the time point and the amount of charge decayed from the previous layer (or from cavity surface for the first layer) subtracting the charge migrating into the next layer [shown in Fig. 5.1(b)]. The amount of charge of the i_{th} layer at time t is calculated as [114]

$$Q_t = Q_{t-dt} + j_{i-1}S_{i-1}dt - j_i S_i dt \tag{5.10}$$

and charge on the cavity wall is calculated as

$$Q_t = Q_{t-dt} - j_1 S_1 dt \tag{5.11}$$

where j is the average current density of the layer, and S is the area of surface between the two consecutive layers. Value of j is extracted from the time-dependent modelling work. As the cavity is spherical, the surface is actually fanshaped. Q_{t-dt} is the number of charges prior to the decay process.

5.3.3 Partial Discharge Occurrence Probability Calculation

Partial discharge is a random process due to the starting electron generation. Starting electron is generated in two ways, namely surface emission and volume generation.

Considering surface emission, including electrons detrapped from traps inside the insulation, electron released via ion impact, field emission from the electrode and surface photo effect, surface emission is satisfied with the Richardson-Schottky scaling and can be expressed as follows:

$$N_{dt0} = \xi(q/e) \tag{5.12}$$

$$N_{dt} = N_{dt0}\exp(-t/\tau) \tag{5.13}$$

$$N_{e1} = N_{dt}v_0\exp(-\frac{\phi - \sqrt{E/(4\pi\varepsilon_0)}}{k_b T}) \tag{5.14}$$

N_{dt0}, N_{dt} and N_{e1} are the number of detrappable electrons produced in discharge, the number of detrapped electrons and the generation rate of the first electron respectively. In these equations, ξ is a factor describing the charge carrier number leading to detrappable electrons, q is the amount of charge on cavity surface, e is the charge value of electron, t is time period since the end of the previous PD activity, τ is decay time constant, v_0 is the fundamental phonon frequency, ϕ is the work function, ε_0 is the vacuum permittivity value, E is cavity field, k_b is the Boltzmann constant and T is the

temperature inside the cavity [49].

The probability of electron generation per second from volume generation, including electron detachment from negative ions and radiative gas ionization [48, 49], is calculated as follows:

$$v = \frac{U_0}{U_0^{inc}} \tag{5.15}$$

$$\eta_i = C_{rad}\phi_{rad}(\rho/p)_0 \tag{5.16}$$

$$V_{eff} = \frac{4}{3}\pi\left(\frac{l}{2}\right)^3(1 - v^{-\beta}) \tag{5.17}$$

$$N_{e2} = \eta_i p V_{eff}(1 - \frac{\eta}{\alpha}) \tag{5.18}$$

where v, η_i, V_{eff} and N_{e2} are the ratio of the applied voltage to the inception voltage, the function describing radiative ionisation mechanism, effective ionisation volume and first electron generation rate respectively. U_0 and U_0^{inc} are the applied voltage and the inception voltage respectively. C_{rad} is the volume ionisation law parameter and it indicates the relationship between gas and radiation. ϕ_{rad} is the radiation quantum density, ρ is the mass density of gas inside void, p is cavity gas pressure and $(\rho/p)_0$ is the pressure reduced gas density. l is the cavity height, β is the exponent in approximation for effective ionisation coefficient, η is gas attachment coefficient and α is the gas ionisation coefficient [48, 49].

Consequently, starting electron generation is expressed as follows:

$$N_e = N_{e1} + N_{e2} \tag{5.19}$$

and the PD occurrence probability is expressed as follows:

$$probability = 1 - \exp(-N_e\Delta t) \tag{5.20}$$

Δt is the time period since the last discharge [44]. Partial discharge is a random process and the probability is compared with a random number between zero and one: if the probability value is higher than this random number, PD occurs.

5.4 Flow Chart

The flow chart is illustrated in Fig. 5.2. In the figure, t_{ramp} is the time length of the ramping stage and $t_{simulation}$ is the length of the whole simulation process (10 hours, 36000s). t_{ramp_step} is the time step used in the ramp stage without PD occurrence (0.01s), t_{step} is the time step in the constant voltage stage without PD occurrence (1s) and t_{PD_step} is the time step used across the discharge (10 nano-seconds). E_{inc} is the inception field and E_{res} is the residual field. The parameter q in the figure includes

the charge induced across the discharge (discharge magnitude) and charge on the cavity surface.
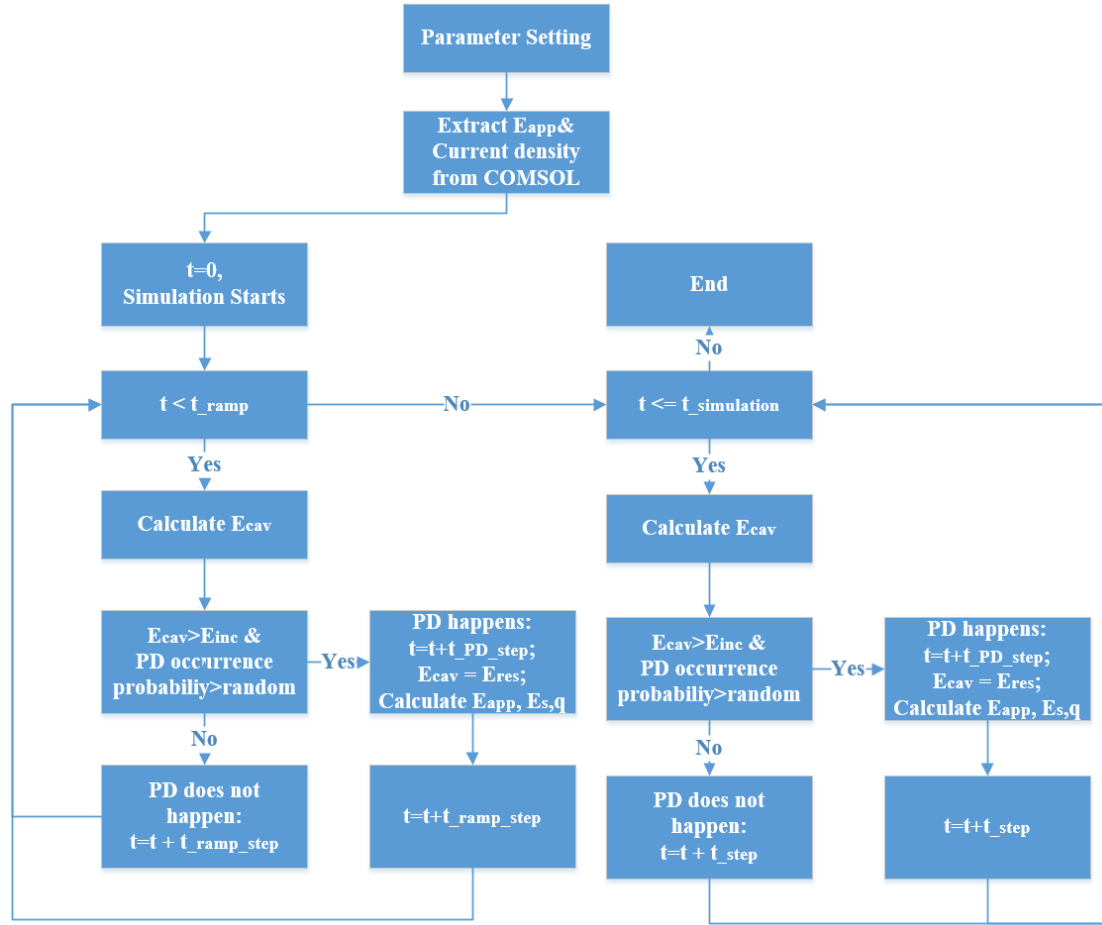

Fig. 5.2. Flow chart for the modelling work.

5.5 Parameters Used in Partial Discharge Modelling Work

The value of the parameters used in DC PD modelling work are listed in Table. 5.1. The cable geometry is different from that used in DC steady state research. The reason is that the cavity field is low compared to the inception field or even lower than the inception field, especially when the cavity is close to the conductor under high temperature difference or loading level. Variation in geometry can possibly lead to different electric field and temperature distribution and the critical temperature difference for field reversal occurrence (as given in Fig. 4.5), but the conclusion is that the equations derived in Chapter 3 should be reasonable for the geometry listed in Table. 5.1. The cable geometry is given in [102] and the electric field in the middle of insulation is 16.67 kV.mm^{-1}, which is much higher than the inception field (3 kV.mm^{-1}).

Table. 5.1. Parameters used for DC PD simulation [49, 102].

Parameter Name	Value	Unit	Explanation
V	150	kV	Applied Voltage
Ramp	5.3	$kV.s^{-1}$	The ramp value
R_i	18	mm	Inner Insulation Radius
R_o	27	mm	Outer Insulation Radius
R_c	1	mm	Cavity Radius
L	1	m	Cable Length
ε_r	2.3		Relative Permittivity
v_0	10^{14}	Hz	Fundamental Photon Frequency
p	101	kPa	Gas Pressure in Cavity
$C_{rad}\phi_{rad}$	2×10^6	$kg^{-1}s^{-1}$	Product of interaction of the radiation of the radiation with the gas and the radiative cosmic and radioactive quantum flux density
$(\rho/p)_0$	10^{-5}	$kg.(m^{-3}Pa^{-1})$	Pressure Reduced Gas Density
ϕ	1	eV	Effective work function
ξ	0.02		Proportionality factor
τ	2	ms	Effective decay time constant
σ_{air}	1×10^{-16}	$S.m^{-1}$	Conductivity of Air without PD Occurrence
a	0.25, 0.5, 0.75		Distance Coefficient
I	1, 2, 4	kA	Current through Conductor
A	3.2781	$A.m^{-2}$	Constant of Fresh Material
	3.6782×10^7	$A.m^{-2}$	Constant of Aged Material
B	2.7756×10^{-7}	$m.V^{-1}$	Constant of Fresh Material
	1.086×10^{-7}	$m.V^{-1}$	Constant of Aged Material
φ	0.56	eV	Thermal Activation Energy of Fresh Material
	0.98	eV	Thermal Activation Energy of Aged Material

5.6 Discussion

There are four points for discussion. First, in the assumption phase, the time step in the ramping stage is set at 10ms. It is derived from the comparison of PD numbers in the ramping stage under the setting of various time step levels. Six time steps are set, namely 1ms, 5ms, 10ms, 50ms, 100ms and 500ms. The comparison indicates that the number of discharge equals the three time steps, which are 1ms, 5ms and 10ms. When the time step is set at 50ms, discharge magnitude is 1 less than that of the condition when the time step is 10ms. When the time step is higher than 50ms, the difference is larger. Therefore, time step should be set at 10ms to reduce the simulation time.

Second, insulation degradation is considered in the modelling work and material properties should change with time. There will be two groups of insulation results: at the early stage, material properties are the same as the fresh material. Under this condition, the applied voltage increases from zero and

reaches a constant magnitude after the ramping stage. To study discharge characteristics when the insulation is greatly degraded, the voltage is constant as the cable is assumed to operate continuously under the constant voltage and the loading level.

Third, to understand the influence of cavity location and loading level (or temperature) on discharge characteristics, three different cavity positions ($a = 0.25$, $a = 0.5$ and $a = 0.75$) and three current levels (1kA, 2kA and 4kA) are used and the occurrence of field reversal is taken into consideration. The maximum current level is set to be 4kA as the temperature in the conductor under the condition (357.55K, 84.4℃) is close to the maximum operating temperature of XLPE (363.15K, 90℃). The corresponding temperature difference across the insulation is 3.52K, 14.09K and 56.40K.

Fourth, to simplify the modelling work, charges accumulated in the bulk are calculated according to the current density in the region between the cavity and the cable sheath. It can result in a confusion that the speed of charge propagation towards the conductor can be different from the speed towards the sheath. According to Fig. 4.17, electrical conductivity of insulation further away from the cable centre is lower. The comparison between the current in the region between the cavity and the conductor (Current 1) and the region between the cavity and the sheath (Current 2) is given in Table. 5.2. The value is calculated as the product of electrical conductivity, electric field and the square of the distance from the cavity centre, which represents the value of jS in Equation (5.10). The value of o indicates the distance from the cavity centre, where the distance is calculated as follows:

$$D_c = oRc \tag{5.21}$$

and the ratio is calculated as Current 1 over Current 2.

Table. 5.2 indicates that the difference between Current 1 and Current 2 is small and the difference is higher in the region further away from the cavity centre. The field produced by the charges decreases with the square of the distance from the cavity centre, and the increase in the difference is acceptable. Therefore, the simplification that only charges propogation towards the cable sheath is calculated is reasonable.

Table. 5.2. Charge propagation speed comparison in two regions.

ΔT	o	Fresh Material		Aged Material		Ratio (%)	
		Current 1 (A)	Current 2 (A)	Current 1 (A)	Current 2 (A)	Fresh material	Aged material
3.52	1.001	5.74E-16	5.86E-16	3.89E-16	4.02E-16	97.93	96.80
	1.1	8.66E-16	9.13E-16	4.48E-16	4.68E-16	94.81	95.80
	1.2	1.21E-15	1.26E-15	5.12E-16	5.36E-16	95.59	95.44
	1.5	2.34E-15	2.52E-15	7.48E-16	7.98E-16	92.75	93.75
	2	4.72E-15	5.17E-15	1.26E-15	1.38E-15	91.32	91.68
14.09	1.001	6.20E-16	6.16E-16	4.82E-16	4.82E-16	100.70	99.86
	1.1	1.03E-15	1.09E-15	5.96E-16	6.08E-16	94.67	98.00
	1.2	1.52E-15	1.59E-15	7.23E-16	7.55E-16	95.51	95.79
	1.5	3.12E-15	3.39E-15	1.16E-15	1.24E-15	92.05	93.59
	2	6.48E-15	7.13E-15	2.09E-15	2.30E-15	90.91	91.25
56.40	1.001	7.00E-16	6.00E-16	3.94E-16	3.42E-16	116.59	115.22
	1.1	1.95E-15	2.15E-15	9.49E-16	9.01E-16	90.87	105.29
	1.2	3.45E-15	3.72E-15	1.60E-15	1.68E-15	92.84	95.52
	1.5	8.15E-15	9.17E-15	3.55E-15	3.78E-15	88.83	93.91
	2	1.80E-14	2.02E-14	7.48E-15	8.20E-15	88.69	91.26

5.7 Conclusions

It is assumed that the geometry and volume of cavity are constant across the simulation. The applied voltage reaches the constant level after the ramping stage, and the temperature and pressure inside the cavity are constant. The three-time step levels are applied in simulation according to the voltage and occurrence of discharge, charges are not trapped in the bulk of insulation and the cavity field is indicated by the level at the cavity centre.

The DC PD process is similar to the AC PD process except the charge decay between the two discharge activities. The discharge recombination can possibly happen on cavity surface due to polarity reversal of applied field at AC voltage, but the phenomenon hardly happens at DC voltage. The reason for charge decay is charge migration into the bulk of insulation. Unlike the charge recombination, though the total amount of charge is constant, the charge field decreases as the distance of the decayed charges from the cavity centre increases.

Niemeyer's model is used in the modelling work with a modification on the charge decay calculation. Equations describing the calculation in the electric field, the number of induced charges in a single event and decayed charges into the insulation bulk, along with the discharge occurrence probability are listed in this chapter. The flow chart and parameters are also listed in this chapter, while the PD results are presented in next chapter.

Chapter 6. HVDC XLPE Cable Partial Discharge Modelling Results

This chapter discusses the influence of cavity location and loading level on PD and the effect of material properties. This research represents preliminary modelling and simulation work on partial discharge in HVDC cable.

6.1 Applied Field Variation under Different Loading Levels

To study the discharge characteristics under different cavity locations and loading levels, the first step is to study the variation of field induced by the applied voltage in the cavity with time. Electrical conductivity determines the electric field distribution in the HVDC cable (as discussed in Chapter 4), which is determined by the local field and temperature.

Cavity field without occurrence of partial discharge when the distance coefficient, a, equals to 0.25 or 0.75 is illustrated in Fig. 6.1. In the ramping stage, cavity field follows the waveform of the applied voltage, which linearly increases. When the cavity location is constant, cavity field value at the end of the ramping stage is nearly independent of the loading level [as given in Fig. 6.1(b)]. The reason is that time length of the ramping process is not long and the temperature changes a little during this stage, even though the current in the conductor is 4kA. The applied voltage is dominant in the electrical conductivity value and therefore, in the cavity field.

| (a) | (b) |
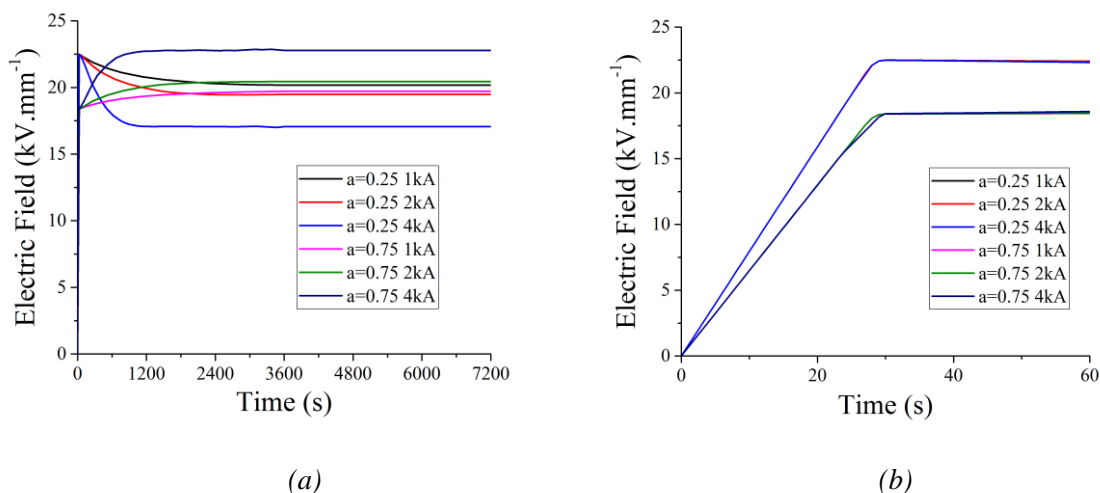
Fig. 6.1. Variation of cavity field without PD occurrence with time for $a = 0.25$ and $a = 0.75$ in (a) 36000s, and (b) 60s.

After the applied voltage reaches the constant stage, the cavity field varies on the transition stage. When the cavity is close to the conductor (a = 0.25), the cavity field keeps decreasing with time and the electric field strength at steady state is lower under higher loading level. When the cavity is further

away from the cable centre (a = 0.75), cavity field keeps increasing with time and field strength at steady state is higher under higher loading level. Field reversal happens when the current is 4kA and this value is chosen to demonstrate the effect of field reversal occurrence on discharge characteristics.

Cavity field without occurrence of partial discharge when the cavity is located in the middle of insulation is illustrated in Fig. 6.2. Field strength is independent of current level. However, the cavity field is slightly higher at higher current level (20.06 kV.mm^{-1} at 4 kA, 20.05 kV.mm^{-1} at 2 kA and 20.02 kV.mm^{-1} at 1 kA). The reason is that electrical conductivity of insulation in the middle of insulation increases with the local temperature or loading level as electric field strength is nearly independent of the temperature at that position. Higher conductivity value leads to higher field enhancement by the air-filled cavity at DC steady state according to Equation (3.34).
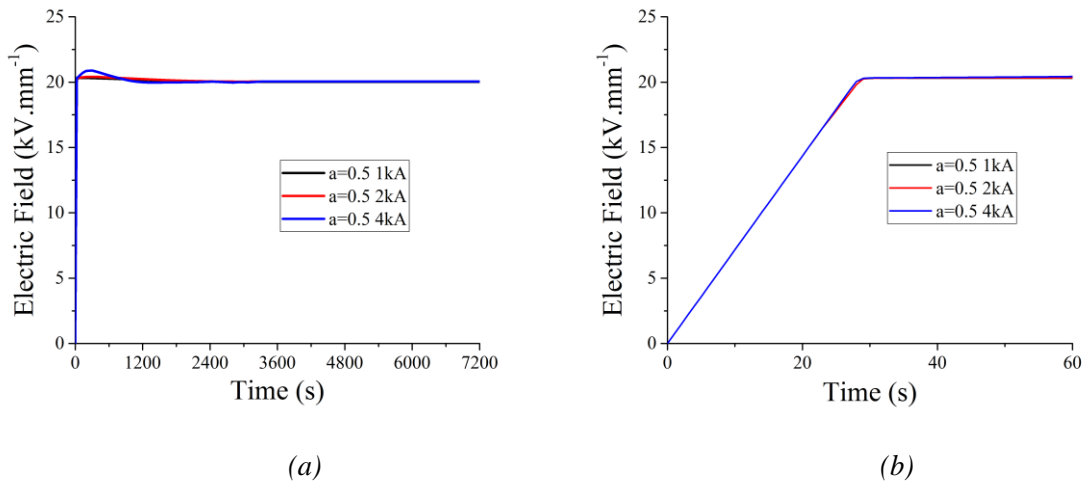
Fig. 6.2. Variation of cavity field without PD occurrence with time for $a = 0.5$ in (a) 36000s, and (b) 60s.

6.2 Partial Discharge under the Reference Condition

It is defined as the reference condition when a single spherical air-filled cavity is in the middle of the insulation and current through conductor is 2kA. Under the condition, both the cavity location and current in the conductor are between the other two cavity locations and two current levels. Cavity field is given in Fig. 6.3. Fig. 6.3 (a) shows the simulation results of the first hour and Fig. 6.3 (b) demonstrates the results of the first six minutes. The black line indicates the electric field in the middle of insulation without the cavity. Blue and red lines indicate the field inside the cavity with and without the occurrence of partial discharge and the pink line indicates the inception field, which is set to be 3kV.mm^{-1}.
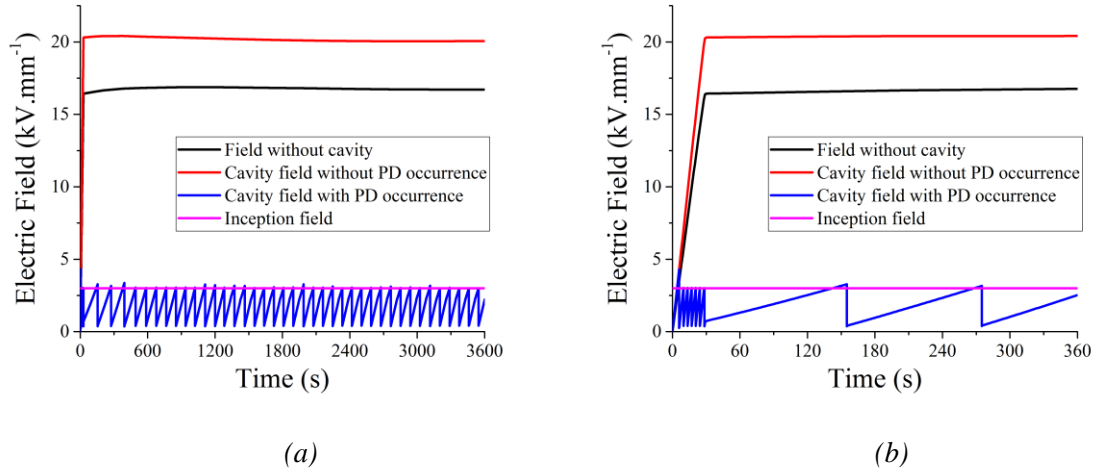
Fig. 6.3. Cavity field across the simulation process ($a = 0.5$, $I = 2kA$) for (a) 3600s, and (b) 360s.

Before the first discharge happens, cavity field equals to the value produced by the applied voltage ($\overrightarrow{E_{app}}$). Cavity field drops to the residual level at the end of the discharge event. Cavity field recovers to the inception field due to charge decay between two activities, and the variation of $\overrightarrow{E_{app}}$ in the ramping stage or transition stage where the applied voltage is constant.

Discharge tends to happen once the cavity field exceeds the inception field. This is due to the generation of the starting electron. Field induced by the applied voltage can be as high as $20kV.mm^{-1}$ and therefore, the field produced by the charges on cavity surface and in the insulation bulk can be higher than $17kV.mm^{-1}$ when the cavity field reaches the inception level. According to Equation (5.2), the number of charges available for the starting electron generation is large. Therefore, discharge occurrence probability is high and PD tends to happen in a short time after the cavity field exceeds the inception level. This phenomenon can indicate that discharge magnitude should possibly be independent of the voltage magnitude if there is a ramping stage before the voltage reaches the constant value: the occurrence field is determined by the inception field instead of the applied field.

The number of discharge activities is 421. Among them, six activities appear in the ramping stage. Time interval between two activities at steady state is around 86.54s (maximum at 126.62s and minimum at 82s). The reason for the long time interval is the slow charge decay between two activities at DC steady state.

The relationship between discharge magnitude and time is plotted in Fig. 6.4. Fig. 6.4 (a) illustrates the discharge magnitude in the first hour and Fig. 6.4 (b) mainly reflects the ramping stage. The induced charge with a high discharge magnitude (628.60 pC) is created across the event. It agrees with the phenomena given in [115] that the first discharge at AC voltage happens at the time point of $T/4$, where the magnitude of applied voltage reaches its peak value and the discharge magnitude is the highest.

97

The electron avalanche is the source to the induced charges in the first event. Cavity field drops to the residual level and the electron avalanche is more significant under higher electric field. The value of residual field therefore is lower under higher electric field [referred to Equation (5.6)]. There are no charges on the cavity surface from the previous one for the generation of starting electron of the first event and surface emission is the only source to the generation of starting electron for the first activity. Lag time is longer, and over voltage and the occurrence field is stronger. Discharge magnitude is determined by the electric field that has collapsed across the partial discharge, and the value for the first event is high.

(a)   *(b)*
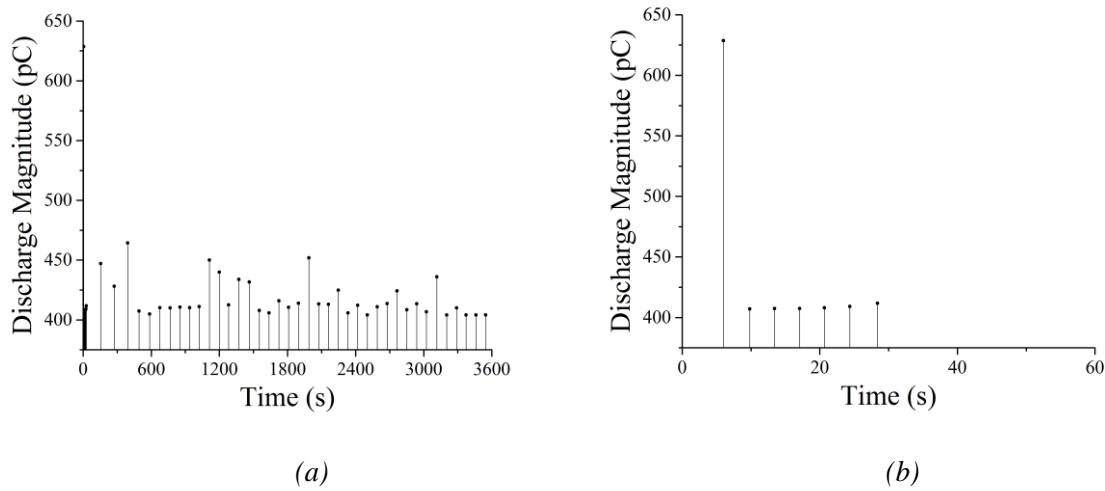
Fig. 6.4. Discharge magnitude across the simulation process ($a = 0.5$, $I = 2kA$) for (a) 3600s, and (b) 60s.

6.3 Partial Discharge Characteristics under Different Loading levels and Cavity Locations

This section researches the influence of loading level and cavity location. The research is conducted for the fresh material, and material properties agree with the fresh material defined in Table. 5.1.

To understand the influence of loading level on discharge characteristics, the simulation, where the cavity is located in the middle of insulation, has been investigated. The position setting can possibly eliminate the influence of the applied field as it varies slightly when the cavity is in the middle of insulation. The cavity field results are illustrated in Figs 6.5 and 6.6 when current through the conductor is 1kA and 4kA. Similar to the discussion in Section 6.2, discharge tends to happen in a short time after the cavity field exceeds the inception level.

When current is 1kA, the results are similar to when the current is 2kA. The discharge repetition rate increases when the current is 4kA and the time interval between two activities decreases. It is due to the

98

increase in the rate of charge decay through the bulk of insulation: electrical conductivity becomes higher when the material is hotter. A faster charge decay leads the cavity field to recover to the level exceeding the inception field in a shorter time and the repetition rate of partial discharge becomes higher at a higher current level. The results agree with the statement given in [21] that the increase in electrical conductivity directly affects the characteristics of PD in XLPE: PD repetition rate increases with electrical conductivity.
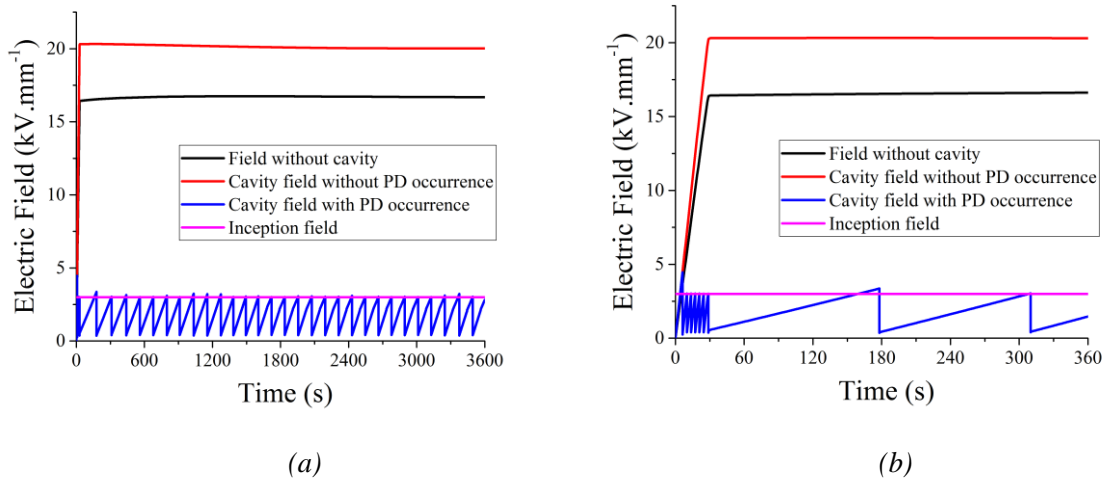
Fig. 6.5. Cavity field across the simulation process ($a = 0.5$, $I = 1kA$) for (a) 3600s, and (b) 360s.
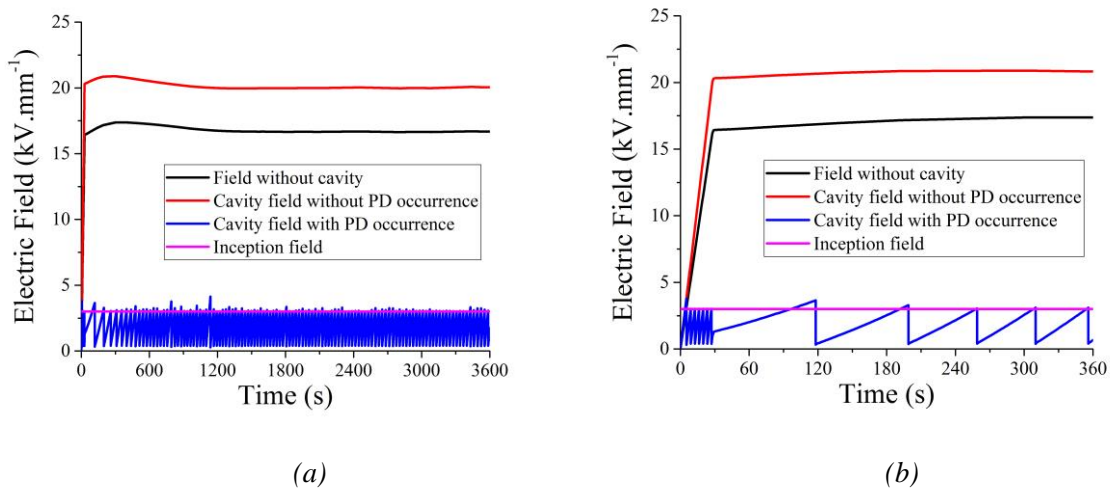
Fig. 6.6. Cavity field across the simulation process ($a = 0.5$, $I = 4kA$) for (a) 3600s, and (b) 360s.

Table. 6.1 shows the influence of loading level on discharge characteristics. Result at the 4kA can be over 3.8 times more frequent that that at 1kA. The difference is mainly at the constant stage and amount of discharge at the ramping stage is nearly independent of the current level, and it seems that the number increases with the current level. It is due to the charge decay speed. The recovery of cavity field from the residual level to the inception field is caused by the increase of applied voltage, and decrease in the

99

absolute magnitude of field produced by the charges on the cavity surface and charges in the insulation bulk due to the charge propagation through the insulation. The recovery speed is faster under higher current level in the ramping stage, and the time interval between two consecutive activities is therefore shorter.

Another effect of charge decay is on the discharge magnitude. Table. 6.1 indicates that the average discharge magnitude increases with the current level. Under the same lag time, charge propagation in the insulation bulk is more significant at a higher current level. Therefore, discharge occurrence field is higher at a higher current level and discharge magnitude is higher as well. When current through the conductor is 4kA, the time interval between two activities is around 30.16s and the rate agrees with the value stated in [21] that the discharge repetition rate can be above 1 per minute.

Table. 6.1. PD characteristics under three current levels through the conductor.

I (kA)	PD Number		Time Interval at Constant Stage (s)		Discharge Magnitude (pC)	
	Ramping stage	Constant stage	Max	Average	Max	Average
1	6	306	149.24	117.46	655.33	408.67
2	6	415	126.62	86.54	628.60	408.55
4	7	1192	90.93	30.16	600.66	411.44

The discharge magnitude comparison is illustrated in Fig. 6.7. The variation in discharge magnitude is slight as the number of charges available for the starting electron generation is large and the lag time for each discharge is short. The results agree with the empirical void discharge results in a 33kV XLPE cable in [116]: activities with high discharge magnitude appear when the magnitude of applied voltage increases and it happens frequently in the transition stage. When the cable reaches a steady state, influence of the magnitude of the applied voltage is not significant.

(a)   *(b)*
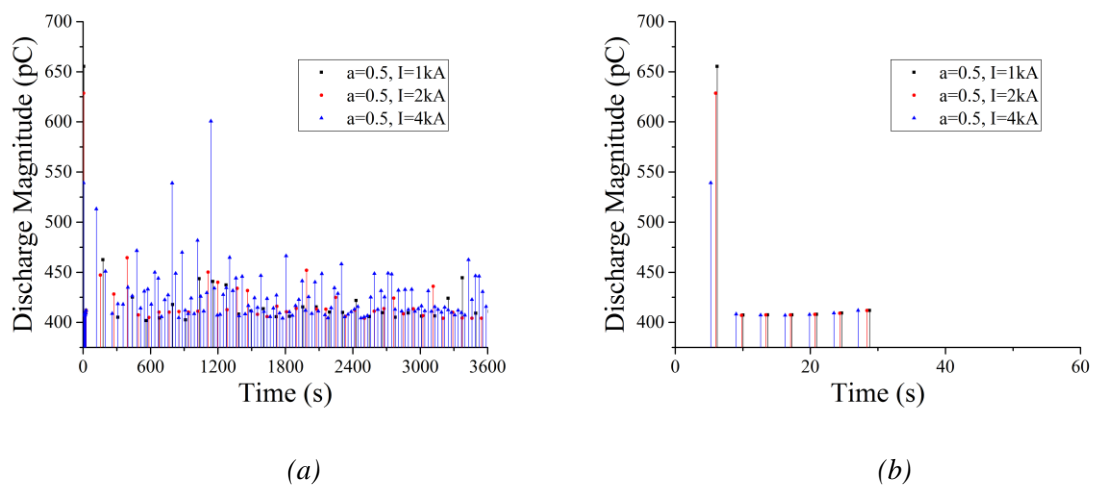
Fig. 6.7. Discharge magnitude across the simulation process ($a = 0.5$) under various current levels for (a) 3600s, and (b) 60s.

When the ramping stage is concentrated on, it is found that except for the first activity, which is highly random, discharge characteristics tend to be nearly independent of the current level in discharge magnitude and time interval between two activities (as listed in Table. 6.2). The reason is that in the ramping stage, the time length for ramp is short and the temperature is not the dominant factor determining the electrical conductivity, and thereby, the cavity field.

Table. 6.2. Discharge time interval at the ramping stage (different in current through conductor).

I (kA)	Time interval Max (s)	Time Interval Min (s)	Time Interval Average (s)
1	3.84	3.61	3.69
2	3.82	3.61	3.68
4	3.76	3.59	3.64

To study the influence of cavity location on discharge characteristics, two conditions are considered to understand the effect of field reversal occurrence. First, current through conductor is 1kA and the cavity is located at different positions and second, current through conductor is 4kA and the cavity is located at different positions.

When the cavity is at different locations under 1kA conductor current, the cavity field over the period of the simulation is illustrated in Figs 6.8 and 6.9. When the cavity is at different locations under 4kA conductor current, the cavity field is illustrated in Figs 6.10 and 6.11.

(a)   *(b)*
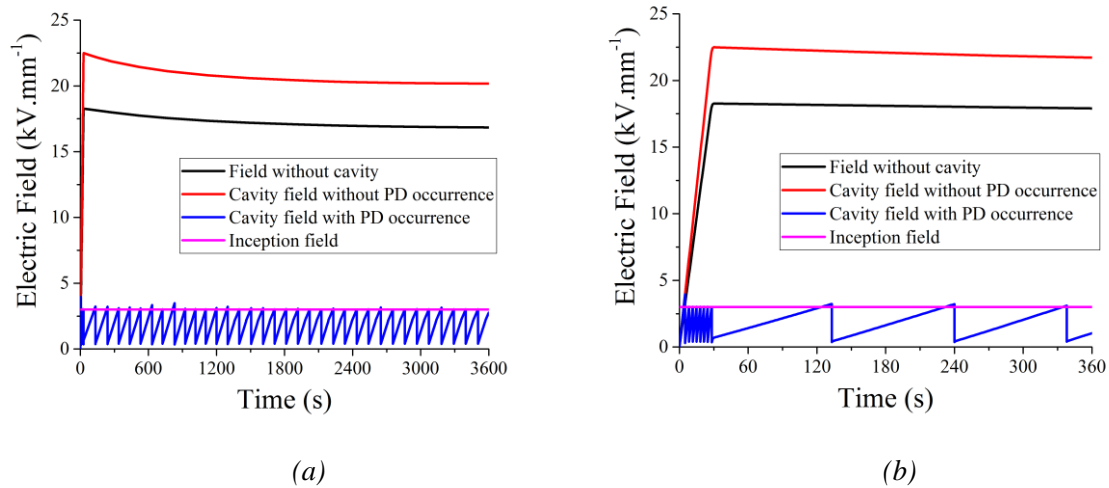
Fig. 6.8. Cavity field across the simulation process ($a = 0.25$, $I = 1kA$) for (a) 3600s, and (b) 360s.
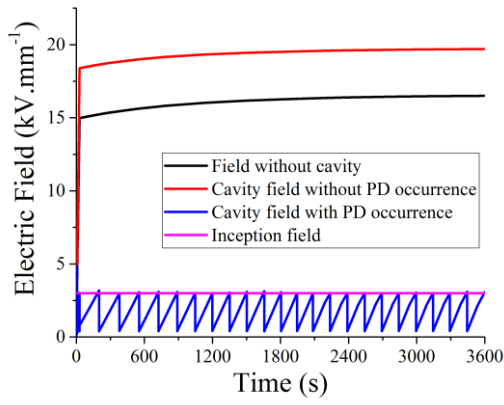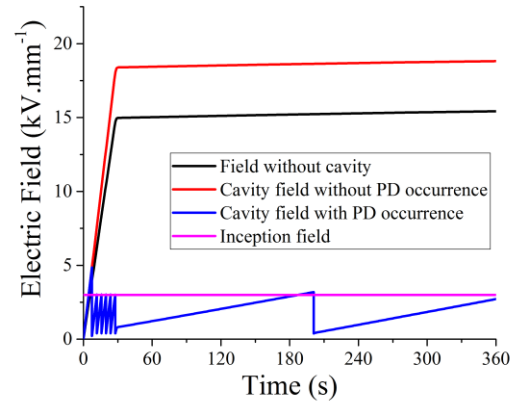
Fig. 6.9. Cavity field across the simulation process ($a = 0.75$, $I = 1kA$) for (a) 3600s, and (b) 360s.
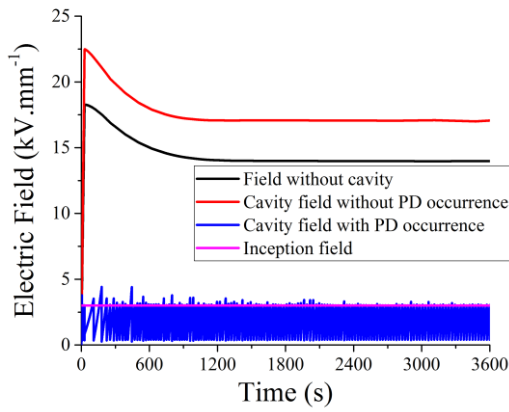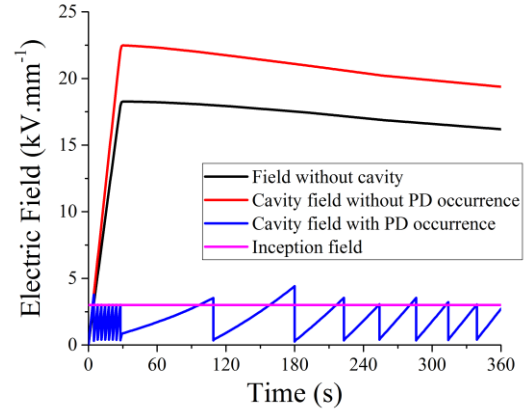
Fig. 6.10. Cavity field across the simulation process ($a = 0.25$, $I = 4kA$) for (a) 3600s, and (b) 360s.
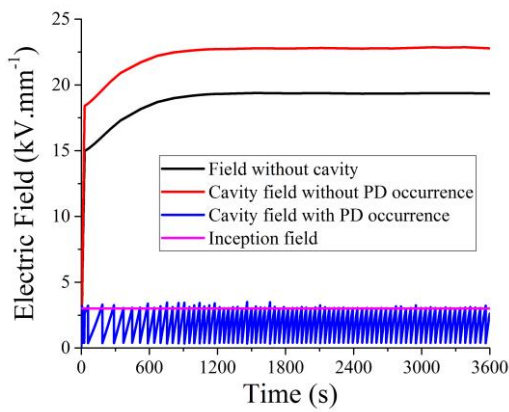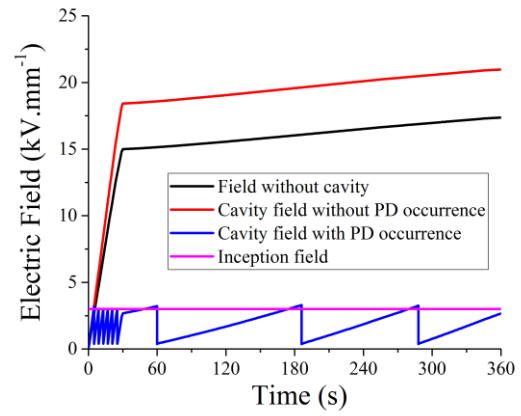
Fig. 6.11. Cavity field across the simulation process ($a = 0.75$, $I = 4kA$) for (a) 3600s, and (b) 360s.

102

Under the condition that $I = 1kA$, when the cavity is closer to conductor (a=0.25), time interval between the last discharge occurring in the ramping stage and the first discharge in the constant voltage stage is shorter than when the cavity is further away from the cable centre (a=0.75). On the contrary, under the condition that $I = 4kA$, the interval between the last discharge occurring in the ramping stage and the first discharge in the constant voltage stage is shorter when the cavity is further away from the cable centre. It is due to the relative speed of variation in field produced by the applied voltage ($\overrightarrow{E_{app}}$) at the transition stage to the speed of charge decay.

The variation in $\overrightarrow{E_{app}}$ in the transission stage when the applied voltage is constant is given in Fig. 6.1(a). When the current level equals to 1kA, the variation in $\overrightarrow{E_{app}}$ is slow, and the short time interval when the cavity is closer to the conductor is caused by the charge decay as temperature closer to the conductor is higher. When the current level equals to 4kA, variation in the magnitude of $\overrightarrow{E_{app}}$ is fast, and it is more dominant in determining the cavity field variation. When the current level equals to 4kA, the time interval is 81.1s for a=0.25, while the value is 34.78s for a=0.75.

Data is listed in Table. 6.3 to help understand the effect of cavity location on discharge characteristics. First, the number of discharge activities occurring over the ramping stage tends to be larger when the cavity is closer to the cable centre. The reason is that in the ramping stage, field reversal does not happen and the cavity field exceeds the inception level later when it is further away from the cable centre.

Table. 6.3. PD characteristics under different cavity locations.

		PD Number		Time Interval at Constant Stage (s)		Discharge Magnitude (pC)	
		Ramping stage	Constant stage	Max	Average	Max	Average
a=0.25	1kA	8	335	114.00	107.16	568.77	408.73
	4kA	8	1406	81.10	25.58	646.41	413.63
a=0.5	1kA	6	306	149.24	117.46	655.33	408.67
	4kA	7	1192	90.93	30.16	600.66	411.44
a=0.75	1kA	6	239	179.00	150.18	721.85	408.49
	4kA	6	813	126.00	44.20	491.33	410.37

Second, under the same current level through conductor, PD number is smaller when the cavity is further away from the cable centre. The trend is more apparent under higher loading level. Charge decay tends to be faster when the cavity is closer to the conductor due to the higher value of temperature, and therefore, current density, and the cavity field recovers to the level exceeding the inception field faster.

Third, higher current level through the conductor enhances the discharge magnitude when the cavity is at the same location, while discharge magnitude is smaller when the cavity is closer to the cable centre under the same current level. Accordingly, when the cavity is closer to the conductor and current

103

through the conductor is 4kA, the average discharge magnitude is the highest. It is due to charge decay as well. Under the same length of lag time, recovery of cavity field is faster at higher temperature and current through the conductor. Discharge occurrence field is higher and therefore, discharge magnitude is higher.

The discharge magnitude comparison is illustrated in Figs 6.12 and 6.13 for 1kA and 4kA respectively. Variation in the discharge magnitude is slight due to the short lag time of each event.
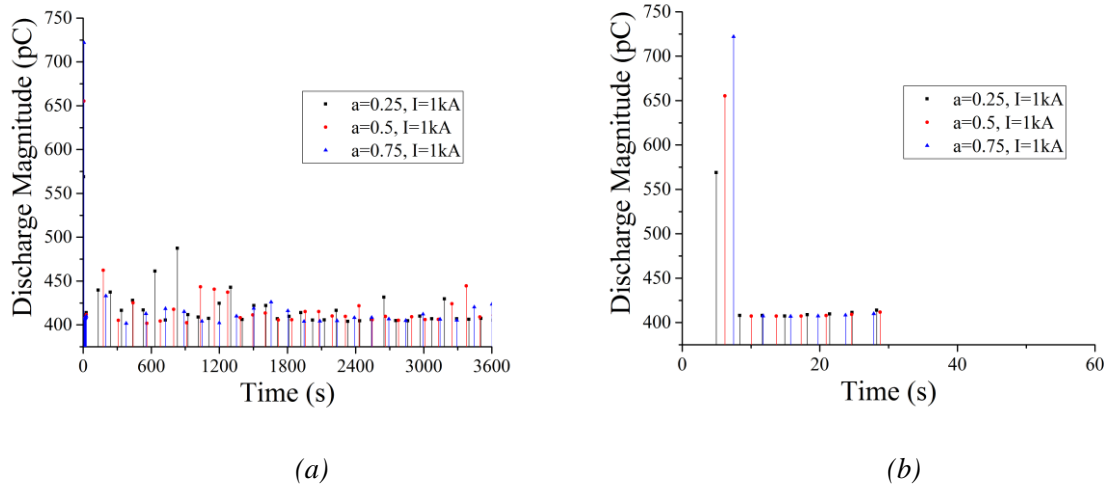

Fig. 6.12. Discharge magnitude across the simulation process ($I = 1kA$) under various cavity location for (a) 3600s, and (b) 60s.
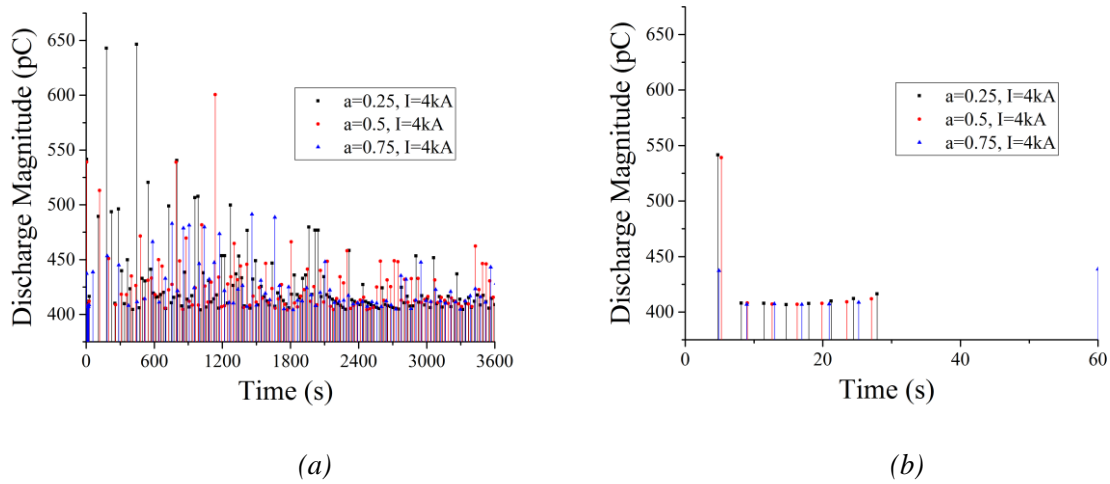
Fig. 6.13. Discharge magnitude across the simulation process ($I = 4kA$) under various cavity location for (a) 3600s, and (b) 60s.

6.4 Partial Discharge Characteristics in Degraded Insulation

Due to their operating conditions, power cables experience electrical, mechanical and thermal stresses,

which may lead to material degradation. Material properties change after degradation and electric field distribution across the insulation varies due to the change in electrical conductivity. Cavity field without PD occurrence is listed in Table. 6.4 when the material is highly degraded (when material properties are regarded as aged material). Field in the middle of insulation tends to be independent of the current level and material properties. The reason for this electric field variation can be as follows: first, the cavity field changes with the electrical conductivity, which is determined by the local field and temperature. Second, cavity field is indicated by the level at cavity centre. However, in aged material, cavity field distribution is not as uniform as when the cavity is in fresh material, which has been indicated in Chapter 4, and a $1.7 \, \text{kV.mm}^{-1}$ field variation appears. Compared to the electric field strength, the variation is small.

Table. 6.4. Cavity field without PD occurrence in fresh or aged material.

		Cavity field for fresh (kV.mm^{-1})	Cavity field for aged (kV.mm^{-1})
a = 0.25	I = 1kA	20.18	22.29
	I = 2kA	19.48	21.77
	I = 4kA	17.06	7.10
a = 0.5	I = 1kA	20.02	20.35
	I = 2kA	20.05	20.81
	I = 4kA	20.06	19.10
a = 0.75	I = 1kA	19.71	19.57
	I = 2kA	20.45	23.07
	I = 4kA	22.78	33.05

When the cavity is closer to the conductor, the cavity field in aged material is similar to that from fresh material when I = 1kA and it even drops to $7 \, \text{kV.mm}^{-1}$ when the conductor is at its maximum operation temperature (I = 4kA). When the cavity is further away from the cable centre, the cavity field without PD occurrence keeps increasing with the current level, and it can even exceed $33 \, \text{kV.mm}^{-1}$, which is 1.5 times of the value under the same position and loading level in fresh material.

It has been discussed in Section 4.4 that aged material can be with higher electrical conductivity value in the region closer to the conductor with the occurrence of field reversal. Parameter values listed in Table. 5.1 lead to different results, and data is listed in Table. 6.5. Electric field strength, E, indicates the location where fresh material and aged material are with the same electrical conductivity value. The corresponding distance coefficient is represented by the a value. The table shows that when current in the conductor is 1kA or 2kA, electrical conductivity of aged material is lower than that of fresh material. When current in the conductor is 4kA and the hottest part of the insulation (357.55K, 84.40℃) nearly reaches its highest operation temperature (363.15K, 90℃), the region that aged material is with higher electrical conductivity value is never higher than 10% of the insulation thickness. Therefore, this condition is not included in this project as the minimum value of a that has been studied in the project is 0.25, and aged material is always with smaller electrical conductivity value.

Table. 6.5. Aged material is with higher electrical conductivity value.

I(kA)	ΔT (K)	E (kV.mm^{-1})	a
1	3.52	N.A.	N.A.
2	14.09	N.A.	N.A.
4	56.40	2.81	0.08

Due to the increase in cavity field because of the variation in material properties by the insulation degradation, and the situation that aged material is with lower electrical conductivity value across the distance coefficient studied in this project, the research on PD characteristics when the insulation is long-term and highly degraded is for the condition when a = 0.75.

The cavity field is illustrated in Fig. 6.14. Simulation work starts from the time point when the previous discharge extinguishes and charges accumulated in the insulation layers are assumed zero at the start of the simulation. When the cable is greatly degraded, discharge repletion rate is low with a long-time interval between two consecutive activities (1512.87s when $I = 1kA$, 971.30s when $I = 2kA$ and 186.76s when $I = 4kA$). The reason is that electrical conductivity of aged material is lower and therefore, current density of each layer is lower. Similar to the conclusion obtained in fresh material, discharge repetition rate increases with current because of the increase in electrical conductivity value.

Average discharge magnitude data is listed in Table. 6.6. It increases with the current due to charge decay. The apparent charge value is 93.64pC, 88.20pC and 44.92pC for I = 1kA, I = 2kA and I = 4kA respectively. The empirical data in [117] indicates that even for a medium voltage XLPE cable (12kV RMS phase voltage), the apparent discharge magnitude can be as high as 200pC at AC voltage when it is long-term degraded. Therefore, discharge magnitude is smaller than that at AC voltage and it agrees with the statement in [21].

(a)   *(b)*

(c)
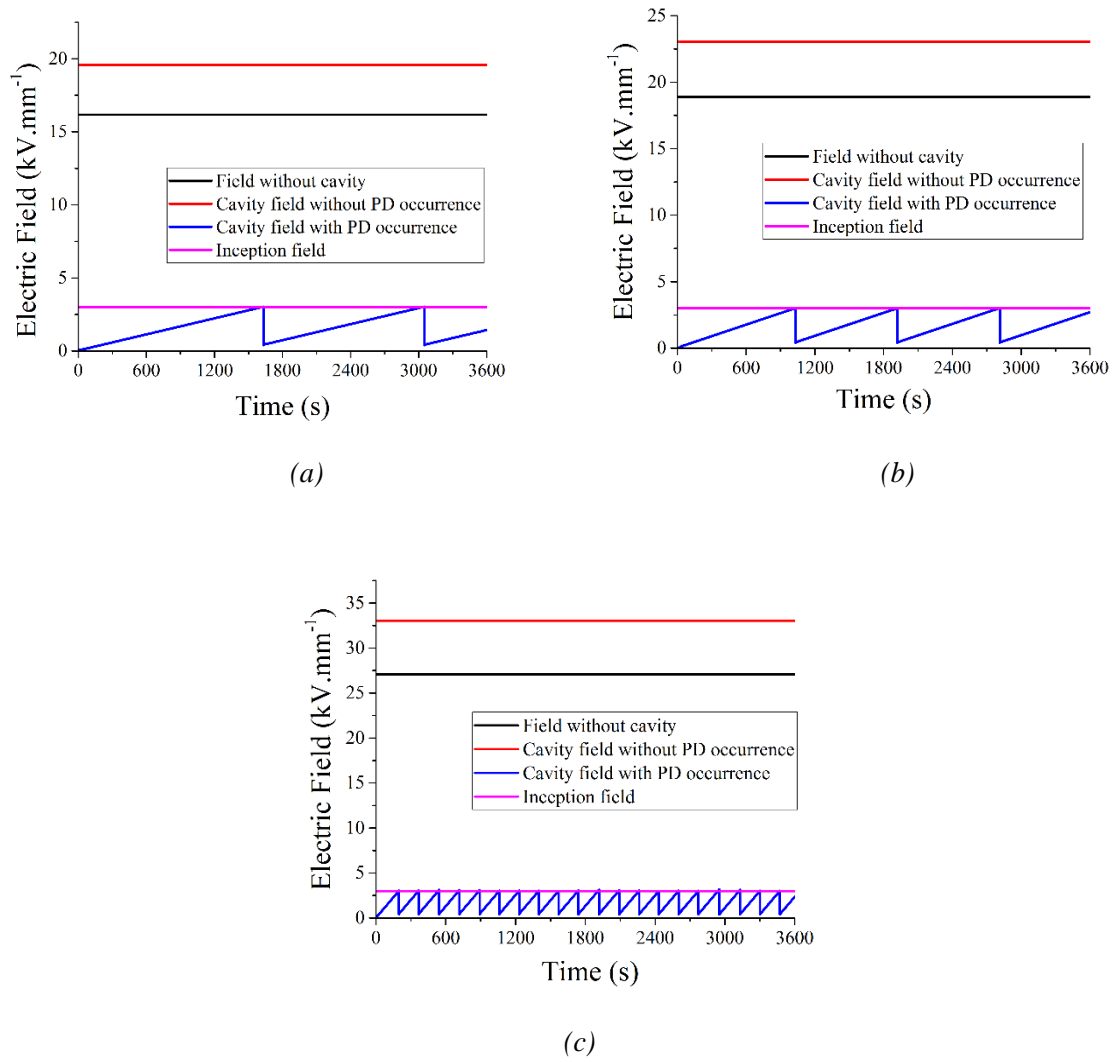
Fig. 6.14. Cavity field across the simulation process ($a = 0.75$) for 3600s when (a) $I = 1kA$, (b) $I = 2kA$, and (c) $I = 4kA$.

Table. 6.6. Discharge magnitude when the cavity is in aged material.

I (kA)	Average PD Magnitude (pC)
1	404.16
2	404.33
4	406.78

6.5 Conclusions

Cavity field without PD occurrence is indicated. Electrical conductivity, which is determined by the local field and temperature, is important in determining cavity field. When the type of voltage with the level starting from zero and keeping constant in magnitude and polarity after a linear ramping stage is applied, cavity field keeps decreasing in the transition stage when the cavity is close to conductor. When

107

the cavity is further away from cable centre, cavity field keeps increasing in the transition stage. When the cavity is in the middle of insulation, electric field, when no cavity appears, should be nearly independent of the loading level.

In this chapter, first, tables and figures indicate that lag time for the occurrence of the first discharge is long as there are no charges from the previous activity for the starting electron generation. Discharge magnitude is high due to the significant electron avalanche. The occurrence time point varies with the field strength induced by the applied field, $\overrightarrow{E_{app}}$.

Second, in the ramping stage, discharge characteristics, such as time interval between two activities and discharge magnitude, are nearly independent of cavity location and current through conductor as the applied voltage is the key factor in this stage.

Third, magnitude of $\overrightarrow{E_{app}}$ is high and therefore, huge number of discharges are ready to be the source to the starting electron in triggering the following discharge. Discharge occurrence probability can therefore be high even if the cavity field just exceeds the inception level. Lag time of each discharge, except the first one, is therefore short, and the variation in discharge magnitude of each activity is slight.

Fourth, charge decay is an important factor determining the PD characteristics. Charge decay is faster when the cavity is closer to the conductor, or the current through the conductor is higher. Faster decay reduces the time interval between two consecutive events, and raises the discharge repetition rate, the number of discharge and average discharge magnitude.

Finally, similar conclusions are drawn for the long-term degraded insulation: both discharge repetition rate and discharge magnitude increase with current through conductor. Compared to the results when cavity is in fresh material, time interval between two consecutive activities is longer as the electrical conductivity of aged material is lower, resulting in slower charge decay recovering the cavity field back to the discharge occurrence field.

Chapter 7. Conclusions and Future Work

Conclusions drawn from the entire project, contributions to the project and the aim and work in the next stage are listed in this chapter.

7.1 Conclusions

At the DC steady state, leakage current through the insulation is steady under a given temperature difference level between the conductor and the sheath. Accordingly, the product value of the local electrical conductivity, electric field strength and distance from the cable centre equals to a constant value, k, under the given temperature difference value and the applied voltage. Equations describing the critical temperature value for field reversal occurrence and temperature and electric field distribution across insulation are derived and proposed. The two expressions in describing the dependence of electrical conductivity on electrical field and temperature are considered in deriving these equations.

The comparison between simulation results and calculation results from the corresponding equations indicates that the equations are reasonable as the error or difference is never higher than 2% under most conditions, except in case of the electric field distribution. For aged material, the error in electric field distribution can be as high as 8%. The source of the error can be that electric field in the middle of insulation actually fluctuates slightly, and the cavity field is indicated by the average value, a more precise meshing work helps improve the value.

In understanding the distortion of a single cavity on the insulation, a 2D model is applied due to simulation efficiency enhancement. However, the 2D model comes with weakness in geometry description and a single spherical cavity is actually a cylindrical one, as the length or height of the cavity is not considered or assumed infinite in the model. Accordingly, the results from published papers cannot be accurate enough. The advantage of a 3D model is that it agrees with the real condition, including the cavity shape and cable length, though the length of simulation process is much longer as more elements need to be calculated.

The comparison between 2D and 3D models provides the references for model selection. In understanding the electrical field and temperature distribution in HVDC cable at a steady state without the cavity presence, there is nearly no difference between results from the 2D model and those from the 3D model. Accordingly, the 2D model is a better choice. When the research is on temperature across insulation, or temperature at the cavity when there is a single air-filled cavity located at the insulation, 2D model can still be the choice: the difference between 2D and 3D model is never higher than 0.3K across the temperature difference levels studied in this project. When the electric field across insulation with the cavity presence is studied, the 2D model is applicable in describing the field far from the cavity

centre (five times larger than the cavity radius), but the 3D model is the only choice for field research at or in the region close to the cavity. Field enhancement level from the 2D model is over 25% higher than that from the 3D model when a 1mm spherical cavity is in the middle of insulation. In obtaining accurate and practical results, the 3D model is applied under the condition, though simulation time is six times longer.

The electric field tends to be resistively graded at DC steady state and electrical conductivity should be the key factor in field enhancement by the air-filled cavity. The speculation in describing field enhancement at DC steady state is that permittivity value in field enhancement equation at AC voltage is straightforwardly replaced by the electrical conductivity. This is proved reasonable with an error percentage between simulation and calculation being never higher than 5.5% of the simulation results in fresh material and 1% of the simulation results in aged material. This conclusion is applicable across the temperature difference levels, cavity shape and cavity location studied in this project.

Field distortion in the region surrounding the single air-filled cavity at DC steady state is researched. When the cavity is in the middle of insulation and temperature difference level is 12K, both field distortion percentage and field strength on xy and xz planes are with high similarity, as the difference is never higher than 0.1 kV.mm^{-1} and 2.2%. Volume of the region with field enhancement equals to that of the region with field reduction. Field strength and field distortion on yz plane are nearly constant with small variation (never higher than 2.3%) when the distance from the cavity centre does not change.

Field distortion can be possibly influenced by the cavity location, temperature difference levels and the material properties as these factors can determine the electrical conductivity of the insulation material in the region where the cavity is located. The trend in field distortion variation follows the value of electrical conductivity that the distortion tends to be more serious in the region closer to the conductor, under higher temperature difference level or in fresh material. Though the volume of region possibly distorted by the cavity increases with the cavity radius, the radius ratio of the possibly distorted region to the cavity keeps constant at 5, when the permissive error percentage is set at 1%.

This project presents the preliminary partial discharge modelling and simulation work. In describing the PD characteristics in HVDC cable applied on with the voltage with constant polarity and magnitude, the difference from that at AC voltage is mainly at the charge decay process between two activities. Charge recombination due to charge migration along the cavity wall is the main source of charge decay at AC voltage. At DC voltage, charges on cavity surface mainly migrate through the insulation bulk according to the local bulk conductivity and therefore, current density. Charges accumulated in the insulation can influence the cavity field and the effect decreases with the distance to the cavity centre.

In the ramping stage, before applied voltage reaches the constant stage, the linear raise in applied voltage or field is the dominant reason for cavity field recovery after the first discharge. In the transition

stage when the magnitude and polarity of applied voltage are constant, the variation in $\overrightarrow{E_{app}}$, which is induced by the applied field in cavity, is significant. At DC steady state, charge decay or insulation temperature is the key factor in field recovery since the previous discharge and the discharge repetition rate. This project also researches the effect of cavity location and current through the conductor on discharge characteristics. The first discharge tends to happen later when the cavity is further away from conductor, and the number of discharge in the ramping stage decreases with the distance from the cable centre. Time interval between two activities in the ramping stage is nearly independent of the location and current.

The lag time of each activity is short, as there are a huge number of charges available for the starting electron generation and discharge magnitude varies slightly. Charge decay is faster when the cavity is closer to the conductor, and the current through the conductor is higher. Faster decay reduces the time interval between two consecutive events, and raises the discharge repetition rate, the number of discharge and average discharge magnitude.

Discharge results in long degraded material shows that discharge repetition rate become lower compared to the condition with the same current value and cavity location. It is due to the low conductivity value at the region near cavity in aged material.

7.2 Contributions

As it has been stated in the previous section, the research in HVDC XLPE cable at DC steady state is mainly conducted on the electric field distribution across the insulation and at the cavity, including the field enhancement by the cavity and cavity distortion on electric field in the region surrounding the cavity.

Results obtained in the project are published in three journal papers, one in English and two in Chinese. Equations describing the critical temperature difference for field reversal occurrence and field distribution across the insulation without cavity presence are proved reasonable, and the field enhancement by a single air-filled cavity at DC steady state with the effect of cavity location and shape, temperature difference and material properties taken into consideration are discussed in [106]. Model comparison in describing the electric field and field enhancement at the cavity is discussed as well, along with the reference for model selection. The possibility in electrical conductivity equations replacement in describing temperature and electric field distribution is discussed in [118]. Electric field distortion by the cavity in the region surrounding the cavity and volume of the region possibly influenced by the cavity are given in [119].

A preliminary research in modelling partial discharge activities in HVDC cable with a constant voltage

applied is attempted in the project using Niemeyer's model. Results obtained can be explained, including the variation in discharge repetition rate with the cavity location and current through the conductor, and the increase of discharge magnitude with current through the conductor. The discharge repetition rate obtained agrees with the statement in [21] that time interval between two events is slightly higher than 60 seconds, the DC PD characteristics agrees with the experical results in [115, 116], and discharge magnitude in long-term degraded cable agrees with [21, 117] that the magnitude of DC PD is lower than that of AC PD.

7.3 Future Work

In understanding the cavity distortion in the region surrounding the cavity and volume of the possibly distorted region, the effect of cavity shape is not considered. It has been shown that when the axis ratio level a_c/b_c is lower than 1, electric field enhancement by the cavity is stronger under a lower value. Therefore, a single ellipsoidal cavity may arguably distort the electric field strength in the surrounding region more seriously than the spherical one. Besides, the radius ratio of the distorted region to the cavity radius may possibly change if the cavity shape is not spherical.

Another point worth researching regarding the field distortion is the amount of cavity. Appearance of multiple cavities should be more destructive than the condition when a single cavity exists in the insulation: when multiple cavities are presented in the insulation, each cavity can be the source to partial discharge and it distorts the local field strength. When two cavities are close enough in distance, interaction exists between them, and the second cavity is with effect on electric field inside the cavity or surrounding the cavity.

To understand the field distortion by two spherical cavities and the interaction between the two, two conditions are to be considered. The first situation is that two cavities vary in their distance from cable centre and they are the same on cable height. The second condition is that the distance from cable centre is the same for these two cavities, while they vary in cable height. Electric field strength inside each cavity and electric field distortion in the region surrounding each cavity and in the region between two cavities are extracted. In indicating the interaction between the two cavities, the extracted data is compared with the corresponding results when only a single spherical cavity is presented in the insulation.

The match between simulation and experiment is needed. Therefore, partial discharge test should be applied on HVDC XLPE cable in future and the empirical results are to be compared to the corresponding simulation results. It can be believed that a numerical particle discharge model is successfully proposed if the match between the experiment results and the corresponding simulation results is acceptable and reasonable.

Appendix 1. Code for a Single Spherical Cavity Field Enhancement at DC Steady State

To avoid mistakes, please run the code via COMSOL 5.2 with MATLAB

```
clear;
clc;

%% Parameter value define%%
Ri = 29.8541/1000;
Ro = 63/1000;
l = 0.5;
U = 150000;
To = 301.15;
deltaT = 3;
while deltaT <= 20
   location = Ri + 0.25*(Ro-Ri);
   while location < Ro
      Rc = 0.5/1000;
      while Rc < 1.501/1000

         %% Model building and calculation%%
         tic;
         import com.comsol.model.*
         import com.comsol.model.util.*
         model = ModelUtil.create('Model');
         model.modelPath('H:\.das\Desktop\final running\3D model\single spherical cavity');
         model.label('3D_single_spherical_cavity.mph');
         model.comments(['3D DC\n\n']);
         model.param.set('Rc', Rc);
         model.param.set('location', location);
         model.param.set('l', l);
         model.param.set('epsilon', '2.3');
         model.param.set('alpha', '0.11[1/K]');
         model.param.set('belta', '0.24[mm/kV]');
         model.param.set('sigma0', '9.1*1e-17[S/m]');
         model.param.set('Tref', '273.15[K]');
         model.param.set('deltaT', deltaT);
         model.param.set('To', To);
         model.param.set('U', '150000[V]');
         model.param.set('S', '1e-16[S/m]');
         model.param.set('Ri', Ri);
         model.param.set('Ro', Ro);
         model.param.set('A', '3.2781[A/m^2]');
         model.param.set('phi', '0.56[eV]');
         model.param.set('q', '1');
         model.param.set('kb', '8.6173324*1e-5[eV/K]');
         model.param.set('B', '2.7756*1e-7[m/V]');
         model.modelNode.create('comp1');
```

```
model.geom.create('geom1', 3);
model.modelNode('comp1').defineLocalCoord(false);
model.mesh.create('mesh1', 'geom1');
model.geom('geom1').create('cyl1', 'Cylinder');
model.geom('geom1').feature('cyl1').set('r', 'Ri');
model.geom('geom1').feature('cyl1').set('h', 'l');
model.geom('geom1').create('cyl2', 'Cylinder');
model.geom('geom1').feature('cyl2').set('r', 'Ro');
model.geom('geom1').feature('cyl2').set('h', 'l');
model.geom('geom1').create('sph1', 'Sphere');
model.geom('geom1').feature('sph1').set('pos', {'location' '0' 'l/2'});
model.geom('geom1').feature('sph1').set('r', 'Rc');
model.geom('geom1').create('dif1', 'Difference');
model.geom('geom1').feature('dif1').selection('input2').set({'cyl1'});
model.geom('geom1').feature('dif1').selection('input').set({'cyl2'});
model.geom('geom1').run;
model.variable.create('var1');
model.variable('var1').model('comp1');
model.variable('var1').set('sigma', 'sigma0*exp(alpha*(T-Tref)+belta*ec.normE)');
model.variable('var1').set('sigma_new', 'A*exp(-
phi*q/(kb*T))*sinh(B*abs(ec.normE+eps))/abs(ec.normE+eps)');
model.view.create('view2', 2);
model.material.create('mat1', 'Common', 'comp1');
model.material.create('mat2', 'Common', 'comp1');
model.material('mat1').selection.set([1]);
model.material('mat2').selection.set([2]);
model.physics.create('ht', 'HeatTransfer', 'geom1');
model.physics('ht').create('temp1', 'TemperatureBoundary', 2);
model.physics('ht').feature('temp1').selection.set([1 2 7 10]);
model.physics('ht').create('temp2', 'TemperatureBoundary', 2);
model.physics('ht').feature('temp2').selection.set([5 6 8 9]);
model.physics.create('ec', 'ConductiveMedia', 'geom1');
model.physics('ec').create('gnd1', 'Ground', 2);
model.physics('ec').feature('gnd1').selection.set([1 2 7 10]);
model.physics('ec').create('pot1', 'ElectricPotential', 2);
model.physics('ec').feature('pot1').selection.set([5 6 8 9]);
model.mesh('mesh1').autoMeshSize(1);
model.result.table.create('tbl1', 'Table');
model.probe.create('pdom1', 'DomainPoint');
model.probe.create('pdom2', 'DomainPoint');
model.probe('pdom1').model('comp1');
model.probe('pdom2').model('comp1');
model.view('view1').set('scenelight', 'off');
model.view('view1').set('transparency', 'on');
model.view('view2').axis.set('abstractviewxscale', '2.9028637800365686E-4');
model.view('view2').axis.set('ymin', '-0.06319160759449005');
model.view('view2').axis.set('xmax', '0.10924475640058517');
model.view('view2').axis.set('abstractviewyscale', '2.9028637800365686E-4');
model.view('view2').axis.set('abstractviewbratio', '-0.04999997094273567');
model.view('view2').axis.set('abstractviewtratio', '0.050000034272670746');
model.view('view2').axis.set('abstractviewrratio', '0.486576646566391');
```

```
model.view('view2').axis.set('xmin', '-0.11543690413236618');
model.view('view2').axis.set('abstractviewlratio', '-0.486576646566391');
model.view('view2').axis.set('ymax', '0.06627611815929413');
model.material('mat1').propertyGroup('def').set('electricconductivity', {'sigma_new' '0' '0' '0' 'sigma_new'
'0' '0' '0' 'sigma_new'});
model.material('mat1').propertyGroup('def').set('relpermittivity', {'epsilon' '0' '0' '0' 'epsilon' '0' '0' '0'
'epsilon'});
model.material('mat1').propertyGroup('def').set('thermalconductivity', {'0.3' '0' '0' '0' '0.3' '0' '0' '0' '0.3'});
model.material('mat1').propertyGroup('def').set('density', '925');
model.material('mat1').propertyGroup('def').set('heatcapacity', '2200');
model.material('mat2').propertyGroup('def').set('electricconductivity', {'S' '0' '0' '0' 'S' '0' '0' '0' 'S'});
model.material('mat2').propertyGroup('def').set('relpermittivity', {'1' '0' '0' '0' '1' '0' '0' '0' '1'});
model.material('mat2').propertyGroup('def').set('thermalconductivity', {'0.0257' '0' '0' '0' '0.0257' '0' '0' '0'
'0.0257'});
model.material('mat2').propertyGroup('def').set('density', '1.205');
model.material('mat2').propertyGroup('def').set('heatcapacity', '1005');
model.physics('ht').feature('init1').set('Tinit', 'To');
model.physics('ht').feature('temp1').set('T0', 'To');
model.physics('ht').feature('temp2').set('T0', 'To+deltaT');
model.physics('ec').feature('pot1').set('V0', 'U');
model.mesh('mesh1').run;
model.result.table('tbl1').label('Probe Table 1');
model.probe('pdom1').setIndex('coords3', 'location', 0, 0);
model.probe('pdom1').setIndex('coords3', '0', 0, 1);
model.probe('pdom1').setIndex('coords3', 'l/2', 0, 2);
model.probe('pdom1').feature('ppb1').set('window', 'window2');
model.probe('pdom1').feature('ppb1').set('expr', 'ec.normE');
model.probe('pdom1').feature('ppb1').set('unit', 'V/m');
model.probe('pdom1').feature('ppb1').set('descr', 'Electric field norm');
model.probe('pdom1').feature('ppb1').set('table', 'tbl1');
model.probe('pdom2').setIndex('coords3', '-location', 0, 0);
model.probe('pdom2').setIndex('coords3', '0', 0, 1);
model.probe('pdom2').setIndex('coords3', 'l/2', 0, 2);
model.probe('pdom2').feature('ppb2').set('window', 'window2');
model.probe('pdom2').feature('ppb2').set('expr', 'ec.normE');
model.probe('pdom2').feature('ppb2').set('unit', 'V/m');
model.probe('pdom2').feature('ppb2').set('descr', 'Electric field norm');
model.probe('pdom2').feature('ppb2').set('table', 'tbl1');
model.study.create('std1');
model.study('std1').create('stat', 'Stationary');
model.sol.create('sol1');
model.sol('sol1').study('std1');
model.sol('sol1').attach('std1');
model.sol('sol1').create('st1', 'StudyStep');
model.sol('sol1').create('v1', 'Variables');
model.sol('sol1').create('s1', 'Stationary');
model.sol('sol1').feature('s1').create('se1', 'Segregated');
model.sol('sol1').feature('s1').create('i1', 'Iterative');
model.sol('sol1').feature('s1').create('i2', 'Iterative');
model.sol('sol1').feature('s1').feature('se1').create('ss1', 'SegregatedStep');
model.sol('sol1').feature('s1').feature('se1').create('ss2', 'SegregatedStep');
model.sol('sol1').feature('s1').feature('se1').create('ll1', 'LowerLimit');
```

```
model.sol('sol1').feature('s1').feature('se1').feature.remove('ssDef');
model.sol('sol1').feature('s1').feature('i1').create('mg1', 'Multigrid');
model.sol('sol1').feature('s1').feature('i2').create('mg1', 'Multigrid');
model.sol('sol1').feature('s1').feature('i2').feature('mg1').feature('pr').create('so1', 'SOR');
model.sol('sol1').feature('s1').feature('i2').feature('mg1').feature('po').create('so1', 'SOR');
model.sol('sol1').feature('s1').feature('i2').feature('mg1').feature('cs').create('d1', 'Direct');
model.sol('sol1').feature('s1').feature.remove('fcDef');
model.result.dataset.create('dset2', 'Solution');
model.result.dataset.create('cpt1', 'CutPoint3D');
model.result.dataset.create('cpt2', 'CutPoint3D');
model.result.dataset.create('cln1', 'CutLine3D');
model.result.dataset('dset2').set('probetag', 'pdom2');
model.result.dataset('cpt1').set('probetag', 'pdom1');
model.result.dataset('cpt1').set('data', 'dset2');
model.result.dataset('cpt2').set('probetag', 'pdom2');
model.result.dataset('cpt2').set('data', 'dset2');
model.result.numerical.create('pev1', 'EvalPoint');
model.result.numerical.create('pev2', 'EvalPoint');
model.result.numerical('pev1').set('probetag', 'pdom1/ppb1');
model.result.numerical('pev2').set('probetag', 'pdom2/ppb2');
model.result.create('pg5', 'PlotGroup1D');
model.result.create('pg6', 'PlotGroup3D');
model.result.create('pg7', 'PlotGroup3D');
model.result.create('pg8', 'PlotGroup3D');
model.result.create('pg9', 'PlotGroup1D');
model.result('pg5').set('probetag', 'window2');
model.result('pg5').create('tblp1', 'Table');
model.result('pg5').feature('tblp1').set('probetag', 'pdom1/ppb1,pdom2/ppb2');
model.result('pg6').create('surf1', 'Surface');
model.result('pg7').create('iso1', 'Isosurface');
model.result('pg8').create('mslc1', 'Multislice');
model.result('pg9').create('lngr1', 'LineGraph');
model.probe('pdom1').genResult([]);
model.probe('pdom2').genResult([]);
model.sol('sol1').attach('std1');
model.sol('sol1').feature('s1').feature('se1').feature('ss1').set('linsolver', 'i1');
model.sol('sol1').feature('s1').feature('se1').feature('ss1').set('segvar', {'comp1_V'});
model.sol('sol1').feature('s1').feature('se1').feature('ss2').set('linsolver', 'i2');
model.sol('sol1').feature('s1').feature('se1').feature('ss2').set('subdamp', '0.8');
model.sol('sol1').feature('s1').feature('se1').feature('ss2').set('segvar', {'comp1_T'});
model.sol('sol1').feature('s1').feature('se1').feature('ll1').set('lowerlimit', 'comp1.T 0');
model.sol('sol1').feature('s1').feature('i1').set('linsolver', 'cg');
model.sol('sol1').feature('s1').feature('i1').feature('mg1').set('prefun', 'amg');
model.sol('sol1').feature('s1').feature('i2').set('rhob', '20');
model.sol('sol1').feature('s1').feature('i2').feature('mg1').feature('cs').feature('d1').set('linsolver', 'pardiso');
model.sol('sol1').runAll;
model.result.dataset('dset2').label('Probe Solution 2');
model.result.dataset('dset2').set('frametype', 'spatial');
model.result.dataset('cpt1').set('data', 'dset2');
model.result.dataset('cpt2').set('data', 'dset2');
model.result.dataset('cln1').set('genpoints', {'Ri' '0' 'l/2'; 'Ro' '0' 'l/2'});
```

```
model.result.dataset.remove('dset3');
model.result.numerical('pev1').setResult;
model.result.numerical('pev2').appendResult;
model.result('pg5').label('Probe Plot Group 5');
model.result('pg5').set('xlabel', 'Electric field norm (V/m), Point: (0.046427, 0, 0.25)');
model.result('pg5').set('windowtitle', 'Probe Plot 2');
model.result('pg5').set('xlabelactive', false);
model.result('pg5').feature('tblp1').label('Probe Table Graph 1');
model.result('pg6').label('Temperature (ht)');
model.result('pg6').feature('surf1').set('colortable', 'ThermalLight');
model.result('pg7').label('Isothermal Contours (ht)');
model.result('pg7').feature('iso1').set('number', '10');
model.result('pg7').feature('iso1').set('colortable', 'ThermalLight');
model.result('pg8').label('Electric Potential (ec)');
model.result('pg8').set('frametype', 'spatial');
model.result('pg8').feature('mslc1').set('expr', 'V');
model.result('pg8').feature('mslc1').set('descr', 'Electric potential');
model.result('pg8').feature('mslc1').set('unit', 'V');
model.result('pg9').set('xlabel', 'Arc length');
model.result('pg9').set('ylabel', 'Electric field norm (V/m)');
model.result('pg9').set('ylabelactive', false);
model.result('pg9').set('xlabelactive', false);
model.result('pg9').feature('lngr1').set('data', 'cln1');
model.result('pg9').feature('lngr1').set('expr', 'ec.normE');
model.result('pg9').feature('lngr1').set('descr', 'Electric field norm');
model.result('pg9').feature('lngr1').set('unit', 'V/m');
 toc;


%% Value Extraction in understanding the trend across the insulation %%
coordinate = Ri;
step = (Ro-Ri)/499;
i = 1;
while coordinate<= Ro
    E_good(i) =  mphinterp(model,'ec.normE','coord',[coordinate;0;l/2]);
    E_good_ref(i) = mphinterp(model,'ec.normE','coord',[-coordinate;0;l/2]);
    T_good(i) =  mphinterp(model,'T','coord',[coordinate;0;l/2]);
    T_good_ref(i) = mphinterp(model,'T','coord',[-coordinate;0;l/2]);
    Cond_x_good(i) = mphinterp(model,'ec.sigmaxx','coord',[coordinate;0;l/2]);
    Cond_y_good(i) = mphinterp(model,'ec.sigmayy','coord',[coordinate;0;l/2]);
    Cond_z_good(i) = mphinterp(model,'ec.sigmazz','coord',[coordinate;0;l/2]);
    Cond_x_good_ref(i) = mphinterp(model,'ec.sigmaxx','coord',[-coordinate;0;l/2]);
    Cond_y_good_ref(i) = mphinterp(model,'ec.sigmayy','coord',[-coordinate;0;l/2]);
    Cond_z_good_ref(i) = mphinterp(model,'ec.sigmazz','coord',[-coordinate;0;l/2]);
    Conductivity_good(i) = sqrt(Cond_x_good(i)^2+Cond_y_good(i)^2+Cond_z_good(i)^2);
    Conductivity_good_ref(i) =
sqrt(Cond_x_good_ref(i)^2+Cond_y_good_ref(i)^2+Cond_z_good_ref(i)^2);
    Product_good(i) = E_good(i)*Cond_x_good(i)*coordinate;
    Product_good_ref(i) = E_good_ref(i)*Cond_x_good_ref(i)*coordinate;
    Location(i) = coordinate*1000;
    coordinate = coordinate + step;
    i = i + 1;
```

```
        end
        Ec_good = mphinterp(model,'ec.normE','coord',[location;0;l/2]);
        Tc_good = mphinterp(model,'ec.normE','coord',[location;0;l/2]);
        location_ratio = (location-Ri)/(Ro-Ri);

        fnamec = strcat('3D good material single spherial cavity across insulation data - Ri =
',num2str(Ri*1000),'[mm]_Ro = ',num2str(Ro*1000),'[mm]_Rc = ',num2str(Rc*1000),'[mm]_Location ratio =
',num2str(location_ratio),'[1]_Temp difference = ',num2str(deltaT),'[K].mat');
        save(fnamec,
'Ro','Ri','Rc','deltaT','location_ratio','E_good','E_good_ref','T_good','T_good_ref','Cond_x_good','Cond_y_good',
'Cond_z_good','Cond_x_good_ref','Cond_y_good_ref','Cond_z_good_ref','Conductivity_good','Conductivity_go
od_ref','Product_good','Product_good_ref','Location','Ec_good','Tc_good');
        disp('Finish good material recording');

        %% Value Extraction in understanding the trend in the cavity %%
        coordinate = location - Rc;
        step = 2*Rc/99;
        i = 1;
        while coordinate <= location + Rc
            E_cav_good(i) =  mphinterp(model,'ec.normE','coord',[coordinate;0;l/2]);
            E_cav_good_ref(i) = mphinterp(model,'ec.normE','coord',[-coordinate;0;l/2]);
            Cond_cav_x_good(i) = mphinterp(model,'ec.sigmaxx','coord',[coordinate;0;l/2]);
            Cond_cav_y_good(i) = mphinterp(model,'ec.sigmayy','coord',[coordinate;0;l/2]);
            Cond_cav_z_good(i) = mphinterp(model,'ec.sigmazz','coord',[coordinate;0;l/2]);
            Cond_cav_x_good_ref(i) = mphinterp(model,'ec.sigmaxx','coord',[-coordinate;0;l/2]);
            Cond_cav_y_good_ref(i) = mphinterp(model,'ec.sigmayy','coord',[-coordinate;0;l/2]);
            Cond_cav_z_good_ref(i) = mphinterp(model,'ec.sigmazz','coord',[-coordinate;0;l/2]);
            Conductivity_cav_good(i) =
sqrt(Cond_cav_x_good(i)^2+Cond_cav_y_good(i)^2+Cond_cav_z_good(i)^2);
            Conductivity_cav_good_ref(i) =
sqrt(Cond_cav_x_good_ref(i)^2+Cond_cav_y_good_ref(i)^2+Cond_cav_z_good_ref(i)^2);
            Location_cav(i) = coordinate*1000;
            coordinate = coordinate + step;
            i = i + 1;
        end
        S = sum(E_cav_good);
        S_ref = sum(E_cav_good_ref);
        E_cav_average = S/100;
        E_cav_ref_average = S_ref/100;
        E_cav_max = max(E_cav_good);
        E_cav_min = min(E_cav_good);
        fnamec = strcat('3D good material single spherial cavity in cavity data - Ri =
',num2str(Ri*1000),'[mm]_Ro = ',num2str(Ro*1000),'[mm]_Rc = ',num2str(Rc*1000),'[mm]_Location ratio =
',num2str(location_ratio),'[1]_Temp difference = ',num2str(deltaT),'[K].mat');
        save(fnamec,
'Ro','Ri','Rc','deltaT','location_ratio','E_cav_good','E_cav_good_ref','Cond_cav_x_good','Cond_cav_y_good','Co
nd_cav_z_good','Cond_cav_x_good_ref','Cond_cav_y_good_ref','Cond_cav_z_good_ref','Conductivity_cav_go
od','Conductivity_cav_good_ref','Location_cav','S','S_ref','E_cav_average','E_cav_ref_average','E_cav_max','E_
cav_min');
        disp('Finish good material recording');
        Rc = Rc + 0.5/1000;
    end
    location = location + 0.25*(Ro-Ri);
```

```
      end
   if deltaT == 3
      deltaT = 7;
   elseif deltaT == 7
      deltaT = 12;
   elseif deltaT == 12
      deltaT = 20;
   else
      deltaT = 100;
   end
end
```

Appendix 2. Code for Partial Discharge in HVDC Cable

```
clear;
clc;

Ri= 18/1000;
Ro = 27/1000;
Rc = 1/1000;
location = Ri+0.5*(Ro-Ri);
I = 2000;
M = xlsread('good material 1mm 0.5 2000A 36000s data.xlsx');

U = 150000;
ramping = 5300;

t_ramp = ceil(U/ramping);
air_noPD = 1e-16;
air_PD = 1e-5;
E_inc = 3*1e6;
E_ext_min = 100;

probability =0;
work_function = 1;
e = 1.6*1e-19;
k = 8.617*1e-5;
Temp = 301.15;
Thickness = Ro - Ri;
E_P_cri = 25.2;
P = 101000;
B = 8.6;
D = 2*Rc;
a = Rc;
b = Rc;
n = 0.5;
belta = 1/n;
v0 = 1e14;
Er0 = 8.854*1e-12;
Er = 2.3;
gamma = 0.35;
tau = 0.002;
Crad_Orad = 2*1e6;
rou_p0 = 1e-5;
ks = 5*1e-6;
sigma_mat_ini = 1e-6;
sigma_air_ini = 1e-16;
K = 3;
epsilon_p = 1;
epsilon_p_n = 50;
epsilon_n = epsilon_p/epsilon_p_n;
epsilon = 1;
```

```
v = 1.22;
virgin_void = 1;
void_condition = 0;
Subject_to_PD = 0;
nPD = 0;
Value_change = 0;
Interval_change = 0;
Es0 = 0;
Charge = 0;
q_constant = Er0*pi*b^2*(1+Er*(K*(a/b)-1));
q_app_constant = -(4/3)*Er0*Er*pi*a*b^2*K*(1/Thickness);
N_dt_constant_1 = e/(4*pi*Er0);
N_dt_constant_2 = k*Temp;
Veff = (4/3)*pi*Rc^3*abs(2*Rc-v^(-belta));
volume = (4/3)*pi*Rc^3;
volume_ratio = 0.5*(1-Veff/volume);
volume_value = volume_ratio*volume;
p_value = 3*volume_value/(pi*Rc^3);
x = 0;
i = 1;
while x <= 1
   y = x^2*(3-x);
   X(i) = x;
   Y(i) = y;

   i = i + 1;
   x = x + 0.001;
end

j = 1;
while j <= i
   if j+1 <= i-1 && (Y(j)-p_value)*(Y(j+1)-p_value) <=0
      m = j;
   end
   j = j + 1;
end

area = 2*pi*Rc^2-2*pi*Rc*X(m)*Rc;

etai_rad = Crad_Orad*rou_p0;
t_inc =((4/3)*Crad_Orad*rou_p0*P*((pi*a*(b^2)))*(1-(v^(-belta))))^(-1);
delta_t = 0;


Time = M(:,1);
E_no_cavity = M(:,2);
E_cavity = M(:,3);
conductivity = M(:,4);
current_density_1 = M(:,8);
current_density_2 = M(:,9);
current_density_3 = M(:,10);
```

```
current_density_4 = M(:,11);
current_density_5 = M(:,12);
current_density_6 = M(:,13);
current_density_7 = M(:,14);
current_density_8 = M(:,15);
current_density_9 = M(:,16);
current_density_10 = M(:,17);
current_density_11 = M(:,18);
current_density_12 = M(:,19);
current_density_13 = M(:,20);
current_density_14 = M(:,21);
current_density_15 = M(:,22);
current_density_16 = M(:,23);
current_density_17 = M(:,24);
current_density_18 = M(:,25);
current_density_19 = M(:,26);
current_density_20 = M(:,27);
current_density_21 = M(:,28);

a1 = 1.001+0/20*(2-1.001);
a2 = 1.001+1/20*(2-1.001);
a3 = 1.001+2/20*(2-1.001);
a4 = 1.001+3/20*(2-1.001);
a5 = 1.001+4/20*(2-1.001);
a6 = 1.001+5/20*(2-1.001);
a7 = 1.001+6/20*(2-1.001);
a8 = 1.001+7/20*(2-1.001);
a9 = 1.001+8/20*(2-1.001);
a10 = 1.001+9/20*(2-1.001);
a11 = 1.001+10/20*(2-1.001);
a12 = 1.001+11/20*(2-1.001);
a13 = 1.001+12/20*(2-1.001);
a14 = 1.001+13/20*(2-1.001);
a15 = 1.001+14/20*(2-1.001);
a16 = 1.001+15/20*(2-1.001);
a17 = 1.001+16/20*(2-1.001);
a18 = 1.001+17/20*(2-1.001);
a19 = 1.001+18/20*(2-1.001);
a20 = 1.001+19/20*(2-1.001);
a21 = 1.001+20/20*(2-1.001);

decay_constant_1 =
a1^2*area*current_density_1+a2^2*area*current_density_2+a3^2*area*current_density_3+a4^2*area*current_
density_4+a5^2*area*current_density_5+...

a6^2*area*current_density_6+a7^2*area*current_density_7+a8^2*area*current_density_8+a9^2*area*current_
density_9+a10^2*area*current_density_10+...

a11^2*area*current_density_11+a12^2*area*current_density_12+a13^2*area*current_density_13+a14^2*area
*current_density_14+a15^2*area*current_density_15+...

a16^2*area*current_density_16+a17^2*area*current_density_17+a18^2*area*current_density_18+a19^2*area
*current_density_19+a20^2*area*current_density_20+a21^2*area*current_density_21;
```

decay_constant_2 =
a2^2*area*current_density_2+a3^2*area*current_density_3+a4^2*area*current_density_4+a5^2*area*current_density_5+...

a6^2*area*current_density_6+a7^2*area*current_density_7+a8^2*area*current_density_8+a9^2*area*current_density_9+a10^2*area*current_density_10+...

a11^2*area*current_density_11+a12^2*area*current_density_12+a13^2*area*current_density_13+a14^2*area*current_density_14+a15^2*area*current_density_15+...

a16^2*area*current_density_16+a17^2*area*current_density_17+a18^2*area*current_density_18+a19^2*area*current_density_19+a20^2*area*current_density_20+a21^2*area*current_density_21;
decay_constant_3 =
a3^2*area*current_density_3+a4^2*area*current_density_4+a5^2*area*current_density_5+...

a6^2*area*current_density_6+a7^2*area*current_density_7+a8^2*area*current_density_8+a9^2*area*current_density_9+a10^2*area*current_density_10+...

a11^2*area*current_density_11+a12^2*area*current_density_12+a13^2*area*current_density_13+a14^2*area*current_density_14+a15^2*area*current_density_15+...

a16^2*area*current_density_16+a17^2*area*current_density_17+a18^2*area*current_density_18+a19^2*area*current_density_19+a20^2*area*current_density_20+a21^2*area*current_density_21;
decay_constant_4 = a4^2*area*current_density_4+a5^2*area*current_density_5+...

a6^2*area*current_density_6+a7^2*area*current_density_7+a8^2*area*current_density_8+a9^2*area*current_density_9+a10^2*area*current_density_10+...

a11^2*area*current_density_11+a12^2*area*current_density_12+a13^2*area*current_density_13+a14^2*area*current_density_14+a15^2*area*current_density_15+...

a16^2*area*current_density_16+a17^2*area*current_density_17+a18^2*area*current_density_18+a19^2*area*current_density_19+a20^2*area*current_density_20+a21^2*area*current_density_21;
decay_constant_5 = a5^2*area*current_density_5+...

a6^2*area*current_density_6+a7^2*area*current_density_7+a8^2*area*current_density_8+a9^2*area*current_density_9+a10^2*area*current_density_10+...

a11^2*area*current_density_11+a12^2*area*current_density_12+a13^2*area*current_density_13+a14^2*area*current_density_14+a15^2*area*current_density_15+...

a16^2*area*current_density_16+a17^2*area*current_density_17+a18^2*area*current_density_18+a19^2*area*current_density_19+a20^2*area*current_density_20+a21^2*area*current_density_21;
decay_constant_6 =
a6^2*area*current_density_6+a7^2*area*current_density_7+a8^2*area*current_density_8+a9^2*area*current_density_9+a10^2*area*current_density_10+...

a11^2*area*current_density_11+a12^2*area*current_density_12+a13^2*area*current_density_13+a14^2*area*current_density_14+a15^2*area*current_density_15+...

a16^2*area*current_density_16+a17^2*area*current_density_17+a18^2*area*current_density_18+a19^2*area*current_density_19+a20^2*area*current_density_20+a21^2*area*current_density_21;
decay_constant_7 =
a7^2*area*current_density_7+a8^2*area*current_density_8+a9^2*area*current_density_9+a10^2*area*current_density_10+...

a11^2*area*current_density_11+a12^2*area*current_density_12+a13^2*area*current_density_13+a14^2*area

*current_density_14+a15^2*area*current_density_15+...

a16^2*area*current_density_16+a17^2*area*current_density_17+a18^2*area*current_density_18+a19^2*area*current_density_19+a20^2*area*current_density_20+a21^2*area*current_density_21;
decay_constant_8 =
a8^2*area*current_density_8+a9^2*area*current_density_9+a10^2*area*current_density_10+...

a11^2*area*current_density_11+a12^2*area*current_density_12+a13^2*area*current_density_13+a14^2*area*current_density_14+a15^2*area*current_density_15+...

a16^2*area*current_density_16+a17^2*area*current_density_17+a18^2*area*current_density_18+a19^2*area*current_density_19+a20^2*area*current_density_20+a21^2*area*current_density_21;
decay_constant_9 = a9^2*area*current_density_9+a10^2*area*current_density_10+...

a11^2*area*current_density_11+a12^2*area*current_density_12+a13^2*area*current_density_13+a14^2*area*current_density_14+a15^2*area*current_density_15+...

a16^2*area*current_density_16+a17^2*area*current_density_17+a18^2*area*current_density_18+a19^2*area*current_density_19+a20^2*area*current_density_20+a21^2*area*current_density_21;
decay_constant_10 = a10^2*area*current_density_10+...

a11^2*area*current_density_11+a12^2*area*current_density_12+a13^2*area*current_density_13+a14^2*area*current_density_14+a15^2*area*current_density_15+...

a16^2*area*current_density_16+a17^2*area*current_density_17+a18^2*area*current_density_18+a19^2*area*current_density_19+a20^2*area*current_density_20+a21^2*area*current_density_21;
decay_constant_11 =
a11^2*area*current_density_11+a12^2*area*current_density_12+a13^2*area*current_density_13+a14^2*area*current_density_14+a15^2*area*current_density_15+...

a16^2*area*current_density_16+a17^2*area*current_density_17+a18^2*area*current_density_18+a19^2*area*current_density_19+a20^2*area*current_density_20+a21^2*area*current_density_21;
decay_constant_12 =
a12^2*area*current_density_12+a13^2*area*current_density_13+a14^2*area*current_density_14+a15^2*area*current_density_15+...

a16^2*area*current_density_16+a17^2*area*current_density_17+a18^2*area*current_density_18+a19^2*area*current_density_19+a20^2*area*current_density_20+a21^2*area*current_density_21;
decay_constant_13 =
a13^2*area*current_density_13+a14^2*area*current_density_14+a15^2*area*current_density_15+...

a16^2*area*current_density_16+a17^2*area*current_density_17+a18^2*area*current_density_18+a19^2*area*current_density_19+a20^2*area*current_density_20+a21^2*area*current_density_21;
decay_constant_14 = a14^2*area*current_density_14+a15^2*area*current_density_15+...

a16^2*area*current_density_16+a17^2*area*current_density_17+a18^2*area*current_density_18+a19^2*area*current_density_19+a20^2*area*current_density_20+a21^2*area*current_density_21;
decay_constant_15 = a15^2*area*current_density_15+...

a16^2*area*current_density_16+a17^2*area*current_density_17+a18^2*area*current_density_18+a19^2*area*current_density_19+a20^2*area*current_density_20+a21^2*area*current_density_21;
decay_constant_16 =
a16^2*area*current_density_16+a17^2*area*current_density_17+a18^2*area*current_density_18+a19^2*area*current_density_19+a20^2*area*current_density_20+a21^2*area*current_density_21;
decay_constant_17 =
a17^2*area*current_density_17+a18^2*area*current_density_18+a19^2*area*current_density_19+a20^2*area

```
*current_density_20+a21^2*area*current_density_21;
decay_constant_18 =
a18^2*area*current_density_18+a19^2*area*current_density_19+a20^2*area*current_density_20+a21^2*area
*current_density_21;
decay_constant_19 =
a19^2*area*current_density_19+a20^2*area*current_density_20+a21^2*area*current_density_21;
decay_constant_20 = a20^2*area*current_density_20+a21^2*area*current_density_21;
decay_constant_21 = a21^2*area*current_density_21;
m = length(E_cavity);
t_start = 0;
t_end = max(Time);
i = 1;
t_step = 1;
t_step_ramp = 0.01;
t_ratio = t_step/t_step_ramp;
t_PD = 1e-8;
z = 1;
j = 1;
w = 1.95;
while j <= m+(t_ratio-1)*t_ramp
    if j <= t_step/t_step_ramp*t_ramp + 1
        if j == 1
            E_with_cavity(j) = E_cavity(1);
            Cond(j) = conductivity(1);
            Decay_new_constant_1(j) = decay_constant_1(1);
            Decay_new_constant_2(j) = decay_constant_2(1);
            Decay_new_constant_3(j) = decay_constant_3(1);
            Decay_new_constant_4(j) = decay_constant_4(1);
            Decay_new_constant_5(j) = decay_constant_5(1);
            Decay_new_constant_6(j) = decay_constant_6(1);
            Decay_new_constant_7(j) = decay_constant_7(1);
            Decay_new_constant_8(j) = decay_constant_8(1);
            Decay_new_constant_9(j) = decay_constant_9(1);
            Decay_new_constant_10(j) = decay_constant_10(1);
            Decay_new_constant_11(j) = decay_constant_11(1);
            Decay_new_constant_12(j) = decay_constant_12(1);
            Decay_new_constant_13(j) = decay_constant_13(1);
            Decay_new_constant_14(j) = decay_constant_14(1);
            Decay_new_constant_15(j) = decay_constant_15(1);
            Decay_new_constant_16(j) = decay_constant_16(1);
            Decay_new_constant_17(j) = decay_constant_17(1);
            Decay_new_constant_18(j) = decay_constant_18(1);
            Decay_new_constant_19(j) = decay_constant_19(1);
            Decay_new_constant_20(j) = decay_constant_20(1);
            Decay_new_constant_21(j) = decay_constant_21(1);
            Y(j) = 1;
            J(j,1) = j;
            Z (j,1) = 1;
        else
            if rem(j-1,t_ratio) > 0
                y = floor((j-1)/t_ratio)+2;
                r = (j-1-(y-1)*t_ratio)/t_ratio+1;
```

```
        J(j,1) = j;
        Y(j,1) = y;
        Z (j,1) = r;
        E_with_cavity(j,1) = E_cavity(y-1) + (E_cavity(y)-E_cavity(y-1))*((j-1-(y-1)*t_ratio)/t_ratio+1);
        Cond(j) = conductivity(y-1) + (conductivity(y)-conductivity(y-1))*((j-1-(y-1)*t_ratio)/t_ratio+1);
        Decay_new_constant_1(j,1) = decay_constant_1(y-1) + (decay_constant_1(y)-decay_constant_1(y-
1))*((j-1-(y-1)*t_ratio)/t_ratio+1);
        Decay_new_constant_2(j,1) = decay_constant_2(y-1) + (decay_constant_2(y)-decay_constant_2(y-
1))*((j-1-(y-1)*t_ratio)/t_ratio+1);
        Decay_new_constant_3(j,1) = decay_constant_3(y-1) + (decay_constant_3(y)-decay_constant_3(y-
1))*((j-1-(y-1)*t_ratio)/t_ratio+1);
        Decay_new_constant_4(j,1) = decay_constant_4(y-1) + (decay_constant_4(y)-decay_constant_4(y-
1))*((j-1-(y-1)*t_ratio)/t_ratio+1);
        Decay_new_constant_5(j,1) = decay_constant_5(y-1) + (decay_constant_5(y)-decay_constant_5(y-
1))*((j-1-(y-1)*t_ratio)/t_ratio+1);
        Decay_new_constant_6(j,1) = decay_constant_6(y-1) + (decay_constant_6(y)-decay_constant_6(y-
1))*((j-1-(y-1)*t_ratio)/t_ratio+1);
        Decay_new_constant_7(j,1) = decay_constant_7(y-1) + (decay_constant_7(y)-decay_constant_7(y-
1))*((j-1-(y-1)*t_ratio)/t_ratio+1);
        Decay_new_constant_8(j,1) = decay_constant_8(y-1) + (decay_constant_8(y)-decay_constant_8(y-
1))*((j-1-(y-1)*t_ratio)/t_ratio+1);
        Decay_new_constant_9(j,1) = decay_constant_9(y-1) + (decay_constant_9(y)-decay_constant_9(y-
1))*((j-1-(y-1)*t_ratio)/t_ratio+1);
        Decay_new_constant_10(j,1) = decay_constant_10(y-1) + (decay_constant_10(y)-
decay_constant_10(y-1))*((j-1-(y-1)*t_ratio)/t_ratio+1);
        Decay_new_constant_11(j,1) = decay_constant_11(y-1) + (decay_constant_11(y)-
decay_constant_11(y-1))*((j-1-(y-1)*t_ratio)/t_ratio+1);
        Decay_new_constant_12(j,1) = decay_constant_12(y-1) + (decay_constant_12(y)-
decay_constant_12(y-1))*((j-1-(y-1)*t_ratio)/t_ratio+1);
        Decay_new_constant_13(j,1) = decay_constant_13(y-1) + (decay_constant_13(y)-
decay_constant_13(y-1))*((j-1-(y-1)*t_ratio)/t_ratio+1);
        Decay_new_constant_14(j,1) = decay_constant_14(y-1) + (decay_constant_14(y)-
decay_constant_14(y-1))*((j-1-(y-1)*t_ratio)/t_ratio+1);
        Decay_new_constant_15(j,1) = decay_constant_15(y-1) + (decay_constant_15(y)-
decay_constant_15(y-1))*((j-1-(y-1)*t_ratio)/t_ratio+1);
        Decay_new_constant_16(j,1) = decay_constant_16(y-1) + (decay_constant_16(y)-
decay_constant_16(y-1))*((j-1-(y-1)*t_ratio)/t_ratio+1);
        Decay_new_constant_17(j,1) = decay_constant_17(y-1) + (decay_constant_17(y)-
decay_constant_17(y-1))*((j-1-(y-1)*t_ratio)/t_ratio+1);
        Decay_new_constant_18(j,1) = decay_constant_18(y-1) + (decay_constant_18(y)-
decay_constant_18(y-1))*((j-1-(y-1)*t_ratio)/t_ratio+1);
        Decay_new_constant_19(j,1) = decay_constant_19(y-1) + (decay_constant_19(y)-
decay_constant_19(y-1))*((j-1-(y-1)*t_ratio)/t_ratio+1);
        Decay_new_constant_20(j,1) = decay_constant_20(y-1) + (decay_constant_20(y)-
decay_constant_20(y-1))*((j-1-(y-1)*t_ratio)/t_ratio+1);
        Decay_new_constant_21(j,1) = decay_constant_21(y-1) + (decay_constant_21(y)-
decay_constant_21(y-1))*((j-1-(y-1)*t_ratio)/t_ratio+1);

    elseif rem(j-1,t_ratio) == 0
        y = (j-1)/t_ratio+1;
        r = (j-(y-1)*t_ratio)/t_ratio;
        J(j,1) = j;
        Y(j,1) = y-1;
        Z (j,1) = r;
```

```
            E_with_cavity(j,1) = E_cavity(y);
            Cond(j,1) = conductivity(y);
            Decay_new_constant_1(j,1) = decay_constant_1(y);
            Decay_new_constant_2(j,1) = decay_constant_2(y);
            Decay_new_constant_3(j,1) = decay_constant_3(y);
            Decay_new_constant_4(j,1) = decay_constant_4(y);
            Decay_new_constant_5(j,1) = decay_constant_5(y);
            Decay_new_constant_6(j,1) = decay_constant_6(y);
            Decay_new_constant_7(j,1) = decay_constant_7(y);
            Decay_new_constant_8(j,1) = decay_constant_8(y);
            Decay_new_constant_9(j,1) = decay_constant_9(y);
            Decay_new_constant_10(j,1) = decay_constant_10(y);
            Decay_new_constant_11(j,1) = decay_constant_11(y);
            Decay_new_constant_12(j,1) = decay_constant_12(y);
            Decay_new_constant_13(j,1) = decay_constant_13(y);
            Decay_new_constant_14(j,1) = decay_constant_14(y);
            Decay_new_constant_15(j,1) = decay_constant_15(y);
            Decay_new_constant_16(j,1) = decay_constant_16(y);
            Decay_new_constant_17(j,1) = decay_constant_17(y);
            Decay_new_constant_18(j,1) = decay_constant_18(y);
            Decay_new_constant_19(j,1) = decay_constant_19(y);
            Decay_new_constant_20(j,1) = decay_constant_20(y);
            Decay_new_constant_21(j,1) = decay_constant_21(y);


        end
    end
else
    E_with_cavity(j,1) = E_cavity(j-(t_ratio-1)*t_ramp);
    Cond(j,1) = conductivity(j-(t_ratio-1)*t_ramp);
    Decay_new_constant_1(j,1) = decay_constant_1(j-(t_ratio-1)*t_ramp);
    Decay_new_constant_2(j,1) = decay_constant_2(j-(t_ratio-1)*t_ramp);
    Decay_new_constant_3(j,1) = decay_constant_3(j-(t_ratio-1)*t_ramp);
    Decay_new_constant_4(j,1) = decay_constant_4(j-(t_ratio-1)*t_ramp);
    Decay_new_constant_5(j,1) = decay_constant_5(j-(t_ratio-1)*t_ramp);
    Decay_new_constant_6(j,1) = decay_constant_6(j-(t_ratio-1)*t_ramp);
    Decay_new_constant_7(j,1) = decay_constant_7(j-(t_ratio-1)*t_ramp);
    Decay_new_constant_8(j,1) = decay_constant_8(j-(t_ratio-1)*t_ramp);
    Decay_new_constant_9(j,1) = decay_constant_9(j-(t_ratio-1)*t_ramp);
    Decay_new_constant_10(j,1) = decay_constant_10(j-(t_ratio-1)*t_ramp);
    Decay_new_constant_11(j,1) = decay_constant_11(j-(t_ratio-1)*t_ramp);
    Decay_new_constant_12(j,1) = decay_constant_12(j-(t_ratio-1)*t_ramp);
    Decay_new_constant_13(j,1) = decay_constant_13(j-(t_ratio-1)*t_ramp);
    Decay_new_constant_14(j,1) = decay_constant_14(j-(t_ratio-1)*t_ramp);
    Decay_new_constant_15(j,1) = decay_constant_15(j-(t_ratio-1)*t_ramp);
    Decay_new_constant_16(j,1) = decay_constant_16(j-(t_ratio-1)*t_ramp);
    Decay_new_constant_17(j,1) = decay_constant_17(j-(t_ratio-1)*t_ramp);
    Decay_new_constant_18(j,1) = decay_constant_18(j-(t_ratio-1)*t_ramp);
    Decay_new_constant_19(j,1) = decay_constant_19(j-(t_ratio-1)*t_ramp);
    Decay_new_constant_20(j,1) = decay_constant_20(j-(t_ratio-1)*t_ramp);
    Decay_new_constant_21(j,1) = decay_constant_21(j-(t_ratio-1)*t_ramp);
```

```
        end
     j = j + 1;
  end


while t_start <= t_ramp
   if t_start == 0 && virgin_void == 1
      if nPD == 0
         Conduc_air = air_noPD;
      end
      t0 = t_start;

      q_s_1 = 0;
      q_s_2 = 0;
      q_s_3 = 0;
      q_s_4 = 0;
      q_s_5 = 0;
      q_s_6 = 0;
      q_s_7 = 0;
      q_s_8 = 0;
      q_s_9 = 0;
      q_s_10 = 0;
      q_s_11 = 0;
      q_s_12 = 0;
      q_s_13 = 0;
      q_s_14 = 0;
      q_s_15 = 0;
      q_s_16 = 0;
      q_s_17 = 0;
      q_s_18 = 0;
      q_s_19 = 0;
      q_s_20 = 0;
      q_s_21 = 0;
      Es0 = 0;
      Time(i) = t_start;
      E_cav0 = E_with_cavity(i)+Es0;
      Time(i) = t_start;
      Field_cav(i,1) = E_cav0;
      Field_s(i) = Es0;
      Charge_surface(i) = q_s_1;
      fprintf('Time:       %d\n', Time(i));
      fprintf('Cavity field:     %d kV/mm \n ', E_cav0);
      fprintf('Surface field:      %d kV/mm \n ', Es0);
      fprintf('Surface charge:     %d\n', q_s_1);
      if nPD == 0
         q_s_1 = 0;
         Es = 0;
      end
      E_cav = E_with_cavity(i+1) + Es;
      i = i + 1;
      virgin_void = 0;
```

```
        t_start = t_start + t_step_ramp;
        Time(i) = t_start;
        Field_cav(i,1) = E_cav;
        Field_s(i) = Es;
        Charge_surface(i) = q_s_1;

        fprintf('Time:      %d\n', Time(i));
        fprintf('Cavity field:     %d kV/mm \n ', Field_cav(i,1));
        fprintf('Surface field:     %d kV/mm \n ', Field_s(i));
        fprintf('Surface charge:     %d\n', Charge_surface(i));
    end

    if (E_cav <= E_inc && virgin_void == 0)
        if nPD == 0
            Conduc_air = air_noPD;
            q_start = q_s_1;
            E_cav_app = E_with_cavity(i+1-nPD);
            q_constant = Er0*pi*b^2*(1+Er*abs(K*(a/b)-1));
            Es = -q_s_1/q_constant;
            E_cav = E_cav_app + Es;
            i = i + 1;
            t_start = t_start + t_step_ramp;
            Time(i) = t_start;
            Field_cav(i,1) = E_cav;
            Field_s(i) = Es;
            Charge_surface(i) = q_s_1;

            fprintf('Time:     %d\n', Time(i));
            fprintf('Cavity field:     %d kV/mm \n ', Field_cav(i,1));
            fprintf('Surface field:     %d kV/mm \n ', Field_s(i));
            fprintf('Surface charge:     %d\n', Charge_surface(i));
        elseif nPD > 0
            Conduc_air = air_noPD;
            q_start = q_s_1;
            q_s_1 = q_s_1 - Decay_new_constant_1(i+1-nPD)*t_step_ramp;
            q_s_2 = q_s_2 + Decay_new_constant_1(i+1-nPD)*t_step_ramp;
            q_s_2 = q_s_2- Decay_new_constant_2(i+1-nPD)*t_step_ramp;
            q_s_3 = q_s_3 + Decay_new_constant_2(i+1-nPD)*t_step_ramp;
            q_s_3 = q_s_3- Decay_new_constant_3(i+1-nPD)*t_step_ramp;
            q_s_4 = q_s_4 + Decay_new_constant_3(i+1-nPD)*t_step_ramp;
            q_s_4 = q_s_4- Decay_new_constant_4(i+1-nPD)*t_step_ramp;
            q_s_5 = q_s_5 + Decay_new_constant_4(i+1-nPD)*t_step_ramp;
            q_s_5 = q_s_5- Decay_new_constant_5(i+1-nPD)*t_step_ramp;
            q_s_6 = q_s_6 + Decay_new_constant_5(i+1-nPD)*t_step_ramp;
            q_s_6 = q_s_6- Decay_new_constant_6(i+1-nPD)*t_step_ramp;
            q_s_7 = q_s_7 + Decay_new_constant_6(i+1-nPD)*t_step_ramp;
            q_s_7 = q_s_7- Decay_new_constant_7(i+1-nPD)*t_step_ramp;
            q_s_8 = q_s_8 + Decay_new_constant_7(i+1-nPD)*t_step_ramp;
            q_s_8 = q_s_8- Decay_new_constant_8(i+1-nPD)*t_step_ramp;
            q_s_9 = q_s_9 + Decay_new_constant_8(i+1-nPD)*t_step_ramp;
            q_s_9 = q_s_9- Decay_new_constant_9(i+1-nPD)*t_step_ramp;
```

```
q_s_10 = q_s_10 + Decay_new_constant_9(i+1-nPD)*t_step_ramp;
q_s_10 = q_s_10- Decay_new_constant_10(i+1-nPD)*t_step_ramp;
q_s_11 = q_s_11 + Decay_new_constant_10(i+1-nPD)*t_step_ramp;
q_s_11 = q_s_11- Decay_new_constant_11(i+1-nPD)*t_step_ramp;
q_s_12 = q_s_12 + Decay_new_constant_11(i+1-nPD)*t_step_ramp;
q_s_12 = q_s_12- Decay_new_constant_12(i+1-nPD)*t_step_ramp;
q_s_13 = q_s_13 + Decay_new_constant_12(i+1-nPD)*t_step_ramp;
q_s_13 = q_s_13- Decay_new_constant_13(i+1-nPD)*t_step_ramp;
q_s_14 = q_s_14 + Decay_new_constant_13(i+1-nPD)*t_step_ramp;
q_s_14 = q_s_14 - Decay_new_constant_14(i+1-nPD)*t_step_ramp;
q_s_15 = q_s_15 + Decay_new_constant_14(i+1-nPD)*t_step_ramp;
q_s_15 = q_s_15 - Decay_new_constant_15(i+1-nPD)*t_step_ramp;
q_s_16 = q_s_16 + Decay_new_constant_15(i+1-nPD)*t_step_ramp;
q_s_16 = q_s_16 - Decay_new_constant_16(i+1-nPD)*t_step_ramp;
q_s_17 = q_s_17 + Decay_new_constant_16(i+1-nPD)*t_step_ramp;
q_s_17 = q_s_17- Decay_new_constant_17(i+1-nPD)*t_step_ramp;
q_s_18 = q_s_18 + Decay_new_constant_17(i+1-nPD)*t_step_ramp;
q_s_18 = q_s_18- Decay_new_constant_18(i+1-nPD)*t_step_ramp;
q_s_19 = q_s_19 + Decay_new_constant_18(i+1-nPD)*t_step_ramp;
q_s_19 = q_s_19- Decay_new_constant_19(i+1-nPD)*t_step_ramp;
q_s_20 = q_s_20 + Decay_new_constant_19(i+1-nPD)*t_step_ramp;
q_s_20 = q_s_20 - Decay_new_constant_20(i+1-nPD)*t_step_ramp;
q_s_21 = q_s_21 + Decay_new_constant_20(i+1-nPD)*t_step_ramp;
q_s_21 = q_s_21 - Decay_new_constant_21(i+1-nPD)*t_step_ramp;


E_cav_app = E_with_cavity(i+1-nPD);
q_constant = Er0*pi*b^2*(1+Er*abs(K*(a/b)-1));
Es = -
(q_s_1/a1^2+q_s_2/a2^2+q_s_3/a3^2+q_s_4/a4^2+q_s_5/a5^2+q_s_6/a6^2+q_s_7/a7^2+q_s_8/a8^2+q_s_9/a9
^2+q_s_10/a10^2+q_s_11/a11^2+q_s_12/a12^2+q_s_13/a13^2+q_s_14/a14^2+q_s_15/a15^2+q_s_16/a16^2+q
_s_17/a17^2+q_s_18/a18^2+q_s_19/a19^2+q_s_20/a20^2+q_s_21/a21^2)/q_constant;
E_cav = E_cav_app + Es;
i = i + 1;
t_start = t_start + t_step_ramp;
Time(i) = t_start;
Field_cav(i,1) = E_cav;
Field_s(i) = Es;
Charge_surface(i) = q_s_1;

fprintf('Time:      %d\n', Time(i));
fprintf('Cavity field:     %d kV/mm \n ', Field_cav(i,1));
fprintf('Surface field:     %d kV/mm \n ', Field_s(i));
fprintf('Surface charge:     %d\n', Charge_surface(i));
    end
  end

  if E_cav > E_inc
    if nPD == 0
      probability = 1-exp(-etai_rad*P*Veff*delta_t);
      random = rand(1);
      fprintf('Time:      %d\n', Time(i));
```

```
fprintf('Probability:    %d\n ', probability);
fprintf('Random:     %d\n', random);
if probability <= random
    Conduc_air = air_noPD;
    q_start = q_s_1;
    q_s_1 = q_s_1 - Decay_new_constant_1(i+1-nPD)*t_step_ramp;
    q_s_2 = q_s_2 + Decay_new_constant_1(i+1-nPD)*t_step_ramp;
    q_s_2 = q_s_2- Decay_new_constant_2(i+1-nPD)*t_step_ramp;
    q_s_3 = q_s_3 + Decay_new_constant_2(i+1-nPD)*t_step_ramp;
    q_s_3 = q_s_3- Decay_new_constant_3(i+1-nPD)*t_step_ramp;
    q_s_4 = q_s_4 + Decay_new_constant_3(i+1-nPD)*t_step_ramp;
    q_s_4 = q_s_4- Decay_new_constant_4(i+1-nPD)*t_step_ramp;
    q_s_5 = q_s_5 + Decay_new_constant_4(i+1-nPD)*t_step_ramp;
    q_s_5 = q_s_5- Decay_new_constant_5(i+1-nPD)*t_step_ramp;
    q_s_6 = q_s_6 + Decay_new_constant_5(i+1-nPD)*t_step_ramp;
    q_s_6 = q_s_6- Decay_new_constant_6(i+1-nPD)*t_step_ramp;
    q_s_7 = q_s_7 + Decay_new_constant_6(i+1-nPD)*t_step_ramp;
    q_s_7 = q_s_7- Decay_new_constant_7(i+1-nPD)*t_step_ramp;
    q_s_8 = q_s_8 + Decay_new_constant_7(i+1-nPD)*t_step_ramp;
    q_s_8 = q_s_8- Decay_new_constant_8(i+1-nPD)*t_step_ramp;
    q_s_9 = q_s_9 + Decay_new_constant_8(i+1-nPD)*t_step_ramp;
    q_s_9 = q_s_9- Decay_new_constant_9(i+1-nPD)*t_step_ramp;
    q_s_10 = q_s_10 + Decay_new_constant_9(i+1-nPD)*t_step_ramp;
    q_s_10 = q_s_10- Decay_new_constant_10(i+1-nPD)*t_step_ramp;
    q_s_11 = q_s_11 + Decay_new_constant_10(i+1-nPD)*t_step_ramp;
    q_s_11 = q_s_11- Decay_new_constant_11(i+1-nPD)*t_step_ramp;
    q_s_12 = q_s_12 + Decay_new_constant_11(i+1-nPD)*t_step_ramp;
    q_s_12 = q_s_12- Decay_new_constant_12(i+1-nPD)*t_step_ramp;
    q_s_13 = q_s_13 + Decay_new_constant_12(i+1-nPD)*t_step_ramp;
    q_s_13 = q_s_13- Decay_new_constant_13(i+1-nPD)*t_step_ramp;
    q_s_14 = q_s_14 + Decay_new_constant_13(i+1-nPD)*t_step_ramp;
    q_s_14 = q_s_14 - Decay_new_constant_14(i+1-nPD)*t_step_ramp;
    q_s_15 = q_s_15 + Decay_new_constant_14(i+1-nPD)*t_step_ramp;
    q_s_15 = q_s_15 - Decay_new_constant_15(i+1-nPD)*t_step_ramp;
    q_s_16 = q_s_16 + Decay_new_constant_15(i+1-nPD)*t_step_ramp;
    q_s_16 = q_s_16 - Decay_new_constant_16(i+1-nPD)*t_step_ramp;
    q_s_17 = q_s_17 + Decay_new_constant_16(i+1-nPD)*t_step_ramp;
    q_s_17 = q_s_17- Decay_new_constant_17(i+1-nPD)*t_step_ramp;
    q_s_18 = q_s_18 + Decay_new_constant_17(i+1-nPD)*t_step_ramp;
    q_s_18 = q_s_18- Decay_new_constant_18(i+1-nPD)*t_step_ramp;
    q_s_19 = q_s_19 + Decay_new_constant_18(i+1-nPD)*t_step_ramp;
    q_s_19 = q_s_19- Decay_new_constant_19(i+1-nPD)*t_step_ramp;
    q_s_20 = q_s_20 + Decay_new_constant_19(i+1-nPD)*t_step_ramp;
    q_s_20 = q_s_20 - Decay_new_constant_20(i+1-nPD)*t_step_ramp;
    q_s_21 = q_s_21 + Decay_new_constant_20(i+1-nPD)*t_step_ramp;
    q_s_21 = q_s_21 - Decay_new_constant_21(i+1-nPD)*t_step_ramp;

    E_cav_app = E_with_cavity(i+1-nPD);
    q_constant = Er0*pi*b^2*(1+Er*abs(K*(a/b)-1));
    Es = -
(q_s_1/a1^2+q_s_2/a2^2+q_s_3/a3^2+q_s_4/a4^2+q_s_5/a5^2+q_s_6/a6^2+q_s_7/a7^2+q_s_8/a8^2+q_s_9/a9
^2+q_s_10/a10^2+q_s_11/a11^2+q_s_12/a12^2+q_s_13/a13^2+q_s_14/a14^2+q_s_15/a15^2+q_s_16/a16^2+q
```

```
_s_17/a17^2+q_s_18/a18^2+q_s_19/a19^2+q_s_20/a20^2+q_s_21/a21^2)/q_constant;
        E_cav = E_cav_app + Es;

        t_start = t_start + t_step_ramp;
        delta_t = delta_t + t_step_ramp;
        i = i + 1;
        Time(i) = t_start;
        Field_cav(i,1) = E_cav;
        Field_s(i) = Es;
        Charge_surface(i) = q_s_1;

        fprintf('Cavity field:     %d kV/mm \n ', Field_cav(i,1));
        fprintf('Surface field:     %d kV/mm \n ', Field_s(i));
        fprintf('Surface charge:     %d\n', Charge_surface(i));

    elseif probability > random
        disp('PD occurs, and this PD is the first one');
        Conduc_air = air_PD;
        Over_field = E_cav-E_inc;
        E_ext = abs(E_ext_min+(E_inc-E_ext_min)*exp((-abs(E_cav+E_inc))/(E_inc-E_ext_min)));
        E_cav_app = E_with_cavity(i);
        E_cav = E_ext;
        Es = E_cav - E_cav_app;
        delta_E = Field_cav(i,1) - E_cav;
        q_constant = Er0*pi*b^2*(1+Er*abs(K*(a/b)-1));
        q_s_1 = -Es*q_constant;
        i = i + 1;
        nPD = nPD + 1;
        delta_t = 0;
        Time_PD(nPD) = t_start;
        Charge_induce(nPD) = q_s_1-Charge_surface(i-1);
        Charge_app(nPD) = delta_E*q_app_constant;
        Field_over(nPD) = Over_field;
        Field_ext(nPD) = E_ext;
        Field_occ(nPD) = Field_cav(i-1);

        t_start = t_start + t_PD;
        Time(i) = t_start;
        Field_cav(i,1) = E_cav;
        Field_s(i) = Es;
        Charge_surface(i) = q_s_1;
        fprintf('Cavity field:     %d kV/mm \n ', Field_cav(i,1));
        fprintf('Surface field:     %d kV/mm \n ', Field_s(i));
        fprintf('Surface charge:     %d\n', Charge_surface(i));

    end

elseif nPD >= 1
    Ndt_0 = epsilon*abs(q_s_1/e);
    Ndt = Ndt_0*exp(-delta_t/tau);
    N_dt = Ndt*v0*exp(-(work_function-sqrt(abs(E_cav)*N_dt_constant_1))/N_dt_constant_2);
```

133

```matlab
Ne = etai_rad*P*Veff;
Ng = N_dt + Ne;
probability = 1-exp(-Ng*delta_t);
random = rand(1);
fprintf('Time:     %d\n', Time(i));
fprintf('Probability:     %d\n ', probability);
fprintf('Random:     %d\n', random);
if probability <= random
    Conduc_air = air_noPD;
    q_start = q_s_1;
    q_s_1 = q_s_1 - Decay_new_constant_1(i+1-nPD)*t_step_ramp;
    q_s_2 = q_s_2 + Decay_new_constant_1(i+1-nPD)*t_step_ramp;
    q_s_2 = q_s_2- Decay_new_constant_2(i+1-nPD)*t_step_ramp;
    q_s_3 = q_s_3 + Decay_new_constant_2(i+1-nPD)*t_step_ramp;
    q_s_3 = q_s_3- Decay_new_constant_3(i+1-nPD)*t_step_ramp;
    q_s_4 = q_s_4 + Decay_new_constant_3(i+1-nPD)*t_step_ramp;
    q_s_4 = q_s_4- Decay_new_constant_4(i+1-nPD)*t_step_ramp;
    q_s_5 = q_s_5 + Decay_new_constant_4(i+1-nPD)*t_step_ramp;
    q_s_5 = q_s_5- Decay_new_constant_5(i+1-nPD)*t_step_ramp;
    q_s_6 = q_s_6 + Decay_new_constant_5(i+1-nPD)*t_step_ramp;
    q_s_6 = q_s_6- Decay_new_constant_6(i+1-nPD)*t_step_ramp;
    q_s_7 = q_s_7 + Decay_new_constant_6(i+1-nPD)*t_step_ramp;
    q_s_7 = q_s_7- Decay_new_constant_7(i+1-nPD)*t_step_ramp;
    q_s_8 = q_s_8 + Decay_new_constant_7(i+1-nPD)*t_step_ramp;
    q_s_8 = q_s_8- Decay_new_constant_8(i+1-nPD)*t_step_ramp;
    q_s_9 = q_s_9 + Decay_new_constant_8(i+1-nPD)*t_step_ramp;
    q_s_9 = q_s_9- Decay_new_constant_9(i+1-nPD)*t_step_ramp;
    q_s_10 = q_s_10 + Decay_new_constant_9(i+1-nPD)*t_step_ramp;
    q_s_10 = q_s_10- Decay_new_constant_10(i+1-nPD)*t_step_ramp;
    q_s_11 = q_s_11 + Decay_new_constant_10(i+1-nPD)*t_step_ramp;
    q_s_11 = q_s_11- Decay_new_constant_11(i+1-nPD)*t_step_ramp;
    q_s_12 = q_s_12 + Decay_new_constant_11(i+1-nPD)*t_step_ramp;
    q_s_12 = q_s_12- Decay_new_constant_12(i+1-nPD)*t_step_ramp;
    q_s_13 = q_s_13 + Decay_new_constant_12(i+1-nPD)*t_step_ramp;
    q_s_13 = q_s_13- Decay_new_constant_13(i+1-nPD)*t_step_ramp;
    q_s_14 = q_s_14 + Decay_new_constant_13(i+1-nPD)*t_step_ramp;
    q_s_14 = q_s_14 - Decay_new_constant_14(i+1-nPD)*t_step_ramp;
    q_s_15 = q_s_15 + Decay_new_constant_14(i+1-nPD)*t_step_ramp;
    q_s_15 = q_s_15 - Decay_new_constant_15(i+1-nPD)*t_step_ramp;
    q_s_16 = q_s_16 + Decay_new_constant_15(i+1-nPD)*t_step_ramp;
    q_s_16 = q_s_16 - Decay_new_constant_16(i+1-nPD)*t_step_ramp;
    q_s_17 = q_s_17 + Decay_new_constant_16(i+1-nPD)*t_step_ramp;
    q_s_17 = q_s_17- Decay_new_constant_17(i+1-nPD)*t_step_ramp;
    q_s_18 = q_s_18 + Decay_new_constant_17(i+1-nPD)*t_step_ramp;
    q_s_18 = q_s_18- Decay_new_constant_18(i+1-nPD)*t_step_ramp;
    q_s_19 = q_s_19 + Decay_new_constant_18(i+1-nPD)*t_step_ramp;
    q_s_19 = q_s_19- Decay_new_constant_19(i+1-nPD)*t_step_ramp;
    q_s_20 = q_s_20 + Decay_new_constant_19(i+1-nPD)*t_step_ramp;
    q_s_20 = q_s_20 - Decay_new_constant_20(i+1-nPD)*t_step_ramp;
    q_s_21 = q_s_21 + Decay_new_constant_20(i+1-nPD)*t_step_ramp;
    q_s_21 = q_s_21 - Decay_new_constant_21(i+1-nPD)*t_step_ramp;
```

```
        E_cav_app = E_with_cavity(i-1-nPD);
        q_constant = Er0*pi*b^2*(1+Er*abs(K*(a/b)-1));



        Es = -
(q_s_1/a1^2+q_s_2/a2^2+q_s_3/a3^2+q_s_4/a4^2+q_s_5/a5^2+q_s_6/a6^2+q_s_7/a7^2+q_s_8/a8^2+q_s_9/a9
^2+q_s_10/a10^2+q_s_11/a11^2+q_s_12/a12^2+q_s_13/a13^2+q_s_14/a14^2+q_s_15/a15^2+q_s_16/a16^2+q
_s_17/a17^2+q_s_18/a18^2+q_s_19/a19^2+q_s_20/a20^2+q_s_21/a21^2)/q_constant;
        E_cav = E_cav_app + Es;
        t_start = t_start + t_step_ramp;
        delta_t = delta_t + t_step_ramp;
        i = i + 1;
        Time(i) = t_start;
        Field_cav(i,1) = E_cav;
        Field_s(i) = Es;
        Charge_surface(i) = q_s_1;

        fprintf('Time:     %d\n', Time(i));
        fprintf('Cavity field:    %d kV/mm \n ', Field_cav(i,1));
        fprintf('Surface field:    %d kV/mm \n ', Field_s(i));
        fprintf('Surface charge:    %d\n', Charge_surface(i));
    elseif probability > random
        disp('PD occurs, and this PD is not the first one');
        Conduc_air = air_PD;
        Over_field = E_cav-E_inc;
        E_ext = abs(E_ext_min+(E_inc-E_ext_min)*exp((-abs(E_cav+E_inc))/(E_inc-E_ext_min)));
        E_cav_app = E_with_cavity(i+1-nPD);
        E_cav = E_ext;
        Es = E_cav - E_cav_app;
        delta_E = Field_cav(i+1-nPD) - E_cav;
        q_constant = Er0*pi*b^2*(1+Er*abs(K*(a/b)-1));
        q_s_1 = -Es*q_constant;
        i = i + 1;
        nPD = nPD + 1;
        delta_t = 0;
        Time_PD(nPD) = t_start;
        Charge_induce(nPD) = q_s_1-Charge_surface(i-1);
        Charge_app(nPD) = delta_E*q_app_constant;
        Field_over(nPD) = Over_field;
        Field_ext(nPD) = E_ext;
        Field_occ(nPD) = Field_cav(i-1);
        t_start = t_start + t_PD;
        Time(i) = t_start;

        Field_cav(i,1) = E_cav;
        Field_s(i) = Es;
        Charge_surface(i) = q_s_1;
        fprintf('Cavity field:    %d kV/mm \n ', Field_cav(i,1));
        fprintf('Surface field:    %d kV/mm \n ', Field_s(i));
        fprintf('Surface charge:    %d\n', Charge_surface(i));
    end
```

```
        end
    end
end

while t_start > t_ramp && t_start<= t_end

    if (abs(E_cav) <= E_inc && virgin_void == 0)
        Conduc_air = air_noPD;
        q_start_1 = q_s_1;
        if E_cav*E_cav_app > 0
            if E_cav > 0
                aa = q_s_1;
                q_s_1 = q_s_1 - Decay_new_constant_1(i+1-nPD)*t_step;
                if aa*q_s_1 >0
                    q_s_2 = q_s_2 + Decay_new_constant_1(i+1-nPD)*t_step;
                    bb = q_s_2;
                    q_s_2 = q_s_2- Decay_new_constant_2(i+1-nPD)*t_step;
                    if bb*q_s_2 >0
                        q_s_3 = q_s_3 + Decay_new_constant_2(i+1-nPD)*t_step;
                        q_s_3 = q_s_3- Decay_new_constant_3(i+1-nPD)*t_step;
                        q_s_4 = q_s_4 + Decay_new_constant_3(i+1-nPD)*t_step;
                        q_s_4 = q_s_4- Decay_new_constant_4(i+1-nPD)*t_step;
                        q_s_5 = q_s_5 + Decay_new_constant_4(i+1-nPD)*t_step;
                        q_s_5 = q_s_5- Decay_new_constant_5(i+1-nPD)*t_step;
                        q_s_6 = q_s_6 + Decay_new_constant_5(i+1-nPD)*t_step;
                        q_s_6 = q_s_6- Decay_new_constant_6(i+1-nPD)*t_step;
                        q_s_7 = q_s_7 + Decay_new_constant_6(i+1-nPD)*t_step;
                        q_s_7 = q_s_7- Decay_new_constant_7(i+1-nPD)*t_step;
                        q_s_8 = q_s_8 + Decay_new_constant_7(i+1-nPD)*t_step;
                        q_s_8 = q_s_8- Decay_new_constant_8(i+1-nPD)*t_step;
                        q_s_9 = q_s_9 + Decay_new_constant_8(i+1-nPD)*t_step;
                        q_s_9 = q_s_9- Decay_new_constant_9(i+1-nPD)*t_step;
                        q_s_10 = q_s_10 + Decay_new_constant_9(i+1-nPD)*t_step;
                        q_s_10 = q_s_10- Decay_new_constant_10(i+1-nPD)*t_step;
                        q_s_11 = q_s_11 + Decay_new_constant_10(i+1-nPD)*t_step;
                        q_s_11 = q_s_11- Decay_new_constant_11(i+1-nPD)*t_step;
                        q_s_12 = q_s_12 + Decay_new_constant_11(i+1-nPD)*t_step;
                        q_s_12 = q_s_12- Decay_new_constant_12(i+1-nPD)*t_step;
                        q_s_13 = q_s_13 + Decay_new_constant_12(i+1-nPD)*t_step;
                        q_s_13 = q_s_13- Decay_new_constant_13(i+1-nPD)*t_step;
                        q_s_14 = q_s_14 + Decay_new_constant_13(i+1-nPD)*t_step;
                        q_s_14 = q_s_14 - Decay_new_constant_14(i+1-nPD)*t_step;
                        q_s_15 = q_s_15 + Decay_new_constant_14(i+1-nPD)*t_step;
                        q_s_15 = q_s_15 - Decay_new_constant_15(i+1-nPD)*t_step;
                        q_s_16 = q_s_16 + Decay_new_constant_15(i+1-nPD)*t_step;
                        q_s_16 = q_s_16 - Decay_new_constant_16(i+1-nPD)*t_step;
                        q_s_17 = q_s_17 + Decay_new_constant_16(i+1-nPD)*t_step;
                        q_s_17 = q_s_17- Decay_new_constant_17(i+1-nPD)*t_step;
                        q_s_18 = q_s_18 + Decay_new_constant_17(i+1-nPD)*t_step;
                        q_s_18 = q_s_18- Decay_new_constant_18(i+1-nPD)*t_step;
                        q_s_19 = q_s_19 + Decay_new_constant_18(i+1-nPD)*t_step;
```

```
        q_s_19 = q_s_19- Decay_new_constant_19(i+1-nPD)*t_step;
        q_s_20 = q_s_20 + Decay_new_constant_19(i+1-nPD)*t_step;
        q_s_20 = q_s_20 - Decay_new_constant_20(i+1-nPD)*t_step;
        q_s_21 = q_s_21 + Decay_new_constant_20(i+1-nPD)*t_step;
        q_s_21 = q_s_21 - Decay_new_constant_21(i+1-nPD)*t_step;
    else
        q_s_2 = 0;
        q_s_3 = q_s_3- Decay_new_constant_3(i+1-nPD)*t_step;
        q_s_4 = q_s_4 + Decay_new_constant_3(i+1-nPD)*t_step;
        q_s_4 = q_s_4- Decay_new_constant_4(i+1-nPD)*t_step;
        q_s_5 = q_s_5 + Decay_new_constant_4(i+1-nPD)*t_step;
        q_s_5 = q_s_5- Decay_new_constant_5(i+1-nPD)*t_step;
        q_s_6 = q_s_6 + Decay_new_constant_5(i+1-nPD)*t_step;
        q_s_6 = q_s_6- Decay_new_constant_6(i+1-nPD)*t_step;
        q_s_7 = q_s_7 + Decay_new_constant_6(i+1-nPD)*t_step;
        q_s_7 = q_s_7- Decay_new_constant_7(i+1-nPD)*t_step;
        q_s_8 = q_s_8 + Decay_new_constant_7(i+1-nPD)*t_step;
        q_s_8 = q_s_8- Decay_new_constant_8(i+1-nPD)*t_step;
        q_s_9 = q_s_9 + Decay_new_constant_8(i+1-nPD)*t_step;
        q_s_9 = q_s_9- Decay_new_constant_9(i+1-nPD)*t_step;
        q_s_10 = q_s_10 + Decay_new_constant_9(i+1-nPD)*t_step;
        q_s_10 = q_s_10- Decay_new_constant_10(i+1-nPD)*t_step;
        q_s_11 = q_s_11 + Decay_new_constant_10(i+1-nPD)*t_step;
        q_s_11 = q_s_11- Decay_new_constant_11(i+1-nPD)*t_step;
        q_s_12 = q_s_12 + Decay_new_constant_11(i+1-nPD)*t_step;
        q_s_12 = q_s_12- Decay_new_constant_12(i+1-nPD)*t_step;
        q_s_13 = q_s_13 + Decay_new_constant_12(i+1-nPD)*t_step;
        q_s_13 = q_s_13- Decay_new_constant_13(i+1-nPD)*t_step;
        q_s_14 = q_s_14 + Decay_new_constant_13(i+1-nPD)*t_step;
        q_s_14 = q_s_14 - Decay_new_constant_14(i+1-nPD)*t_step;
        q_s_15 = q_s_15 + Decay_new_constant_14(i+1-nPD)*t_step;
        q_s_15 = q_s_15 - Decay_new_constant_15(i+1-nPD)*t_step;
        q_s_16 = q_s_16 + Decay_new_constant_15(i+1-nPD)*t_step;
        q_s_16 = q_s_16 - Decay_new_constant_16(i+1-nPD)*t_step;
        q_s_17 = q_s_17 + Decay_new_constant_16(i+1-nPD)*t_step;
        q_s_17 = q_s_17- Decay_new_constant_17(i+1-nPD)*t_step;
        q_s_18 = q_s_18 + Decay_new_constant_17(i+1-nPD)*t_step;
        q_s_18 = q_s_18- Decay_new_constant_18(i+1-nPD)*t_step;
        q_s_19 = q_s_19 + Decay_new_constant_18(i+1-nPD)*t_step;
        q_s_19 = q_s_19- Decay_new_constant_19(i+1-nPD)*t_step;
        q_s_20 = q_s_20 + Decay_new_constant_19(i+1-nPD)*t_step;
        q_s_20 = q_s_20 - Decay_new_constant_20(i+1-nPD)*t_step;
        q_s_21 = q_s_21 + Decay_new_constant_20(i+1-nPD)*t_step;
        q_s_21 = q_s_21 - Decay_new_constant_21(i+1-nPD)*t_step;
    end
else
    q_s_1 = 0;
    bb =  q_s_2;
    q_s_2 = q_s_2- Decay_new_constant_2(i+1-nPD)*t_step;
    if bb*q_s_2>0
        q_s_3 = q_s_3 + Decay_new_constant_2(i+1-nPD)*t_step;
```

```
q_s_3 = q_s_3- Decay_new_constant_3(i+1-nPD)*t_step;
q_s_4 = q_s_4 + Decay_new_constant_3(i+1-nPD)*t_step;
q_s_4 = q_s_4- Decay_new_constant_4(i+1-nPD)*t_step;
q_s_5 = q_s_5 + Decay_new_constant_4(i+1-nPD)*t_step;
q_s_5 = q_s_5- Decay_new_constant_5(i+1-nPD)*t_step;
q_s_6 = q_s_6 + Decay_new_constant_5(i+1-nPD)*t_step;
q_s_6 = q_s_6- Decay_new_constant_6(i+1-nPD)*t_step;
q_s_7 = q_s_7 + Decay_new_constant_6(i+1-nPD)*t_step;
q_s_7 = q_s_7- Decay_new_constant_7(i+1-nPD)*t_step;
q_s_8 = q_s_8 + Decay_new_constant_7(i+1-nPD)*t_step;
q_s_8 = q_s_8- Decay_new_constant_8(i+1-nPD)*t_step;
q_s_9 = q_s_9 + Decay_new_constant_8(i+1-nPD)*t_step;
q_s_9 = q_s_9- Decay_new_constant_9(i+1-nPD)*t_step;
q_s_10 = q_s_10 + Decay_new_constant_9(i+1-nPD)*t_step;
q_s_10 = q_s_10- Decay_new_constant_10(i+1-nPD)*t_step;
q_s_11 = q_s_11 + Decay_new_constant_10(i+1-nPD)*t_step;
q_s_11 = q_s_11- Decay_new_constant_11(i+1-nPD)*t_step;
q_s_12 = q_s_12 + Decay_new_constant_11(i+1-nPD)*t_step;
q_s_12 = q_s_12- Decay_new_constant_12(i+1-nPD)*t_step;
q_s_13 = q_s_13 + Decay_new_constant_12(i+1-nPD)*t_step;
q_s_13 = q_s_13- Decay_new_constant_13(i+1-nPD)*t_step;
q_s_14 = q_s_14 + Decay_new_constant_13(i+1-nPD)*t_step;
q_s_14 = q_s_14 - Decay_new_constant_14(i+1-nPD)*t_step;
q_s_15 = q_s_15 + Decay_new_constant_14(i+1-nPD)*t_step;
q_s_15 = q_s_15 - Decay_new_constant_15(i+1-nPD)*t_step;
q_s_16 = q_s_16 + Decay_new_constant_15(i+1-nPD)*t_step;
q_s_16 = q_s_16 - Decay_new_constant_16(i+1-nPD)*t_step;
q_s_17 = q_s_17 + Decay_new_constant_16(i+1-nPD)*t_step;
q_s_17 = q_s_17- Decay_new_constant_17(i+1-nPD)*t_step;
q_s_18 = q_s_18 + Decay_new_constant_17(i+1-nPD)*t_step;
q_s_18 = q_s_18- Decay_new_constant_18(i+1-nPD)*t_step;
q_s_19 = q_s_19 + Decay_new_constant_18(i+1-nPD)*t_step;
q_s_19 = q_s_19- Decay_new_constant_19(i+1-nPD)*t_step;
q_s_20 = q_s_20 + Decay_new_constant_19(i+1-nPD)*t_step;
q_s_20 = q_s_20 - Decay_new_constant_20(i+1-nPD)*t_step;
q_s_21 = q_s_21 + Decay_new_constant_20(i+1-nPD)*t_step;
q_s_21 = q_s_21 - Decay_new_constant_21(i+1-nPD)*t_step;
else
q_s_2 = 0;
q_s_3 = q_s_3- Decay_new_constant_3(i+1-nPD)*t_step;
q_s_4 = q_s_4 + Decay_new_constant_3(i+1-nPD)*t_step;
q_s_4 = q_s_4- Decay_new_constant_4(i+1-nPD)*t_step;
q_s_5 = q_s_5 + Decay_new_constant_4(i+1-nPD)*t_step;
q_s_5 = q_s_5- Decay_new_constant_5(i+1-nPD)*t_step;
q_s_6 = q_s_6 + Decay_new_constant_5(i+1-nPD)*t_step;
q_s_6 = q_s_6- Decay_new_constant_6(i+1-nPD)*t_step;
q_s_7 = q_s_7 + Decay_new_constant_6(i+1-nPD)*t_step;
q_s_7 = q_s_7- Decay_new_constant_7(i+1-nPD)*t_step;
q_s_8 = q_s_8 + Decay_new_constant_7(i+1-nPD)*t_step;
q_s_8 = q_s_8- Decay_new_constant_8(i+1-nPD)*t_step;
q_s_9 = q_s_9 + Decay_new_constant_8(i+1-nPD)*t_step;
```

```
                    q_s_9 = q_s_9- Decay_new_constant_9(i+1-nPD)*t_step;
                    q_s_10 = q_s_10 + Decay_new_constant_9(i+1-nPD)*t_step;
                    q_s_10 = q_s_10- Decay_new_constant_10(i+1-nPD)*t_step;
                    q_s_11 = q_s_11 + Decay_new_constant_10(i+1-nPD)*t_step;
                    q_s_11 = q_s_11- Decay_new_constant_11(i+1-nPD)*t_step;
                    q_s_12 = q_s_12 + Decay_new_constant_11(i+1-nPD)*t_step;
                    q_s_12 = q_s_12- Decay_new_constant_12(i+1-nPD)*t_step;
                    q_s_13 = q_s_13 + Decay_new_constant_12(i+1-nPD)*t_step;
                    q_s_13 = q_s_13- Decay_new_constant_13(i+1-nPD)*t_step;
                    q_s_14 = q_s_14 + Decay_new_constant_13(i+1-nPD)*t_step;
                    q_s_14 = q_s_14 - Decay_new_constant_14(i+1-nPD)*t_step;
                    q_s_15 = q_s_15 + Decay_new_constant_14(i+1-nPD)*t_step;
                    q_s_15 = q_s_15 - Decay_new_constant_15(i+1-nPD)*t_step;
                    q_s_16 = q_s_16 + Decay_new_constant_15(i+1-nPD)*t_step;
                    q_s_16 = q_s_16 - Decay_new_constant_16(i+1-nPD)*t_step;
                    q_s_17 = q_s_17 + Decay_new_constant_16(i+1-nPD)*t_step;
                    q_s_17 = q_s_17- Decay_new_constant_17(i+1-nPD)*t_step;
                    q_s_18 = q_s_18 + Decay_new_constant_17(i+1-nPD)*t_step;
                    q_s_18 = q_s_18- Decay_new_constant_18(i+1-nPD)*t_step;
                    q_s_19 = q_s_19 + Decay_new_constant_18(i+1-nPD)*t_step;
                    q_s_19 = q_s_19- Decay_new_constant_19(i+1-nPD)*t_step;
                    q_s_20 = q_s_20 + Decay_new_constant_19(i+1-nPD)*t_step;
                    q_s_20 = q_s_20 - Decay_new_constant_20(i+1-nPD)*t_step;
                    q_s_21 = q_s_21 + Decay_new_constant_20(i+1-nPD)*t_step;
                    q_s_21 = q_s_21 - Decay_new_constant_21(i+1-nPD)*t_step;
                end
            end
        end
    end
    E_cav_app = E_with_cavity(i+1-nPD);
    q_constant = Er0*pi*b^2*(1+Er*abs(K*(a/b)-1));
    Es = -
(q_s_1/a1^2+q_s_2/a2^2+q_s_3/a3^2+q_s_4/a4^2+q_s_5/a5^2+q_s_6/a6^2+q_s_7/a7^2+q_s_8/a8^2+q_s_9/a9
^2+q_s_10/a10^2+q_s_11/a11^2+q_s_12/a12^2+q_s_13/a13^2+q_s_14/a14^2+q_s_15/a15^2+q_s_16/a16^2+q
_s_17/a17^2+q_s_18/a18^2+q_s_19/a19^2+q_s_20/a20^2+q_s_21/a21^2)/q_constant;
    E_cav = E_cav_app + Es;
    i = i + 1;
    t_start = t_start + t_step;
    Time(i) = t_start;
    Field_cav(i,1) = E_cav;
    Field_s(i) = Es;
    Charge_surface(i) = q_s_1;

    fprintf('Time:      %d\n', Time(i));
    fprintf('Cavity field:     %d kV/mm \n ', Field_cav(i,1));
    fprintf('Surface field:     %d kV/mm \n ', Field_s(i));
    fprintf('Surface charge:     %d\n', Charge_surface(i));
end

if abs(E_cav) > E_inc
    if nPD == 0
        Ndt_0 = epsilon*abs(q_s_1/e);
```

```matlab
Ndt = Ndt_0*exp(-delta_t/tau);
N_dt = Ndt*v0*exp(-(work_function-sqrt(abs(E_cav)*N_dt_constant_1))/N_dt_constant_2);
Ne = etai_rad*P*Veff;
Ng = N_dt + Ne;
probability = 1-exp(-Ng*delta_t);
random = rand(1);
fprintf('Time:    %d\n', Time(i));
fprintf('Probability:    %d\n ', probability);
fprintf('Random:    %d\n', random);
if probability <= random
    Conduc_air = air_noPD;
    aa = q_s_1;
    q_s_1 = q_s_1 - Decay_new_constant_1(i+1-nPD)*t_step;
    if aa*q_s_1 >0
        q_s_2 = q_s_2 + Decay_new_constant_1(i+1-nPD)*t_step;
        bb = q_s_2;
        q_s_2 = q_s_2- Decay_new_constant_2(i+1-nPD)*t_step;
        if bb*q_s_2>0
            q_s_3 = q_s_3 + Decay_new_constant_2(i+1-nPD)*t_step;
            q_s_3 = q_s_3- Decay_new_constant_3(i+1-nPD)*t_step;
            q_s_4 = q_s_4 + Decay_new_constant_3(i+1-nPD)*t_step;
            q_s_4 = q_s_4- Decay_new_constant_4(i+1-nPD)*t_step;
            q_s_5 = q_s_5 + Decay_new_constant_4(i+1-nPD)*t_step;
            q_s_5 = q_s_5- Decay_new_constant_5(i+1-nPD)*t_step;
            q_s_6 = q_s_6 + Decay_new_constant_5(i+1-nPD)*t_step;
            q_s_6 = q_s_6- Decay_new_constant_6(i+1-nPD)*t_step;
            q_s_7 = q_s_7 + Decay_new_constant_6(i+1-nPD)*t_step;
            q_s_7 = q_s_7- Decay_new_constant_7(i+1-nPD)*t_step;
            q_s_8 = q_s_8 + Decay_new_constant_7(i+1-nPD)*t_step;
            q_s_8 = q_s_8- Decay_new_constant_8(i+1-nPD)*t_step;
            q_s_9 = q_s_9 + Decay_new_constant_8(i+1-nPD)*t_step;
            q_s_9 = q_s_9- Decay_new_constant_9(i+1-nPD)*t_step;
            q_s_10 = q_s_10 + Decay_new_constant_9(i+1-nPD)*t_step;
            q_s_10 = q_s_10- Decay_new_constant_10(i+1-nPD)*t_step;
            q_s_11 = q_s_11 + Decay_new_constant_10(i+1-nPD)*t_step;
            q_s_11 = q_s_11- Decay_new_constant_11(i+1-nPD)*t_step;
            q_s_12 = q_s_12 + Decay_new_constant_11(i+1-nPD)*t_step;
            q_s_12 = q_s_12- Decay_new_constant_12(i+1-nPD)*t_step;
            q_s_13 = q_s_13 + Decay_new_constant_12(i+1-nPD)*t_step;
            q_s_13 = q_s_13- Decay_new_constant_13(i+1-nPD)*t_step;
            q_s_14 = q_s_14 + Decay_new_constant_13(i+1-nPD)*t_step;
            q_s_14 = q_s_14 - Decay_new_constant_14(i+1-nPD)*t_step;
            q_s_15 = q_s_15 + Decay_new_constant_14(i+1-nPD)*t_step;
            q_s_15 = q_s_15 - Decay_new_constant_15(i+1-nPD)*t_step;
            q_s_16 = q_s_16 + Decay_new_constant_15(i+1-nPD)*t_step;
            q_s_16 = q_s_16 - Decay_new_constant_16(i+1-nPD)*t_step;
            q_s_17 = q_s_17 + Decay_new_constant_16(i+1-nPD)*t_step;
            q_s_17 = q_s_17- Decay_new_constant_17(i+1-nPD)*t_step;
            q_s_18 = q_s_18 + Decay_new_constant_17(i+1-nPD)*t_step;
            q_s_18 = q_s_18- Decay_new_constant_18(i+1-nPD)*t_step;
            q_s_19 = q_s_19 + Decay_new_constant_18(i+1-nPD)*t_step;
```

```
    q_s_19 = q_s_19- Decay_new_constant_19(i+1-nPD)*t_step;
    q_s_20 = q_s_20 + Decay_new_constant_19(i+1-nPD)*t_step;
    q_s_20 = q_s_20 - Decay_new_constant_20(i+1-nPD)*t_step;
    q_s_21 = q_s_21 + Decay_new_constant_20(i+1-nPD)*t_step;
    q_s_21 = q_s_21 - Decay_new_constant_21(i+1-nPD)*t_step;
  else
    q_s_2 = 0;
    q_s_3 = q_s_3- Decay_new_constant_3(i+1-nPD)*t_step;
    q_s_4 = q_s_4 + Decay_new_constant_3(i+1-nPD)*t_step;
    q_s_4 = q_s_4- Decay_new_constant_4(i+1-nPD)*t_step;
    q_s_5 = q_s_5 + Decay_new_constant_4(i+1-nPD)*t_step;
    q_s_5 = q_s_5- Decay_new_constant_5(i+1-nPD)*t_step;
    q_s_6 = q_s_6 + Decay_new_constant_5(i+1-nPD)*t_step;
    q_s_6 = q_s_6- Decay_new_constant_6(i+1-nPD)*t_step;
    q_s_7 = q_s_7 + Decay_new_constant_6(i+1-nPD)*t_step;
    q_s_7 = q_s_7- Decay_new_constant_7(i+1-nPD)*t_step;
    q_s_8 = q_s_8 + Decay_new_constant_7(i+1-nPD)*t_step;
    q_s_8 = q_s_8- Decay_new_constant_8(i+1-nPD)*t_step;
    q_s_9 = q_s_9 + Decay_new_constant_8(i+1-nPD)*t_step;
    q_s_9 = q_s_9- Decay_new_constant_9(i+1-nPD)*t_step;
    q_s_10 = q_s_10 + Decay_new_constant_9(i+1-nPD)*t_step;
    q_s_10 = q_s_10- Decay_new_constant_10(i+1-nPD)*t_step;
    q_s_11 = q_s_11 + Decay_new_constant_10(i+1-nPD)*t_step;
    q_s_11 = q_s_11- Decay_new_constant_11(i+1-nPD)*t_step;
    q_s_12 = q_s_12 + Decay_new_constant_11(i+1-nPD)*t_step;
    q_s_12 = q_s_12- Decay_new_constant_12(i+1-nPD)*t_step;
    q_s_13 = q_s_13 + Decay_new_constant_12(i+1-nPD)*t_step;
    q_s_13 = q_s_13- Decay_new_constant_13(i+1-nPD)*t_step;
    q_s_14 = q_s_14 + Decay_new_constant_13(i+1-nPD)*t_step;
    q_s_14 = q_s_14 - Decay_new_constant_14(i+1-nPD)*t_step;
    q_s_15 = q_s_15 + Decay_new_constant_14(i+1-nPD)*t_step;
    q_s_15 = q_s_15 - Decay_new_constant_15(i+1-nPD)*t_step;
    q_s_16 = q_s_16 + Decay_new_constant_15(i+1-nPD)*t_step;
    q_s_16 = q_s_16 - Decay_new_constant_16(i+1-nPD)*t_step;
    q_s_17 = q_s_17 + Decay_new_constant_16(i+1-nPD)*t_step;
    q_s_17 = q_s_17- Decay_new_constant_17(i+1-nPD)*t_step;
    q_s_18 = q_s_18 + Decay_new_constant_17(i+1-nPD)*t_step;
    q_s_18 = q_s_18- Decay_new_constant_18(i+1-nPD)*t_step;
    q_s_19 = q_s_19 + Decay_new_constant_18(i+1-nPD)*t_step;
    q_s_19 = q_s_19- Decay_new_constant_19(i+1-nPD)*t_step;
    q_s_20 = q_s_20 + Decay_new_constant_19(i+1-nPD)*t_step;
    q_s_20 = q_s_20 - Decay_new_constant_20(i+1-nPD)*t_step;
    q_s_21 = q_s_21 + Decay_new_constant_20(i+1-nPD)*t_step;
    q_s_21 = q_s_21 - Decay_new_constant_21(i+1-nPD)*t_step;
  end
else
  q_s_1 = 0;
  bb = q_s_2;
  q_s_2 = q_s_2- Decay_new_constant_2(i+1-nPD)*t_step;
  if bb*q_s_2 >0
    q_s_3 = q_s_3 + Decay_new_constant_2(i+1-nPD)*t_step;
```

```
q_s_3 = q_s_3- Decay_new_constant_3(i+1-nPD)*t_step;
q_s_4 = q_s_4 + Decay_new_constant_3(i+1-nPD)*t_step;
q_s_4 = q_s_4- Decay_new_constant_4(i+1-nPD)*t_step;
q_s_5 = q_s_5 + Decay_new_constant_4(i+1-nPD)*t_step;
q_s_5 = q_s_5- Decay_new_constant_5(i+1-nPD)*t_step;
q_s_6 = q_s_6 + Decay_new_constant_5(i+1-nPD)*t_step;
q_s_6 = q_s_6- Decay_new_constant_6(i+1-nPD)*t_step;
q_s_7 = q_s_7 + Decay_new_constant_6(i+1-nPD)*t_step;
q_s_7 = q_s_7- Decay_new_constant_7(i+1-nPD)*t_step;
q_s_8 = q_s_8 + Decay_new_constant_7(i+1-nPD)*t_step;
q_s_8 = q_s_8- Decay_new_constant_8(i+1-nPD)*t_step;
q_s_9 = q_s_9 + Decay_new_constant_8(i+1-nPD)*t_step;
q_s_9 = q_s_9- Decay_new_constant_9(i+1-nPD)*t_step;
q_s_10 = q_s_10 + Decay_new_constant_9(i+1-nPD)*t_step;
q_s_10 = q_s_10- Decay_new_constant_10(i+1-nPD)*t_step;
q_s_11 = q_s_11 + Decay_new_constant_10(i+1-nPD)*t_step;
q_s_11 = q_s_11- Decay_new_constant_11(i+1-nPD)*t_step;
q_s_12 = q_s_12 + Decay_new_constant_11(i+1-nPD)*t_step;
q_s_12 = q_s_12- Decay_new_constant_12(i+1-nPD)*t_step;
q_s_13 = q_s_13 + Decay_new_constant_12(i+1-nPD)*t_step;
q_s_13 = q_s_13- Decay_new_constant_13(i+1-nPD)*t_step;
q_s_14 = q_s_14 + Decay_new_constant_13(i+1-nPD)*t_step;
q_s_14 = q_s_14 - Decay_new_constant_14(i+1-nPD)*t_step;
q_s_15 = q_s_15 + Decay_new_constant_14(i+1-nPD)*t_step;
q_s_15 = q_s_15 - Decay_new_constant_15(i+1-nPD)*t_step;
q_s_16 = q_s_16 + Decay_new_constant_15(i+1-nPD)*t_step;
q_s_16 = q_s_16 - Decay_new_constant_16(i+1-nPD)*t_step;
q_s_17 = q_s_17 + Decay_new_constant_16(i+1-nPD)*t_step;
q_s_17 = q_s_17- Decay_new_constant_17(i+1-nPD)*t_step;
q_s_18 = q_s_18 + Decay_new_constant_17(i+1-nPD)*t_step;
q_s_18 = q_s_18- Decay_new_constant_18(i+1-nPD)*t_step;
q_s_19 = q_s_19 + Decay_new_constant_18(i+1-nPD)*t_step;
q_s_19 = q_s_19- Decay_new_constant_19(i+1-nPD)*t_step;
q_s_20 = q_s_20 + Decay_new_constant_19(i+1-nPD)*t_step;
q_s_20 = q_s_20 - Decay_new_constant_20(i+1-nPD)*t_step;
q_s_21 = q_s_21 + Decay_new_constant_20(i+1-nPD)*t_step;
q_s_21 = q_s_21 - Decay_new_constant_21(i+1-nPD)*t_step;
else
q_s_2 = 0;
q_s_3 = q_s_3- Decay_new_constant_3(i+1-nPD)*t_step;
q_s_4 = q_s_4 + Decay_new_constant_3(i+1-nPD)*t_step;
q_s_4 = q_s_4- Decay_new_constant_4(i+1-nPD)*t_step;
q_s_5 = q_s_5 + Decay_new_constant_4(i+1-nPD)*t_step;
q_s_5 = q_s_5- Decay_new_constant_5(i+1-nPD)*t_step;
q_s_6 = q_s_6 + Decay_new_constant_5(i+1-nPD)*t_step;
q_s_6 = q_s_6- Decay_new_constant_6(i+1-nPD)*t_step;
q_s_7 = q_s_7 + Decay_new_constant_6(i+1-nPD)*t_step;
q_s_7 = q_s_7- Decay_new_constant_7(i+1-nPD)*t_step;
q_s_8 = q_s_8 + Decay_new_constant_7(i+1-nPD)*t_step;
q_s_8 = q_s_8- Decay_new_constant_8(i+1-nPD)*t_step;
q_s_9 = q_s_9 + Decay_new_constant_8(i+1-nPD)*t_step;
```

```
                q_s_9 = q_s_9- Decay_new_constant_9(i+1-nPD)*t_step;
                q_s_10 = q_s_10 + Decay_new_constant_9(i+1-nPD)*t_step;
                q_s_10 = q_s_10- Decay_new_constant_10(i+1-nPD)*t_step;
                q_s_11 = q_s_11 + Decay_new_constant_10(i+1-nPD)*t_step;
                q_s_11 = q_s_11- Decay_new_constant_11(i+1-nPD)*t_step;
                q_s_12 = q_s_12 + Decay_new_constant_11(i+1-nPD)*t_step;
                q_s_12 = q_s_12- Decay_new_constant_12(i+1-nPD)*t_step;
                q_s_13 = q_s_13 + Decay_new_constant_12(i+1-nPD)*t_step;
                q_s_13 = q_s_13- Decay_new_constant_13(i+1-nPD)*t_step;
                q_s_14 = q_s_14 + Decay_new_constant_13(i+1-nPD)*t_step;
                q_s_14 = q_s_14 - Decay_new_constant_14(i+1-nPD)*t_step;
                q_s_15 = q_s_15 + Decay_new_constant_14(i+1-nPD)*t_step;
                q_s_15 = q_s_15 - Decay_new_constant_15(i+1-nPD)*t_step;
                q_s_16 = q_s_16 + Decay_new_constant_15(i+1-nPD)*t_step;
                q_s_16 = q_s_16 - Decay_new_constant_16(i+1-nPD)*t_step;
                q_s_17 = q_s_17 + Decay_new_constant_16(i+1-nPD)*t_step;
                q_s_17 = q_s_17- Decay_new_constant_17(i+1-nPD)*t_step;
                q_s_18 = q_s_18 + Decay_new_constant_17(i+1-nPD)*t_step;
                q_s_18 = q_s_18- Decay_new_constant_18(i+1-nPD)*t_step;
                q_s_19 = q_s_19 + Decay_new_constant_18(i+1-nPD)*t_step;
                q_s_19 = q_s_19- Decay_new_constant_19(i+1-nPD)*t_step;
                q_s_20 = q_s_20 + Decay_new_constant_19(i+1-nPD)*t_step;
                q_s_20 = q_s_20 - Decay_new_constant_20(i+1-nPD)*t_step;
                q_s_21 = q_s_21 + Decay_new_constant_20(i+1-nPD)*t_step;
                q_s_21 = q_s_21 - Decay_new_constant_21(i+1-nPD)*t_step;
            end
        end


        E_cav_app = E_with_cavity(i+1-nPD);
        q_constant = Er0*pi*b^2*(1+Er*abs(K*(a/b)-1));

        Es = -
(q_s_1/a1^2+q_s_2/a2^2+q_s_3/a3^2+q_s_4/a4^2+q_s_5/a5^2+q_s_6/a6^2+q_s_7/a7^2+q_s_8/a8^2+q_s_9/a9
^2+q_s_10/a10^2+q_s_11/a11^2+q_s_12/a12^2+q_s_13/a13^2+q_s_14/a14^2+q_s_15/a15^2+q_s_16/a16^2+q
_s_17/a17^2+q_s_18/a18^2+q_s_19/a19^2+q_s_20/a20^2+q_s_21/a21^2)/q_constant;
        E_cav = E_with_cavity(i+1) + Es;
        t_start = t_start + t_step;
        delta_t = delta_t + t_step;
        i = i + 1;
        Time(i) = t_start;
        Field_cav(i,1) = E_cav;
        Field_s(i) = Es;
        Charge_surface(i) = q_s_1;


        fprintf('Cavity field:     %d kV/mm \n ', Field_cav(i,1));
        fprintf('Surface field:     %d kV/mm \n ', Field_s(i));
        fprintf('Surface charge:     %d\n', Charge_surface(i));

    elseif probability > random
        disp('PD occurs, and this PD is the first one');
```

```
Es1 = -q_s_1/(a1^2*q_constant);
Es2 = -q_s_2/(a2^2*q_constant);
Es3 = -q_s_3/(a3^2*q_constant);
Es4 = -q_s_4/(a4^2*q_constant);
Es5 = -q_s_5/(a5^2*q_constant);
Es6 = -q_s_6/(a6^2*q_constant);
Es7 = -q_s_7/(a7^2*q_constant);
Es8 = -q_s_8/(a8^2*q_constant);
Es9 = -q_s_9/(a9^2*q_constant);
Es10 = -q_s_10/(a10^2*q_constant);
Es11 = -q_s_11/(a11^2*q_constant);
Es12 = -q_s_12/(a12^2*q_constant);
Es13 = -q_s_13/(a13^2*q_constant);
Es14 = -q_s_14/(a14^2*q_constant);
Es15 = -q_s_15/(a15^2*q_constant);
Es16 = -q_s_16/(a16^2*q_constant);
Es17 = -q_s_17/(a17^2*q_constant);
Es18 = -q_s_18/(a18^2*q_constant);
Es19 = -q_s_19/(a19^2*q_constant);
Es20 = -q_s_20/(a20^2*q_constant);
Es21 = -q_s_21/(a21^2*q_constant);
Conduc_air = air_PD;
Over_field = E_cav-E_inc;
if E_cav > 0
    E_ext = abs((E_ext_min+(E_inc-E_ext_min)*exp((-abs(E_cav+E_inc))/(E_inc-E_ext_min))));
else
    E_ext = -abs((E_ext_min+(E_inc-E_ext_min)*exp((-abs(E_cav+E_inc))/(E_inc-E_ext_min))));
end
E_cav_app = E_with_cavity(i);
E_cav = E_ext;
Es = E_cav - E_cav_app;
delta_E = Field_cav(i,1) - E_cav;
q_constant = Er0*pi*b^2*(1+Er*abs(K*(a/b)-1));
q_s_1 = -(Es-Es2-Es3-Es4-Es5-Es6-Es7-Es8-Es9-Es10-Es11-Es12-Es13-Es14-Es15-Es16-Es17-Es18-
Es19-Es20-Es21)*q_constant;
i = i + 1;
nPD = nPD + 1;
delta_t = delta_t+t_step;
Time_PD(nPD) = t_start;
Charge_induce(nPD) = q_s_1-Charge_surface(i-1);
Charge_app(nPD) = delta_E*q_app_constant;
Field_over(nPD) = Over_field;
Field_ext(nPD) = E_ext;
Field_occ(nPD) = Field_cav(i-1);

t_start = t_start + t_PD;
Time(i) = t_start;
Field_cav(i,1) = E_cav;
Field_s(i) = Es;
Charge_surface(i) = q_s_1;
fprintf('Cavity field:    %d kV/mm \n ', Field_cav(i,1));
```

144

```matlab
        fprintf('Surface field:    %d kV/mm \n ', Field_s(i));
        fprintf('Surface charge:    %d\n', Charge_surface(i));

    end

elseif nPD >= 1
    Ndt_0 = epsilon*abs(q_s_1/e);
    Ndt = Ndt_0*exp(-delta_t/tau);
    N_dt = Ndt*v0*exp(-(work_function-sqrt(abs(E_cav)*N_dt_constant_1))/N_dt_constant_2);
    Ne = etai_rad*P*Veff;
    Ng = N_dt + Ne;
    probability = 1-exp(-Ng*delta_t);
    random = rand(1);
    fprintf('Time:    %d\n', Time(i));
    fprintf('Probability:    %d\n ', probability);
    fprintf('Random:    %d\n', random);
    if probability <= random
        Conduc_air = air_noPD;
        q_start = q_s_1;
        if E_cav > 0
            q_s_1 = q_s_1 - Decay_new_constant_1(i+1-nPD)*t_step;
            q_s_2 = q_s_2 + Decay_new_constant_1(i+1-nPD)*t_step;
            q_s_2 = q_s_2- Decay_new_constant_2(i+1-nPD)*t_step;
            q_s_3 = q_s_3 + Decay_new_constant_2(i+1-nPD)*t_step;
            q_s_3 = q_s_3- Decay_new_constant_3(i+1-nPD)*t_step;
            q_s_4 = q_s_4 + Decay_new_constant_3(i+1-nPD)*t_step;
            q_s_4 = q_s_4- Decay_new_constant_4(i+1-nPD)*t_step;
            q_s_5 = q_s_5 + Decay_new_constant_4(i+1-nPD)*t_step;
            q_s_5 = q_s_5- Decay_new_constant_5(i+1-nPD)*t_step;
            q_s_6 = q_s_6 + Decay_new_constant_5(i+1-nPD)*t_step;
            q_s_6 = q_s_6- Decay_new_constant_6(i+1-nPD)*t_step;
            q_s_7 = q_s_7 + Decay_new_constant_6(i+1-nPD)*t_step;
            q_s_7 = q_s_7- Decay_new_constant_7(i+1-nPD)*t_step;
            q_s_8 = q_s_8 + Decay_new_constant_7(i+1-nPD)*t_step;
            q_s_8 = q_s_8- Decay_new_constant_8(i+1-nPD)*t_step;
            q_s_9 = q_s_9 + Decay_new_constant_8(i+1-nPD)*t_step;
            q_s_9 = q_s_9- Decay_new_constant_9(i+1-nPD)*t_step;
            q_s_10 = q_s_10 + Decay_new_constant_9(i+1-nPD)*t_step;
            q_s_10 = q_s_10- Decay_new_constant_10(i+1-nPD)*t_step;
            q_s_11 = q_s_11 + Decay_new_constant_10(i+1-nPD)*t_step;
            q_s_11 = q_s_11- Decay_new_constant_11(i+1-nPD)*t_step;
            q_s_12 = q_s_12 + Decay_new_constant_11(i+1-nPD)*t_step;
            q_s_12 = q_s_12- Decay_new_constant_12(i+1-nPD)*t_step;
            q_s_13 = q_s_13 + Decay_new_constant_12(i+1-nPD)*t_step;
            q_s_13 = q_s_13- Decay_new_constant_13(i+1-nPD)*t_step;
            q_s_14 = q_s_14 + Decay_new_constant_13(i+1-nPD)*t_step;
            q_s_14 = q_s_14 - Decay_new_constant_14(i+1-nPD)*t_step;
            q_s_15 = q_s_15 + Decay_new_constant_14(i+1-nPD)*t_step;
            q_s_15 = q_s_15 - Decay_new_constant_15(i+1-nPD)*t_step;
            q_s_16 = q_s_16 + Decay_new_constant_15(i+1-nPD)*t_step;
            q_s_16 = q_s_16 - Decay_new_constant_16(i+1-nPD)*t_step;
```

```
q_s_17 = q_s_17 + Decay_new_constant_16(i+1-nPD)*t_step;
q_s_17 = q_s_17- Decay_new_constant_17(i+1-nPD)*t_step;
q_s_18 = q_s_18 + Decay_new_constant_17(i+1-nPD)*t_step;
q_s_18 = q_s_18- Decay_new_constant_18(i+1-nPD)*t_step;
q_s_19 = q_s_19 + Decay_new_constant_18(i+1-nPD)*t_step;
q_s_19 = q_s_19- Decay_new_constant_19(i+1-nPD)*t_step;
q_s_20 = q_s_20 + Decay_new_constant_19(i+1-nPD)*t_step;
q_s_20 = q_s_20 - Decay_new_constant_20(i+1-nPD)*t_step;
q_s_21 = q_s_21 + Decay_new_constant_20(i+1-nPD)*t_step;
q_s_21 = q_s_21 - Decay_new_constant_21(i+1-nPD)*t_step;
else

q_s_1 = q_s_1 + Decay_new_constant_1(i+1-nPD)*t_step;
q_s_2 = q_s_2 - Decay_new_constant_1(i+1-nPD)*t_step;
q_s_2 = q_s_2 + Decay_new_constant_2(i+1-nPD)*t_step;
q_s_3 = q_s_3 - Decay_new_constant_2(i+1-nPD)*t_step;
q_s_3 = q_s_3 + Decay_new_constant_3(i+1-nPD)*t_step;
q_s_4 = q_s_4 - Decay_new_constant_3(i+1-nPD)*t_step;
q_s_4 = q_s_4 + Decay_new_constant_4(i+1-nPD)*t_step;
q_s_5 = q_s_5 - Decay_new_constant_4(i+1-nPD)*t_step;
q_s_5 = q_s_5 + Decay_new_constant_5(i+1-nPD)*t_step;
q_s_6 = q_s_6 - Decay_new_constant_5(i+1-nPD)*t_step;
q_s_6 = q_s_6 + Decay_new_constant_6(i+1-nPD)*t_step;
q_s_7 = q_s_7 - Decay_new_constant_6(i+1-nPD)*t_step;
q_s_7 = q_s_7 + Decay_new_constant_7(i+1-nPD)*t_step;
q_s_8 = q_s_8 - Decay_new_constant_7(i+1-nPD)*t_step;
q_s_8 = q_s_8 + Decay_new_constant_8(i+1-nPD)*t_step;
q_s_9 = q_s_9 - Decay_new_constant_8(i+1-nPD)*t_step;
q_s_9 = q_s_9 + Decay_new_constant_9(i+1-nPD)*t_step;
q_s_10 = q_s_10 - Decay_new_constant_9(i+1-nPD)*t_step;
q_s_10 = q_s_10 + Decay_new_constant_10(i+1-nPD)*t_step;
q_s_11 = q_s_11 - Decay_new_constant_10(i+1-nPD)*t_step;
q_s_11 = q_s_11 + Decay_new_constant_11(i+1-nPD)*t_step;
q_s_12 = q_s_12 - Decay_new_constant_11(i+1-nPD)*t_step;
q_s_12 = q_s_12 + Decay_new_constant_12(i+1-nPD)*t_step;
q_s_13 = q_s_13 - Decay_new_constant_12(i+1-nPD)*t_step;
q_s_13 = q_s_13 + Decay_new_constant_13(i+1-nPD)*t_step;
q_s_14 = q_s_14 - Decay_new_constant_13(i+1-nPD)*t_step;
q_s_14 = q_s_14 + Decay_new_constant_14(i+1-nPD)*t_step;
q_s_15 = q_s_15 - Decay_new_constant_14(i+1-nPD)*t_step;
q_s_15 = q_s_15 + Decay_new_constant_15(i+1-nPD)*t_step;
q_s_16 = q_s_16 - Decay_new_constant_15(i+1-nPD)*t_step;
q_s_16 = q_s_16 + Decay_new_constant_16(i+1-nPD)*t_step;
q_s_17 = q_s_17 - Decay_new_constant_16(i+1-nPD)*t_step;
q_s_17 = q_s_17 + Decay_new_constant_17(i+1-nPD)*t_step;
q_s_18 = q_s_18 - Decay_new_constant_17(i+1-nPD)*t_step;
q_s_18 = q_s_18 + Decay_new_constant_18(i+1-nPD)*t_step;
q_s_19 = q_s_19 - Decay_new_constant_18(i+1-nPD)*t_step;
q_s_19 = q_s_19 + Decay_new_constant_19(i+1-nPD)*t_step;
q_s_20 = q_s_20 - Decay_new_constant_19(i+1-nPD)*t_step;
q_s_20 = q_s_20 + Decay_new_constant_20(i+1-nPD)*t_step;
```

```matlab
                q_s_21 = q_s_21 - Decay_new_constant_20(i+1-nPD)*t_step;
                q_s_21 = q_s_21 + Decay_new_constant_21(i+1-nPD)*t_step;
            end
            E_cav_app = E_with_cavity(i+1-nPD);
            q_constant = Er0*pi*b^2*(1+Er*abs(K*(a/b)-1));



            Es = -
(q_s_1/a1^2+q_s_2/a2^2+q_s_3/a3^2+q_s_4/a4^2+q_s_5/a5^2+q_s_6/a6^2+q_s_7/a7^2+q_s_8/a8^2+q_s_9/a9
^2+q_s_10/a10^2+q_s_11/a11^2+q_s_12/a12^2+q_s_13/a13^2+q_s_14/a14^2+q_s_15/a15^2+q_s_16/a16^2+q
_s_17/a17^2+q_s_18/a18^2+q_s_19/a19^2+q_s_20/a20^2+q_s_21/a21^2)/q_constant;
            E_cav = E_cav_app + Es;
            t_start = t_start + t_step;
            delta_t = delta_t + t_step;
            i = i + 1;
            Time(i) = t_start;
            Field_cav(i,1) = E_cav;
            Field_s(i) = Es;
            Charge_surface(i) = q_s_1;

            fprintf('Time:      %d\n', Time(i));
            fprintf('Cavity field:     %d kV/mm \n ', Field_cav(i,1));
            fprintf('Surface field:     %d kV/mm \n ', Field_s(i));
            fprintf('Surface charge:     %d\n', Charge_surface(i));
        elseif probability > random
            disp('PD occurs, and this PD is not the first one');
            Es1 = -q_s_1/(a1^2*q_constant);
            Es2 = -q_s_2/(a2^2*q_constant);
            Es3 = -q_s_3/(a3^2*q_constant);
            Es4 = -q_s_4/(a4^2*q_constant);
            Es5 = -q_s_5/(a5^2*q_constant);
            Es6 = -q_s_6/(a6^2*q_constant);
            Es7 = -q_s_7/(a7^2*q_constant);
            Es8 = -q_s_8/(a8^2*q_constant);
            Es9 = -q_s_9/(a9^2*q_constant);
            Es10 = -q_s_10/(a10^2*q_constant);
            Es11 = -q_s_11/(a11^2*q_constant);
            Es12 = -q_s_12/(a12^2*q_constant);
            Es13 = -q_s_13/(a13^2*q_constant);
            Es14 = -q_s_14/(a14^2*q_constant);
            Es15 = -q_s_15/(a15^2*q_constant);
            Es16 = -q_s_16/(a16^2*q_constant);
            Es17 = -q_s_17/(a17^2*q_constant);
            Es18 = -q_s_18/(a18^2*q_constant);
            Es19 = -q_s_19/(a19^2*q_constant);
            Es20 = -q_s_20/(a20^2*q_constant);
            Es21 = -q_s_21/(a21^2*q_constant);
            Conduc_air = air_PD;
            Over_field = E_cav-E_inc;
            if E_cav>0
                E_ext = abs((E_ext_min+(E_inc-E_ext_min)*exp((-abs(E_cav+E_inc))/(E_inc-E_ext_min))));
            else
```

```matlab
        E_ext = -abs((E_ext_min+(E_inc-E_ext_min)*exp((-abs(E_cav+E_inc))/(E_inc-E_ext_min)))));
    end
    E_cav_app = E_with_cavity(i+1-nPD);
    E_cav = E_ext;
    Es = E_cav - E_cav_app;
    delta_E = Field_cav(i+1-nPD) - E_cav;
    q_constant = Er0*pi*b^2*(1+Er*abs(K*(a/b)-1));
    q_s_1 = -(Es-Es2-Es3-Es4-Es5-Es6-Es7-Es8-Es9-Es10-Es11-Es12-Es13-Es14-Es15-Es16-Es17-Es18-
Es19-Es20-Es21)*q_constant;
    i = i + 1;
    nPD = nPD + 1;
    delta_t = delta_t+t_step;
    Time_PD(nPD) = t_start;
    Charge_induce(nPD) = q_s_1-Charge_surface(i-1);
    Charge_app(nPD) = delta_E*q_app_constant;
    Field_over(nPD) = Over_field;
    Field_ext(nPD) = E_ext;
    Field_occ(nPD) = Field_cav(i-1);
    t_start = t_start + t_PD;
    Time(i) = t_start;
    Field_cav(i,1) = E_cav;
    Field_s(i) = Es;
    Charge_surface(i) = q_s_1;
    fprintf('Cavity field:    %d kV/mm \n ', Field_cav(i,1));
    fprintf('Surface field:    %d kV/mm \n ', Field_s(i));
    fprintf('Surface charge:    %d\n', Charge_surface(i));
            end
        end
    end
end
position_ratio = (location-Ri)/(Ro-Ri);
Shijian = Time_PD';


fnamec_part_new = strcat('Fresh_material_PD analysis_Ri = ',num2str(Ri*1000),'[mm]_Ro =
',num2str(Ro*1000),'[mm]_Rc = ',num2str(Rc*1000),'[mm]_Position_Ratio =
',num2str(position_ratio),'[1]_Time = ',num2str(t_end),'[s]_Time step = ',num2str(t_step),'[s]_I =
',num2str(I),'[A].mat');
save(fnamec_part_new,'Ri','Ro','Rc','Time','Time_PD','Charge_induce','Charge_app','Field_ext','Field_over','Fiel
d_occ','Field_cav','Field_s','Charge_surface','nPD','Shijian');
```

References

[1] W. Long and S. Nilsson, "HVDC transmission: yesterday and today", *IEEE Power and Energy Magazine*, vol. 5, no. 2, pp. 22-31, 2007;

[2] G. Mazzanti and M. Marzinotto, *Extruded cables for high-voltage direct-current transmission*, 1st ed. Piscataway, NJ: IEEE Press, 2013;

[3] D. Valenza and G. Cipollini, "HVDC submarine power cable systems-state of the art and future developments", *Proceedings 1995 International Conference on Energy Management and Power Delivery EMPD '95*, vol. 1, pp. 283-287;

[4] M. Jeroense, "HVDC, the next generation of transmission highlights with focus on extruded cable systems", *2008 International Symposium on Electrical Insulating Materials (ISEIM 2008)*, pp. 10-15, 2008;

[5] G. Chen, M. Hao, Z. Xu, A. Vaughan, J. Cao and H. Wang, "Review of high voltage direct current cables", *CSEE Journal of Power and Energy Systems*, vol. 1, no. 2, pp. 9-21, 2015;

[6] H. Ghorbani, M. Jeroense, C. Olsson and M. Saltzer, "HVDC Cable Systems— Highlighting Extruded Technology", *IEEE Transactions on Power Delivery*, vol. 29, no. 1, pp. 414-421, 2014;

[7] *HVDC Light Cables: Submarine and land power cables*, ABB's high voltage cable unit Sweden, 2006, pp.5.

[8] J. Zha, Y. Wu, S. Wang, D. Wu, H. Yan and Z. Dang, "Improvement of space charge suppression of polypropylene for potential application in HVDC cables", *IEEE Transactions on Dielectrics and Electrical Insulation*, vol. 23, no. 4, pp. 2337-2343, 2016;

[9] A. Fazal, M. Hao, A. Vaughan, G. Chen, J. Cao and H. Wang, "The effect of composition and processing on electric characteristics of XLPE in HVDC cable applications", *2016 IEEE Electrical Insulation Conference (EIC)*, pp. 440-443, 2016;

[10] E. Kimbark, *Direct current transmission*, 1st ed. New York: Wiley-Interscience, 1971;

[11] Limiting global climate change to 2 degrees Celsius the way ahead for 2020 and beyond. Communication from the commission to the council, the European Parliament, the Eur. Econ. and Social Committee and the Committee of the regions', http://eurlex.europa.eu/LexUriServ/LexUriServ.do?uri=COM:2007:0002: FIN:EN:PDF;

[12] H. O, T. Blackburn, B. Phung, H. Zhang and R. Khawaja, "Investigation of Electric Field Distribution in Power Cables with Voids", *2006 IEEE 8th International Conference on Properties and applications of Dielectric Materials*, pp. 637-640, 2006;

[13] S. Lachini, A. Gholami and M. Mirzaie, "Determining electric field distribution in high voltage cable in presence of cavity," *45th International Universities Power Engineering Conference (UPEC)*, pp. 1-7, 2010;

[14] A. Nosseir, "Calculation of Discharge Inception Voltage Due to the Presence of Voids in Power Cables", *IEEE Transactions on Electrical Insulation*, vol. -14, no. 2, pp. 117-120, 1979;

[15] F. Cheng, "Insulation thickness determination of polymeric power cables", *IEEE Transactions on Dielectrics and Electrical Insulation*, vol. 1, no. 4, pp. 624-629, 1994;

[16] J. Jackson, *Classical electrodynamics*, 1st ed. New York: Wiley, 1962;

[17] R. Schwarz, T. Judendorfer and M. Muhr, "Review of Partial Discharge Monitoring techniques used in High Voltage Equipment", *2008 Annual Report Conference on Electrical Insulation and Dielectric Phenomena*, pp. 400-403, 2008;

[18] *High-voltage test technique-Partial discharge measurements (3rd edition)*, IEC60270, 2000-2012;

[19] E. Lemke, S. Berlijin, E. Gulski, M. Muhr, E. Pultrum, T. Strehl, W. Hauschild, J. Rickmann and G. Rizzi, "Guide for electrical partial discharge measurements in compliance to IEC 60270," *Technical Brochure,* vol. D1, no.241, pp.61- 67, 2008;

[20] Y. R. Chaudhari, N. R. Bhosale, P. M. Kothoke, "Composite Analysis of Phase Resolved Partial Discharge Patterns using Statistical Techniques," *International Journal of Modern Engineering Research* (IJMER), vol. 3, no. 4, pp. 1947-1957, 2013;

[21] P. Morshuis and J. Smit, "Partial discharges at dc voltage: their mechanism, detection and analysis", *IEEE Transactions on Dielectrics and Electrical Insulation*, vol. 12, no. 2, pp. 328-340, 2005;

[22] H. Suzuki, K. Aihara and T. Okamoto, "Complex behaviour of a simple partial-discharge model", *Europhysics Letters (EPL)*, vol. 66, no. 1, pp. 28-34, 2004;

[23] Z. Achillides, G. Georghiou and E. Kyriakides, "Partial discharges and associated transients: the induced charge concept versus capacitive modeling", *IEEE Transactions on Dielectrics and Electrical Insulation*, vol. 15, no. 6, pp. 1507-1516, 2008;

[24] J. Kim, D. Kim, K. Nam, W. Choi, B. Lee and J. Koo, "Characteristics of partial discharge by AC and DC", *2012 IEEE International Conference on Condition Monitoring and Diagnosis*, pp. 489-492, 2012;

[25] H. Niu, A. Cavallini and G. Montanari, "Identification of Partial Discharge Phenomena in HVDC Apparatus", *Conference Record of the 2008 IEEE International Symposium on Electrical Insulation*, pp. 373-376, 2008.

[26] M. Danikas, "The definitions used for partial discharge phenomena", *IEEE Transactions on Electrical Insulation*, vol. 28, no. 6, pp. 1075-1081, 1993;

[27] F. Peek, *Dielectric phenomena in high voltage engineering*, 2nd ed. New York: McGraw-Hill Book Company, Inc., 1920;

[28] E. Kuffel, W. Zaengl and J. Kuffel, *High voltage engineering*, 1st ed. Oxford: Butterworth-Heinemann/Newnes, 2000;

[29] T. Dakin, H. Philofsky and W. Divens, "Effect of electric discharges on the breakdown of solid insulation", *Transactions of the American Institute of Electrical Engineers, Part I: Communication and Electronics*, vol. 73, no. 2, pp. 155-162, 1954;

[30] F. Kreuger, *Partial discharge detection in high-voltage equipment*, 1st ed. London: Butterworths, 1989;

[31] M. Danikas, R. Bartnikas and J. Novak, "On the spark to pseudoglow and glow transition mechanism and discharge detectability (Discussion, with reply by R. Bartnikas and J.P. Novak)", *IEEE Transactions on Electrical Insulation*, vol. 28, no. 3, pp. 429-431, 1993;

[32] T. Tanaka, "Internal Partial Discharge and Material Degradation", *IEEE Transactions on Electrical Insulation*, vol. -21, no. 6, pp. 899-905, 1986;

[33] R. Bartnikas, "A Commentary on Partial Discharge Measurement and Detection", *IEEE Transactions on Electrical Insulation*, vol. -22, no. 5, pp. 629-653, 1987;

[34] R. Altenburger, C. Heitz and J. Timmer, "Analysis of phase-resolved partial discharge patterns of voids based on a stochastic process approach", *Journal of Physics D: Applied Physics*, vol. 35, no. 11, pp. 1149-1163, 2002;

[35] C. Heitz, "A generalized model for partial discharge processes based on a stochastic process approach", *Journal of Physics D: Applied Physics*, vol. 32, no. 9, pp. 1012-1023, 1999;

[36] R. Van Brunt, "Stochastic properties of partial-discharge phenomena", *IEEE Transactions on Electrical Insulation*, vol. 26, no. 5, pp. 902-948, 1991;

[37] R. Bodega, A. Cavallini, P. Morshuis and F. Wester, "The effect of voltage frequency on partial discharge activity", *Annual Report Conference on Electrical Insulation and Dielectric Phenomena*, pp. 685-689;

[38] H. Illias (2011) Measurement and simulation of partial discharges within a spherical cavity in a solid dielectric material. *University of Southampton, Electronics and Computer Science: EEE, Doctoral Thesis*, 236pp;

[39] C. Forssen and H. Edin, "Influence of cavity size and cavity location on partial discharge frequency dependence", *The 17th Annual Meeting of the IEEE Lasers and Electro-Optics Society, 2004. LEOS 2004.*, pp. 438-441;

[40] G. Karady, R. Roy and S. Domitz, "Effect of temperature on the partial discharge initiation voltage of capacitors", *IEEE Transactions on Dielectrics and Electrical Insulation*, vol. 2, no. 3, pp. 499-502, 1995;

[41] C. Vibhakar and S. Kanitkar, "Novel investigation for specimens aging tests under partial discharges and temperature", *2009 IEEE Conference on Electrical Insulation and Dielectric Phenomena*, pp. 433-436, 2009;

[42] H. Illias, G. Chen and P. Lewin, "Partial discharge within a spherical cavity in a dielectric material as a function of cavity size and material temperature", *IET Science, Measurement & Technology*, vol. 6, no. 2, pp. 52-62, 2012;

[43] S. Dodd, N. Chalashkanov and J. Fothergill, "Statistical Analysis of Partial Discharges from Electrical Trees Grown in a Flexible Epoxy Resin", *2008 Annual Report Conference on Electrical Insulation and Dielectric Phenomena*, pp. 666-669, 2008;

[44] R. Van Brunt, "Physics and chemistry of partial discharge and corona. Recent advances and future challenges", *IEEE Transactions on Dielectrics and Electrical Insulation*, vol. 1, no. 5, pp. 761-784, 1994;

[45] "Digital techniques for partial discharge measurements", *IEEE Transactions on Power Delivery*, vol. 7, no. 2, pp. 469-479, 1992;

[46] P. Morshuis, "Partial discharge mechanisms in voids related to dielectric degradation", *IEE Proceedings - Science, Measurement and Technology*, vol. 142, no. 1, pp. 62-68, 1995;

[47] G. Crichton, P. Karlsson and A. Pedersen, "Partial discharges in ellipsoidal and spheroidal voids", *IEEE Transactions on Electrical Insulation*, vol. 24, no. 2, pp. 335-342, 1989;

[48] L. Niemeyer, "A generalized approach to partial discharge modeling", *IEEE Transactions on Dielectrics and Electrical Insulation*, vol. 2, no. 4, pp. 510-528, 1995;

[49] F. Gutfleisch and L. Niemeyer, "Measurement and simulation of PD in epoxy voids", *IEEE Transactions on Dielectrics and Electrical Insulation*, vol. 2, no. 5, pp. 729-743, 1995;

[50] R. Bartnikas and E. McMahon, *Engineering dielectrics*, 1st ed. Philadelphia: ASTM, 1979.

[51] Z. He, J. Li, T. Jiang, L. Bao and C. Cheng, "Partial discharge characteristics influenced by different temperatures under pulsating DC voltages", *2013 IEEE International Conference on Solid Dielectrics (ICSD)*, pp. 1001-1004, 2013;

[52] A. Bradwell, *Electrical insulation*, 1st ed. London, U.K.: P. Peregrinus on behalf of the Institution of Electrical Engineers, 1983;

[53] L. Dissado and J. Fothergill, *Electrical degradation and breakdown in polymers*, 1st ed. London: P. Peregrinus, 1992;

[54] M. Sparks, D. Mills, R. Warren, T. Holstein, A. Maradudin, L. Sham, E. Loh and D. King, "Theory of electron-avalanche breakdown in solids", *Phys. Rev. B*, vol. 24, no. 6, pp. 3519-3536, 1981;

[55] H. Raether, *Electron avalanches and breakdown in gases*, 1st ed. Washington: Butterworths, 1964;

[56] J. Townsend, *Electrons in gases*, 1st ed. London: Hutchinson's Scientific and Technical Publications, 1948;

[57] M. Góngora-Nieto, P. Pedrow, B. Swanson and G. Barbosa-Cánovas, "Impact of air bubbles in a dielectric liquid when subjected to high field strengths", *Innovative Food Science & Emerging Technologies*, vol. 4, no. 1, pp. 57-67, 2003;

[58] E. Husain and R. Nema, "Analysis of Paschen Curves for air, N2 and SF6 Using the Townsend Breakdown Equation", *IEEE Transactions on Electrical Insulation*, vol. -17, no. 4, pp. 350-353, 1982;

[59] J. Meek and J. Craggs, *Electrical breakdown of gases*, 1st ed. Chichester: Wiley, 1978;

[60] A. Pedersen, "Criteria for Spark Breakdown in Sulfur Hexafluoride", *IEEE Transactions on Power Apparatus and Systems*, vol. -89, no. 8, pp. 2043-2048, 1970;

[61] W. Carey, A. Wiebe, R. Nord and L. Altgilbers, "Characterization of Paschen curve anomolies at high P*D values", *2011 IEEE Pulsed Power Conference*, pp. 741-744, 2011;

[62] L. Leob, *Basic process of gaseous electronics*, 2nd ed. Berkeley and Los Angeles, California: University of California Press, 1961.

[63] M. Bhalla and J. Craggs, "Measurement of Ionization and Attachment Coefficients in Sulphur Hexafluoride in Uniform Fields", *Proceedings of the Physical Society*, vol. 80, no. 1, pp. 151-160, 1962;

[64] K. Kao, *Dielectric phenomena in solids*, 1st ed. Amsterdam: Academic Press, 2004;

[65] V. Jain and A. Bajaj, *A textbook of design of electrical installations*, 1st ed. New Delhi: LAXMI PUBLICATIONS(P) LTD, 2004.

[66] J. Crine, "A molecular model to evaluate the impact of aging on space charges in polymer dielectrics", *IEEE Transactions on Dielectrics and Electrical Insulation*, vol. 4, no. 5, pp. 487-495, 1997;

[67] J. Crine, J. Parpal and G. Lessard, "A model of aging of dielectric extruded cables", *Proceedings of the 3rd International Conference on Conduction and Breakdown in Solid Dielectrics*, pp. 347-351;

[68] Y. Shibuya, S. Zoledziowski and J. Calderwood, "Void formation and electrical breakdown in epoxy resin", *IEEE Transactions on Power Apparatus and Systems*, vol. 96, no. 1, pp. 198-207, 1977;

[69] Bok-Hee Youn, Dae-Hee Cho and Sung-Ik Shim, "Improvement of breakdown strength by additives and curing conditions on XLPE insulation for power cable", *Conference Record of the 2004 IEEE International Symposium on Electrical Insulation*, pp. 347-350;

[70] K. Kao, "New theory of electrical discharge and breakdown in low-mobility condensed insulators", *Journal of Applied Physics*, vol. 55, no. 3, pp. 752-755, 1984;

[71] L. Harvanek, J. Hornak, V. Mentlik, P. Trnka and T. Dzugan, "Influence of nano and microparticles on the development of electrical trees", *2016 IEEE International Conference on Dielectrics (ICD)*, pp. 92-95, 2016;

[72] G. Chen and C. Tham, "Electrical treeing characteristics in XLPE power cable insulation in frequency range between 20 and 500 Hz", *IEEE Transactions on Dielectrics and Electrical Insulation*, vol. 16, no. 1, pp. 179-188, 2009;

[73] K. Zhou, M. Huang, W. Tao, M. He and M. Yang, "A possible water tree initiation mechanism for service-aged XLPE cables: Conversion of electrical tree to water tree", *IEEE Transactions on Dielectrics and Electrical Insulation*, vol. 23, no. 3, pp. 1854-1861, 2016;

[74] M. Stanley (2000) Sprites and their Parent Discharges, *New Mexico Institute of Mining and Technology, Physics, Doctoral Thesis*, pp328;

[75] R. Patsch and F. Berton, "Pulse Sequence Analysis - a diagnostic tool based on the physics behind partial discharges", *Journal of Physics D: Applied Physics*, vol. 35, no. 1, pp. 25-32, 2001;

[76] U. Fromm, "Interpretation of partial discharges at dc voltages", *IEEE Transactions on Dielectrics and*

Electrical Insulation, vol. 2, no. 5, pp. 761-770, 1995;

[77] G. Hoogenraad and J. Beyer, "Digital HVDC partial discharge testing", *Conference Record of the 2000 IEEE International Symposium on Electrical Insulation (Cat. No.00CH37075)*, pp. 448-451;

[78] R. Bever, "Ramp Technique for DC Partial Discharge Testing", *IEEE Transactions on Electrical Insulation*, vol. -20, no. 1, pp. 38-46, 1985;

[79] M. Hikita, K. Yamada, A. Nakamura, T. Mizutani, A. Oohasi and M. Ieda, "Measurements of partial discharges by computer and analysis of partial discharge distribution by the Monte Carlo method", *IEEE Transactions on Electrical Insulation*, vol. 25, no. 3, pp. 453-468, 1990;

[80] W. McDermid, "IEEE guide for the measurement of partial discharges in AC electric machinery", *2012 IEEE International Symposium on Electrical Insulation*, pp. 659-660, 2012;

[81] K. Engel, *Bewertung von Teilentladungen in spaltförmigen Isolierstoffdefekten*, 1st ed. Aachen: Shaker, 1998.

[82] S. Karmakar, N. K. Roy, and P. Kumbhakar, "Detection of Partial Discharges Using Optelectronic Method," *International Conference on Optics and Photonics (ICOP)*, 2009;

[83] J. Pearson, O. Farish, B. Hampton, M. Judd, D. Templeton, B. Pryor and I. Welch, "Partial discharge diagnostics for gas insulated substations", *IEEE Transactions on Dielectrics and Electrical Insulation*, vol. 2, no. 5, pp. 893-905, 1995;

[84] T. Kim, J. Nam and K. Suh, "Acoustic monitoring of HV equipment with optical fiber sensor", *Proceedings of 2001 International Symposium on Electrical Insulating Materials (ISEIM 2001). 2001 Asian Conference on Electrical Insulating Diagnosis (ACEID 2001). 33rd Symposium on Electrical and Electronic Insulating Materials and Applications in System*, pp. 241-244;

[85] M. MacAlpine, Z. Zhiqiang and M. Demokan, "Development of a fibre-optic sensor for partial discharges in oil-filled power transformers", *Electric Power Systems Research*, vol. 63, no. 1, pp. 27-36, 2002;

[86] I. Kemp, "Partial discharge plant-monitoring technology: present and future developments", *IEE Proceedings - Science, Measurement and Technology*, vol. 142, no. 1, pp. 4-10, 1995;

[87] H. Kranz, "PD pulse sequence analysis and its relevance for on-site PD defect identification and evaluation", *IEEE Transactions on Dielectrics and Electrical Insulation*, vol. 12, no. 2, pp. 276-284, 2005;

[88] E. Gulski, "Digital analysis of partial discharges", *IEEE Transactions on Dielectrics and Electrical Insulation*, vol. 2, no. 5, pp. 822-837, 1995;

[89] L. Satish and B. Gururaj, "Use of hidden Markov models for partial discharge pattern classification", *IEEE Transactions on Electrical Insulation*, vol. 28, no. 2, pp. 172-182, 1993;

[90] W. Ziomek, H. Schlemper and K. Feser, "Computer aided recognition of defects in GIS", *Conference Record of the 1996 IEEE International Symposium on Electrical Insulation*, pp. 91-94;

[91] A. Contin, G. Montanari and C. Ferraro, "PD source recognition by Weibull processing of pulse height distributions", *IEEE Transactions on Dielectrics and Electrical Insulation*, vol. 7, no. 1, pp. 48-58, 2000;

[92] H. Illias, Teo Soon Yuan, A. Bakar, H. Mokhlis, G. Chen and P. Lewin, "Partial discharge patterns in high voltage insulation", *2012 IEEE International Conference on Power and Energy (PECon)*, pp. 750-755, 2012;

[93] R. Patsch, M. Hoof M and C. Reuter, "Pulse-sequence-analysis, a promising diagnostic tool", *Proceeding of the 8th International Symposium on High-voltage Engineering (ISH)*, vol. 4, pp 157–160, 1993;

[94] R. Patsch and M. Hoof, "Pulse-sequence-analysis, the physics behind", proceeding of the joint conference: international workshop on electrical insulation and 25th symposium on electrical insulation materials, pp 111–114, 1993;

[95] M. Hoof and R. Patsch, "Analyzing partial discharge pulse sequences-a new approach to investigate degradation phenomena", *Proceedings of 1994 IEEE International Symposium on Electrical Insulation*, pp. 327-331;

[96] M. Hoof and R. Patsch, "Pulse-sequence analysis: a new method for investigating the physics of PD-induced ageing", *IEE Proceedings - Science, Measurement and Technology*, vol. 142, no. 1, pp. 95-101, 1995;

[97] M. Hoof, B. Freisleben and R. Patsch, "PD source identification with novel discharge parameters using counterpropagation neural networks", *IEEE Transactions on Dielectrics and Electrical Insulation*, vol. 4, no. 1, pp. 17-32, 1997;

[98] R. Patsch and M. Hoof, "Electrical treeing-physical details obtained by pulse-sequence-analysis", *Proceedings of 1995 IEEE 5th International Conference on Conduction and Breakdown in Solid Dielectrics*, pp. 344-349.

[99] B. Du, Q. Zhang, Y. Lu and X. Zhang, "PD Pattern Classification for dc System Based on Fractal Dimensions Combined with Statistical Features", *2006 IEEE 8th International Conference on Properties and applications of Dielectric Materials*, pp. 427-430, 2006;

[100] U. Fromm and E. Gulski, "Statistical behaviour of internal partial discharges at DC voltage", *Proceedings of 1994 4th International Conference on Properties and Applications of Dielectric Materials (ICPADM)*, pp. 670-673;

[101] H. Ye, E. Boudoudou, E. Scholz, M. Clemens, "Coupled Electro-Thermal Field Simulations in HVDC-Cables", *COMSOL Conference*, 2011;

[102] S. Boggs, D. Damon, J. Hjerrild, J. Holboll and M. Henriksen, "Effect of insulation properties on the field grading of solid dielectric DC cable", *IEEE Transactions on Power Delivery*, vol. 16, no. 4, pp. 456-461, 2001;

[103] Z. Huang, J. Pilgrim, P. Lewin, S. Swingler and G. Tzemis, "Thermal-Electric Rating Method for Mass-Impregnated Paper-Insulated HVDC Cable Circuits", *IEEE Transactions on Power Delivery*, vol. 30, no. 1, pp. 437-444, 2015;

[104] M. Jeroense (1997) Charges and Discharges in HVDC Cables: In Particular in Mass-impregnated HVDC Cables. *Delft University, Electrical Engineering, Mathematics and Computer Science, Doctoral Thesis*, 222pp;

[105] R. Hampton, "Feature article - Some of the considerations for materials operating under high-voltage, direct-current stresses", *IEEE Electrical Insulation Magazine*, vol. 24, no. 1, pp. 5-13, 2008;

[106] M. He, G. Chen and P. Lewin, "Field distortion by a single cavity in HVDC XLPE cable under steady state", *High Voltage*, vol. 1, no. 3, pp. 107-114, 2016;

[107] G. Chen and F. Baharudin, "Partial discharge modelling based on a cylindrical model in solid dielectrics", *2008 International Conference on Condition Monitoring and Diagnosis*, pp. 74-78, 2008;

[108] J. Mathews and K. Fink, *Numerical methods using MATLAB*, 1st ed. Upper Saddle River, N.J.: Pearson, 2004;

[109] H. Illias, G. Chen and P. Lewin, "Partial discharge modelling in a spherical cavity within a dielectric insulation material as a function of frequency", *2009 IEEE Electrical Insulation Conference*, pp. 55-59, 2009;

[110] C. Forssen and H. Edin, "Modeling partial discharges in a cavity at different applied frequencies", *2007 Annual Report - Conference on Electrical Insulation and Dielectric Phenomena*, pp. 132-135, 2007;

[111] S. Pawar, P. Murugavel and D. Lal, "Effect of relative humidity and sea level pressure on electrical conductivity of air over Indian Ocean", *Journal of Geophysical Research*, vol. 114, no. 2, 2009;

[112] L. Magid, *Electromagnetic fields, energy, and waves*, 1st ed. New York: Wiley, 1972;

[113] B. Weedy and D. Chu, "HVDC Extruded Cables-Parameters for Determination of Stress", *IEEE Power Engineering Review*, vol. -4, no. 3, pp. 43-44, 1984;

[114] D. Taylor and T. Williams, "Decay of surface charge in the presence of a time-dependent bulk conductivity", *Journal of Physics C: Solid State Physics*, vol. 11, no. 1, pp. 111-117, 1977;

[115] L. Christophorou and D. James, *Gaseous dielectrics VII*, 1st ed. New York: Plenum Press, 1994;

[116] M. Seltzer-Grant, R. Giussani, W. Siew, E. Corr, X. Hu, M. Zhu, M. Judd, A. Reid, A. Neumann, and J. Awodola, "Laboratory and field partial discharge measurement in HVDC power cables", *9th International Conference on Insulated Power Cables*, pp. 21-25, 2015;

[117] Z. Ahmed, G. Hussain, M. Lehtonen, L. Varacka and J. Kudelcik, "Analysis of partial discharge signals in medium voltage XLPE cables", *2016 17th International Scientific Conference on Electric Power Engineering (EPE)*, pp. 1-6, 2016;

[118] M. He, and G. Chen, "Comparison Between Electrical Conductivity Equations in Descrbing HVDC Cable Insulating Materials", *Journal of Southern Power System Technology*, vol. 10, no. 4, pp. 78-84, 2016;

[119] M. He, G. Chen, and P. L. Lewin, "Analysis of Influence of Internal Defect on Electric Field Distortion of HVDC Cable with Finite Element Method", *Journal of Southern Power System Technology*, vol. 9, no. 10, pp. 83-91, 2015.

Publication List

M. He, G. Chen and P. Lewin, "Field distortion by a single cavity in HVDC XLPE cable under steady state", *High Voltage*, vol. 1, no. 3, pp. 107-114, 2016;

M. He, and G. Chen, "Comparison Between Electrical Conductivity Equations in Descrbing HVDC Cable Insulating Materials", *Journal of Southern Power System Technology*, vol. 10, no. 4, pp. 78-84, 2016;

M. He, G. Chen, and P. L. Lewin, "Analysis of Influence of Internal Defect on Electric Field Distortion of HVDC Cable with Finite Element Method", *Journal of Southern Power System Technology*, vol. 9, no. 10, pp. 83-91, 2015;

N. Liu, M. He, H. Alghamdi, G. Chen, M. Fu, R. Li and S. Hou, "An improved model to estimate trapping parameters in polymeric materials and its application on normal and aged low-density polyethylenes", *J. Appl. Phys.*, vol. 118, no. 6, p. 064102, 2015;

M. He, D. Qiang, N. Liu, G. Chen and P. Lewin, "Investigation of charge injection threshold field in epoxy resin", *2015 IEEE Electrical Insulation Conference (EIC)*, pp. 49-52, 2015;

D. Qiang, M. He, G. Chen and T. Andritsch, "Influence of nano-SiO_2 and BN on space charge and AC/DC performance of epoxy nanocomposites", *2015 IEEE Electrical Insulation Conference (EIC)*, pp. 492-495, 2015;

He, M, Tian, J, Chen, G and Lewin, P L, "Investigation of Partial Discharge in Solid Dielectric under DC Voltage," *UHVNet,* 2014.